CADMIUM SULPHIDE TRANSDUCERS

Thick Vacuum-Deposited Films for Ultrasonic Shear-Mode Low-Frequency Operation

by

SADIQ BAKER HUSSAIN

A thesis submitted for the degree of

Doctor of Philosophy, University of Warwick, August 1971

A B S T R A C T

The primary aim of this research project was to deposit thick-film (low-frequency) s-mode CdS piezoelectric transducers directly onto copper or aluminium rods which formed part of the welding-electrode of a spot-welding machine. These transducers were to replace the discrete transducers used in a set-up for the "on-machine" evaluation of spot-welds. A secondary aim was to deposit very thin CdS films on glass slides for use as microwave resonators. The dependence of film adhesion on film thickness, and crystallographic orientation changes with thickness imposed an upper limit on the thickness of transducers with adequate properties for applications. The final goal, established through experience on the project, was to determine how thick piezoelectric films could be deposited to make useful transducers.

Highly stoichiometric (deviations from stoichiometry of the order of 1 part in 10^{13}) and highly resistive (> 10^{10} Ω.m.), and highly oriented films up to 100 μm thick have been successfully deposited on Aℓ rod substrates. Two deposition techniques were used : CdS/S electron beam bombardment evaporation and Cd/S isothermal cells. Provided that the temperature of the vapour molecules was less than 400°C and that the pumping speed could be increased at will, then, the faster the deposition rate, the sharper the oblique c-axis preferred orientation, and the better the piezoelectric performance of the films. The pumping speed limited the deposition rate to 10 $\mu m.h^{-1}$.

Appreciable thermal stresses in the films gave rise to large forces which induced the thick-films to flake off or disintegrate. The dependence of film adhesion on film thickness is explained in terms of the inequality between the forces which bind the film to the substrate (independent of thickness) and the forces which induce the film to flake off (proportional to thickness). Thick CdS films were made to adhere to the substrate by making the substrate surface rougher

so that the films "keyed-in".

No appreciable temperature gradients existed in the CdS films during growth, either across their thicknesses or along their surfaces. No changes in temperature gradients occurred in the films due to changes in film orientation, and vice versa.

Up to a certain critical thickness, the c-axes of most CdS film crystallites aligned themselves with the direction of the vapour beam. When the thickness of the film exceeded the critical thickness, the growth of oblique crystallites was stifled and the film's c-axis tilted towards the substrate-normal and eventually became parallel to it. This was confirmed by etching-back a thick CdS film which was deposited at oblique vapour incidence. A model is presented for the "stifling process" which gives the relation between the critical thickness, the grain size and the deposition angle of the film. For a given deposition environment, the stifling process imposed an upper limit on the thickness of an s-mode transducer.

The use of copper substrates, and of copper parts inside the deposition chamber, was abandoned because of the corrosive action of sulphur on copper. Cu/CdS junctions were nearly ohmic, and the anomalous behaviour of these junctions is explained in terms of the reaction between Cu and S to form Cu_2S.

CdS s-mode transducers with untuned two-way insertion loss of 35 dB in a 50 ohm system have been successfully deposited on glass slides for operation at frequencies down to 20 MHz. The stress in CdS films on glass slides was much less than that on Aℓ rods. It is possible that the higher stress in films on Aℓ rods weakened their piezoelectric performance.

C O N T E N T S

P R E F A C E

I started working on this project in October 1967 after graduating from University College, Cardiff. All of the work reported here is entirely my own unless otherwise credited in the text. So far as I know, no thesis similar to this one has been submitted at any other university. I have already published parts of this work (see Appendix III), other parts will be submitted for publication in the near future.

Sadiq Baker Hussain
August 1971

A C K N O W L E D G E M E N T S

This work was initiated and supported by the Ministry of Technology (now the Ministry of Aviation Supply) as part of their research contract on the ultrasonic evaluation of electrical resistance spot-welds (Ministry Agreement No. PD/187/02/ADM). I am indebted to them for granting me financial support.

The subject of thin films is inter-disciplinary by nature and in the course of this investigation I had the opportunity to discuss a number of problems with chemists, physicists as well as engineers. In the School of Engineering Science I wish to thank the Chairman, Professor J.A. Shercliff, for providing facilities for this project; my Supervisor, Dr. D.I. Crecraft for his help and guidance throughout; Mr. M.K. McPhun for his help during the design of the r.f. sputtering apparatus; Dr. D.K. Bowen and Dr. R.G. Rhodes for useful discussions on crystals and crystallography; Dr. A.J. Pritchard, Dr. C.J.N. Alty and Dr. G.B. Wallis for discussing my results on temperature profiles in thin films; Dr. H.V. Shurmer for a discussion on semiconductor junctions.

Thanks are also due to co-worker Geoff Warner especially for his help during the design of welding-electrode-inserts and the slot in the seam-welding wheel-electrode; to Kemal Mehmet, Dave Michie and Richard Butlin, of the microwave-integrated circuits group, for their cooperation; particularly for allowing me (sometimes!) to monopolise two deposition chambers. From the technical staff I must single-out Mr. J.L. Baker, Chief Technician, for his unfailing help throughout. I also wish to thank Mr. J.J. Darmon for doing some of the "Talysurf" measurements; Mr. H.J. Fowkes and Mr. F.A. Holloway for machining some of the

substrates; Mr. P.J. Smith for his help throughout, especially for making some of the substrate holders; Mr. R. Fathers for machining some of the substrate holders; Mr. D. Wood for his help in some of the drawings of the r.f. sputtering apparatus and Mrs. T. Richards for tracing most of the diagrams. Thanks also to Mr. H.G. Woodgate and Mr. C.G. Lovatt for their help in photographic work. Thanks also to Allan Coles for cleaning the deposition chamber in the last two deposition runs. In the School of Physics I would like to thank Dr. H. Mykura for the use of the X-ray set, and helpful discussions on the diffraction patterns obtained; and Dr. R.L. Segall for discussions on aluminium epitaxy. In the School of Molecular Sciences I wish to thank Mr. K. Holden for his help throughout especially for making the cadmium and sulphur pyrex cells; Dr. O.W. Howarth who, in his capacity as Warden of Rootes Hall, allowed me to stay in residence on campus longer than is normally allowed. This made it easier for me to carry out my "marathon" deposition runs which often ran continuously for twenty hours. In the Library I wish to acknowledge the unfailing assistance of Miss M. Cooper and Mr. M. Davies. Admiration and gratitude for Miss Daphne Twigger for taking on the difficult task of making a reasonable typescript out of my scribbled manuscript.

Outside the University I wish to thank Mr. J. Pink of Hewlett-Packard for the loan of the F.E.T. probe used in piezoelectric polarity determination; Mr. J.W. Dove of W. Canning & Co. for gold-plating the seam-welding wheel-electrode free of charge; Mr. A. Richards of Industrial Pharmaceutical Service Ltd. for the supply of a free sample of surgical masks; Mr. D.W. Brown of Morganite Research and Development for his cooperation in the supply of the non-standard large cermet crucibles used in this work; and Mr. D. Luff of the Admiralty Materials Research Laboratory for kindly presenting us with a P.Z.T. sputtering

disc and P.Z.T. granuals. Thanks also to Mr. R.W. Gibson and Mr. R.F. Mitchell of Mullards Research Labs. for helping us during the start of this project and especially for showing us their substrate cleaning arrangements; Dr. P.D. Fochs of G.E.C. Hirst Research Centre for showing us their CdS single crystal growing apparatus. I also wish to thank Dr. S.J. Welles of EPIC (Electronic Properties Information Centre) for sending us the data tables on Group II-VI compounds, and the EPIC Bulletin.

Isla has been to me a delightful human-dictionary whom I consulted concerning spelling. Bravo to her for not being too jealous of "my machine"!

It is to my parents that I dedicate this work for their patience in their long wait for me to go back home.

Sadiq Baker Hussain

C H A P T E R 1

Introduction

The first aim of this project was to fabricate low-frequency (down to 10 MHz) s-mode CdS transducers. The CdS transducers were to be deposited directly onto welding-electrode-inserts (Fig. 1.1), and be used instead of the discrete ceramic transducers which formed part of the set-up for the "on-machine" ultrasonic inspection of spot-welds devised by Crecraft and Warner [1]. In electrical resistance spot-welding the two parts to be joined, which are usually in the form of sheet metal, are pressed together between two copper electrodes. A short pulsed electric current is passed through the electrodes and the workpieces. The circuit resistance is largely confined to the workpieces, so that sufficient heat develops to melt the metal over a small area. The region of fused metal is known as the weld "nugget", and it forms at the junction of the metal sheets between the tips of the electrodes. The quality of the weld is mainly determined by the quality of the weld nugget, and its position relative to the finished thickness of the joined sheets. The ultrasonic inspection entails [2] transmitting a short pulse of shear waves from a discrete transducer mounted in the welding-electrode through the electrode tip and into the nearest sheet being welded. Shear waves are used for two reasons. Firstly, the molten weld nugget, being liquid, has no shear stiffness and will not support shear waves. It therefore presents an almost perfect acoustic impedance mismatch to waves arriving at its boundary from the parent metal and a good reflection results. Secondly, the velocity is about half that of longitudinal waves and thus results in a doubling of echo return times from, typically, 100 ns to 200 ns, a great help to the electronic instrumentation. Some of the ultra-

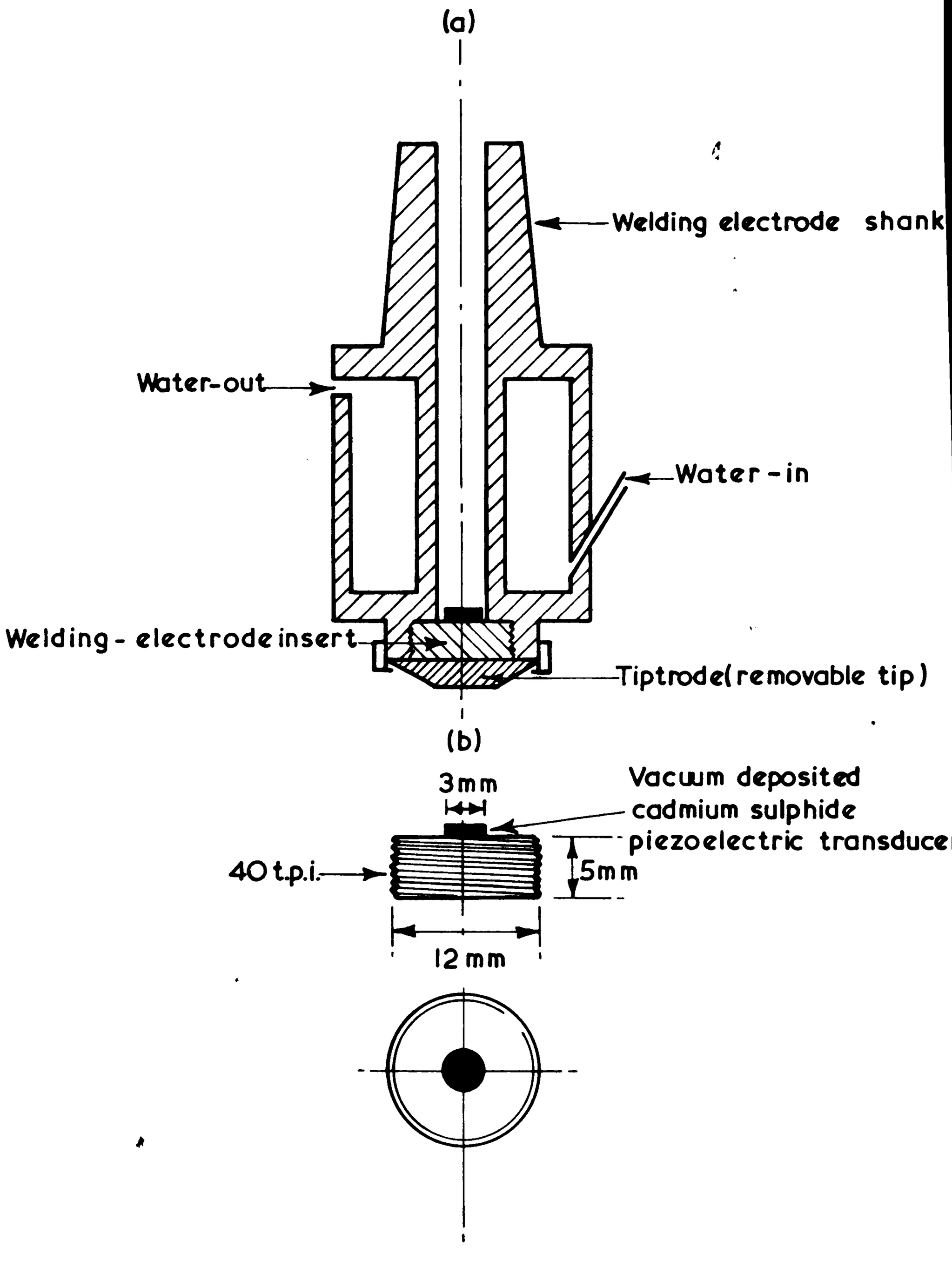

FIG.1.1 (a) Welding electrode
(b) Piezoelectric film transducer on welding electrode insert

sound energy is reflected at the boundary between the electrode tip and the sheet surface, due to the inevitable acoustic mismatch between the electrode copper and the sheet metal. The echo is returned to the transducer followed by the echo from the molten weld nugget. Their time of separation is measured continuously and represents the depth of the weld below the surface. The main limitation of this method is its resolution. In practice the shortest pulse shape of a received echo is a "chad" consisting of 1.5 cycles and for electronic circuitry to resolve the echoes from the tip and the weld successfully, there must be at least one half cycle spacing. This means that when the weld has grown to the largest size allowed, 70% penetration, say, its depth below the surface must accommodate at least two wavelengths. For a typical example of 1 mm sheets, this leaves 0.3 mm of unmolten material with a return path length of 0.6 mm, which is traversed in about 0.2 μs at 3 mm. μs^{-1}. For two cycles the frequency must be 10 MHz. The resolution is limited somewhat further because the ideal "chad" pulse shape can not be obtained. This is because coupling becomes more difficult as the frequency is raised due to surface imperfections. In addition attenuation and dispersion affect pulse propagation at frequencies above 10 MHz. It was hoped that the use of CdS film transducers would improve coupling at 10 MHz, and provide a practical way of raising the frequency to 15 MHz to improve the resolution of the system. Thus, it seemed advantageous to turn to the vacuum-deposition of CdS films direct onto welding-electrode-inserts. The electrode-inserts are designed to screw inside the welding electrode (Fig. 1.1). Copper inserts are used in order to eliminate acoustic mismatches between the insert and the electrode-tip copper. It was hoped to deposit CdS films onto domed electrode-inserts (with 12 mm radius of curvature), so that the ultrasonic beam would be focussed on the spot-weld.

This would increase the ultrasonic signal to noise ratio. Because the electrode-inserts carry part of the welding current, the use of more conventional delay-line materials, e.g. quartz, as inserts was ruled out. The use of quartz would also have created transducer to earth electrical contact problems, and would have introduced cracking and machining difficulties.

When this project started thin-film transducer technology was in its infancy, and the realms of thick-film (low-frequency) transducers were still unexplored. However, it seemed likely that it would not be too difficult to extend the thickness range of film transducers. The fields of depositing film transducers direct onto polycrystalline metal rods, or onto curved surfaces, were also new. Film transducers offer the following advantages over discrete transducers. Firstly, film transducers are deposited direct onto the propagation medium, and, therefore, all the problems associated with bonding a discrete (fragile) transducer onto the propagation medium are eliminated. Secondly, the transducer insertion-loss is decreased by an amount equivalent to the loss associated with the bonding layer. Thirdly, the waves generated by the film transducers are directly coupled to the propagation medium. This is of particular advantage when s-mode waves are to be launched since the problems associated with transmission through a coupling medium are avoided. Fourthly, film transducer materials e.g. cadmium sulphide and zinc oxide, have much lower permittivities than those of ceramic materials, and, therefore, for a given thickness, the film transducers are much easier to drive electrically in view of their lower capacitance. This is of great advantage when good transient performance is required, since a short rise-time pulse is then used to drive the transducer. Finally, with thin-film techniques it may be possible to deposit transducers direct onto curved surfaces, in order to focus the ultrasonic beam. Also,

conventional methods of cutting slabs from a single crystal of a piezoelectric material, and polishing them down to the desired thickness, cannot be used to make slabs thinner than a few micrometres, because they become extremely difficult to handle. With thin film vacuum-deposition techniques transducers can be made as thin as 100 nm, and these transducers are as rugged as the substrates they are deposited on. Most of the work on thin-film transducers was concentrated on materials of binary compounds e.g. cadmium sulphide (CdS), zinc sulphide (ZnS) and zinc oxide (ZnO). The binary compound materials CdS and ZnO have the highest piezoelectric coupling coefficients, with the latter being better than the former. In the present work, CdS was chosen for three main reasons. Firstly, it was, and still is, the best known material in this group. Secondly, it is much easier to deposit stoichiometric films of CdS than of ZnO. Thirdly, for a given frequency a ZnO s-mode transducer has to be about 1.5 times thicker than a CdS one. For example, 10 MHz CdS and ZnO transducers have to be 90 and 135 μm thick.

If and when the fabrication of low-frequency s-mode CdS transducers onto curved surfaces proved feasible, a continuous curved CdS film would be deposited direct onto one side of a slot milled into a wheel-electrode of the type used in seam-welding (Fig. 1.2). In seam-welding a line of overlapping weld nuggets is produced in two or more thicknesses of metal by the passage of an interrupted electric current between the periphery of two wheel electrodes, which are continuously rotated and to which a predetermined load is applied. It was hoped that the CdS film transducer in the wheel-electrode would enable the inspection of seam-welds to be carried out in a manner essentially similar to that of the spot-welds. The various ultrasonic techniques for

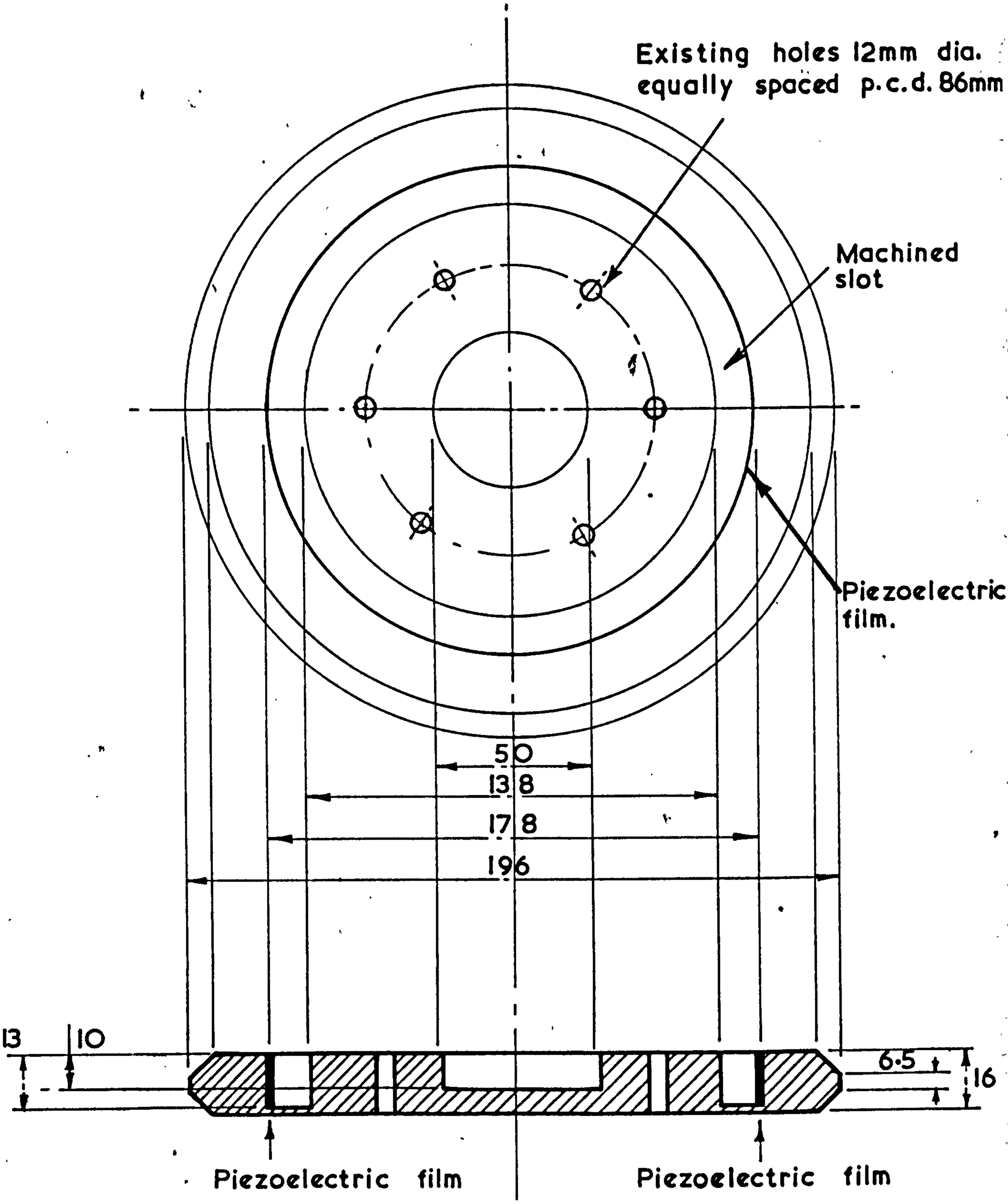

FIG.1.2 Seam welding electrode (dimensions in mm)

the inspection of spot- and seam-welds have been recently reviewed [2]. Time permitting, it was also hoped, to deposit very thin CdS films on glass slides for use as microwave resonators.

SI units are used throughout the Thesis, except in Chapters 4 and 5 where the torr is used as the unit of pressure because it is still widely used in vacuum work. The SI unit of pressure is the $N.m^{-2}$ and is given the name "pascal" (Pa). The pascal is related to the torr by the equation :

1 torr = 1 mm of mercury = 133 Pa.

CHAPTER 1

REFERENCES

1. D.I. Crecraft and G. Warner, *Ultrasonic evaluation of electrical resistance spot-welds*, Non-destructive Testing, 2, p. 40 (1969).

2. E.T. Hall and D.I. Crecraft, *NDT of resistance spots, roll-spot, stitch and seam welds*, Non-destructive Testing, 4, p. 181 (1971).

C H A P T E R 2

Piezoelectricity

2.1. Introduction

In this chapter the theory of piezoelectricity in single crystals [1, 2] is presented with particular reference to wurtzite and sphalerite crystals to which cadmium sulphide belongs in its hexagonal class 6 mm form and cubic class $\bar{4}$ 3 m form, respectively. The conditions necessary for shear-mode generation in thin films of wurtzite [3, 4, 5] and sphalerite structures are presented after discussing the conditions necessary for s-mode generation in single crystals [1, 6, 7] of the same structure. Piezoelectric multi-layers and piezoelectric coupling coefficients [8] for various modes are considered. A table of piezoelectric and other physical constants is given for cadmium sulphide and other piezoelectric and ceramic transducer materials. The reader is referred to Chapter 7 for an introduction to crystals and crystallography.

2.2. Piezoelectricity

Piezoelectricity (pressure-electricity) was first observed by the Curie brothers in 1880 when they found that the application of pressure to slabs of certain crystals resulted in electric charges appearing across the slabs. Piezoelectricity may be defined as the electric polarization (charge per unit area) produced by mechanical strain in crystals belonging to certain classes, the polarization being proportional to the strain, and changing sign with it. This is known as the direct piezoelectric effect. Closely related to it is the converse effect, whereby a piezoelectric crystal becomes strained, when an electric field is applied across it, by an

amount proportional to the field. The direct and converse piezoelectric effects are reversible and they are a manifestation of the same fundamental property of the crystal : the lack of a centre of symmetry. Out of the 32 crystal classes 20 classes lack a centre of symmetry and may exhibit piezoelectric properties.

2.2.1. The direct piezoelectric effect

When a stress is applied to certain crystals they develop an electric moment whose magnitude is proportional to the applied stress. For example if a uniaxial tensile stress σ is applied along the c-axis of cadmium sulphide crystal (hexagonal class 6 mm), the magnitude of the electric moment per unit volume, or the polarization charge per unit area is given by

$$P = d\sigma \qquad \ldots\ldots\ldots \qquad (2.1)$$

where P is the polarization

d is the appropriate piezoelectric coefficient, and

σ is the mechanical stress.

As implied by equation (2.1) a change from a tensile to a compressive stress reverses the direction of the polarization.

In general a state of stress is specified by a second-rank tensor with nine components, while the polarization of a crystal, being a vector, is specified by three components. It is found that when a general stress σ_{ij} acts on a piezoelectric crystal each component of the resulting polarization P_i is linearly related to all the components of σ_{ij} :-

$P_1 = d_{111}\sigma_{11} + d_{112}\sigma_{12} + d_{113}\sigma_{13} + d_{121}\sigma_{21} + \ldots\ldots\ldots + d_{133}\sigma_{33}$ and two similar equations for P_2 and P_3.

Using the summation convention the equations become :-

$$P_1 = d_{1jk}\sigma_{jk}$$

$$P_2 = d_{2jk}\sigma_{jk} \quad \ldots\ldots\ldots \quad (2.2)$$

$$P_3 = d_{3jk}\sigma_{jk}$$

It can be shown, from considerations of symmetry, that

$$\sigma_{ij} = \sigma_{ji}, \text{ and } d_{ijk} = d_{ikj} \quad \ldots\ldots\ldots \quad (2.3)$$

In equation (2.2) the 27 coefficients d_{ijk} form a third rank tensor and because of the symmetry element expressed in equation (2.3) only 18 independent coefficients exist. Writing the coefficients of equation (2.2) in full we thus have :

$$\begin{array}{ccccccccc} d_{111} & d_{112} & d_{113} & d_{211} & d_{212} & d_{213} & d_{311} & d_{312} & d_{313} \\ (d_{121}) & d_{122} & d_{123} & (d_{221}) & d_{222} & d_{223} & (d_{312}) & d_{322} & d_{323} \\ (d_{131}) & (d_{132}) & d_{133} & (d_{231}) & (d_{232}) & d_{233} & (d_{331}) & (d_{332}) & d_{333} \end{array}$$

where the coefficients without brackets are independent coefficients. Using matrix notation the representation of the eighteen independent coefficients can be further simplified. The first suffix, of every coefficient, remains the same as in the tensor notation, but the second and third suffixes are replaced by a single suffix running from 1 to 6 as follows :

tensor notation	:	11	22	33	23,32	31,13	12,21
matrix notation	:	1	2	3	4	5	6

Thus in matrix notation the array of d_{ij} becomes :

$$\begin{array}{cccccc} d_{11} & d_{12} & d_{13} & d_{14} & d_{15} & d_{16} \\ d_{21} & d_{22} & d_{23} & d_{24} & d_{25} & d_{26} \\ d_{31} & d_{32} & d_{33} & d_{34} & d_{35} & d_{36} \end{array}$$

2.2.2. The converse piezoelectric effect

When an electric field is applied in a piezoelectric crystal the shape of the crystal changes slightly, and it is found that there is a linear relationship between the components of the vector E_i giving the components of the electric field within the crystal and the components of the strain tensor ε_{ij} which describe the change of shape. Moreover the coefficients connecting the electric field and the mechanical strain in the converse effect are the same as those connecting the stress and the polarization in the direct effect: when the direct effect is written as $P_i = d_{ijk}\sigma_{jk}$, then the converse effect is written as $\varepsilon_{jk} = d_{ijk} E_i$. Again since $\varepsilon_{jk} = \varepsilon_{kj}$ it follows that d_{ijk} is symmetrical in j and k.

The following scheme summarises the piezoelectric equations in matrix notation. Read horizontally by rows it gives the direct effect, and read vertically by columns it gives the converse effect :

		ε_1	ε_2	ε_3	ε_4	ε_5	ε_6		
		σ_1	σ_2	σ_3	σ_4	σ_5	σ_6		
E_1	P_1	d_{11}	d_{12}	d_{13}	d_{14}	d_{15}	d_{16}	.....	(2.4)
E_2	P_2	d_{21}	d_{22}	d_{23}	d_{24}	d_{25}	d_{26}		
E_3	P_3	d_{31}	d_{32}	d_{33}	d_{34}	d_{35}	d_{36}		

The choice of E and σ as independent variables is arbitrary. A separate pair of piezoelectric equations correspond to a different choice of independent variables. In the same way that the choice of E and σ as independent variables gave rise to the "d" piezoelectric coefficients, the choice of P and σ as independent variables give rise to the "g" piezoelectric coefficients, and that of ε and E as independent variables to the "e" coefficients, and finally the choice of ε and P as independent variables gives rise to the "h" piezoelectric coefficients.

2.2.3. Piezoelectric coefficients for wurtzite and sphalerite crystals

The wurtzite CdS structure is illustrated in Fig. 2.1. This structure [7, 9] consists of two interpenetrating close-packed hexagonal lattices, one composed of cadmium atoms and the other of sulphur atoms. Each cadmium atom is at the centre of a tetrahedron whose corners are occupied by sulphur atoms, and each sulphur atom is at the centre of a tetrahedron of cadmium atoms. The lack of symmetry along the c-axis is apparent from Fig. 2.1. The sphalerite structure is illustrated in Fig. 2.2. It consists [7, 9] of two interpenetrating face-centred cubic lattices. The lattice of cadmium atoms is displaced with respect to the lattice of sulphur atoms by one quarter of the cube diagonal. The basic building blocks of this lattice are again tetrahedra, with sulphur atoms at the centre of a tetrahedron of cadmium atoms and vice versa.

Because of the high degree of symmetry in wurtzite and sphalerite structures, many of the general piezoelectric coefficients of equation (2.4) are equal to zero. (Of course a piezoelectric crystal must not have a centre of symmetry, but it may have other forms of symmetry, e.g. symmetry about a given axis or in a given plane).

For wurtzite crystals only d_{15}, d_{24}, d_{31}, d_{32} and d_{33} have non-zero values, and because of crystal symmetry $d_{15} = d_{24}$ and $d_{31} = d_{32}$. Therefore, for wurtzite crystals the following matrix may be written to represent the piezoelectric equations (2.4) above :

		ε_1	ε_2	ε_3	ε_4	ε_5	ε_6
		σ_1	σ_2	σ_3	σ_4	σ_5	σ_6
ε_1	P_1	0	0	0	0	d_{15}	0
ε_2	P_2	0	0	0	d_{24}	0	0
ε_3	P_3	d_{31}	d_{32}	d_{33}	0	0	0

..... (2.5)

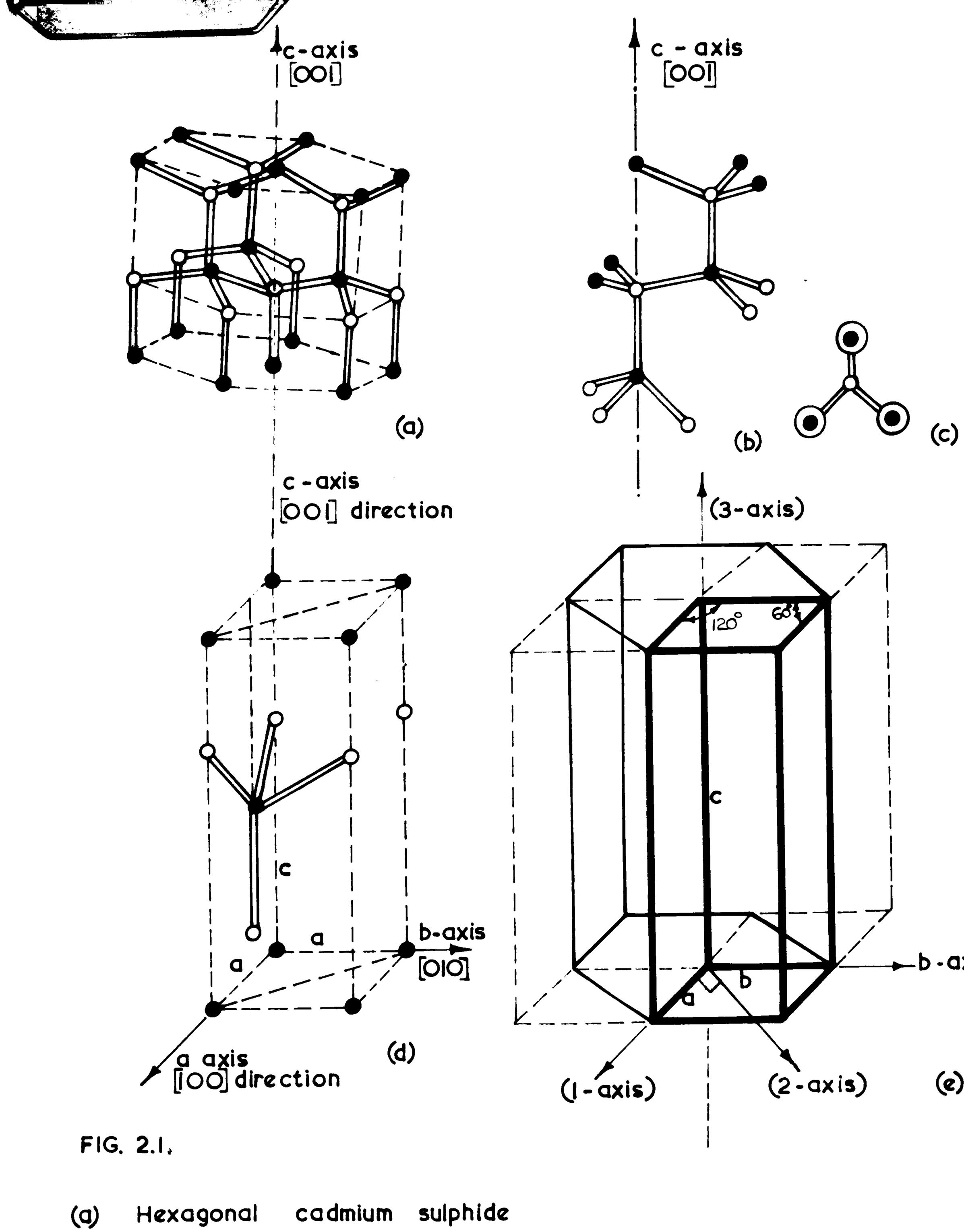

FIG. 2.1.

(a) Hexagonal cadmium sulphide

(b) Stacking arrangement: Aa Bb Aa Bb.....

(c) Looking along c - axis

(d) Unit-cell of Hexagonal cadmium sulphide

(e) Relationship between unit cell (heavy line) and hexagonal prism

● Cadmium atom ○ Sulpher atom ═ Atomic bond
(a=0·4150nm c=0·6737nm)

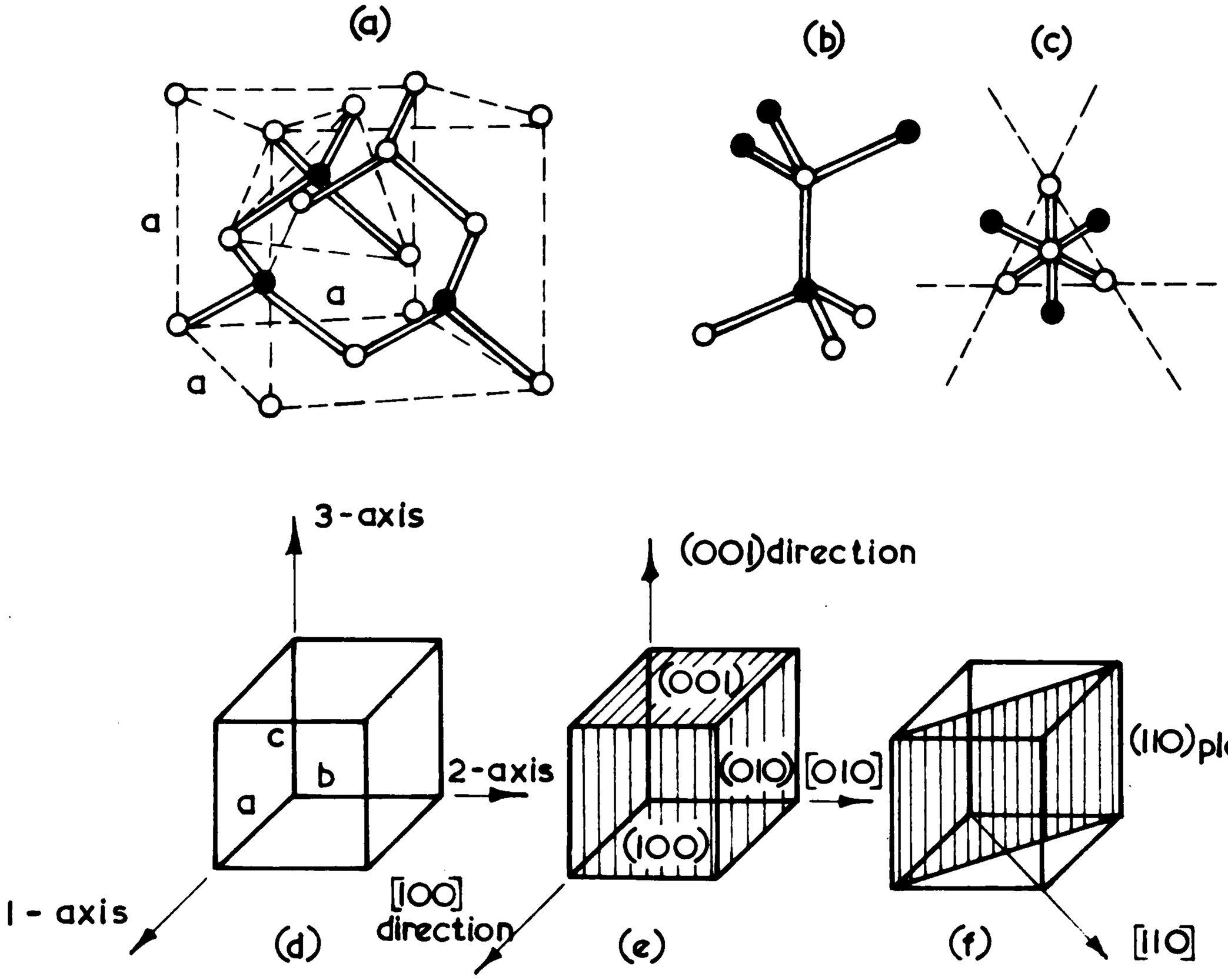

FIG. 2.2 (a) Cubic (sphalerite) cadmium sulphide

(b) Stacking arrangment Aa Bb Cc Aa Bb Cc .....

(c) Looking along [111] direction

(d) Relationship between cube-edges and the orthogonal axes

(e) (f) and (d) Various crystal planes ( ), and directions [ ]

or writing the converse piezoelectric effect in full :

$$\varepsilon_1 = d_{31} E_3 , \quad \varepsilon_2 = d_{32} E_3 , \quad \varepsilon_3 = d_{33} E_3$$

$$\varepsilon_4 = d_{24} E_2 , \quad \varepsilon_5 = d_{15} E_1 , \quad \varepsilon_6 = 0 \qquad \ldots\ldots\ldots (2.6)$$

where $d_{15} = d_{24}$ and $d_{31} = d_{32}$

The suffixes 1, 2, 3 refer to compressional components of strain and 4, 5, 6 refer to shear components.

The numerical values of d_{33}, d_{31}, and d_{15} for cadmium sulphide and other relevant materials are shown in Table 2.1 (at the end of this chapter).

Similarly for sphalerite crystals the piezoelectric matrix may be written as follows :

$$\begin{matrix} 0 & 0 & 0 & d_{14} & 0 & 0 \\ 0 & 0 & 0 & 0 & d_{25} & 0 \\ 0 & 0 & 0 & 0 & 0 & d_{16} \end{matrix} \qquad \ldots\ldots\ldots (2.7)$$

where $d_{14} = d_{15} = d_{16}$

The converse piezoelectric effect may be written as :

$$\varepsilon_4 = d_{14} E_1$$

$$\varepsilon_5 = d_{25} E_2 \qquad \ldots\ldots\ldots (2.8)$$

$$\varepsilon_6 = d_{36} E_3$$

For the binary compounds of Group II - VI the piezoelectric coefficients of the sphalerite phase are markedly lower than those for the wurtzite phase of the same compound [15].

2.3. Conditions for shear-mode generation

The results obtained above are only valid provided that the crystallographic axes b and c are related to the 1, 2 and 3 axes in a certain manner [2]. The 1, 2, and 3 axes, unlike the a, b, and c

axes are always mutually orthogonal. For hexagonal crystals the 3 axis is taken to be along the c axis, the 1 axis along the a axis and the 2 axis is taken to be in the plane of the a, and b axes, and at right angles to the 1 and 3 axes, so that they form a right handed set of axes, see Fig. 2.1e. For cubic crystals the a, b, and c axes are taken to be along the 1, 2, and 3 axes respectively, see Fig. 2.2d.

Equations (2.6) show that when an electric field is applied along the positive direction of the c axis (3 axis) no shear strains will develop. However, compressional strains, ε_1, ε_2, and ε_3, will develop along the c axis and along the 1, and 2 axes, the magnitude of the strains being dependent on the values of the appropriate piezoelectric coefficients and on the strength of the electric field. Of these three compressional strains only ε_3 is piezoelectrically active, because the other two are transverse to the applied field [1, 7]. By active it is implied that an ultrasonic stress wave may propagate in the material along the 3 axis. From equations (2.6) it can also be seen that when an electric field has a component perpendicular to the 3 axis, then, in general two types of shear strain will be present : $\varepsilon_4 = d_{24} E_2$ and $\varepsilon_5 = d_{15} E_1$. In general, then, two shear-mode waves with different velocities [6] will propagate when the electric field is in the basal plane. For generation of only one shear-wave the electric field must be either along the 1 axis or along the 2 axis.

For cubic (sphalerite) crystals equations (2.8) show that unilateral electric fields parallel to a cube edge produce only transverse shear strains and such strains are piezoelectrically inactive [1, 7].

The effect of rotating the c axis (or a cube-edge) away from the 3 axis by an angle θ will now be discussed since the results are applicable to thin films whose c-axis (or cube-edge) is inclined at

an angle to the substrate normal, as is the case with films for shear-mode generation. The piezoelectric matrix (2.4) must be transformed to take account of this change in axes. It can be shown [1] that the new (transformed) components of the piezoelectric matrix may be, in general, expressed in terms of the original coefficients by equations of the form :

$$d'_{33} = d_{33} \cos^3\theta + (d_{31} + 2\,d_{15}) \cos\theta \sin^2\theta + d_{11} \sin^3\theta$$
$$+ \sin\theta \cos\theta\,(d_{13} + 2\,d_{35}) \qquad \ldots\ldots\ldots (2.9)$$

Where the prime indicates a transformed piezoelectric coefficient, and d_{33}, d_{31}, ... etc are the original coefficients of equations (2.4).

This transformed matrix can then be applied to particular crystal systems. Thus for wurtzite crystals the equations may be reduced to [3, 4, 5]

$$d'_{tc} = d'_{33} = d_{33} \cos^3\theta + (2\,d_{15} + d_{31}) \sin^2\theta \cos\theta$$
$$d'_{ts} = d'_{35} = -d_{15} \sin\theta \cos 2\theta + \frac{1}{2}(d_{33} - d_{31}) \cos\theta \sin 2\theta$$
$$\ldots\ldots\ldots (2.10)$$

Where d'_{tc} is the compressional-thickness piezoelectric coefficient and d'_{ts} is the shear-thickness piezoelectric coefficient. For sphalerite crystals the transformed equations may again be derived [7] from the general equations, and will be of the form :

$$d'_{14} = d_{14} \cos^2\theta - d_{25} \sin^2\theta$$
$$d'_{15} = d_{25} \sin\theta \cos\theta \qquad \ldots\ldots\ldots (2.11)$$

From equations (2.10) and equations (2.11) it can be seen that when the c-axis (or a cube edge) is inclined at an angle θ to the 3-axis, then, in general, both shear-mode and compressional mode excitations are possible when the electric field is applied along the 3-axis.

2.4. Piezoelectricity in thin films

The theory presented above applies to single crystals, and, therefore, it can be readily applied to epitaxially deposited films of cadmium sulphide and other materials of wurtzite or sphalerite structure. Moreover, since the wurtzite [2, 3, 4] and sphalerite [15, 17] single crystal structures have complete dielectric, piezoelectric and elastic isotropy in the (001) and (111) planes, respectively, their orientation can be sufficiently described by specifying the [001] (c-axis) direction and the [111] direction respectively. Thus the above theory may also be applied to non-epitaxial films with preferred orientation. (See Fig. 2.2 for illustrations of various lattice planes and directions).

Although with microwave cavity techniques [6, 18] it is possible to apply an electric field at an angle to the normal to the plane of a deposited film, provided that it is deposited onto an insulating substrate, in most applications a piezoelectric thin film is sandwiched between two metallic films (electrodes) and the electric field is applied between the two electrodies i.e. at right angles to the plane of the film (parallel to the 3-axis). In the following discussion only the latter case will be considered, where it will be assumed that the electric field is always applied in the direction of the 3-axis.

For hexagonal cadmium sulphide films whose c-axis is inclined at an angle, θ, to the substrate-normal it can be seen from equations (2.10) that there will be no coupling to the c-mode when $\theta = 38.5^{o}$, and 90^{o}, and no coupling to the shear-mode when $\theta = 0^{o}$, and 63.5^{o} [3, 4, 5].

For sphalerite crystals when a cube edge is inclined at an angle of 45^{o} to the 3-axis, then compressional-mode excitation is possible, and when the (110) plane is perpendicular to the 3-axis shear-mode excitation is possible [7]. For sphalerite films, then, the condition necessary for compressional-mode [17] generation is that the

(111) plane of the film be parallel to the substrate, and for shear-mode generation the (110) plane must be parallel to the substrate.

For deposited cadmium sulphide films to be suitable for shear-mode generation, then, the c-axis of hexagonal films must be either parallel to the plane of the film, or inclined at an angle of about 40^{o} to the normal [3, 4, 5], or the (110) plane of a cubic film must be parallel to the substrate. This is to be expected in view of the close relation which exists [7, 9] between the wurtzite and sphalerite structures when these two structures are viewed along the [001] and [111] directions respectively, they only differ by 60^{o} rotation of the tetrahedra.

In the literature [19, 20] there is some controversy as to whether a non-epitaxially grown cadmium sulphide film whose c-axis is normal to the substrate, may be excited for shear-mode generation by applying the electric field at right-angles to the c-axis. DeKlerk [19] maintains that an epitaxial film [6] is needed for such excitation, whereas Foster [20] maintains that a non-epitaxial film whose c-axis is normal to the substrate would be capable of producing shear-mode waves but that the problem is hypothetical since, in practice, no electric field could be applied parallel to the substrate.

From the theory presented above it would seem that Foster [20] is correct when he states that such a film would be capable of generating shear-mode waves. However, the problem is not hypothetical since it is possible with microwave cavity techniques to apply the field at an angle to the substrate normal, provided that the substrate is non-metallic, and that there is no metallic electrode between the piezoelectric film and the substrate. The experimental results of Weber [18] seem to confirm this for non-epitaxial films, and the results of DeKlerk [6] for epitaxial films.

2.4.1. Coupling coefficient for piezoelectric transducers

In the piezoelectric conversion of electromagnetic into acoustic

radiation (or vice versa) it is not possible [21] to satisfy simultaneously both frequency and wave vector conservation, hence this process cannot proceed in a uniform piezoelectric medium. Piezoelectric transducers rely on a variation of piezoelectric coefficient with position either by using a slab of finite thickness as is the case with conventional piezoelectric transducers or a variation of piezoelectric constant along a surface as is the case with surface-mode transducers. In the case of a piezoelectric slab, maximum efficiency of conversion of ultrasonic energy to electrical energy (or vice versa) is achieved when the relevant dimension is equal to half a wavelength [1, 8]. For thickness-mode transducers, for example, the thickness, t, is equal to half a wavelength :

$$t = \frac{\lambda}{2} \quad , \quad \text{but} \quad \lambda = \frac{v}{f} \qquad \therefore \quad f = \frac{v}{2t} \qquad \ldots\ldots\ldots\ldots (2.12)$$

where v is the appropriate velocity of acoustic waves, and f is the frequency.

The coupling coefficient of a piezoelectric transducer may be defined as the square root of the conversion efficiency of the transducer, or

$$k^2 = \frac{\text{electrical energy out}}{\text{total mechanical energy in}}$$

The coupling coefficient, k, is a function of elastic, piezoelectric and dielectric properties of the transducer material, and of boundary conditions. For example, it can be shown [8] that :

$$k_{33} = \frac{d_{33}}{\sqrt{\kappa_{33} S_{33}}} \qquad \ldots\ldots\ldots\ldots (2.13)$$

where k_{33} is the static compressional-mode coupling coefficient for a piezoelectric resonator whose piezoelectric coefficient along the 3-axis is d_{33} and whose elastic constant and dielectric permittivity along the

same axis are S_{33} and κ_{33} respectively.

Also it may be shown [8] that :

$$k_{31} = \frac{d_{31}}{\sqrt{\kappa_{33} S_{11}}} \qquad \ldots\ldots\ldots (2.14)$$

and

$$k_{tc} = h_{33} \frac{\kappa_{33}}{\sqrt{c_{33}}}$$

where k_{tc} is the coupling coefficient of a transducer operating in it compressional-thickness-mode, and h and c are piezoelectric and elastic stiffness coefficients respectively.

In dynamic systems the coupling coefficients are dependent upon the stress distribution and are, in general, less than the static ones because not all the elastic (mechanical) energy is coupled. Piezoelectric coupling factors characterize a piezoelectric material better for power transduction than do the sets of elastic, dielectric and piezoelectric constants and the bandwidth of a transducer is also dependent upon the appropriate coupling coefficient. Furthermore, the coupling factors of piezoelectric materials with considerably different values of permittivity and/or compliance may be directly compared, and this is done in Table 2.1.

The coupling coefficient is not a tensor and therefore does not obey the tensor transformation formulae of the type given in equations (2.9). Thus, when axis transformations are performed the new (transformed) coupling coefficient is obtained by substituting the new (transformed) elastic, dielectric, and piezoelectric constants in the original equation, e.g.

$$k'_{33} = \frac{d'_{33}}{\sqrt{S'_{33} \kappa'_{33}}} \qquad \ldots\ldots\ldots (2.15)$$

where d'_{33} is the transformed piezoelectric coefficient given in equation (2.10) and s'_{33} , κ'_{33} are the transformed electric and dielectric constants. Similarly the rotated thickness-shear k'_{ts} , and thickness-compressional k'_{tc} coupling coefficients are given by

$$k'_{ts} = h'_{35} \frac{\kappa'_{33}}{\sqrt{c'_{44}}}$$

$$k'_{tc} = h'_{33} \frac{\kappa'_{33}}{\sqrt{c'_{33}}}$$

Since all these transformed constants are dependent upon the angle of rotation, then the coupling coefficient is also a function of the angle. Gibson [3] and Foster [4] have given a plot for the thickness-mode coupling coefficient, k_t, for compressional- and shear-mode excitation versus inclination of the c-axis to the normal for hexagonal CdS and ZnO (Figure 2.3).

2.4.2. Multi-layers

It has been shown [15] that when the top layer of a cadmium-sulphide single crystal consists of cadmium atoms, then negative charge appears on the top face of the slab when a compressive stress is applied in the direction of the c-axis. Conversely, when the top layer consists of sulphur atoms, then positive charge appears on the top face for the same stress. This phenomenum is known as crystal inversion and is a consequence of the anisotropy along the c-axis, i.e. if a fixed point on the c-axis is considered then the atoms above and below it are at different distances. When the crystal is deformed by a given stress then it will always deform in a manner that is biased one way. This manifests itself in the piezoelectric polarity. Thus

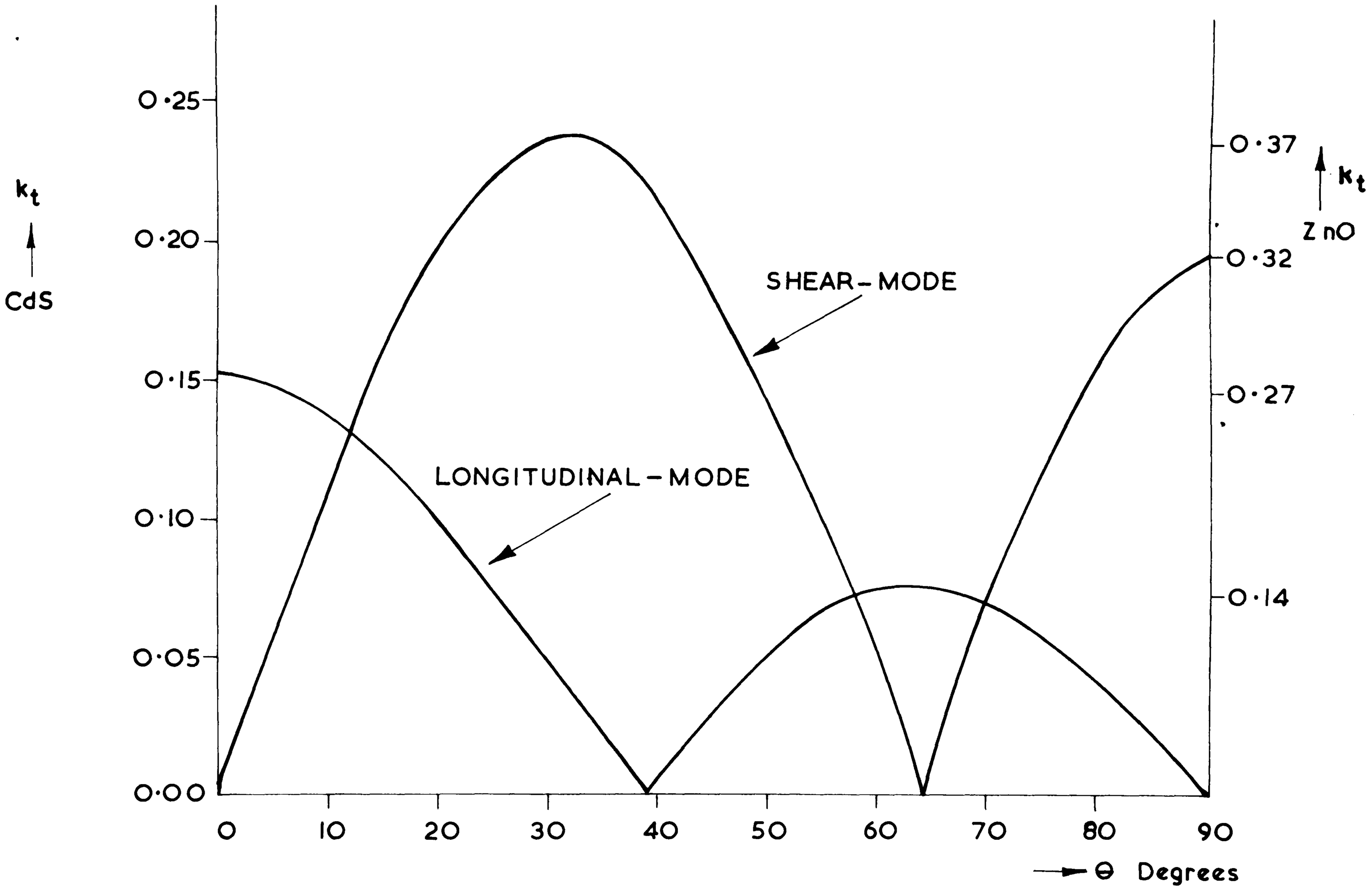

FIG. 2.3 Variation of s-mode and c-mode coupling coefficients with inclination of c-axis to substrate normal for wurtzite CdS and ZnO (after Gibon,[3] & Foster[4])

when a crystal is turned upside down, then, for the same stress, positive electric charge will appear at the same face as when the crystal was up-right, the only difference being that what used to be the top face is now the bottom face. The effect of piezoelectric polarity on various multi-layers of a piezoelectric material will be considered.

When a voltage impulse is applied to a piezoelectric transducer bonded (or deposited) onto a propagation medium it can be shown [22] that :

(a) the ultrasonic pulse generated *at the front face* of the transducer is of the same shape and time-duration as the voltage pulse,

(b) the ultrasonic pulse generated *at the back face* of the transducer is also the same as the voltage pulse but has a negative amplitude relative to that of the front face. By the time this (back face) pulse reaches the front face of the transducer it lags the front face pulse by $\frac{t}{v}$ seconds, where t is the transducer thickness, and v is the ultrasonic wave velocity in the transducer material.

(c) the ultrasonic pulse generated in the propagation medium (substrate) is the phasor sum of (a) and (b) above, and is approximately one cycle of a sine wave with a periodic time, T, approximately equal to $\frac{2t}{v}$ seconds.

The apparent frequency, f, of the ultrasonic wave is, therefore, given by $f = \frac{1}{T} = \frac{v}{2t}$, $\therefore t = \frac{v}{2f} = \frac{\lambda}{2}$ where λ is the wavelength of the ultrasonic wave. Thus, as indicated in 2.4.1 (equation (2.12)), resonance occurs when the transducer is half a wavelength thick.

The polarity of the ultrasonic pulse relative to that of the voltage pulse is determined by the piezoelectric polarity of

the transducer material e.g. when materials of opposite polarity are used the resulting ultrasonic pulses have opposite polarity (180^{o} out of phase). Consider two $\frac{\lambda}{2}$ piezoelectric layers arranged in such away that the positive directions of the c-axes of the two layers are opposite i.e. the two layers have opposite polarity (Fig. 2.4b). When a voltage impulse is applied to such an arrangement each layer will generate in the propagation medium (substrate) an ultrasonic impulse whose shape is approximately a sine-wave and whose duration is approximately T seconds. However, because the two $\frac{\lambda}{2}$ layers have opposite polarity the two ultrasonic pulses generated will have opposite polarity i.e. they will be 180^{o} out of phase with each other. The ultrasonic pulse generated by the top piezoelectric layer has to traverse an extra distance equal to the thickness of the bottom layer before it reaches the substrate, i.e. the path difference between the two pulse waves generated by the top and bottom piezoelectric layers is $\frac{\lambda}{2}$. This $\frac{\lambda}{2}$ path difference cancels the effect of the opposing polarity of the two ultrasonic pulses, i.e. constructive rather than destructive interference takes place, and an ultrasonic pulse is propagated whose duration ($\frac{3T}{2}$ seconds) is longer than the pulse generated by a single $\frac{\lambda}{2}$ layer (T seconds). When the electric field gradient is made to be the same across a single $\frac{\lambda}{2}$ layer or two $\frac{\lambda}{2}$ layers of opposite polarity, i.e. when the amplitude of the voltage impulse in the latter case is made to be twice that of the former, then the amplitude of the ultrasonic pulse generated by the latter will have twice the amplitude of the former. Because the amplitude of the voltage applied across a thin film is limited by the breakdown voltage of the material of the film (a few volts for a film whose thickness is of the order of one micrometre), two $\frac{\lambda}{2}$ piezoelectric layers of opposite polarity have been used [23] to generate ultrasonic wave pulses at microwave frequencies, so that the applied voltage across the film thickness

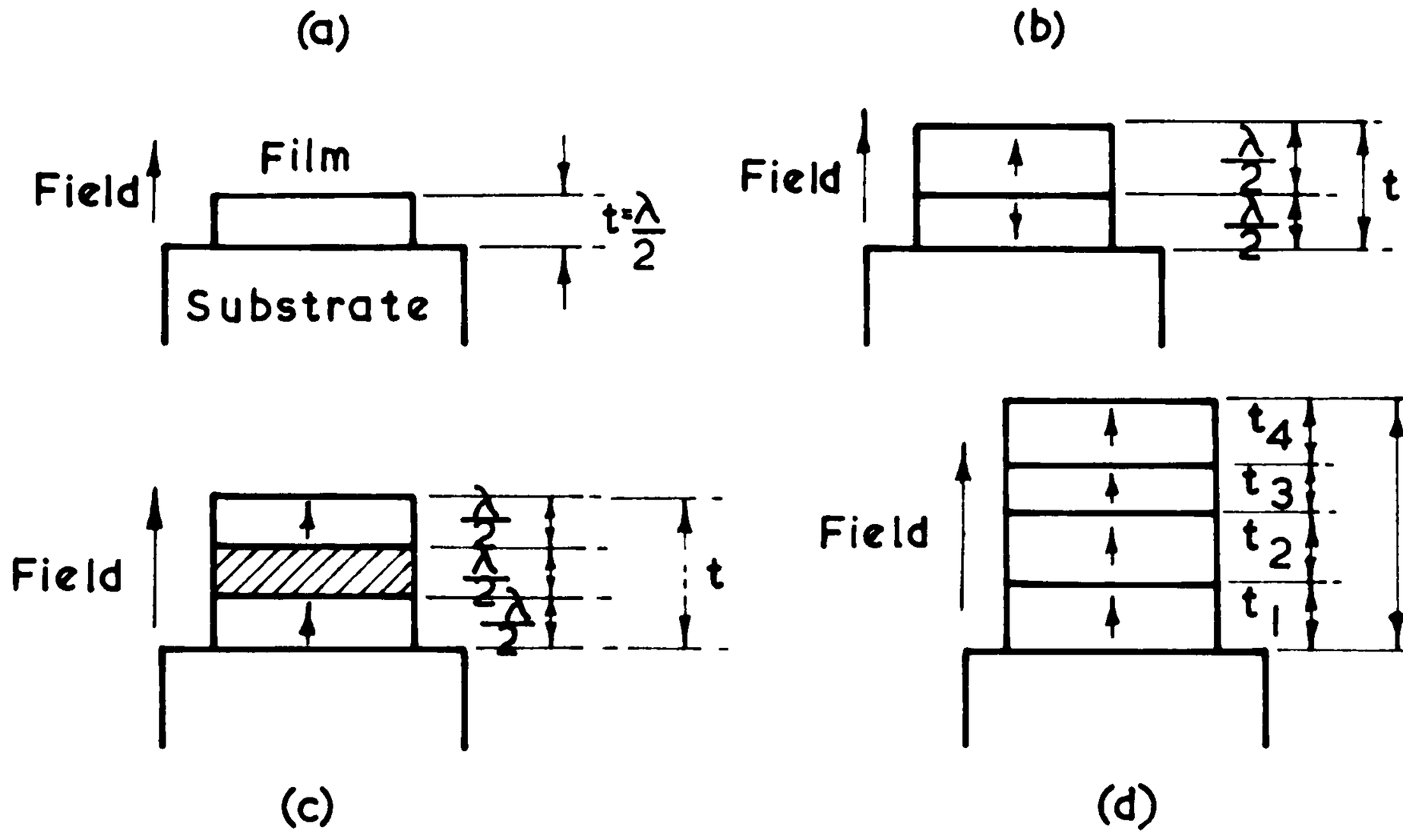

FIG. 2.4 Piezoelectric Multi - layer Transducers

(a) Single layer, $t=\frac{\lambda}{2}$

(b) Two inverted layers, $t=\lambda$

(c) Two $\frac{\lambda}{2}$ layers of same polarity sandwiching a $\frac{\lambda}{2}$ passive layer $t=\frac{3\lambda}{2}$

(d) Piezoelectric multilayers of same polarity,

$t_t=\frac{\lambda}{2}$

may be doubled resulting in a doubling of the ultrasonic power output of the transducer, and a halving of the capacitance of the film making the transducer easier to drive.

Similarly, it can be argued that an ultrasonic pulse of duration $\frac{3T}{2}$ seconds is generated in the propogation medium (substrate), when a voltage impulse is applied to a transducer consisting of a $\frac{\lambda}{2}$ passive layer sandwiched between two $\frac{\lambda}{2}$ active layers of the same polarity (Fig. 2.4c). Such a transducer [21, 24] will have the same advantages as those of a transducer consisting of two $\frac{\lambda}{2}$ active layers of opposite polarity with the disadvantage that for two such transducers to give the same ultrasonic output power, the voltage impulse applied to the former will have to be 1.5 times greater than that applied to the latter (but the capacitance of the former will be less than that of the latter).

Consider now multi-layers of a piezoelectric material stacked in such a manner that all layers have the same polarity (Fig. 2.4d). In this case the multi-layer is equivalent to a single layer whose thickness is the sum of the individual thickness of the layers, and since there is no discontinuity in the piezoelectric constant along the thickness of the multi-layer it may be regarded as a single $\frac{\lambda}{2}$ transducer. In this case, however, the resonance frequency is decreased, according to the formula given in equation (2.12), by the proportional increase in thickness. Such multi-layers have been fabricated in the present investigation (see Chapter 5) and they fall in two categories :

(a) layers of CdS films on CdS films up to 10 in number (about 100 μm thick) have been fabricated, since, due to the limitation on the size of the crucible in electron beam bombardment evaporation, [25] no single continuous thick film could be deposited,

(b) layers of CdS films about 10 μm thick sandwiching a very thin (less than 0.1 μm) passive layer of quartz (SiO_2) were deposited so that the change of orientation of cadmium sulphide crystallites with film thickness may be studied (Chapter 8). Since the thickness of the SiO_2 passive layer is very much less than that of the active cadmium sulphide layer, and, therefore, much less than an acoustic wavelength, this arrangement may be regarded as equivalent to that of (a) above provided that the CdS layers have the same piezoelectric polarity.

The piezoelectric polarity of as-deposited cadmium sulphide films was determined from their electrical response to a force impulse of short duration (section 9.3.3). It was found that cadmium sulphide films deposited on chromium films, copper films and quartz films have the same polarity : a compressive stress produced negative charge on the top face of the film. The response of as-deposited films to a nanosecond voltage impulse was also studied (section 9.3.1) Depending on the crystallographic orientation of the film it either generated pure-shear mode ultrasonic pulse waves or pure compressional-mode or both waves simultaneously, and the shape and duration of the ultrasonic pulse was as that predicted [22]. The crystallographic orientation inferred from these tests were confirmed by X-ray diffraction techniques (Chapter 7).

TABLE 2.1. Physical constants of some piezoelectric transducer materials

Material	Density	Melting Point	Relative Permittivity	Wave Velocity		Acoustic Impedance		Coupling coefficients				Piezoelectric Coefficients pC.N^{-1}			References (Chapter 2)
	10^3kg.m^{-3}	^oC	κ_r	m.s^{-1}		10^6kg.m^{-1}.s^{-1}		k_{33}	k_{15}	k_{tc}	k_{ts}	d_{15}	d_{33}	d_{31}	
				v_c	v_s	z_c	z_s								
Quartz (SiO_2)	2.65	1730	4.58	5700	3800	15.2	10.0 (k_{26})	0.10	0.14	-	-	-	+2.31 (d_{11})	+0.73 (d_{14})	8,10,11,12
Zinc sulphide (ZnS)	4.09	1830	8.9	5850	3370	19.8	13.8	0.05	0.08	-	-	+2.8	+3.2	-1.1	8,10,11,12
Cadmium sulphide (CdS)	4.82	1475	8.5 - 8.9	4500	1800	21.7	8.68	0.26	0.19	0.16	0.23	-14	+10.3	-5.8	3,4,8,10,14,15
Zinc oxide (ZnO)	5.6	1975	7.8 - 8.7	6110	2740	34.2	15.3	0.36	0.29	0.27	0.37	-12	+12	-4.7	4,8,10,11,14,15
Cadmium selenide (CdSe)	5.68	1239	9.7 -	3860	1540	22.4	8.96	0.19	0.13	-	-	-10.5	+7.8	-3.92	8,10,11,13,14,15
Lead zirconate titanate (PZT)	7	-	1200	4400	2300	31	16	0.7	0.7	0.7	0.7	+496	+289	-123	8,10
Sodium potassium niobate (PSN)	4.5	-	375	6200	3000	28	13.5	-	-	0.6	0.6	-	-	-	10
Lithium niobate ($LiNbO_3$)	4.64	-	30-84	7200	3700	34	17.8	-	-	0.19	0.7	-	-	-	10
Lithium titanate ($LiTaO_3$)	7.45	1650	45-51	7200	3800	52.4	28	-	-	0.3	0.4	-	-	-	10,16
Barium titanate ($BaTaO_3$)	5.7	-	1700	-	-	-	-	0.5	0.5	0.4	-	+392	+86	-34	8

C H A P T E R 2

REFERENCES

1. W.G. Cady, *Piezoelectricy*, Dover Publications (1964).

2. J.F. Nye, *Physical Properties of Crystals*, Oxford Univ. Press (1964).

3. R.W. Gibson, *Cadmium sulphide ultrasonic transducers*, Elect. Lett., 2, 6, p. 213 (1966).

4. N.F. Foster et al, *CdS and ZnO thin film transducers*, IEEE Trans. SU-15, 1, p. 28 (1962).

5. M. Nagao, *High efficiency CdS film transducers for the shear-mode*, JAP, 37, p. 4591 (1966).

6. J. DeKlerk, *Thin film piezoelectric transducers*, JAP, 37, p. 4522 (1966).

7. J.H. Mcfee, *Transmission and amplification of acoustic waves in piezoelectric semi-conductors*, Physical Acoustics, Vol. 4A ed. W.P. Mason Academic Press (1964).

8. D.A. Berlincourt et al, *Piezoelectric and Piezomagnetic materials and their function as transducers*, Physical Acoustics, Vol. 1A ed. W.P. Mason Academic Press (1964).

9. C.S. Barret et al, *Structure of metals : crystallographic methods, principles and data*, McGraw-Hill (1966).

10. R.F. Mitchell, *Some new materials for ultrasonic transducers*, Ultrasonics, April 1968, p. 112.

11. D. Beecham, *Ultrasonic transducers for frequencies above 50 MHz*, Ultrasonics, January 1967, p. 19.

12. Data sheet, Haraues Ltd., Bath Road, Slough, Bucks.

13. M. Aven et al ed., *Physical and Chemical properties of II-VI compounds*, North-Holland (1967).

14. EPIC, *II-VI semiconducting compounds data tables*, by M. Neuberger (1969).

15. D.A. Berlincourt et al, *Electro-elastic properties of the sulphides selenides and tellurides of zinc and cadmium*, Phys. Rev., 129, 3, p. 1009 (1963).

16. A.W. Warner, *Low temperature coefficient of frequency of $LiNbO_3$ resonator*, Proc. IEEE, 55, p. 450 (1967).

17. S.A. Semiletov et al, *Thin Film piezoelectric textures*, Sov. Phys. Crystallography, 12, 2, p. 562 (1967).

18. R. Weber, *Comparative data on CdS transducers*, Proc. IEEE, 54, p. 333 (1966).

19. J. DeKlerk, *Author's reply*, JAP, 39, p. 4461 (1968).

20. N.F. Foster, *Insertion loss and coupling factors in thin film transducers*, JAP, 39, p. 4466 (1968).

21. J. DeKlerk, *Multi-layer enhancement of microwave piezoelectric converstion in CdS-SiO layers*, App. Phys. Lett., 7, p. 10 (1965).

22. M. Redwood, *A study of waveforms in the generation and detection of short ultrasonic pulses*, App. Mat. Res., April 1963, p. 76.

23. J. DeKlerk, *C axis flapping for multilayer piezoelectric thin film transducers*, App. Phys. Lett., 13, p. 102 (1968).

24. J. DeKlerk, *Multi-layer thin film piezoelectric transducers*, IEEE Trans. SU-13, p. 99 (1966).

25. R. Weber, *Electron bombardment technique for the deposition of CdS film transducers*, Rev. Sci. Inst., 37, p. 955 (1966).

C H A P T E R 3

A review of thin film transducer technology

3.1. Introduction

In this chapter a survey of the progress in thin- and thick-film transducer technology is given. The various transducer deposition methods are briefly discussed including the ones used in the present work. Various piezoelectric materials are discussed in terms of their suitability for thin film transducers. The advantages of thin film transducers over discrete (conventional) transducers are outlined. A summary of other thin film devices is given. It is stated that CdS s-mode films have been deposited thicker than those hitherto reported in the literature, and that c-mode transducers up to 100 μm thick have also been deposited.

3.2. Materials for piezoelectric transducers (PET's)

Materials for piezoelectric transducers may be classified in three groups as follows :

(a) Single crystal materials : any insulating material which has a crystal structure that is non-centrosymmetric may exhibit piezoelectricity, e.g. quartz (SiO_2) and cadmium sulphide (CdS). Such materials are called piezoelectric materials.

(b) Polycrystalline materials that may be poled by a strong electric field, i.e. ferroelectric materials. In their poled (permanent polarization) form such materials are called piezoelectric ceramics in view of the similarity of their manufacturing process to that of thermal insulation ceramics. Lead zirconate citanate (PZT) and potassium sodium niobate (PSN) belong to this group of materials.

(c) Materials that may exist in either of the two forms above, i.e., they are at once piezoelectric (when in single crystals), and ferroelectric (when poled, if they are polycrystalline). Such materials are exemplified by lithium niobate ($LiNbO_3$) and barium titanate ($BaTiO_3$) and they are called ferroelectric-piezoelectric materials. Very often no distinction is made between the last two groups of materials and they are both referred to as piezoelectric ceramics.

The main advantages of ceramics over single crystal piezoelectric materials are that they can be fabricated in almost any shape or size [1, 2] (not possible with single crystal piezoelectric cuts, but may be possible with thin film techniques); and their electrical and piezoelectric properties may be adjusted by varying [1,2,3] the composition of their solid solutions. Also ceramics have a higher piezoelectric coupling coefficient than other piezoelectric materials (see Table 2.1, at the end of Chapter 2). The main disadvantages of ceramic materials is their high relative dielectric permittivities, κ, which makes the static capacitance of a ceramic transducer much higher than that of other piezoelectric materials (Tables 2.1 and 3.1). This makes ceramic transducers much more difficult to drive, because of electrical impedance matching problems at high frequencies [4].

It is difficult to make a comparison between the properties of ferroelectric-piezoelectric materials in their single crystal and their poled forms since few materials have been made in both forms. A recent review paper [1] presented comparative data on various solid solutions of ceramic materials, e.g. barrium titanate/calcium zirconate and lithium posphates/lithium tartrates. Solid solutions of Group II-VI compounds (e.g. CdS and ZnS) have also been investigated [5]. A bibliography of literature on piezoelectric and piezomagnetic materials has recently been published [6].

Single crystal cuts of quartz and Rochelle salt (sodium potassium tartrate) dominated the field of piezoelectric transducers (PET's) until the advent of ADP (ammonium dihydrogen posphate) and lithium sulphate crystals [7]. However, the discovery of poled piezoelectricity in ferroelectric materials, first in $BaTiO_3$ then in PZT, and later in PSN, led to their extensive use as transducer materials due to their higher piezoelectric conversion efficiency [2, 3, 7]. Thin ceramic plates required for high frequency transducers can be sliced [2] from a block of the ceramic material by a diamond saw and then ground or lapped to their final required thickness. Poling can be done before or after cutting [2]. However, there is a limit to how thin a ceramic plate or a single crystal slab may be lapped because they become very fragile. This limitation in "thickness", and, therefore, in frequency range, provided the impetus for the deposition of piezoelectric thin films using vacuum deposition techniques. Thus, the era of thin film transducer technology began, and with it materials of Group II-VI binary compounds [5] came to prominence. The elements that constitute the Group II-VI binary compounds belong to Group II and Group VI of the Periodic Table. Cadmium (Cd), zinc (Zn) and mercury (Hg) constitute Group II, while oxygen (O_2), sulphur (S), selenium (Se), and tellerium (Te) make up Group VI.

3.3. Thin film piezoelectric transducers

It was shown in Chapter 2 that the fundamental resonance frequency, f, of a piezoelectric transducer operating in its thickness mode may be written as $f = \frac{v}{2t}$, where f is the resonance frequency, t is the transducer thickness and v is the appropriate acoustic velocity in the transducer medium. Using the above equation, and the values of v_c and v_s from Table 2.1, the resonance frequency of a piezoelectric transducer may be plotted versus transducer thickness, and this is done in Fig. 3.1 for cadmium sulphide transducers. It can be seen from this figure that s-mode resonance frequencies of 10 MHz, 100 MHz, and 1 GHz correspond

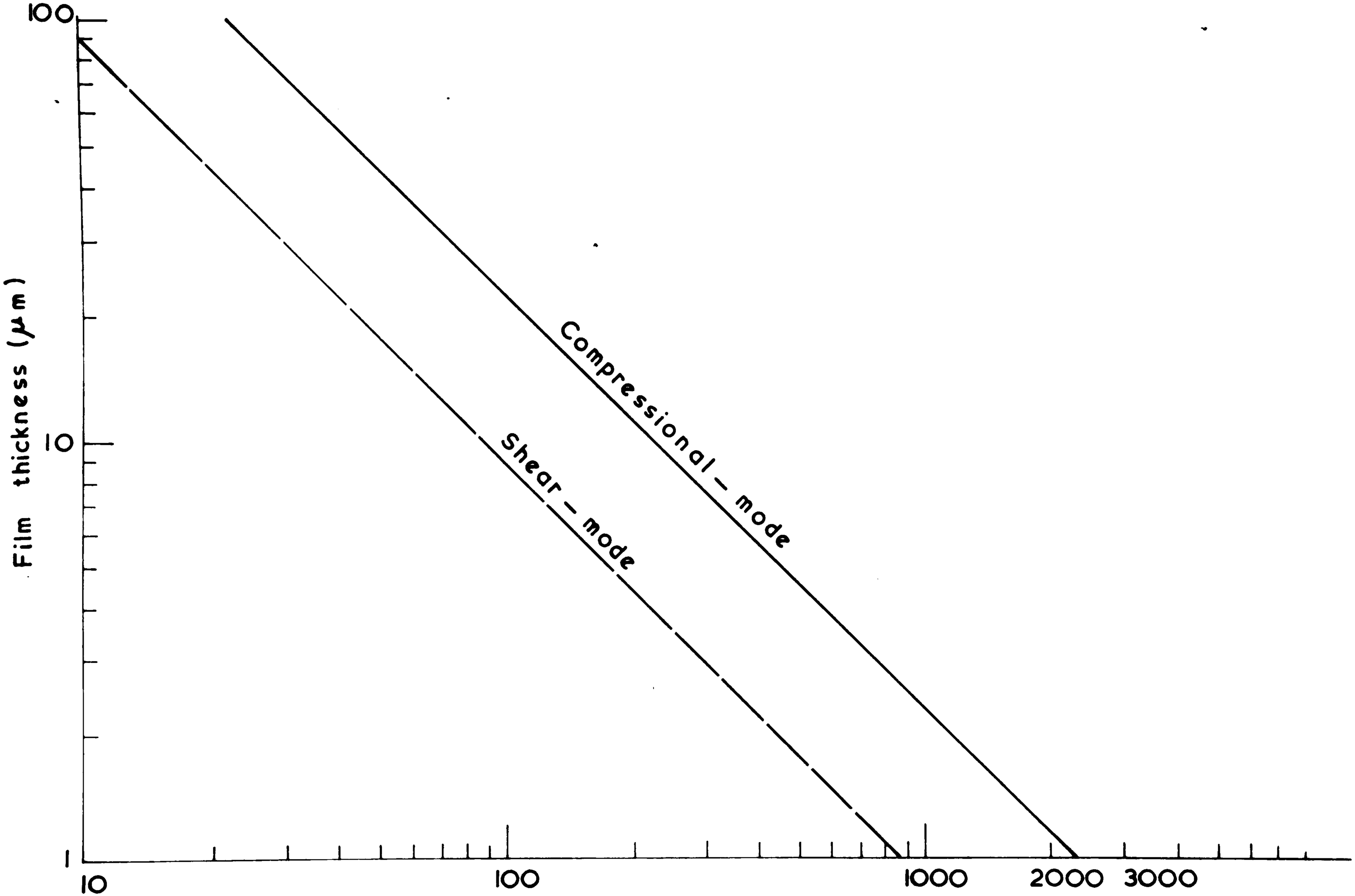

FIG 3.1. CdS film thickness versus resonance frequency

to transducer thickness of 90 μm, 9 μm and 900 nm respectively. Fig. 3.2 is a schematic diagram of a vacuum deposited transducer.

The transducer thickness determines the wavelength of the acoustic wave generated in the transducer material, while the operating frequency is decided by the appropriate velocity of propagation of acoustic waves in the transducer material. Thus transducers of different material having the same resonance frequency and operating in the same mode will have thicknesses directly proportional to the velocity of acoustic waves in their respective materials. The thicknesses and static capacitances of a 10 MHz s-mode piezoelectric transducer are compared in Table 3.1 for various materials.

With thin film techniques it is possible to deposit piezoelectric films thinner than 100 nm, the minimum thickness being limited by the development of the crystallographic orientation of the deposited film (see Chapter 8). The deposition of thin piezoelectric films of CdTe [8,9,10] CdSe [8,11,12], ZnS [12,13,14], ZnSe [8,12], ZnTe [8,12], and ZnO [13,15,16], and CdS has been reported. Varying degrees of success have been achieved with the deposition of thin ferroelectric films of $LiNbO_3$ [17], $BaTiO_3$ [17,18], AlN (aluminium nitride) [13], and PZT [17] showing piezoelectric behaviour. The deposition of some piezomagnetic films has also been reported, e.g. YIG (yttrium iron garnet) [19].

So far, most of the published work on thin film PET's has been concentrated on materials from Group II-VI. These materials are chemically less complex than the ternary compounds of ferroelectric materials like PZT, PSN, and $LiNbO_3$, and, therefore, much easier to deposit in a stoichiometric form. Also the constituent elements of Group II-VI compounds have much lower melting points [5] than their compounds, e.g. Cd, Zn, and S melt at 321, 420, and 119°C while ZnS and CdS melt at 1830 and 1475°C respectively; and oxygen boils [20] at -183°C while ZnO melts at 1975°C. Because of their high melting points these binary compounds dissociate [5,13] before reaching their boiling points.

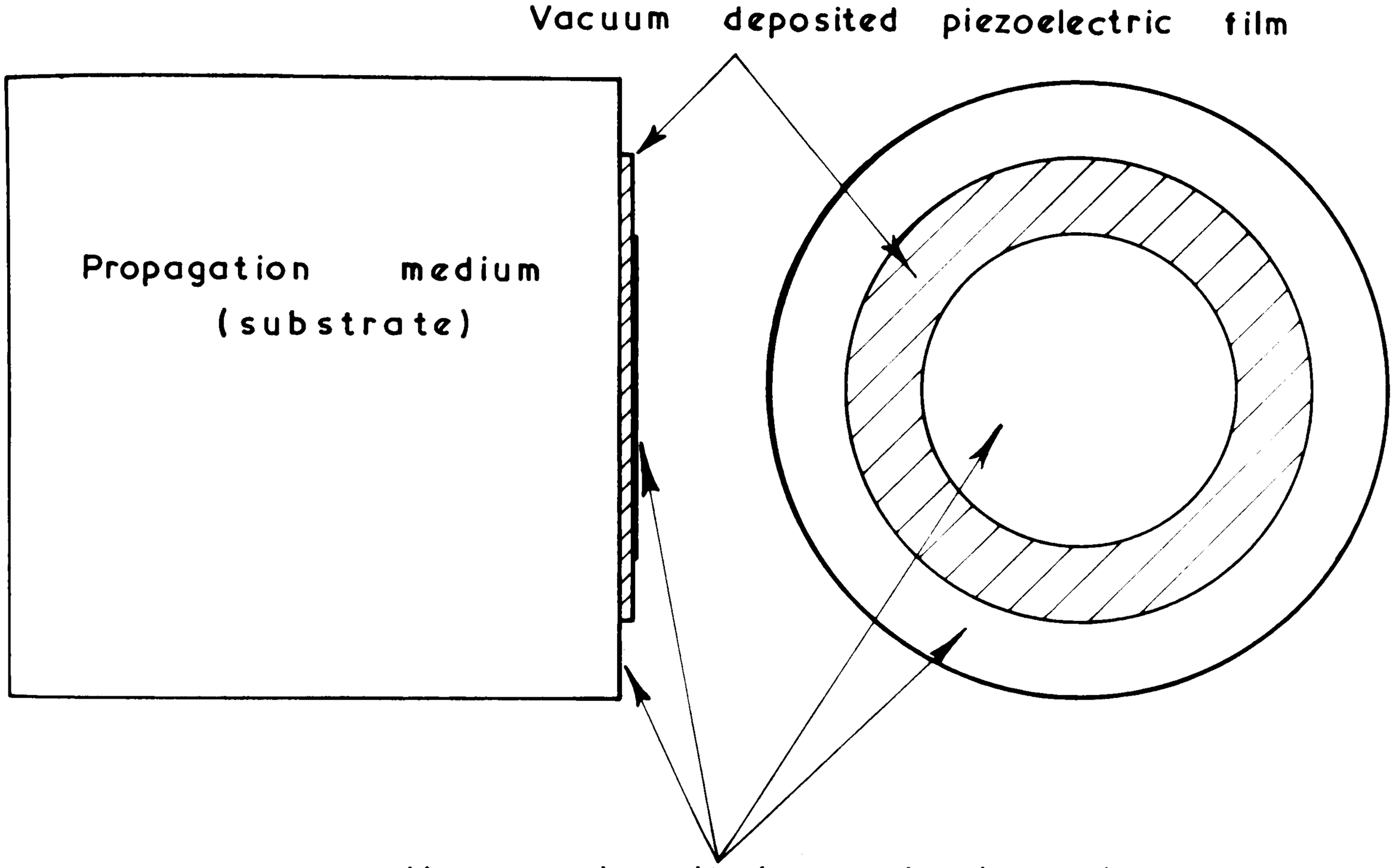

FIG. 3.2. Schematic diagram of piezoelectric film transducer.

From the binary compounds of Group II-VI CdS and ZnO have the highest piezoelectric coupling coefficients (Table 2.1), and from these two compounds CdS is much easier [3] to vapourize. It sublimes [21] in vacuum at temperatures as low as 600-800°C. CdS melts [5] at a temperature of 1475°C at a minimum pressure of 3.8 atmospheres, and because of the high temperatures and pressures involved most of the work on CdS thin film deposition has been concentrated on sublimation in vacuum of CdS, or the co-evaporation of cadmium and sulphur simultaneously. Most of the work reported on growing CdS single crystals [5,13,22-26] is also concerned with growing from the vapour phase, rather than from the melt. CdS films have also been deposited using sputtering techniques [13,16,27,28]. Much of the work on ZnO film deposition has been done by sputtering, because it is difficult to evaporate due to disproportionation [13]. Deposition rates by sputtering are very slow and typically [13] of the order of $1\mu.h^{-1}$. However, recently DeKlerk [15] has reported on the vapour deposition of ZnO films by the sublimation of zinc in a controlled oxygen environment with the substrate cooled to a temperature of -150°C, with typical deposition rates of 1 $\mu m.h^{-1}$. Clearly, deposition rates of this order are unsuitable for the deposition of thick films (thicker than 30 μm, say). Because of the high relative dielectric permittivity of a ceramic piezoelectric material compared with that of CdS or ZnO, it seems likely that in most transducer applications the latter materials will be preferred, because they are much easier to drive.

3.3.1. Shear-mode and compressional-mode thin film PET's

Since the binary compounds of Group II-VI have higher piezoelectric coupling coefficients in their wurtzite (hexagonal) phase, than those of the sphalerite (cubic) phase (Chapter 2), and since most [13] deposited films of CdS and ZnO belong to the former phase, only wurtzite piezoelectric films will be considered. A deposited film of wurtzite cadmium sulphide or zinc oxide may either have its

c-axis oriented normal to the substrate or parallel to it, or it may be inclined at an angle, θ, to the substrate normal. In most applications the piezoelectric film is sandwiched between two metallic electrodes, with the result that an electric field may only be applied across the film thickness (Fig. 3.2). It was shown in Chapter 2 that in such a case the film will generate s-mode waves only when its c-axis is parallel to the substrate (hereafter referred to as s-mode Type I), or when its c-axis is inclined at an angle of about 40^{o} to the substrate normal (s-mode Type II), Figs. 3.3a and b. When the film's c-axis makes an angle θ to the substrate normal, then, in general both s-mode and c-mode excitations will result, Fig. 3.3d, and when its c-axis is perpendicular to the substrate only c-mode excitation will result, Fig. 3.3e.

The appropriate coupling coefficients [7,29] for s-mode Type I and s-mode Type II transducers, operating in their thickness mode, are k_{15} and k_{ts} respectively, and from Table 2.1 it is seen that, at the optimum angle of 40^{o}, k_{ts} is 1.2 times greater than k_{15}. It would seem, therefore, that, in theory at least, a Type II transducer is about 1.5 times as efficient as a Type I transducer, under the same operating conditions. So far as is known, no deposition of a CdS s-mode Type I transducer has been reported yet, although Foster [13, 30] has reported the deposition of a thin film ZnO transducer of this type, using a triode sputtering technique. Various authors have reported on the deposition of s-mode Type II transducers, as well as c-mode transducers, and a short historical survey is given below of the progress made in cadmium sulphide transducers in terms of improvement in deposition techniques, making the films thicker (lower frequencies), and controlling the crystallographic orientation of the deposited films.

3.3.2. A short historical survey of CdS thin film PET's

The crystallographic orientation of evaporated cadmium sulphide

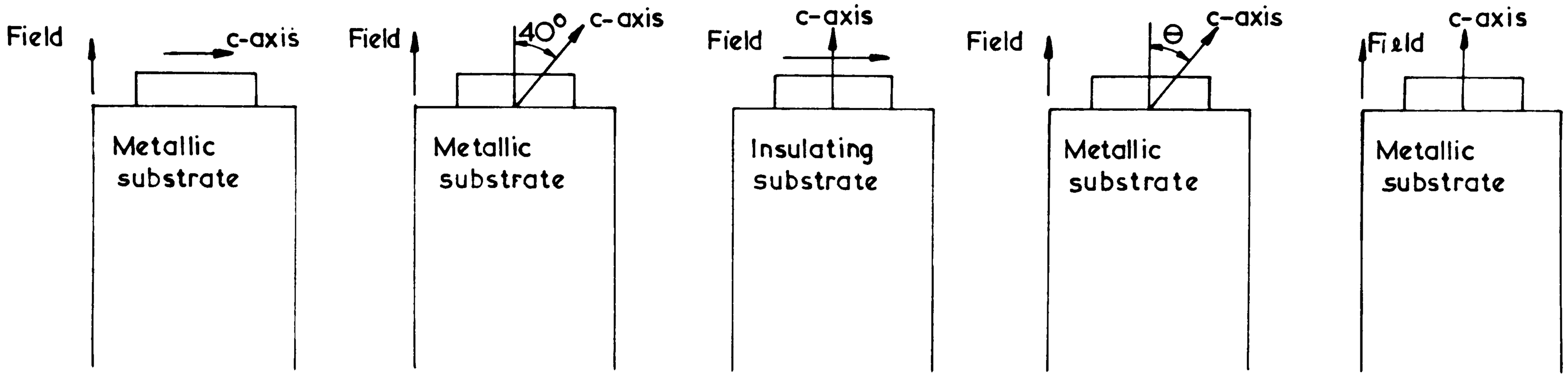

FIG. 3.3 Types of film transducers

films has been examined by many workers since the mid 1950's [5,8,10,11,13,31-37]. Much of the earlier work was concerned with photoresistive and photosensitive studies. CdS films deposited rapidly onto unheated substrates were characteristically of low resistivity, whereas slower deposition rates on heated substrates yield high electrical resistivity films [13]. One of the earliest studies on the structure of CdS films was by Semiletov [8] in 1956 on films deposited onto heated mica and rock salt substrates. The films were found to consist of both cubic (sphalerite) and hexagonal (wurtzite) phases with the hexagonal crystals oriented with their c-axis normal to the substrate. Shalimova [32] and Anrushko [35] reported on the structure of CdS films both in as-deposited state and after recrystallization. Their results showed that deposition at 30^{o} from the substrate-normal produced films oriented with their c-axes inclined at an angle to the substrate. The results of Dresner et al [36] also agreed with previous results, and a further investigation by Addiss [37] showed that under his conditions, the initial 0.1 μm of the film was randomly oriented, with the highly preferred normal c-axis orientation appearing at later stages. Apart from the sphalerite and wurtzite phases of CdS, a third phase has been reported [5]. This phase has the NaCl (common salt) structure which is centrosymmetric, and, therefore, would exhibit no piezoelectricity.

It was in 1964 that the use of vapour deposited thin films of cadmium sulphide as ultrasonic transducers was first reported by Foster [17] and DeKlerk [38]. Since then Foster and co-workers, and DeKlerk and co-workers have continued reporting on improvements in their fabrication techniques, with the former [13, 29] concentrating on thin films up to 4.5 μm thick suitable as s-mode Type II transducers, while the latter [40-42] reporting on very thin films and multi-layer thin films up to 8 μm thick suitable for s-mode Type III and c-mode transducers. It is reported [8] that the use of CdS thin films as piezoelectric transducers was predicted as early as 1946. In 1960 piezoelectricity

in wurtzite CdS and ZnO was discussed [43]. Vapour-deposited thin film transducers superceded depletion-layer and diffusion-layer transducers, reported [4], respectively, by White in 1961 and Foster in 1963. In 1965 Crofut published a paper on diffusion-layer transducer [4] limitations, and Foster [17] switched over from diffusion-layer transducers to vapour deposited transducers.

In 1966 Gibson [29] reported on the theoretical conditions necessary for s-mode generation in wurtzite CdS thin films. Nagao [44] reported on the fabrication of CdS s-mode Type II transducers up to 9 μm thick, and on the theoretical conditions necessary for s-mode generation; he also reported that to achieve oblique c-axis orientation it was necessary to deposit the aluminium film substrate (i.e. the bottom electrode of the CdS transducer) as well as the CdS film at oblique incidence. In the same year Weber [45] reported on the deposition of CdS transducers with normal c-axis up to 62 μm thick using an electron beam bombardment technique, and Page [46] reported on cadmium sulphide thin film devices. Also in 1966, DeKlerk [47] published a review article on thin film transducer fabrication and Gunther [48] reported on theoretical conditions necessary for the deposition of stoichiometric films, and experimental processes occurring with condensation of Group II-VI compounds. Sputtering of CdS was reported by Foster [13] at deposition rates of up to 3 $\mu m.h^{-1}$, and Winslow et al [49] reported the deposition of c-mode PET's as multiple films.

In 1967 Sliker et al [50] reported the deposition of CdS film transducers with oblique c-axis up to 8 μm thick using Foster's technique. In the same year a comprehensive article appeared by Beecham [4] dealing with depletion layer, diffusion layer as well as vapour deposited cadmium sulphide layers. Semiletov et al [8] reported on cadmium sulphide piezoelectric textures. An article by Foster [51] on various crystallographic orientations of CdS films observed under

the same deposition conditions was published. He found in some cases that although the vapour beam was hitting the substrate at an angle the CdS film grew with its c-axis normal to the substrate, and attributed the effect to the epitaxial growth of the CdS film on the gold substrate film (bottom gold electrode of CdS transducer), typically deposited on quartz or sapphire.

In 1968 Foster [39] reported on the theoretical conditions necessary for shear-mode generation in cadmium sulphide films using a different approach from the one used earlier by Gibson [29] but arriving at the same conclusions. Duncan et al [52] reported on the effect of neutron irradiation on the acoustic performance of evaporated CdS films. Mitchell's [3] review article on new materials for ultrasonic transducers complimented Beecham's [4] earlier review. Deposition of very thin CdS films (< 2 μm) by a chemical deposition technique was reported by Nagao [53]. It can be said that this deposition technique is not suitable [54] for the fabrication of thick films, thicker than 30 μm, say.

In 1969 the optimum conditions for the deposition of CdS film transducers with normal c-axis were discussed by King [55], and the deposition of films with normal c-axis up to 100 μm thick was reported by Llewellyn et al [56]. Curtis reported the deposition of CdS transducers with oblique c-axis up to 20 μm thick using a silver diffusion technique [57]. In the same year the present author presented a paper at a meeting of The British Acoustical Society in which he reported on the fabrication of CdS film transducers with oblique c-axis up to 16 μm thick. An expanded version of this paper was later published (see Appendix III).

In 1970 a bibliography of thin film ultrasonic transducers was reported by Smith et al [6], and values for the piezoelectric coefficient, d, were reported by Don [58] et al, for CdS thin films with oblique and normal c-axis orientations. Mitchell [59] reported that Curtis' [57] technique for the fabrication of s-mode Type II CdS transducers by silver

diffusion was always unreliable, and that it was not suitable for the regular production of transducers. Meitzler et al [60] published an article on the use of optical bifringence in CdS to investigate properties of very thin (< 1 μm) piezoelectric transducers. Earlier, in 1963 Addiss [37] used the optical bifringence properties of CdS to study recrystallization of vacuum deposited films. Towards the end of the year Beecham [61] reported a new isothermal technique for the deposition of CdS transducers suitable for s-mode Type II, and Curtis [62] reported on epitaxial films of CdS on gallium arsenide. A review article appeared by Foster [13] on piezoelectric thin films.

Outside the present work, as far as is known, no deposition of CdS films thicker than 20 μm whose c-axis is inclined at an angle to the substrate has been reported, and the deposition of a 100 μm thick film whose c-axis is normal to the substrate has only recently been reported by another worker [56]. The deposition of oblique c-axis films is far more difficult to achieve from a technological point of view [59]. Polycrystalline copper rods, and later polycrystalline aluminium rods have been used for the first time as the propagation media of ultrasonic waves generated by thin film piezoelectric transducers. The present work represents the first non-destructive testing application of a vacuum deposited piezoelectric transducer.

3.4. Thin film transducer fabrication techniques

In order to put in perspective the techniques of vacuum deposition used for thin film transducer fabrication, a mention is made here of other techniques [63] used for the deposition of thin films. They are :

(a) Electrolytic deposition where the films are deposited either on a metallic cathode or on the anode (anodization). Examples of the former are gold plating and of the latter the formation of oxide coatings on aluminium.

(b) Chemical deposition whereby only a solution, an activator and a sensitizor are used to achieve chemical reduction;

(c) Polymerization whereby a thin film of monomeric material is spread on and polymerization is initiated either thermally or by electromagnetic irradiation e.g. ultra-violet light or electron beam, e.g. fabrication of lacquer-film capacitors.

All the techniques mentioned above may be used to deposit thin films with varying degrees of purity and crystallographic orientation. A particular technique may lend itself as being more suitable than others for a particular application. For high purity insulating piezoelectric films with controlled crystallographic orientations, vacuum deposition techniques are the most suited.

3.4.1. Vacuum evaporation

Various methods for the vacuum evaporation of materials are used, and they may be divided into two categories, the first being resistance wire heating which is the conventional type of evaporation whereby the material is either hung onto a filament and stays on when melted due to surface tension, or the material is placed in a crucible (or a cell) that is heated by winding a filament around it or placing it inside a furnace. The second category is electron beam bombardment (e.b.b.) evaporation, where heat may be generated direct in the evaporant by the action of a beam of electrons which are accelerated by a high voltage towards the evaporant. The advantages of e.b.b. evaporation are :

(a) Heat can be generated direct in the evaporant which is of particular use when the evaporant is a very bad thermal conductor, e.g. cadmium sulphide;

(b) the amount of heat radiated from the vapour source (crucible) is very much less than that radiated when conventional evaporation is used, and this is of great importance when the

temperature of the substrate is to be controlled within about 10 degrees as is the case with CdS deposition;

(c) focussing arrangements can be used to focus the electron beam, thus localising the heat power;

(e) the holder of the evaporant may be cooled to prevent interaction between crucible and evaporant. Some of the disadvantages of e.b.b. evaporation are that the equipment is more complicated and that if the vacuum is not high enough, residual gas molecules and some of the evaporant molecules may become ionised by the electrons (see Chapter 4). However, the ionisation of residual gas molecules could be used, in the form of a discharge at rough vacuua, as ionic bombardment cleaning [13] for the substrates before evaporation starts (see Chapter 5).

Vacuum evaporated piezoelectric films of binary compounds have been prepared in a variety of ways. As the temperatures required for vapourizing these materials are well in excess of their decomposition temperatures [5, 13], the vapour phase is in all cases composed of the elemental species. In a CdS system, because of the higher tendency of the sulphur to re-evaporate from the substrate as compared with the cadmium, films grown under conditions of equal cadmium and sulphur fluxes (e.g. as from a single CdS source) are normally sulphur deicient [13,61] When using a single CdS source the stoichiometry is considerably improved by heating the substrate to reduce the residence time of free cadmium on the surface, and by reducing the deposition rate [13]. The stoichiometry can also be improved by introducing excess sulphur in the system. An alternative method for increasing the resistivity is to co-evaporate a suitable monovalent metal (e.g. silver or copper) which acts as an electron acceptor [4, 13] in the deposited film (see section 9.2.1).

Two principal types of evaporation system have been used. In

the direct deposition system there is a direct line-of-sight between source and substrate, and the mean-free path is larger than the substrate-to-source-distance. In the indirect evaporation system there is no direct path from source to substrate, and, in general, the mean-free-path is smaller than the substrate to source distance, with the consequent loss of vapour beam directionality necessary for the deposition of films whose c-axis is inclined at an angle to the substrate normal. Within these two principal types of deposition system, various techniques have evolved. These are described below.

3.4.1.1. The Method of Foster

In his first report, in 1964, on the vacuum deposition of CdS transducers, Foster used direct evaporation of a single CdS source on a copper film substrate. Post evaporation treatment was required to diffuse the copper through the CdS film thickness, i.e. this transducer was, in fact, the same as the diffusion layer transducer [4], reported by him in 1963, with the whole of the thickness of the transducer acting as the diffusion layer. In 1965 Foster [17] modified his technique so that no post evaporation diffusion was necessary, and he used a technique whereby CdS and sulphur (S), were evaporated simultaneously from two separate crucibles. In their latest version (1968) Foster and co-workers [39] reported that the individually controlled CdS and S sources were housed in a water cooled enclosure equipped with a short cooled cylinder to condense out scattered (random) vapour molecules. Foster [13] reported that it was found necessary to use gold electrodes as the substrate metal film because of reaction between sulphur and copper films. This reaction was observed in the present work during the deposition of CdS films onto copper welding electrode inserts (see Chapter 5). Typical deposition rates of 0.03 $\mu m.min^{-1}$ were reported [13], for the fabrication of s-mode Type II transducers. Foster [13] reported that in most cases the c-axis of a deposited film

aligned itself along the direction of the vapour beam, although in some cases [51] it did not.

3.4.1.2. The method of DeKlerk

This arrangement, first reported [38] in 1965, uses individual cadmium and sulphur sources and incorporates a baffle between the sources and the substrate. The whole assembly is enclosed in a heated inner chamber, thereby creating an atmosphere containing substantial vapour pressures of cadmium and sulphur from which deposition takes place indirectly onto suitably placed substrates. Typical conditions are substrate temperature 200°C, inner-chamber wall temperature 160°C, sulphur source temperature 150°C, cadmium temperature 400°C, and deposition rate up to 0.6 $\mu m.min^{-1}$. Later DeKlerk reported [40-42] the deposition of epitaxial multi-layers. DeKlerk's films always turn out with their c-axes normal to the substrate because the vapour beam is non-directive, i.e. complete molecular disorder (chaos) exists inside the deposition chamber. This arrangement, therefore, is not suitable for the deposition of films whose c-axes are to be inclined at an angle to the substrate-normal.

3.4.1.3. The method of Beecham

This is a direct deposition method, and, therefore, suitable for oblique deposition. First reported [61] in 1970, it uses an isothermal source, the deposition rate being controlled by the area of orifices in the cadmium and sulphur cells as well as by the temperature of the cells. A typical deposition rate for s-mode Type II transducers is 1.8 $\mu m.min^{-1}$, with an isothermal source temperature of 420°C. The cadmium and sulphur cells are placed inside a furnace which is heated by a resistance wire. This method was used in some (later) experiments in the present investigation which are described in Chapter 5.

3.4.1.4. Other methods

Page [46] used a method essentially similar to that of DeKlerk

except that he used a crystallization dish instead of the baffle in DeKlerk's system. This method was also used by Llewellyn [56] et al. Weber [45] used an indirect deposition technique to vapourize CdS pellets and sulphur pellets from the same crucible using e.b.b. evaporation. Curtis [57] used direct CdS e.b.b. deposition with post-evaporation silver diffusion, with a typical rate of 0.4 $\mu m.min^{-1}$. Nagao [44] used evaporation of CdS pellets with direct deposition on aluminium film substrate influenced the direction of the c-axis relative to the vapour beam direction. He used fused quartz and Z-cut sapphire as substrates. The as-deposited films had low resistivity and were placed in a sealed quartz tube with sulphur and heated for 10 hours at 300-450^{o}C. High resistivity films then resulted.

3.4.1.5. Methods used in the present investigation

Because, from the outset, the present research project was concerned with the fabrication of s-mode transducers, this ruled out all deposition methods employing indirect evaporation e.g. those of DeKlerk [38], Weber [45], and Page [46]. The methods involving post-deposition treatment e.g. copper or silver diffusion were also thought to be unsuitable for very thick films, since it was reported [4] that there was a limit on how thick a diffusion layer could be. In any case, it was thought more desirable to eliminate one extra step (post-deposition treatment) from the production process. Also, it was later claimed [59] that the deposition of s-mode Type II CdS transducers by silver diffusion was unreliable, and that it could not be used for the regular production of transducers.

Two principal deposition methods were used. The first was a direct electron beam bombardment (e.b.b.) evaporation where Cd and S granules were evaporated from the same crucible (hereafter referred to as the e.b.b. isothermal technique). It was found that the c-axis

of a deposited film aligned itself with the direction of the vapour beam, and s-mode Type II transducers were fabricated up to about 45 μm thick. The thickest such film reported in the literature to date is 20 μm. However, when thicker films were deposited using the same deposition procedure as for the thin films, it was found that they would only operate as c-mode transducers. This meant that their c-axes did not align with the vapour beam, in contradiction with our earlier results with thinner films. Using crystallographic techniques it was established that the bottom layer of a thick film did indeed align its c-axis with the vapour beam, and that the orientation of the films was thickness-dependent. For a given deposition environment there is a critical thickness above which the film's c-axis starts to tilt towards the substrate-normal, depending on deposition rate and deposition angle. These effects were attributed to a "stifling process" whereby orientation changes occur during film growth. The studies made on orientation effects in thin- and thick-films, and the stifling process are discussed in Chapter 8, and it is stated there that one of the parameters controlling the stifling process is the size of the grains. CdS films suitable for c-mode generation have also been fabricated using this technique, up to 100 μm thick.

In Chapter 4, where evaporation and condensation phenomena are discussed, it is shown that the evaporation rate of a given material may be increased either by increasing its temperature or by increasing its surface area. For a given evaporation system, and for a given crucible, the only way to increase the deposition rate, therefore, is to raise the temperature of the crucible. This means that the rate of arrival of vapour molecules at the substrate is dependent on their temperature. Therefore, it could not be established, for a given deposition environment, whether it was the higher rate of arrival of molecules that affected the orientation of as-deposited films, or whether it was their temperature, or, indeed, both. It seemed expedient,

therefore, to make the deposition rate independent of the temperature of the source in order to establish which one of these parameters is the most important in determining the change of orientation from oblique c-axis to normal c-axis.

One way of achieving this would be to use crucibles with different top surface areas, in different deposition runs, keeping the crucible temperature the same. However the Birvac RG2 electron ring gun used imposes an upper limit on the top surface of the crucible of about 1 cm^2 (Chapter 5). In order to vary the deposition rate by on order of magnitude, therefore, the crucible would either be too small to hold enough evaporant material or too large to be heated by the electron beam. In any case small surface areas are essential if the beam is to have any directional-properties relative to the substrates. Since the ring gun proved itself a nuisance to further experimentation it was decided to dismantle it from the deposition apparatus, and use resistance wire heating.

The second deposition method was direct evaporation from a cadmium cell placed on top of a sulphur cell in such a way that sulphur molecules escaping from an orifice in the sulphur cell are concentric with cadmium molecules emitted from an annular orifice in the cadmium cell (Beecham's [31] isothermal source). The two cells are housed inside a furnace, and their temperature is approximately the same. The advantage of using cadmium and sulphur rather than CdS and sulphur is that cadmium and sulphur have much lower melting points [5] than CdS, and therefore it is possible to experiment with relatively cool molecules hitting the substrate at rates suitable for thick film deposition. For example, with the e.b.b. isothermal technique typical temperatures of molecules were 600-800^{o}C at deposition rates of 0.03 - 0.1 $\mu m.min^{-1}$ compared with temperatures of 300-400^{o}C with rates of 0.1 - 2 $\mu m.min^{-1}$ in Beecham's technique.

3.4.2. Sputtering techniques

Another approach to the vacuum deposition of thin films is sputtering [64]. In this technique atoms or molecules are ejected from a material by bombarding a target of the material, inside a vacuum chamber, either with positive ions (d.c. sputtering) or alternately with positive and negative ions (r.f. sputtering). The atoms (or molecules) are then deposited on a suitably placed substrate. D.C. sputtering is used when the target is metallic, while r.f. sputtering is used for insulating targets to prevent the accumulation of ions on the target. In order to establish a discharge inside a sputtering chamber (to provide the bombarding ions) the residual pressure has to be relatively high [13] (of the order of 10^{-1} torr). Under such conditions the sputtered molecules have a very short mean free path, and, therefore, have no directivity. With triode sputtering [13] a discharge may be obtained at about 10^{-3} torr, thus increasing the mean free path of the sputtered molecules by two orders of magnitudes. However, the deposition rate remains very low even under such conditions, and it is of the order of 1 μm per hour for cadmium sulphide [13]. Sputtering techniques will prove to be very useful for the deposition of very thin films in view of the very low deposition rates possible. Also these techniques would be useful for the deposition of chemically-complex compounds like ceramic piezoelectric materials. However, for thick films the long deposition times involved (tens of hours) make them very unattractive. The use of diode sputtering for depositing ZnO piezoelectric thin films was first reported [13], followed by a report on the deposition of cadmium sulphide films at rates of up to 0.3 $\mu m.h^{-1}$. Films of lithium niobate and zinc oxide have also been sputtered [13] using triode sputtering techniques at rates of about 1 $\mu m.h^{-1}$.

When this research project started in October 1967, one of its goals was to deposit very thin piezoelectric films for microwave ultrasonic work, and to this end the author designed an r.f. sputtering

apparatus, essentially similar to that of Probyn [65], which was made in the University Workshops (see Appendix I). The author also designed and built the H.T. power supply for the r.f. oscillator for the sputtering apparatus, complete with its automatic safety cut-outs in case of vacuum pump failures or oscillator valve heater failure, etc. Details of this power pack and safety circuits are given in Appendix I.

Due to shortage of time, in view of the unforeseen difficulties in the fabrication of thick CdS films suitable for s-mode generation, the author did not have the opportunity to make use of the sputtering apparatus. However, it gives the author great pleasure that this apparatus has been used a great deal by some of the author's colleagues, in the microwave-integrated-circuits group, for the deposition of very thin films of silicon dioxide [66].

3.4.3. Other techniques

The deposition of very thin cadmium sulphide films using a chemical deposition technique has been reported [53]. However it is not likely [54] that such films will have a strong crystallographic orientation. In any case, it is claimed that the chemical-deposition technique is not [54] suitable for the deposition of thick films.

3.5. Film transducers versus discrete transducers

The main impetus for the fabrication of thin film transducers was the basic technological limit imposed on the thinness of a particular transducer with conventional fabrication techniques, e.g. the fabrication of transducers a few micrometres thick. However, in some applications vacuum deposited film transducers are preferred to discrete transducers even though these deposited transducers are quite thick (thicker than 30 μm, say). Film transducers are superior to discrete transducers for the following reasons :-

(1) Film transducers are deposited direct onto the propagation medium, and therefore, all the problems [4, 56] associated with bonding a discrete (fragile) transducer onto the propagation medium are eliminated. This has many consequences. Firstly no-matter how thin a deposited transducer is, it is as rugged as the substrate it is deposited on, provided that certain precautions have been taken to match the transducer material to the substrate material from a thermal-expansion point of view (see Chapter 6). Secondly the transducer insertion-loss is decreased by an amount equivalent to the loss associated with the bonding layer. Bonding layer losses of 5 - 15 dB have been reported [67]. Thirdly, the waves generated by the film transducer are directly coupled to the propagation medium. This is of particular advantage when s-mode waves are to be launched since the problems associated with transmission through a coupling medium are avoided.

(2) The most efficient film transducer materials to date are cadmium sulphide and zinc oxide. These materials have much lower relative dielectric permittivities than those of ceramic material and, therefore, for a given thickness, the thin film transducers will be much easier to drive electrically in view of their lower capacitance. This is of great advantage when good transient performance is required, since a short rise-time pulse is then required to drive the transducer. The capacitances of a 10 MHz s-mode transducer for various materials are compared in Table 3.1.

(3) With thin film techniques it is possible to deposit piezoelectric transducers direct onto curved surfaces, for example in the manufacture of focussed ultrasonic probes. In the present project CdS piezoelectric transducers have been

successfully deposited onto domed spot-welding electrode inserts (with 12 mm radius of curvature), so that the ultrasonic beam may be focussed on the spot-weld. An extension of this may be the deposition of a piezoelectric film directly onto one side of a slot milled onto a wheel electrode of the type used for seam welding (see Chapter 1) to enable the quality of the seam-welds to be evaluated ultrasonically on-machine. So far as is known, no deposition of thin piezoelectric films on curved surfaces (outside the present work) has been reported in the literature to date.

3.6. Other thin film devices

The Group II-VI compounds are rather a special class of materials, they are not only important for advancing the basic understanding of solid-state physics, solid-state chemistry [5], and crystal chemistry [5, 22], but also they exhibit many interesting phenomena. Some examples are found in electroluminescence [5, 26], photo-voltaic and photo-sensitive effects [5, 26, 64], piezoelectric and piezoresistive effects [64], semiconducting effects [5, 26, 64, 68], electron-phonon interaction and ultrasonic-microwave amplification effects [69]. In many cases these effects have been studied by utilizing thin film layers [5, 26, 64, 70].

Most of the interest in thin film studies exists for technological reasons, and a lot of progress has been made in the field of micro-electronics [64, 71], in the manufacture of thin film integrated circuits [66] both in its lumped and strip line forms, in thin film capacitors and resistors [64], thin film field-effect transistors and diodes [64]. In the photo-voltaic field solar cells have also been made from thin films of cadmium sulphide [72]. Thin film piezoelectric and piezo-resistive strain-gauges have also been made [64]. An interesting strain-gauge thin film FET device which combines piezoelectric and semiconducting properties

of CdS has also been reported [13] which has potential advantages over conventional strain-gauges.

3.7. Very recent developments

In 1971 Holt et al [73] reported on crystallographic defects in thin epitaxial layers of sphalerite and wurtzite CdS grown on (100) and (110), and on (111) planes, respectively, of NaCl (sodium chloride). By heat treating the films at high temperatures they found that the defect content of the films was reduced. The wurtzite films had their c-axes normal to the substrate, and this was not affected by the heat treatment. However, the sphalerite films under-went a phase transformation to the wurtzite structure. They found that CdS grew epitaxially with substrate temperatures down to $0^{o}C$. In the same year, the dependence of the piezoelectric coupling coefficient on dislocation density in single crystal cadmium sulphide was reported [74]. It was found that the coupling coefficient stays constant over a wide range of dislocation densities, but falls very rapidly to zero when the dislocation density exceeds a certain value. A study on the effect of electron irradiation on the conductivity of CdS crystals was published [75]. The growth of cadmium sulphide films by sulphidation of cadmium films was reported [76]. Although studies on piezoelectricity in naturally occurring polymers such as cellulose and keratine have been reported earlier, it was in 1971 that measurements on piezoelectricity in films of synthetic polymer materials, e.g. polyvinylchloride, were reported [77].

TABLE 3.1 Comparative data on a 10 MHz s-mode transducer

Material	$\frac{v}{v_{CdS}}$	$\frac{t}{t_{CdS}}$	$\frac{\kappa_r}{\kappa_{r_{CdS}}}$	$\frac{C}{C_{CdS}}$	Transducer Thickness (μm)	Transducer capacitance (disc 3mm diameter)
CdS	1	1	1	1	90	30
ZnO	1.5	1.5	1	0.7	135	21
PSN	1.7	1.7	3.8	22	150	660
$Si\ O_2$	2.1	2.1	0.5	0.2	190	6
CdSe	0.9	0.9	1	1.1	81	33
PZT	1.3	1.3	140	110	117	3300
$Li\ Nb\ O_3$	2.1	2.1	3.5	1.7	190	51

C H A P T E R 3

REFERENCES

1. D. Luff, *Materials for piezoelectric transducers*, paper presented at B.A.S. meeting (1970).

2. *Mullards' Piezoelectric Ceramics Handbook*, ed. J. von Randeraat (1968).

3. R.F. Mitchell, *Some new materials for ultrasonic transducers*, Ultrasonics April 1968, p.112.

4. D. Beecham, *Ultrasonic transducers for frequencies above 50 MHz*, Ultrasonics, Jan. 1967, p.19.

5. M. Aven et al, *Physical and chemical properties of II-VI compounds*, North-Holland (1967).

6. A.B. Smith et al, *A bibliography of microwave ultrasonics*, IEEE Trans. SU-17, p. 86 (1970).

7. D.A. Berlincourt et al, *chapter in Physical Acoustics Vol. 1A* ed. W.P. Mason, Academic Press (1964).

8. S.A. Semiletov et al, *Thin film piezoelectric textures*, Sov. Phys. Cryst. 12, 2, p. 362 (1967).

9. M. Weinstein et al, *The growth of wurtzite CdTe and sphalerite type CdS single crystal films*, App. Phys. Lett. 6, p. 73 (1965).

10. Z.A. Magomedov et al, *Structure of epitaxial CdS thin films obtained by sputtering*, Sov. Phys. Cryst. 12, p. 470 (1967).

11. F.V. Shallcross, *Effect of fabrication parameters on structural and electronic properties of thin CdS and CdSe films*, Trans. Met. Soc. of AIME 236, p. 309 (1966).

12. K.K. Muravjera et al, *Growth and electro-physical properties of mono-crystalline films of cadmium and zinc chalcogenides*, Thin Solid Films, 5, p. 7 (1970).

13. N.F. Foster, chapter in *Handbook of t.f. technology*, ed. L.I. Maissel et al, McGraw-Hill (1970).

14. J. DeKlerk *Elastic constant of α ZnS*, J. Phys. Chem. Solids 28, p. 1831 (1967).

15. J. DeKlerk, *ZnO evaporated transducers*, Ultrasonics July 1970 p.

16. G.A. Rozgonyi et al, *Epitaxial thin films of ZnO on CdS and sapphire*, J. Vac. Sci. Tech. 6, p. 115 (1969).

17. N. Foster, *CdS evaporated-layer transducers*, Proc. IEEE 53, p.1400 (1965).

18. J.R. Slack et al, *Flash evaporation of ferroelectric thin films*, Thin Solid Films, 6, p. 233 (1970).

19. J.H. Collins et al, *Shear-mode generation at microwave frequencies using epitaxial YIG films on YAG*, App. Phys. Lett. 13, p. 93 (1968).

20. J.C. Bailor et al, *University Chemistry*, Heat & Co., Boston (1965).

21. G.A. Somorjai, *The evaporation rate and mechanism of CdS and CdSe*, Proc. Intl, Sympm. on evaporation and Dayton, Ohio (1962).

22. F.A. Kroger, *The chemistry of imperfect crystals*, North-Holland (1964).

23. D.C. Shotton et al, *The growth of CdS crystals*, GPO Res. Rep. No. 6 (1968).

24. P.D. Fochs et al, *Growth of CdS single crystals of controlled composition from the vapour phase*, J. Cryst. Growth, 3, p. 122 (1968).

25. M.R. Lorenz, chapter in *Physical and chemical properties of II-VI compounds*, Ed. M. Aven et al, North-Holland (1967).

26. G. Thomas ed. *II-VI semiconducting compounds*, Benjamin, N.Y. (1967).

27. I. Lagnado et al, *R.F. sputtered CdS thin crystals*, J. Vac. Sci. Tech., 7, p. 318 (1970).

28. T.K. Lakshmanan et al, *Some properties of sputtered CdS films*, Trans. 10th Nat. Vacm. Sympm., Macmillan (1963).

29. R.W. Gibson, *CdS ultrasonic transducers*, Elect. Lett., 2, 6, p. 213 (1966).

30. N.F. Foster et al, *Crystallographic orientation of ZnO films deposited by triode sputtering*, J. Vac. Sci. Tech., 6, p. 111 (1969).

31. R.J. Miller et al, *Production of CdS crystals by co-evaporation in vacuum*, JAP, 29, p. 1277 (1958).

32. K.V. Shalimova, *Crystal structure of CdS thin films as affected by deposition conditions*, Sov. Phys. Cryst. 8, p. 618 (1964).

33. R.Zuleeg et al, *Space charge limited currents and Schotky-emission currents in t.f. CdS diodes*, Sol. Stat. Elecs. 7, p. 575 (1964).

34. J.M. Gilles et al, *Photoconductivity and crystal size in evaporated layers of CdS*, Nature, 18, p. 862 (1958).

35. A.F. Andrushko, *Orientation of the micro-crystals of t.f's of CdS*, Sov. Phys. Cryst., 7, 2, p.172 (1962).

36. J. Dresner et al, *Crystallinity and electronic properties of CdS films*, JAP, 34, 8, p. 2390 (1963).

37. R.R. Addis, *Recrystallization of CdS films*, Trans. 10th Nat. Vacm. Sympm. p. 354 Macmillan N.Y. (1963).

38. J. DeKlerk et al, *Vapour-deposited thin film piezo-electric transducers*, Rev. Sci. Inst., 36, p. 506 (1965).

39. N.F. Foster et al, *CdS and ZnO t.f. transducers*, IEEE Trans. SU-15, 1, p. 28 (1968).

40. J. DeKlerk, *Multi-layer enhancement of microwave piezoelectric conversion in CdS-SiC layers*, App. Phys. Lett., 7, p. 10 (1965).

41. J. DeKlerk, *C-axis flipping for multi-layer piezoelectric transducers*, App. Phys. Lett. 13, 3, p. 102 (1968).

42. J. DeKlerk, *Multi-layer t.f. piezoelectric transducers*, IEEE Trans. SU-13, p. 99 (1966).

43. A.R. Hutson, *Piezoelectricity and conductivity in ZnO and CdS*, Physl. Rev. Lett., 4, p. 505 (1960).

44. M. Nagao, *High efficiency CdS film transducers for the shear-mode*, JAP 37, p. 4591 (1966).

45. R. Weber, *Electron bombardment technique for the deposition of CdS film transducers*, Rev. Sci. Inst., 37, p. 955 (1966).

46. D.J. Page, *CdS thin film devices*, Proc. IERE-IEE Joint Conf. Applications of t.f's, paper 9 (1966).

47. J. DeKlerk, chapter in *Physical Acoustics*, ed. W.P. Mason, Vol. 4A, Academic Press (1966).

48. K.G. Gunther, chapter in *Use of t.f's in physical investigations*, ed. J.C. Anderson, Academic Press (1966).

49. D.K. Winslow et al, *Multiple film microwave acoustic transducers*, IEEE Intl. Con. Recd., 14, p. 26 (1966).

50. T.R. Sliker et al, *A thin film CdS quartz composite resonator*, JAP 38, p. 2350 (1967).

51. N.F. Foster, *Structure of CdS evaporated films in relation to their use as ultrasonic transducers*, JAP, 38, p. 149 (1967).

52. W. Duncan et al, *Effect of neutron irradiation on the acoustic performance of evaporated CdS films*, JAP 39, p. 5987 (1968).

53. M. Nagao et al, *Chemically deposited thick CdS films*, Japan JAP 7, p. 684 (1968).

54. M. Nagao, *Private Communication*.

55. P.J. King, *The optimum conditions for the evaporation of CdS films*, Brit. J. App. Phys. 2, p. 1349 (1969).

56. J.D. Llewellyn et al, *Apparatus for the deposition of low frequency CdS transducers*, J. Sci. Inst. (J. of Physics E), 2, p. 535 (1969).

57. B.J. Curtis, *The preparation of s-mode evaporated CdS ultrasonic transducers by silver diffusion*, JAP 40, p. 433 (1969).

58. A. Doi, *Dependence of piezoelectric constant of evaporated CdS thin films upon their deposition rate*, Japan JAP 9, p. 723 (1970).

59. R.F. Mitchell, *Mullards Res. Labs. Rep. No. 2732* (1970).

60. A.H. Meitzler et al, *Use of optical bifringence in monitoring properties of GHz piezoelectric transducers*, IEEE Trans. SU-17, p. 60 (1970).

61. D. Beecham, *Cadmium/sulphur isothermal source for CdS deposition*, Rev. Sci. Inst. 41, p. 1654 (1970).

62. B.J. Curtis et al, *The epitaxial growth of CdS on gallium arsenide substrates*, J. Cryst. Growth 6, p. 269 (1970).

63. R.W. Berry et al, *Thin film technology*, Van Nostrand (1968).

64. L.I. Maissel et al ed. *Handbook of thin film technology*, McGraw-Hill (1970).

65. B.A. Probyn, *Sputtering of insulators in r.f. discharge*, Vacuum, 18, p. 253 (1968).

66. K. Mehmet, *Ph.D. Thesis*, University of Warwick (1970).

67. J.D. Llewellyn, *Ph.D. Thesis*, University of Lancaster (1970).

68. N.B. Hannay ed. *Semiccnductors*, Chapman & Hall, London (1960).

69. J.H. McFee, chapter in *Physical Acoustics*, ed. W.P. Mason, Vol. 4A, Academic Press (1964).

70. J.C. Anderson ed. *The use of thin films in physical investigations*, Academic Press (1966).

71. L. Holland ed. *Thin film microelectronics*, Chapman & Hall (1965).

72. IRD Newsletter *CdS thin film solar cells*, November 1969.

73. D.B. Halt et al, *Crystallographic defects in epitaxial layers of CdS*, J. Cryst. Growth, 9, p. 193, (1971).

74. N. Chubachi et al, *Influence of dislocations in CdS crystal on its electromechanical coupling factors*, JAP, 42, 3, p. 962 (1971).

75. M. Kitagawa et al, *Annealing of electron-irradiated CdS*, App. Phys. Lett. 18, 2, p. 41 (1971).

76. G. Hecht et al, *Nucleation and oriented growth of chemically formed sulphide and oxide films*, J. Vac. Sci. Tech. 7, 5, p. 547 (1970).

77. J. Cohen, *Direct pie-effect in polyvinyl-chloride films*, JAP 42, 2. p. 893 (1971).

C H A P T E R 4

Vacuum evaporation and condensation theory

4.1. Introduction

In this chapter existing theories [1,2,3] on vacuum evaporation and deposition phenomena are presented with critical comments by the author on their agreement with experimental results on CdS reported by various authors. The chemistry [4,5] and, in particular, the stoichiometry of deposited films of cadmium sulphide are also discussed. Values of the mean-free-path of sulphur and cadmium vapour atoms at various pressures are given together with percentages of vapour atoms reaching a substrate without colliding with each other. Critical values of substrate temperatures (temperatures above which no condensation is possible), and critical values of vapour pressures (pressures below which no deposition is possible) are given for deposition of sulphur, cadmium, and cadmium sulphide. Although the torr is not the SI unit for pressure, it is very widely used at present. In fact, all of the pressure gauges used in the present work were calibrated in torr, and this is why it is used in this and in the following chapter. The torr is related [6] to the SI unit of pressure (the pascal) by the following equation :

1 torr = 1 mm of mercury = 133 pascal.

4.2. Gas Kinetics

In the kinetic theory of gases,[1] a gas is conceived as a large number of minute hard particles (molecules) moving about at random with very high velocities. The pressure and temperature which are terms used to describe the observed macroscopic phenomena can then be

explained in terms of the microscopic behaviour of the molecules. Thus, pressure is regarded as the average force per unit area on the walls of a container due to bombardment by the molecules, and the absolute temperature is regarded as being proportional to the mean of the squares of the velocities of the molecules i.e. to their average kinetic energy of translation.

4.2.1. The mole and molecular weights

Since in chemical reactions it is impossible to experiment with a single molecule (or atom), a certain number of molecules (or atoms) may be used as a standard of the amount of matter involved in a reaction instead of a single molecule (or atom), provided that the same number is always used. By convention [5] this number is taken to be 6.02×10^{23} (known as Avogadro's number), and it represents one mole of the substance. The mole is one of the basic SI units [7] and is given the symbol "mol". It occupies a volume of 22.4 litre at 760 torr and 273 K. The weight in grammes of 1 mole of a substance is the molecular (or atomic) weight of that substance. For example, the molecular weights of nitrogen (N_2) and water vapour (H_2O) are, respectively, 28 and 18. By definition, the molecular weight of a compound is equal to the sum of the molecular (or atomic) weights of its constituent molecules (or atoms), e.g. the atomic weights of sulphur (S) and cadmium (Cd) are 32 and 112, respectively, and, therefore the molecular weight of cadmium sulphide (CdS) is 32 + 112 = 144. It follows immediately that 32 g of sulphur combine with 112 g of cadmium to form 114 g of cadmium sulphide, i.e. CdS is 77.5% cadmium by weight.

4.2.2. Gas pressure

When a gas is removed from a vessel by some means of pumping, the gas pressure in the vessel falls, i.e. the number of molecules, n, per unit volume in the vessel decreases and the average separation

between the molecules increases. For an ideal gas the pressure, P, is given by [6] :

$$P = n k T \qquad \ldots\ldots\ldots (4.1)$$

where T is the temperature in kelvin, and k is the Boltzmann constant. The most probable speed, v_m, of a molecule is given by [6,8] $v_m = \left(\frac{2kT}{m} \right)^{\frac{1}{2}}$ where m is the mass of the molecule. The speeds of the molecules have a Maxwellion distribution, with an average speed given by [6,8] $r_a = \frac{2}{\sqrt{\pi}}$ $v_m = 145.5 \sqrt{\frac{T}{M}}$ where M is the molecular weight and v_a is in cm.$^{s-1}$. For example the average velocities of air molecules, sulphur, S_2, molecules and cadmium vapour atoms at 100^{o}C are 940, 620 and 460 m.s^{-1}, respectively. With a substrate-to-source-distance, inside a vacuum chamber, of 10 cm, say, it would take a cadmium atom about 0.2 ms to reach the substrate, provided that the mean free path of the molecule is greater than 10 cm. Since such short time intervals are involved it may be assumed that the vapour molecules cool down very little en route to the substrate.

4.2.3. Mean free path

The mean-free-path (m.f.p.) is a measure of how readily molecules will travel through a gas, and is given by [6] :

$$L = \frac{1}{\pi \sqrt{2}\, n\, d_o^{\,2}} \qquad \ldots\ldots\ldots (4.2)$$

where L is the m.f.p., n is the number of molecules per unit volume, and d_o is the diameter of the molecule. For example air molecules have m.f.p's of [8] 67 nm, 51 cm, and 51 m at pressures of 760, 10^{-4}, and 10^{-6} torr respectively. When the pressure is low collisions between molecules and the walls of the container predominate and there is so-called molecular flow [1]. If most collisions are between the molecules themselves, there is viscous flow [1]. In such a case individual molecules

have no directivity when travelling between source and substrate and the gas may be treated as a fluid i.e. a continuum. For viscous flow to occur the m.f.p. of molecules must be small compared with the dimensions of the container.

4.2.4. The rate of arrival of gas molecules

Gas molecules bombard the walls of a container at a rate, R_a, given by [6] :

$$R_a = P \left(\frac{1}{2\pi mkT} \right)^{\frac{1}{2}} \qquad \text{..... .... (4.3a)}$$

where P is the pressure inside the container. When P is expressed in torr, the above equation becomes :

$$R_a = 3.51 \times 10^{22} P \left(\frac{1}{TM} \right)^{\frac{1}{2}} \text{ molecules cm}^{-2}.\text{s}^{-1} \qquad \text{.....(4.3b)}$$

Since 1 mole represents 6.02×10^{23} molecules, R_a may be written as :

$$R_a = 0.058 P \left(\frac{1}{TM} \right)^{\frac{1}{2}} \qquad \text{..... (4.3c)}$$

Further, since 1 mole weighs M grammes

$$R_a = 0.058 P \left(\frac{M}{T} \right)^{\frac{1}{2}} \quad \text{g.cm}^{-2}.\text{s}^{-1} \qquad \text{..... (4.3d)}$$

Alternatively, the rate of arrival of molecules may be expressed in terms of deposited film thickness assuming that every arriving molecule sticks onto the substrate :

$$R_a = \frac{580}{\rho} P \left(\frac{M}{T} \right)^{\frac{1}{2}} \quad \mu\text{m.s}^{-1} \qquad \text{..... (4.3e)}$$

where ρ is the density of the condensing material in g.cm^{-3}. For example, the deposition rate of cadmium at a pressure of 5×10^{-5} and a temperature of 400°C is approximately 0.1 $\mu\text{m.min}^{-1}$. In actual fact some cadmium atoms re-evaporate, their rate of evaporation being dependent on the temperature of the substrate, and the deposition rate

would be less than predicted by the above equation. When gas moelcules (or atoms) hit the walls of a deposition chamber they are reflected diffusely because the walls of the container are rough on an atomic scale.

The rate at which molecules are adsorbed may be written as [1] :

$$\frac{d_{na}}{dt} = c_s R_a = 3.5 \times 10^{22} c_s P \left(\frac{1}{TM}\right)^{\frac{1}{2}} \quad \text{molecules. cm}^{-2}.\text{s}^{-1}$$

where c_s is the sticking coefficient, defined as the probability that an incident molecule be adsorbed. When both sides are multiplied by kT, the amout of gas adsorbed may be written as

$$\frac{d(PV)}{dt} = 3640 c_s P \left(\frac{T}{M}\right)^{\frac{1}{2}} \quad \text{torr. litre. cm}^{-2}.\text{s}^{-1}$$

where T is the temperature of the molecules, and n_a molecules occupy volume V. In a mono-layer the distance between the centres of the adsorbed molecules is approximately equal to the diameter of a molecule. It is equal [1] to 3.7×10^{-8} cm for nitrogen molecules, and, therefore, a nitrogen mono-layer contains 7.3×10^{14} molecules. If $c_s = 1$, the mono-layer will form [1] in 2s at 10^{-6} torr. The number of molecules in a mono-layer depends on the surface structure, e.g. the lattice constant of the adsorbent, and the size of the molecule. The sticking coefficient is a function of the number of sites available for adsorption. When adsorbed gases are suddenly released e.g. when the wall of a vacuum chamber is heated, the pressure inside the chamber rises. If a mono-layer of nitrogen (78% of the atmosphere) is suddenly released from the substrate holder, say, inside a vacuum chamber, the pressure would increase [1] by 10^{-2} torr. How long this pressure rise would last before going back to the original vacuum depends on the pumping speed of the vacuum pumping system.

4.2.5. Vapour pressure [8]

The pressure exerted by a vapour in equilibrium with its solid form (sublimation) or liquid form (vapourization) is known as the equilibrium vapour pressure, P_e, of the substance. Condensation onto a substrate from the vapour phase is possible if the vapour pressure is higher than the equilibrium vapour pressure, i.e. if the vapour is super-saturated. The driving force for condensation (deposition) is the ratio between these two pressures i.e. the degree of super-saturation. The equilibrium vapour pressure may be calculated thermodynamically and may be written as [1,9] :

$P_e = A\, e^{-\frac{\Delta G}{kT}}$, where A is a constant and ΔG is the heat of vapourization. This equation holds provided that P_e does not exceed tens of torrs. When P_e is large the dependence of log P_e on $\frac{1}{T}$ becomes non-linear, see Fig. 4.1.

4.3. Vacuum evaporation

The expressions for the rate of arrival of gas molecules (equations (4.3)) may be used [2] to express the rate of evaporation, R_e, of molecules from a solid (sublimation) or a liquid (vapourization). The equilibrium between vapour and bulk material (solid or liquid) is dynamic with molecules continually leaving and returning to the emitting surface of the bulk substance. If all arriving molecules stick to the substance, then, at equilibrium, this is also the rate of evaporation. The evaporation rate remains the same [1] if no equilibrium exists and more substance evaporates than condenses on the emitting surface as long as the bulk supply lasts. If the evaporating molecules are immediately removed, e.g. in a vacuum system that is continually exhausted, such that none return to the bulk substance, the net rate of evaporation is a maximum. Thus we may write for the rate of evaporation, R_e, of a substance in a vacuum :

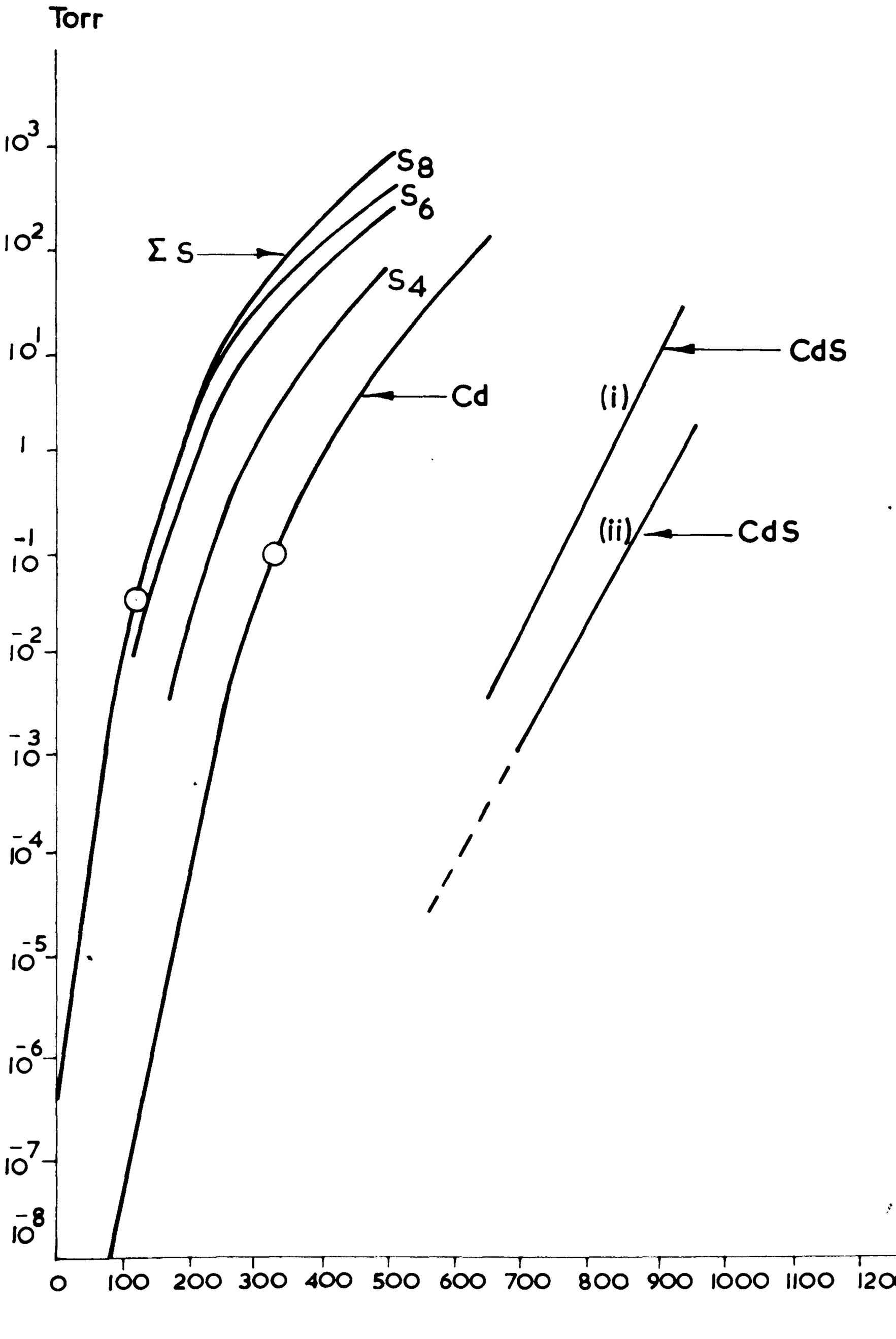

FIG. 4.1 Vapour pressure versus temperature.
—○— Melting point. (i) Equilibrium, (ii) Evaporation
(Data from Beecham[11] and Somarjai[12])

$$R_e = 3.51 \times 10^{33} P_e \left(\frac{1}{TM}\right)^{\frac{1}{2}} \text{ molecules. cm}^{-2}.\text{s}^{-1}$$

or $$R_e = 0.058 P_e \left(\frac{M}{T}\right)^{\frac{1}{2}} \text{ g.cm}^{-2}.\text{s}^{-1}$$

..... (4.4)

The vapour pressure, P_e, changes rapidly with temperature (Fig. 4.1). This influence determines the dependence of evaporation rate on temperature rather than the $T^{-\frac{1}{2}}$ term in equations (4.4).

If the vapour pressure is allowed to build-up, e.g. if the pumping speed is too low, some of the vapour molecules would return to the emitting surface, reducing the condensation coefficient [1]. For materials in equilibrium with their vapour, a is nearly unity [2]. However, in all deposition runs in the present investigation, the residual gas pressure was less than 10^{-4} torr and, therefore, equations (4.4) hold for the evaporation rate in all of the deposition experiments in the present work.

Since the squares of the diametres of the atoms of cadmium, sulphur, and nitrogen are [5] approximately in the ratio 3:2:1, it follows from equation (4.2) that their m.f.p's will be in the ratio 1:2:3, i.e. $L_{Cd} : L_S : L_N = 1 : 2 : 3$. Using the m.f.p. of nitrogen [6] as a reference, values for L_{Cd} and L_S were calculated and they are given in Table 4.1a. Water vapour and hydrocarbon vapours form the principal components [2] of the residual gases in a dynamic pumping system, and their m.f.p's are also given in this table. The mean free path, L_e, of an electron passing through a gas (vapour) whose mean free path is L, is given by [6] $L_e = 5.66L$. In some vacuum systems electron beam bombardment evaporation is used instead of filament heating, and it is of interest to determine the m.f.p. of electrons in such a system during evaporation. From Table 4.1 it is seen that for sulphur vapour at 10^{-4} torr, the m.f.p. is 34 cm and, since the electron beam traverses a distance of less than one centimetre in the Birvac RG2 electron ring

Molecule	m.f.p. at gas pressure in torr							Reference
	760	10^{-1}	10^{-2}	10^{-3}	10^{-4}	10^{-5}	10^{-6}	
Air	67 nm	510 μm	5.1 mm	5.1 cm	51 cm	5.1 m	51 m	6
Water vapour	44 nm	340 μm	3.4 mm	3.4 cm	34 cm	3.4 m	34 m	2
Cadmium	22 nm	170 μm	1.7 mm	1.7 cm	17 cm	1.7 m	17 m	
Sulphur	44 nm	340 μm	3.4 mm	3.4 cm	34 cm	3.4 m	34 m	

(a)

$\frac{\ell}{L_v}$	0.01	0.05	0.1	0.25	0.5	0.75	1.0	2	3	4	5	10
$\frac{N}{N_o}$ %	99	95	90	78	60	47	37	14	5	2	1	0

(b)

Vapour atom	Pressure (torr)	ℓ/L_v	N/N_o % (approx.)
Cd	10^{-4}	0.47	60
	10^{-5}	0.05	100
S	10^{-4}	0.24	80
	10^{-5}	0.02	100

(c)

TABLE 4.1 (a) m.f.p. for various vapours, (b) percentage of molecules reaching substrate for various values of the ratio, ℓ/L_v, of substrate-crucible-distance to the m.f.p., (c) percentage of Cd and S vapour atoms reaching substrate for substrate-to-crucible-distance of 8 cm.

gun, it may be stated that almost all the electrons reach the crucible without colliding with the vapour molecules. However, some workers have reported on interactions between electron beams and vapour molecules [10].

It can be shown [2,6] that the fraction, N, of the molecules emitted, N_o, from a source (crucible), inside a vacuum chamber, which traverses a distance ℓ without experiencing collisions with residual gas molecules is given by :

$N = N_o e^{-\frac{\ell}{L_v}}$ where L_v is the m.f.p. of the vapour molecules in the residual gas. The ratio $\frac{N}{N_o}\%$ for various values of $\frac{\ell}{L_v}$, ℓ, and L_v are given in Table 4.1b.

For deposition at oblique incidence, ideally, all arriving molecules should hit the substrate at the required angle. In practice, however, because of deposition angle, deposition rate, and substrate temperature control limitations the distance between the substrate and the source is not short enough, compared with m.f.p., to ensure that all molecules hit the substrate at an oblique angle. For example, in most film deposition work in the present investigation, the residual pressure was less than 5×10^{-5} torr, with a substrate to source distance of about 7 cm, i.e. more than 90% of the molecules hit the substrate at oblique incidence. The substrate area is negligible compared with the total surface area inside the chamber, and, therefore, it could be reasonably assumed that very few of the "random" molecules (i.e. the molecules that collide with each other) reach the substrate. Nevertheless, a very small proportion of random molecules may do so.

4.4. Vacuum deposition (condensation)

Some substances e.g. noble metals can be vapourised and condensed to form deposits in the atmosphere, but such coatings often lack a smooth texture [2]. Chemical reactions between the evaporant and

air (oxygen) may prevent condensation of a deposit or give rise to the other compounds, e.g. when cadmium is volatised in air, cadmium oxide "smoke" deposits are formed. Contamination of the deposit may be prevented by replacing the air with an inert gas e.g. argon, but for most metals and inorganic compounds the evaporation temperature has to be very high to obtain the necessary vapour pressures required for a reasonable deposition rate. This is because the m.f.p. is very small at atmospheric pressures and room temperature (Table 4.1) which means that some vapour molecules return to the bulk material after colliding with each other instead of reaching the substrate. If the vapour molecules are required to hit the substrate at a given angle then the pressure has to be less than 10^{-4} torr for a substrate to source distance of few centimetres. As indicated by equation (4.2) the m.f.p. increases as the pressure is lowered and a larger percentage of the vapour molecules reach the substrate without collisions with each other. This assumes that the pumping system is fast enough to evacuate some of the vapour molecules introduced into the vacuum chamber by the vapour source, in order to maintain the value of the m.f.p. during deposition. The percentages of sulphur and cadmium vapour atoms reaching the substrate are given in Table 4.1c for various gas pressures at a substrate to source distance of 8 cm. From equations (4.5) the rate of arrival of vapour molecules at a substrate, R_{ar}, inside a vacuum chamber may be written as :

$$R_{ar} = 3.51 \times 10^{22} P \left(\frac{1}{TM} \right)^{\frac{1}{2}} \quad \text{molecules.cm}^{-2}.\text{s}^{-1}$$

where P is the residual gas pressure. When a molecule (particle) strikes a surface it may either suffer an elastic collision and rebound immediately with no loss of energy (reflection and diffraction) or it may suffer an inelastic collision in which case it may either lose or gain energy. A special case of an inelastic collision is for

the molecule to lose so much energy that it remains adsorbed on the surface. In the case of adsorption the molecule can either remain permanently on the surface (condensation) or it may remain for only a short time and then be restituted to the vapour phase (re-evaporation). The rate of condensation, R_c, may be written as $R_c = a R_{av}$, where a is the accommodation coefficient [1,2] which depends on how clean the substrate surface is and how cold the substrate is relative to the temperature of the vapour molecules. In vapour-phase deposition for a clean surface the accommodation coefficient is nearly unity [1,11], and one may write $R_c = R_a$.

There will be net condensation on a substrate provided that [3] the rate of condensation (arrival of molecules), R_a, is greater than the rate of re-evaporation from the substrate, R_{es}, :

$$R_{av} > R_{es} \text{ , i.e. } \frac{P}{\sqrt{T_m}} > \frac{P}{\sqrt{T_s}} \qquad \ldots\ldots\ldots (4.5)$$

where P is the gas pressure inside the deposition chamber and P_e is the vapour pressure of the condensing material at temperature T_s (substrate temperature), and T_m is the temperature of the molecules. From equation (4.5) it can be seen that, for a given material, there is a critical substrate temperature above which no condensation will be possible. For example, taking a typical sublimation temperature of CdS (600^oC) and a typical gas pressure of 5×10^{-5} torr, then, for condensation to occur $\frac{P_e}{\sqrt{T_s}} < \frac{5 \times 10^{-5}}{\sqrt{600}}$. From vapour pressure data (Fig. 4.1), for sulphur condensation on sulphur the critical substrate temperature, T_{sc}, is about 30^oC. For the sake of brevity this temperature will be referred to as T_{sc}(S/S). Similarly, it can be deduced that T_{sc}(Cd/Cd) is about 150^oC, and T_{sc}(CdS/CdS) is about 400^oC. Also, critical temperatures for condensation of sulphur (or cadmium) atoms on cadmium sulphide may be worked out. For this the evaporation rate of sulphur (or cadmium) atoms from cadmium sulphide must be known. Assuming

that during evaporation cadmium sulphide dissociates into cadmium atoms and sulphur atoms, then the evaporation rate of sulphur (or cadmium) atoms is equal to the evaporation rate of CdS. The evaporation rate from the basal plane of cadmium sulphide single crystals has been experimentally determined[12] in terms of rise in gas pressure inside the vacuum chamber (Fig. 4.1), and from this it may be deduced that T_{sc}(S/CdS) and T_{sc}(Cd/CdS) are equal to about 550°C. Similar critical substrate temperatures may be worked out for other residual pressures and temperatures, and this is done in Table 4.2a.

From equation (4.5) it can also be seen that for a given substrate temperature, T_s, and a given temperature of arriving molecules, T_m, there is a minimum rate of arrival of vapour molecules below which no condensation occurs. The rate of arrival of gas molecules is proportional to the gas pressure inside the chamber (equations (4.3). For example, for T_s = 170°C and T_m = 600°C, the critical pressure for condensation of sulphur vapour on sulphur is given by : $P_{crit}(S/S) \simeq 10^{-1}$ torr. Similarly $P_{crit}(Cd/Cd) \simeq 10^{-4}$ torr, and $P_{crit}(Cd/CdS) \simeq 10^{-11}$ torr. Table 4.2b gives critical fluxes for other substrates and molecule temperatures. During deposition and condensation of the first mono-layer of the incident vapour on an unlike substrate, the interfacial forces and consequently the critical values of the substrate temperature and incident flux may change reaching constant value when the deposited layer itself acts as substrate. When continuous deposition is considered, however, the deposition of the first mono-layer is only a negligible part of the process as a whole, and the above equations may be assumed to hold for deposition on unlike substrates.

Although the above theory is not very precise because it assumes that the accommodation (sticking) coefficient of, sulphur atoms, is the same as that for cadmium atoms, it predicts, nevertheless, with reasonable accuracy, the substrate temperature ranges at which a

Pressure	Critical substrate temperature, ^{o}C				Temperature of vapour molecules, ^{o}C
	S/S	Cd/Cd	S/CdS	Cd/CdS	
5×10^{-5}	30	150	550	550	600
5×10^{-4}	50	190	600	600	600
5×10^{-5}	40	180	530	530	800
5×10^{-4}	60	200	610	570	400

(a)

Substrate temperature T_s ^{o}C	Molecule temperature T_m ^{o}C	Critical pressure, P_{crit}, torr			
		S/S	Cd/Cd	S/CdS	Cd/CdS
170	600	10^{-1}	10^{-4}	10^{-11}	10^{-11}
170	400	8×10^{-2}	8×10^{-5}	8×10^{-12}	8×10^{-12}
100	600	5×10^{-3}	3×10^{-6}	10^{-12}	10^{-12}
300	600	5×10^{-1}	2×10^{-2}	10^{-8}	10^{-8}

(b)

TABLE 4.2 (a) Critical substrate temperatures,

(b) Critical deposition rates expressed in terms of vapour pressures.

material may condense. It predicts for example that cadmium vapour atoms will not deposit on a cadmium film substrate above about 190°C at residual pressures of about 5×10^{-4} torr. This is in good agreement with the experimental results of King [13] where he found that cadmium will not deposit above a temperature of about 180°C on a range of substrate materials (e.g. glasses, quartz, silicon, germanium, brass and steel). However, in his paper King states that his findings are in disagreement with earlier experimental results published by DeKlerk [14] where he (DeKlerk) found that cadmium would deposit at substrate temperatures above 200°C. It would seem that DeKlerk was depositing under different vapour pressure conditions (i.e. different evaporation rates) than those of King. Unfortunately, however, neither DeKlerk nor King give values for the pressure in their vacuum chambers during cadmium deposition. King also reported that, in agreement with DeKlerk's experiments, sulphur will not deposit at temperatures higher than about 50°C, which is in good agreement with theoretical predictions, provided that the gas pressure during deposition is greater than 5×10^{-4} torr. During cadmium sulphide deposition (Chapter 5), it was observed that only sulphur deposited at the cooler parts of the deposition chamber, e.g. the base-plate which is in good agreement with the above results.

4.5. Chemistry of binary crystals

Although most of the following applies to any compound of Group II-VI, only cadmium sulphide will be considered. Cadmium and sulphur have a relatively low melting point (321 and 119°C at atmospheric pressure, respectively) whereas the compound itself melts at 1475°C at a minimum pressure of 3.8 atmospheres [4]. However CdS sublimes [12] at temperatures as low as 600°C, and this is why most of the work on crystal growth of CdS has been concentrated on growth from the vapour-phase rather than from the melt. Nevertheless growth

from the melt has also been reported [15].

In the vapour phase the metal cadmium exists as mono-atomic vapour [4,16] whereas the vapour-phase species of sulphur are somewhat more complex since they can exist in several forms depending on temperature and pressure. Sulphur is known to exist [11,16] in the mono-atomic (S), di-atomic (S_2), pento-atomic (S_4), hexo-atomix (S_6) and octo-atomic (S_8) states. In general a sulphur vapour molecule may be written as S_{2n}, where n is an integer, and $1 < n < 4$. Cadmium sulphide dissociates [4,12,17] during evaporation into cadmium mono-atomic vapour (Cd) and sulphur di-atomic molecules (S_2) according to the reaction :

$$2\ CdS\ (solid \rightleftarrows 2\ Cd\ (gas) + S_2\ (gas) \qquad \ldots\ldots\ldots\ (4.6)$$

In general CdS may dissociate during evaporation according to the reaction :

$$2n\ CdS\ (solid) \rightleftarrows 2n\ Cd\ (gas + S_{2n}\ (gas)$$

This equation indicates that the partial vapour pressures of sulphur and cadmium are not independent. They are coupled by the equilibrium constant [4], K, of the reaction as follows :

$$K = P_{Cd}^{2n}\ P_{S_{2n}} \qquad \ldots\ldots\ldots\ (4.7)$$

where P_{Cd} and $P_{S_{2n}}$ are the vapour pressures of cadmium and sulphur, respectively, and n has the same significance as before. Alternatively, the values of K may be calculated from other thermodynamic data [4] by means of the equation : $\Delta G = \Delta H - T\Delta S = -RT \log_e K$, where ΔG is the change in the Gibbs free energy of the dissociation reaction (the negative value of the formation free energy), and ΔH and ΔS are the corresponding enthalpy and entropy changes. From equation (4.6) it can be seen that the constant for the reaction of equation (4.7) is

given by :

$$K = P_{Cd}^{2} \times P_{S_2} \qquad \ldots\ldots\ldots (4.8)$$

The total vapour pressure, P, over solid CdS, assuming only elemental Cd and S_2 exist in the vapour phase, is given by : $P = P_{Cd} + P_{S_2}$. The only constraint on this system is equation (4.10), i.e. the product of the partial pressures must stay constant. This is analogous to the constraint imposed on the concentrations [4] of electrons, n, and holes, p, in a semiconductor : $np = K_i$, and is known [4] as the Equation of State. Cadmium and sulphur molecules may recombine at a substrate to form [4,12,18] cadmium sulphide (solid). However, it has been claimed [19] that the growth of cadmium sulphide occurs from undissociated cadmium sulphide (gas) molecules, even though these undissociated molecules constituted only 5% of the total sublimed cadmium sulphide (solid).

When a substrate is exposed to a vapour beam, some of the impinging atoms (or molecules) condense and may later re-evaporate depending on the temperature of the substrate. Re-evaporation is inhibited if the condensed atoms migrate to a more favourable site with a greater bonding energy. Condensed atoms can agglomerate into a relatively stable unit whose probability of future growth is greater than that of evaporation. The smallest such unit is a crystal nucleus. Nucleation from the vapour is possible if the pressure of the gas molecules above the substrate is higher than the equilibrium vapour pressure. The driving force for condensation is the super-saturation: the ratio between these two pressures. Once the nucleus has formed, it begins to grow. The super-saturation required for growth is generally much less than for nucleation, but must still be greater than unity. The rate of crystal growth increases with an increase in the vapour pressure of the system (see equations 4.3). Any substrate may be considered to offer a number of nucleation

sites each of which is characterised by a particular super-saturation needed for its activation. A low super-saturation (i.e. low pressure during deposition) should therefore reduce the number of nuclei which develop and thus limit polycrystallinity (i.e. increase the grain size of the growing crystal). Except in epitaxial growth, a significant number of nuclei always form, but they subsequently grow at different rates and it is possible to arrange for one particular orientation to predominate (see Chapter 8).

4.5.1. Stoichiometry of deposited CdS films

A stoichiometric binary compound is one which has no excess of either of its constituent elements. For example, a cadmium sulphide crystal is said to be stoichiometric if it contains no excess cadmium i.e. no cadmium atoms exist on inter-stitial lattice sites, or alternatively if no sulphur lattice sites are vacant. Cadmium sulphide crystals are either completely stoichiometric (the ideal case) or contain excess cadmium (e.g. sulphur vacancies). No crystals with excess sulphur have been grown to date [4], and non-stoichiometric cadmium sulphide is always n-type [4,12,20] because of the presence of free electrons (rather than free holes) in the crystal lattice. The resistivity of cadmium sulphide may vary by more than 15 orders of magnitude depending on its stoichiometry, and the higher the stoichiometry the higher the resistivity of the crystal. Resistivities in the range 10^{1} - 10^{16} ohm.m have been reported [15] for single crystal CdS.

If the composition of a compound deviates markedly from that expected on the basis of a simple stoichiometric composition, this can be found by quantitative analysis of the consituents. Since conventional [21] methods of quantitative analysis have an error of ± 0.1%, deviations from stoichiometry of less than 0.1% can not be detected in this way. However, recent developments such as microprobe analysis may extend the range of detection of non-stoichiometry. Deviations from stoichiometry of less

than 10^{-1} p.p.m. may be determined by measuring the physical properties of the solid insofar as these are determined by it. For instance the electrical resistivity of cadmium sulphide is known [11,22] to decrease with decreasing stoichiometry. Of course factors other than the stoichiometry of a deposited film may contribute to the value of its electrical resistivity, for example it is known that the crystallographic structure plays a part in this. For films with good crystallographic structure, however, the stoichiometry is the dominant factor in determining the resistivity.

As stated above when cadmium sulphide is heated, the vapour dissociates into cadmium atoms and sulphur molecules, which recombine on cooling. At any given temperature the partial pressures of sulphur (S_2) and cadmium (Cd) are related by equation (4.8), where it can be seen that if a small excess of cadmium is present, the sulphur vapour pressure is reduced, and as a consequence the vapourization of CdS is reduced. If the system is continuously exhausted, as in vacuum deposition the excess cadmium vapour will fall rapidly until the cadmium to sulphur ratio in the vapour is similar to that in the solid, and the sublimation is then termed congruent [12,15]. Thus at equilibrium the more stoichiometric the starting material, the more stoichiometric is the vapour from which condensation is to take place and this is why ultra-high purity cadmium sulphide has been used as the starting material in all deposition experiments carried out by the author. A slow growth rate [15] is necessary if congruent evaporation is to be achieved in order to give the vacuum pumping system enough time to exhaust the excess vapour. At residual gas pressures of the order of 10^{-5} cadmium sulphide evaporates congruently [12].

When films are deposited in vacuum by sublimation of cadmium sulphide, in most cases the films tend to have excess cadmium in them even when congruent evaporation is used. This is because of the

difference in the accommodation coefficients [11] of sulphur and cadmium atoms on the substrate. To ensure the stoichiometry of a deposited film, excess sulphur must be present during deposition. Excess sulphur may be introduced into the deposition chamber either by evaporating sulphur from a separate crucible or by adding extra sulphur in the cadmium sulphide crucible. The latter method has been used to deposit stoichiometric films in most experiments in this work. The amount of excess sulphur vapour used must not be so large that the pressure inside the deposition chamber is so high that little cadmium sulphide vapourization occurs. Too much excess sulphur also means that a lot of sulphur deposits on the cooler part of the deposition chamber, e.g. the base-plate and the diffusion pump inlet making their cleaning (for a consequent deposition run) much more difficult, apart from the waste of high purity material.

The co-evaporation of cadmium and sulphur has also been used by many authors to produce stoichiometric films of cadmium sulphide (see Chapter 3). Their methods fall broadly into two categories. The first is the co-evaporation from crucibles of roughly the same area whose temperatures are independently controlled to give the required ratio of sulphur to cadmium atoms incident on the substrate and the required deposition rate. The second method is to vapourize cadmium and sulphur from two separate concentric cells held at the same temperature whose orifice areas are controlled to give the required ratio between rate of arrival of sulphur molecules, N_S, and cadmium molecules, N_{Cd}. This method is more versatile since it offers the advantage of varying the evaporation rate without varying the temperature of the source by changing the area of the orifice. In all the other methods, for a given pumping speed and a given substrate temperature, the only way to increase the evaporation rate is to increase the temperature of the source. Because vapour pressure depends very strongly on temperature (see Fig. 4.1), the ratio [11]

between sulphur vapour pressure and cadmium vapour pressure varies with temperature as shown in Fig. 4.2. When the two cells are held at the same temperature (isothermal source), the ratio $\frac{N_S}{N_{Cd}}$ is determined by the ratio between the orifice areas. From equations (4.3) it follows that :

$$\frac{N_S}{N_{Cd}} = \left(\frac{M_{Cd}}{M_S}\right)^{\frac{1}{2}} \frac{A_S}{A_{Cd}} \cdot \frac{\Sigma(2n)^{\frac{1}{2}} P_{S_{2n}}}{P_{Cd}} \qquad \ldots\ldots\ldots (4.9)$$

where A_S and A_{Cd} are the areas of the sulphur and cadmium orificies, respectively, and the other symbols have the same significance as before. The Σ term is introduced [11] to account for all possible species of the sulphur molecules (S_{2n}). Equation (4.9) can now be used to determine the orifice areas of the sulphur and cadmium cells. For example, for cells at a temperature of 420°C, when a sulphur orifice of 0.5 mm diameter is used, then a cadmium orifice area of 48 mm is required to give a sulphur to cadmium ratio of 5 at the substrate. The actual area of orifices used depends on the deposition rate required and on the pumping speed of the pumping system. This method has also been used in the present work because it has the advantage that the vapour molecules are less hot than those from CdS evaporation. The effect of the temperature of the vapour molecules on the nucleation and the crystallogric structure of as-deposited films is discussed in section 8.4.3.

Because the transit speeds of cadmium and sulphur vapour atoms are different (section 4.2.2), it may be possible to increase the stoichiometry of a deposited film by using a rotating-vane particle velocity filter to increase the ratio of sulphur to cadmium atoms incident on a substrate. The use of such filters has been reported [23] for the deposition of low scattering dielectric mirrors for laser applications. Another factor that may affect the stoichio-

$$B = \frac{\sum_{n=1}^{4} (2n)^{1/2} \; P_{S_{2n}}}{P_{Cd}}$$

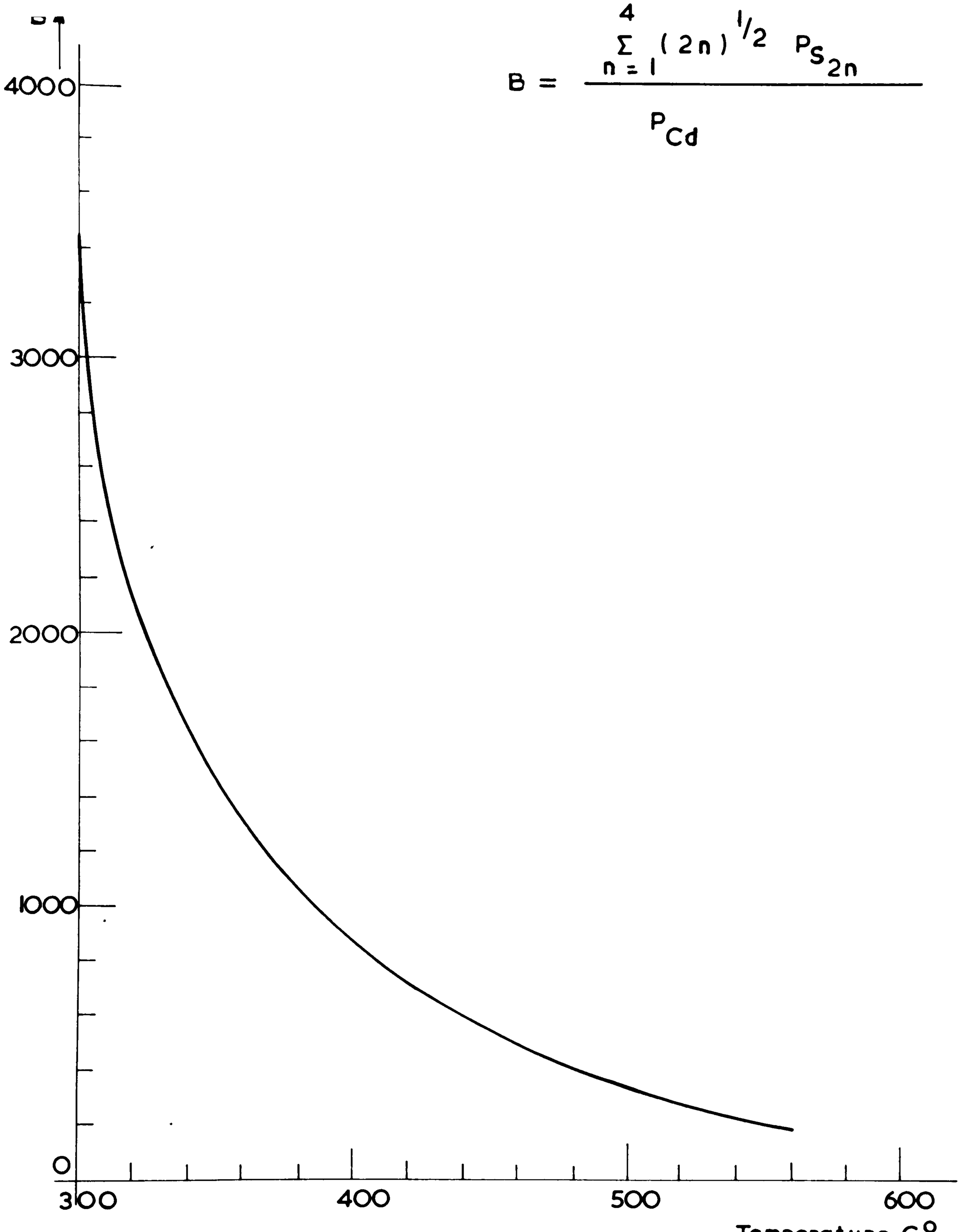

FIG 4.2. Variation of ratio of vapour pressure of sulphur to that of cadmium with temperature (after Beecham[11])

metry of a deposited film is thermo-diffusion [21] : When a gaseous mixture of atomic (or molecular) species of different molecular weights is subjected to a temperature gradient, a stationary state is set up in which the gas mixture at the hot (crucible) side is enriched in the heavier (cadmium) species, whereas that at the cold (substrate) side is enriched in the ligher (sulphur) species.

4.5.2. Evaporation mechanism of cadmium-sulphide

Since one of the products (S_2) of the dissociation of CdS does not occur as a unit in the crystal lattice, the evaporation must proceed by a number of steps. One possible sequence [12] is :

(i) The formation of Cd and S surface atoms at their lattice positions :

$$CdS\ (\text{solid molecule}) \xrightarrow{H_1} Cd\ (\text{surface atom}) + S\ (\text{surface atom})$$

(ii) Diffusion of Cd and S atoms on the surface

(iii) Recombination of S atoms to form S_2 molecules :

$$S\ (\text{atom}) + S\ (\text{atom}) \xrightarrow{H_2} S_2\ (\text{molecule})$$

(iv) Evaporation of Cd atom from the surface into vacuum :

$$Cd\ (\text{atom}) \xrightarrow{H_3} Cd\ (\text{gas})$$

(v) Evaporation of S_2 molecule from the surface into vacuum :

$$S_2\ (\text{molecule}) \xrightarrow{H_4} S_2\ (\text{gas})$$

In this sequence all the steps are endothermic i.e. they require activation (heat) energy, except (iii) which is exothermic. The H's represent the enthalpies of the reactions and by convention [5] they are taken to be positive for endothermic, and negative for exothermic reactions. They represent the heats absorbed or evolved during the reaction by one mole of the material. During condensation of CdS the reverse of the above sequence may represent the formation of cadmium sulphide (solid) from cadmium vapour atoms and sulphur vapour molecules, with all the steps being exothermic except (iii) which is endothermic.

Another possible sequence for the formation of a CdS crystal from Cd (vapour) and S_2 (vapour) is :

(i) Conversion of gaseous cadmium atoms and sulphur molecules to solid (exothermic: heat of condensation H_c)

(ii) Conversion of solid S_2 molecules to S atoms (endothermic : dissociation energy H_d)

(iii) Conversion of sulphur atoms to sulphur ions by gain of electrons (exothermic: electron affinity H_e)

(iv) Conversion of cadmium atoms to cadmium ions by loss of electrons (endothermic : ionization energy H_i)

(v) Combination of cadmium and sulphur ions to form crystalline cadmium sulphide (exothermic : lattice energy H_ℓ)

A direct reaction between cadmium and sulphur atoms gives cadmium sulphide, the entholpy of the reaction being the heat of formation, H_f. In as much as the direct and step-wise paths give crystalline CdS the total energy change must be the same i.e. $-H_f = -H_c + H_d - H_e + H_i - H_\ell$. It is the lattice energy, H_ℓ, which is chiefly responsible [5] for the substantial amount of energy released during the formation of the crystal. It is a measure of the attraction between the negative ions $S^=$ and the positive ions Cd^{++}, and this energy of attraction takes up most of the heat supplied during vapourization. The heat of sublimation of CdS is equal [4] to 2.1 $kJ.g^{-1}$. The effect of the heat energy released by the vapour molecules during vapour deposition on the temperature of the growing face of a deposited film, and on thermal stresses in the film are discussed in Chapter 6.

In the above model it was assumed that the bond between sulphur and cadmium atoms in cadmium sulphide is ionic rather than co-valent. However, the bonds [4] in most II-VI compounds are not adequately described by any of these extreme types of bond, but have characteristics intermediate to those usually associated with

the terms ionic and co-valent. More fundamental research is needed to understand the nature of the bonds in these compounds, as well as their evaporation mechanism.

C H A P T E R 4

REFERENCES

1. G. Lewin, *Fundamentals of vacuum science and technology*, McGraw-Hill (1965).

2. L. Holland, *Vacuum depositing thin films*, Chapman & Hall (1966).

3. K.G. Gunther, chapter in *The use of thin films in physical investigations*, ed. J.C. Anderson, Academic Press (1966).

4. M. Aven et al ed. *Physical and chemical properties of II--VI compounds*, North-Holland (1967).

5. J.C. Bailar et al, *University chemistry*, Heath & Co. Boston (1965).

6. J. Yarwood, *High vacuum techniques*, Chapman & Hall (1967).

7. G.H. Rayner et al, *SI units*, NPL (1970).

8. R.W. Berry et al, *Thin film technology*, Van-Nostrand (1968).

9. M.W. Zemansky, *Heat and thermodynamics*, McGraw-Hill (1957).

10. K. Mehmet, *Ph.D. Thesis*, University of Warwick (1970).

11. D. Beecham, *Cadmium/sulphur isothermal source CdS deposition*, Rev. Sci. Inst. 41, 11, p. 1654 (1970).

12. G.A. Somarjai et al, *Evaporation mechanism of CdS single crystals*, J. Cheml. Phys. 41, 5, p. 1389 (1964).

13. P.J. King, *The optimum conditions for the evaporation of CdS films*, Brit. J. App. Phys. 2, p. 1349 (1969).

14. J. DeKlerk et al, *Vapour deposited t.f. piezoelectric transducers*, Rev. Sci. Inst. 36, p. 506 (1965).

15. D.C. Shotton et al, *The growth of CdS crystals*, G.P.O. Res. Dept. Rep. No. 6 (1968).

16. A.N. Nesmeyanov, *Vapour pressure of the elements*, Infosearch, London (1963).

17. P.D. Fochs et al, *Growth of CdS single crystals of controlled composition from the vapour phase*, J. Cryst. Growth 3, p. 122 (1968).

18. D.W.G. Ballentyne,et al, *Kinetics of vapour growth of II-VI compounds in a sealed tube*, J. Cryst. Growth 7, p. 79 (1970)

19. R.J. Caveny, *The role of dissociation in the growth of CdS crystals*, J. Cryst. Growth 7, p. 102 (1970).

20. N.B. Hannay ed. *Semiconductors*, Chapman & Hall (1960).

21. F.A. Kroger, *The chemistry of imperfect crystals*, North-Holland (1964).

22. N.F. Foster, *CdS evaporated-layer transducers*, Proc. IEEE 53, p.1400 (1965).

23. Ministry of Technology, *Particle filtration*, Tech-Link No. 588 (1970).

C H A P T E R 5

Film deposition: experimental work

5.1. Introduction

The author's own work on the vacuum deposition of s-mode CdS transducers suitable for low frequency operation is described in this chapter. The two isothermal methods used, namely the CdS/S electron beam evaporation and the Cd/S furnace evaporation are discussed in detail. The procedure undertaken in a typical CdS/S or Cd/S deposition run is described together with a versatile substrate holding arrangement enabling the deposition of films with a wide-range of deposition angles and film thicknesses in one deposition run. It is pointed-out that no such holding arrangement has been reported outside this work. A survey of the CdS deposition runs is also given.

5.2. Pumping-down the vacuum chamber

A conventional manually-controlled high vacuum pumping system was used (Birvac Torr Plan Type T4). The system (Fig. 5.1) incorporates a rotary pump (Edwards Model ES150) which backs on oil vapour diffusion pump (Edwards Model E04) whose maximum un-baffled pumping speed is 600 litres s^{-1}. The rotary pump has a gas-ballast facility to reduce the vapour condensation inside it. Air from the atmosphere is admitted to the pump via a one-way gas-ballast valve at a suitable time in the revolution of the rotor. The diffusion pump has a magnetic valve delay device to protect it in case of rotors pump failure and a liquid nitrogen trap to prevent the back-diffusion of oil vapour into the deposition chamber and to improve the ultimate vacuum achieved.

A pumping cycle starts by evacuating the backing line of the diffusion pump to a pressure of better than 1 torr. The diffusion

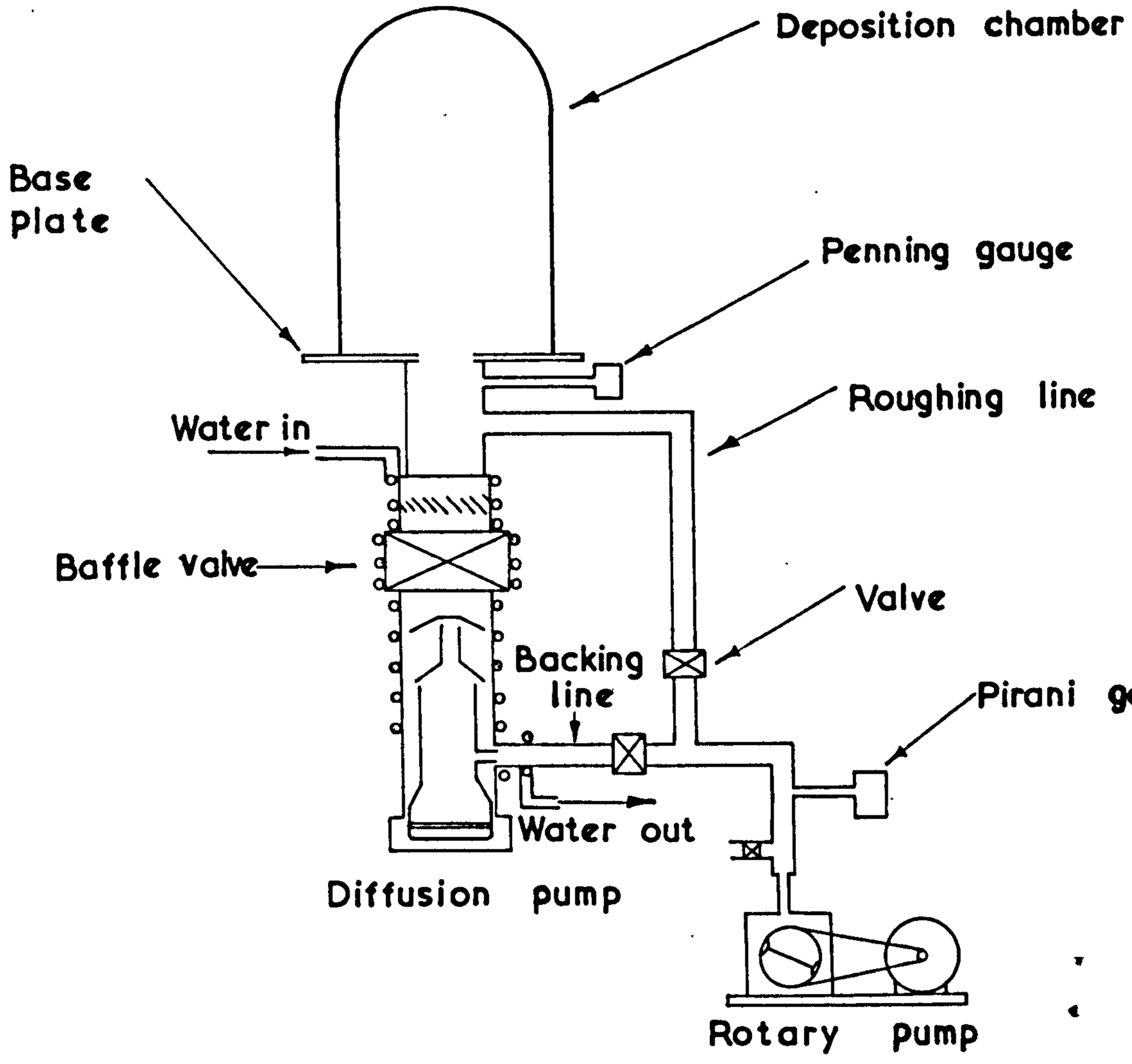

FIG. 5.1 Schematic diagram of high- vacuum pumping system

pump takes about 20 minutes to heat up during part of which the deposition chamber is evacuated through the roughing line, with the backing line valve closed. This valve is then closed and the backing line valve opened. After filling the liquid nitrogen trap the baffle valve is opened. The time the pumping system takes to evacuate the deposition chamber to better than 10^{-5} torr varies from one to six hours depending on the temperature, the surface area and the number of items to be out-gassed inside the deposition chamber. A Pirany gauge monitors the backing line pressure (typically 0.1 torr) while a Penning gauge indicates the pressure inside the chamber. The liquid nitrogen trap is topped-up every three hours. The use of an automatic liquid nitrogen trap topper has been reported [1]. To shut down the pumping system, the baffle valve is closed and the diffusion pump heater switched off. The rotary pump stays on backing the diffusion pump while it is cooling down for about 10 min. The backing line valve is then closed and the rotary pump switched off.

A plastic tube carried the exhaust from the rotary pump outlet out of the laboratory where the deposition experiments were carried out. This reduced the danger of exposing the experimenter to the highly toxic [2,3] cadmium vapours. Cadmium metal particles are also known to be highly poisonous [2,3]. During some deposition runs the author wore "Filtron" surgical masks (supplied by Industrial Pharmaceutical Service Ltd.).

5.3. Setting-up the deposition chamber

In all film deposition experiments carried out by the author, the deposition chamber (Fig. 5.2) incorporated the following :

(1) A pyrex bell jar 300 mm diameter and 350 mm high with a "Viton" gasket. A shutter to stop the direct vapour beam from reaching the substrates. A variety of shutters were used depending on the requirements of a particular deposition run. Provisions were included

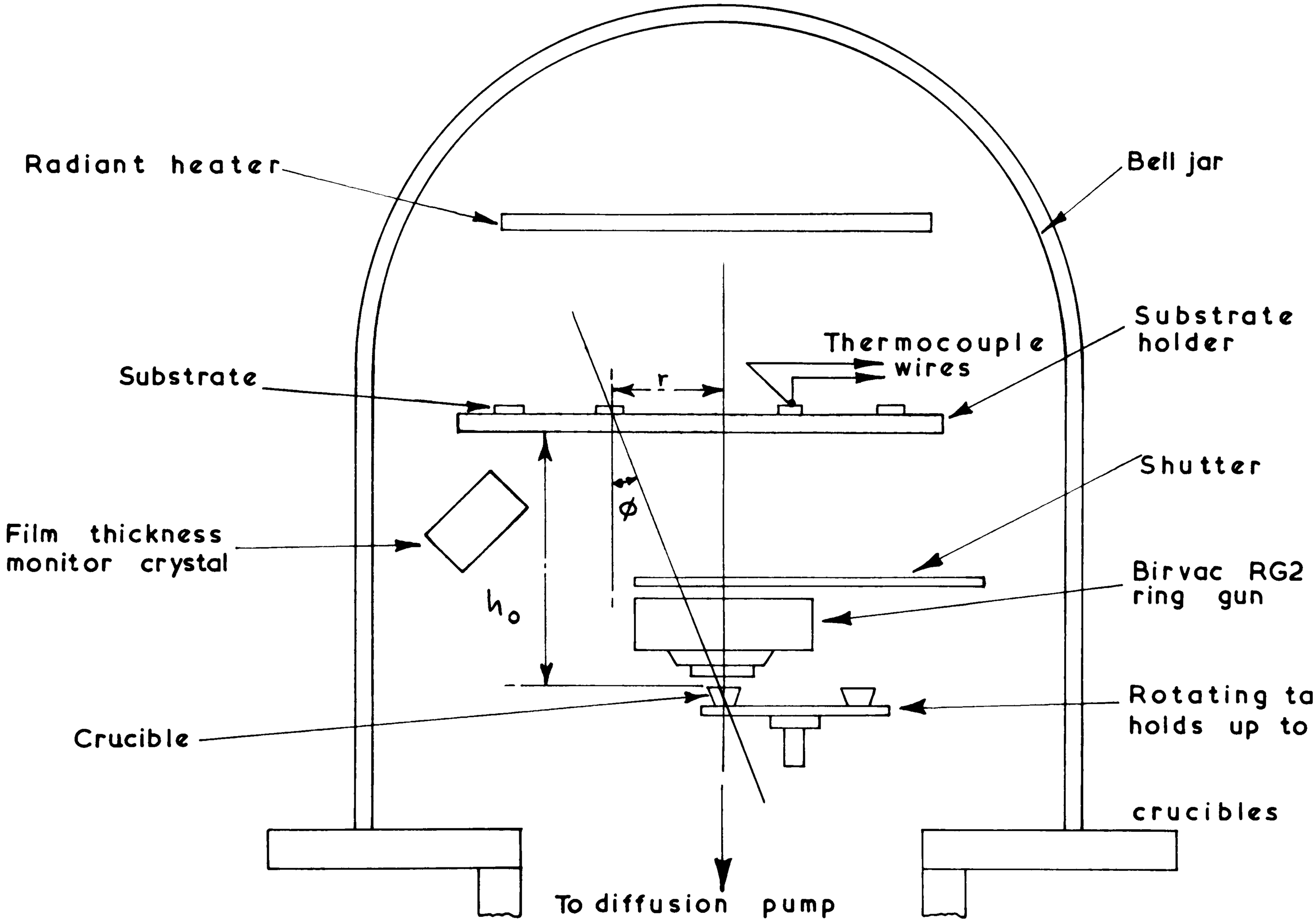

FIG. 5.2 Schematic diagram of electron beam bombardment evaporation chamber.

for rotating the shutter from outside the chamber using a vacuum-tight rotary shaft (Birvac TR8S).

(2) A thermocouple to monitor the substrate temperature. The thermocouple wires (chromel-alumel supplied by British Driver Harris Ltd.) were spot-welded to form a junction. The thermocouple junction was secured inside a hole drilled in a dummy substrate. The thermocouple wires were fed through a vacuum lead-through (Edwards Type TL8). This was preferred to the other more convenient (and more expensive) lead-through (Type TL4A) because in the latter the thermocouple wires terminate at the lead-through posts *inside* the vacuum chamber. This meant that the thermocouple cold-junction was not at room temperature. It was measured to be about 40^{o}C when the substrate temperature was held at 200^{o}C. This would introduce an appreciable error in substrate temperature measurement. To eliminate this error the thermocouple junction must be *outside* the deposition chamber. Therefore, the thermocouple wires were actually made to go through the lead-through and set in "Araldite" which formed a good vacuum-seal.

(3) A substrate heater to raise the substrate temperature to the required value. A 1 kW ceramic boiling ring heater (Metway Ltd.) was used. Later, a metallic ring heater (Electricity Board) of the type used in modern cookers was used. The former was unreliable because its resistance wire was liable to break during a deposition run. When this happend it meant that film deposition had to be interrupted to replace the heater. The deposited films would be exposed to the atmosphere during heater replacement. This might lead to the formation of thin oxide layers on the surfaces of the films which might mean that consequent deposited layers would flake-off. The heaters were always out-gassed and baked in vacuum before being used in a deposition run. The power input to the heater was fed

through a 10A "Quadrac" thyristor unit (West Instruments Ltd. Type THL-10A-250). The thyristor was fired in a cycle syncopation mode by pulses from a "Gaurdian" three-term (proportional + derivative + integral) controller (West Type Q3X). This controller compared the substrate thermocouple signal with a highly stabilised reference voltage corresponding to the set-point temperature. The difference between them would be amplified and used to control the firing pulses to drive the thyristor.

(4) A vapour source which consisted of a cermet crucible heated by electron beam bombardment (e.b.b.) The e.b.b. ring gun (Fig. 5.3) was supplied by Birvac Ltd. complete with its Type RC power pack. This gun focusses electrons from a circular molybdenum filament (hot-cathode) on a crucible which is mounted on a stainless steel turn-table. The turn-table can hold up to six crucibles so that different materials can be evaporated without breaking the vacuum inside the chamber. Provisions for rotating the turn-table from outside the chamber are included. The electrons are work-accelerated when the H.T. voltage is applied between the gun and the crucible. The electrons lose most of their kinetic energy as heat generated direct in the evaporant. The power pack provides an L.T. filament supply of up to 30A at 10V and an H.T. supply of up to 300 mA at 4.5 kV. Geometric focussing is used, and it is varied by moving the crucible up or down relative to the ring gun. In most CdS deposition experiments in the present work, the electron beam was diffused to cover most of the area of the top face of the crucible. Under such conditions the variation of crucible temperature with H.T. beam power was as shown in Fig. 5.4. Because the top face of the crucible was very close to the bottom of the gun which was at a high potential, it was not possible to measure the temperature there. Instead the temperature at the wall of the crucible where it touched its securing molybdenum clip was measured. Another difficulty

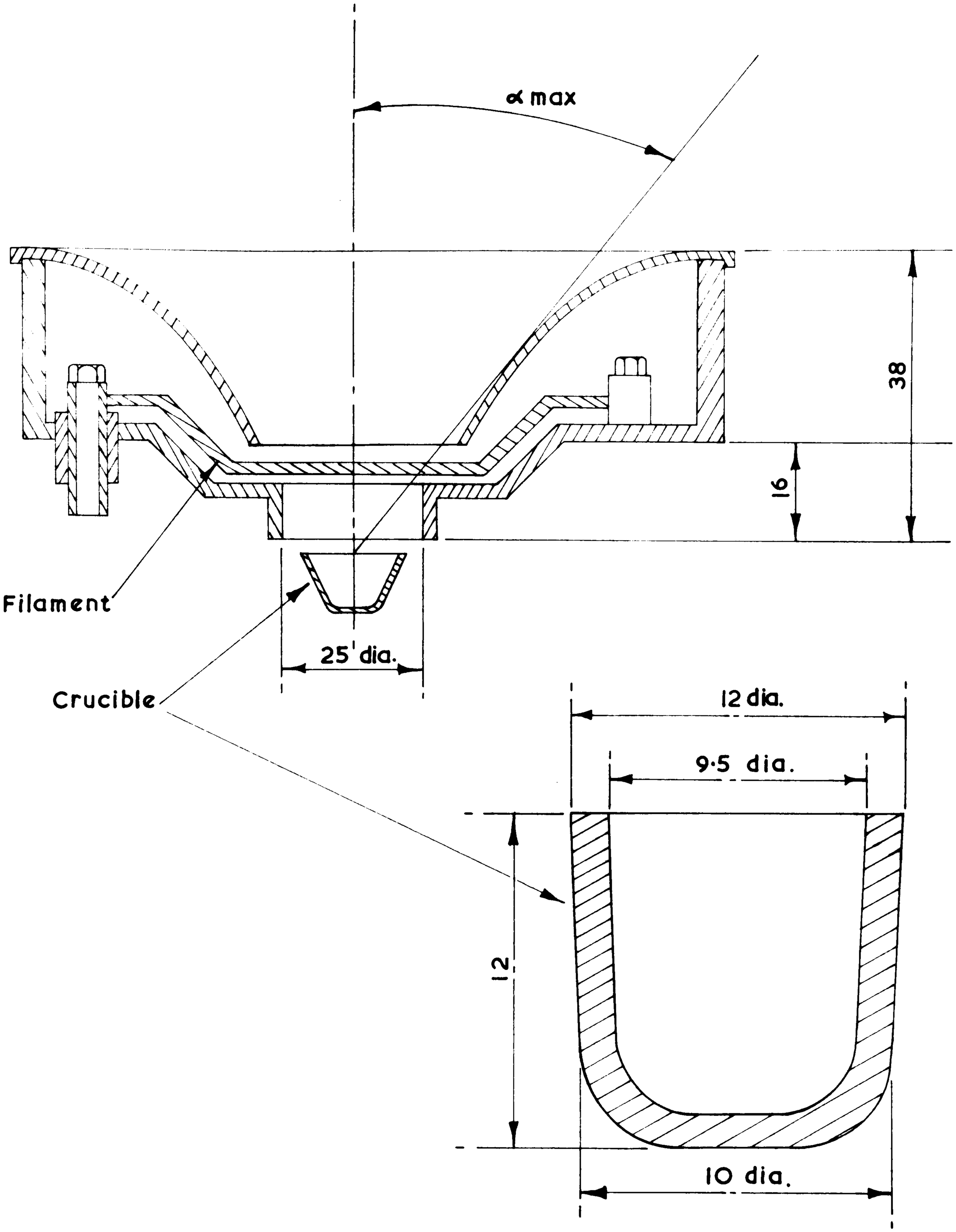

FIG. 5.3

RG2 Ring Gun.
(Dimensions in mm)

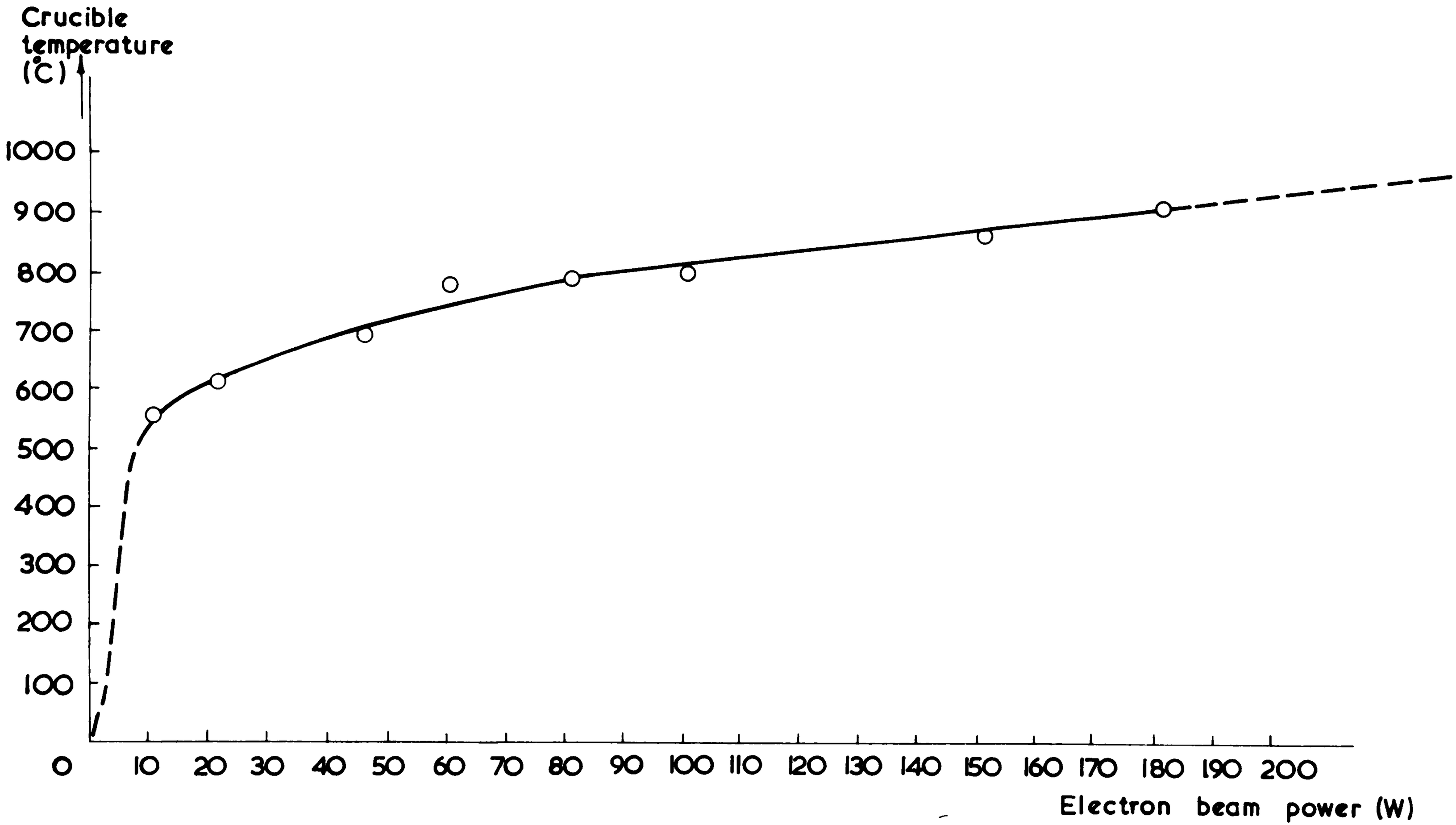

FIG. 5.4. Variation of crucible temperature with electron beam power.

during the measurement of crucible temperature was the interference of the electron beam with thermocouple (millivoltmeter) voltage indication, making it oscillate. Therefore, the temperature given in Fig. 5.4 were those recorded after switching off the H.T. supply. Because of the high temperatures involved the crucible would cool by at least few tens of degrees before its temperature was recorded. Also, the temperature of the evaporant is thought to be about 150^{o} higher than that measured. This is because the clip forms part of the turn-table which acts as a heat-sink for the crucible. It is claimed [4] that when the electron beam is focussed to a spot 1 mm diameter the temperature at the spot would be about $4000^{o}C$. The cermet crucibles (80% molybdenum by weight and 20% alumina with their walls lined with molybdenum) were supplied by Morganite Research and Development Ltd. for use up to $1900^{o}C$ ("Metamic" 519 Type C44). Cermet crucibles are preferred to carbon ones because the latter material is easier to evaporate at higher temperatures thus contaminating the deposited films. The advantages of using e.b.b. heating are discussed in section 3.4.1.

(5) As an alternative to (4) above the vapour source consisted of two concentric pyrex cells heated inside an alumina furnace (Fig. 5.5). The furnace and its a.c. power supply were designed by the author. The furnace comprised an alumina tubing 64 mm I/D and 75 mm O/D, and 120 mm long. About 20 turns of 20 S.W.G. (0.9 mm) "Kanthal" resistance wire were wound around it with a pitch of about 5 mm. The "Kanthal" wire was supplied by Hall & Pickles Ltd. Slots were cut on the outside of the wall of the alumina tubing to accommodate the wire and securing clips through which every turn of the wire was threaded. This ensured that the coil turns did not sag and short-circuit when the furnace was in use. An alumina-silica-fibre "Kaowool" blanket of very

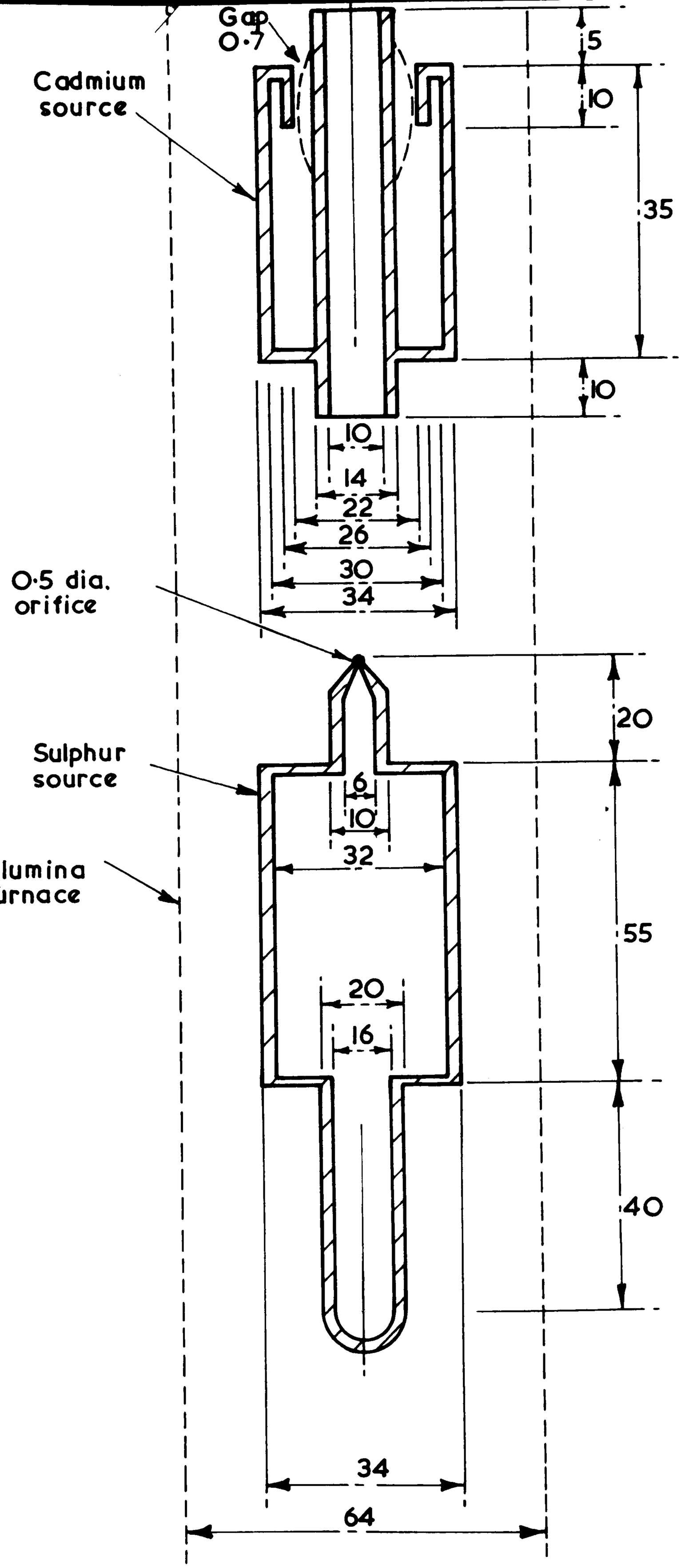

FIG 5.5 — Cadmium / Sulphur isthermal source (MK II)
(Dimensions in mm)

low thermal conductivity was then made to surround the furnace in order to increase the ultimate temperature attainable inside the furnace and to decrease the temperature rise time-constant. The "Kaowool" blanket was supplied by Morganite Ceramic Fibres Ltd., and contained no organic binders. Therefore, there was no danger of it contaminating the substrates. As a further precaution against contamination from the furnace, and to reduce its radiation heat loss, a thin-walled aluminium tubing (125 mm diameter) was made to surround the furnace. To the top of the aluminium shield was attached an annular ring whose I/D was the same as that of the alumina tubing and whose O/D slightly overlapped the aluminium shield. This insured that no part of the furnace was "seen" by the substrates. The furnace was connected across the secondary of a 2:1 transformer and drew up to 11A at 110V. The temperature inside the furnace went up to 400^{o}C in 2 min. The primary of the transformer was connected in series with a 20A thyristor unit (West Type TH-KD-P-20A-250) complete with its anti-surge RC network to prevent the large on-and-off in-rush currents in the transformer from burning out the thyristor. The furnace temperature was controlled using a "Gaurdian" controller in the same manner as discussed in (3) above. The author also designed the cadmium and sulphur pyrex cells (Fig. 5.5) on lines similar to those described by Beacham [5]. Various orifice sizes were used depending on the evaporation rate and film thickness required, see section 5.5 below. The cells were made in the University Workshops. A sulphur cell would be filled with sulphur first, and its bottom tube drawn and sealed as shown in Fig. 5.5. A cadmium cell would be filled with the required amount by feeding cadmium shots (1-3 mm) through the side arm which would later be drawn and sealed. There would be plenty of room for the sulphur and cadmium to expand inside the cells on melting.

(6) A Pirani gauge head (Birvac Type H202) and a Penning head (Type H2002) to monitor the vacuum inside the chamber. Because of the position of the outlet of the head of the Penning gauge in the deposition chamber, thin-film particles often got in and made the gauge give a false reading to its control unit (Birvac Type T2002). When this happened, the gauge head would be dismantled and cleaned. It was also cleaned after every deposition run. The use of a fine stainless steel mesh was thought to be insufficient to prevent small particles from getting inside the head.

(7) A monitor crystal complete with its heat shield. This crystal (6 MHz s-mode quartz) formed part of the Edwards Film Thickness Monitor (FTM) Model 1. Its principle of operation is the change in the natural resonance frequency of the monitor crystal as it gets loaded by a depositing film. A second (reference) crystal whose resonance frequency is 6.5 MHz is mounted in an oscillator unit outside the vacuum chamber. The difference between the two crystal frequencies is amplified within this unit and fed into a main unit where it is mixed with a variable oscillator to produce a final difference frequency of between 0 and 150 kHz. The mass of a depositing thin film causes a reduction in the resonance frequency of the monitor crystal, causing an increase in the final difference frequency. This change is converted to a d.c. signal which actuates a frequency shift meter and a rate-meter. The manufacturers claim [6] that the frequency shift is proportional to the film thickness. Using the manufacturers calibration line for aluminium films, the dependence of frequency shift on film thickness for various materials was plotted (Fig. 5.6). Optical and "Talysurf" thickness measurements were used as a check on CdS film thickness which was also inferred from static capacitance measurements (see Chapter 9). It turned out that the films were

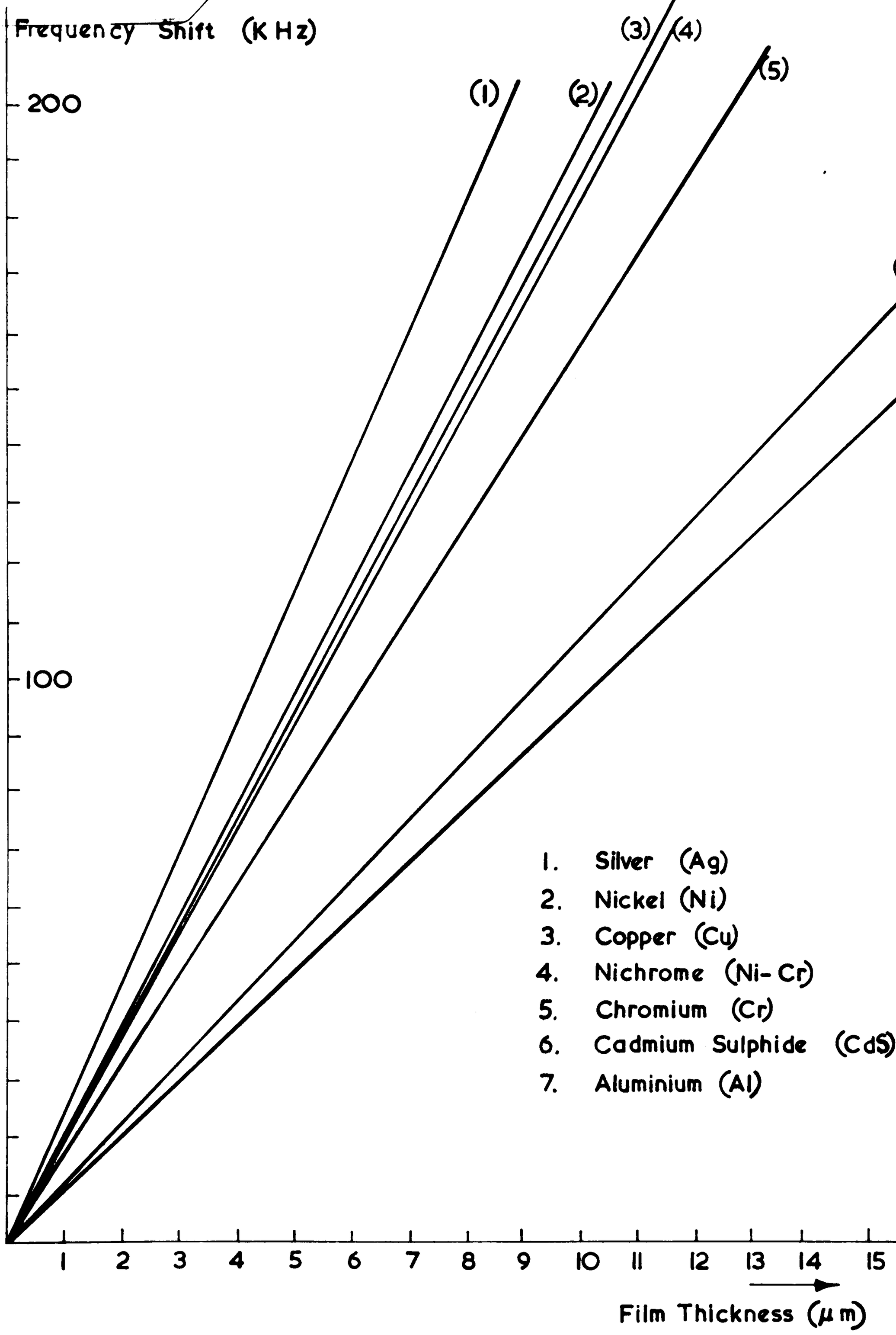

FIG. 5.6 Calibration chart for Film Thickness Monitor.

approximately half as thick as predicted by the calibration chart. It is thought that the difference arises because the manufacturer's calibration crystal frequency is approximately proportional to the mass of the deposited film, whereas it should, in fact, be the square root of the mass. To a first approximation the change in square root of the mass may be taken as equal to half the change in mass. Using this as a basis for calibration, excellent agreement was found between predicted (Fig. 5.6) and measured film thickness. Another problem encountered with the film thickness monitor was the burning out of the first stage of the amplifier in the oscillator unit during film deposition. This was due to excessive charge build-up from the electron beam on the monitor crystal leads. The crystal itself was shielded in an earthed can, but its wires were insulated from earth in order to carry the crystal signal. This was overcome by putting the two insulated crystal leads inside the outer braid of a co-axial cable and earthing it.

(8) A substrate holder. Various holders were made of non-magnetic stainless steel (Cashmores Ltd. Type EN58J). Figure 5.7 shows a disc holder 9 mm thick suitable for holding welding-electrode-insert substrates, (Mk. IIIb) while in Fig. 5.8 a 3 mm thick holder is shown for holding glass slides and 0.5 inch (12.5 mm) rod substrates (Mk. II). The holes for the rod substrates were arranged on pitch circles whose radii determined the horizontal distance, r, between the centre of the disc (which is vertically above the centre of the vapour source) and the substrate. The dimension, r together with the height, h_o, of the holder above the source determined the deposition angle, $\emptyset$, between the vapour beam and the substrate-normal. Thus, $\emptyset = \tan^{-1} \frac{r}{h_o}$. All substrates on the same P.C.D. had the same deposition angle. For a given holder height the deposition angle may be varied by varying r. Alternatively, for a fiven r the deposition angle may be varied by varying h_o.

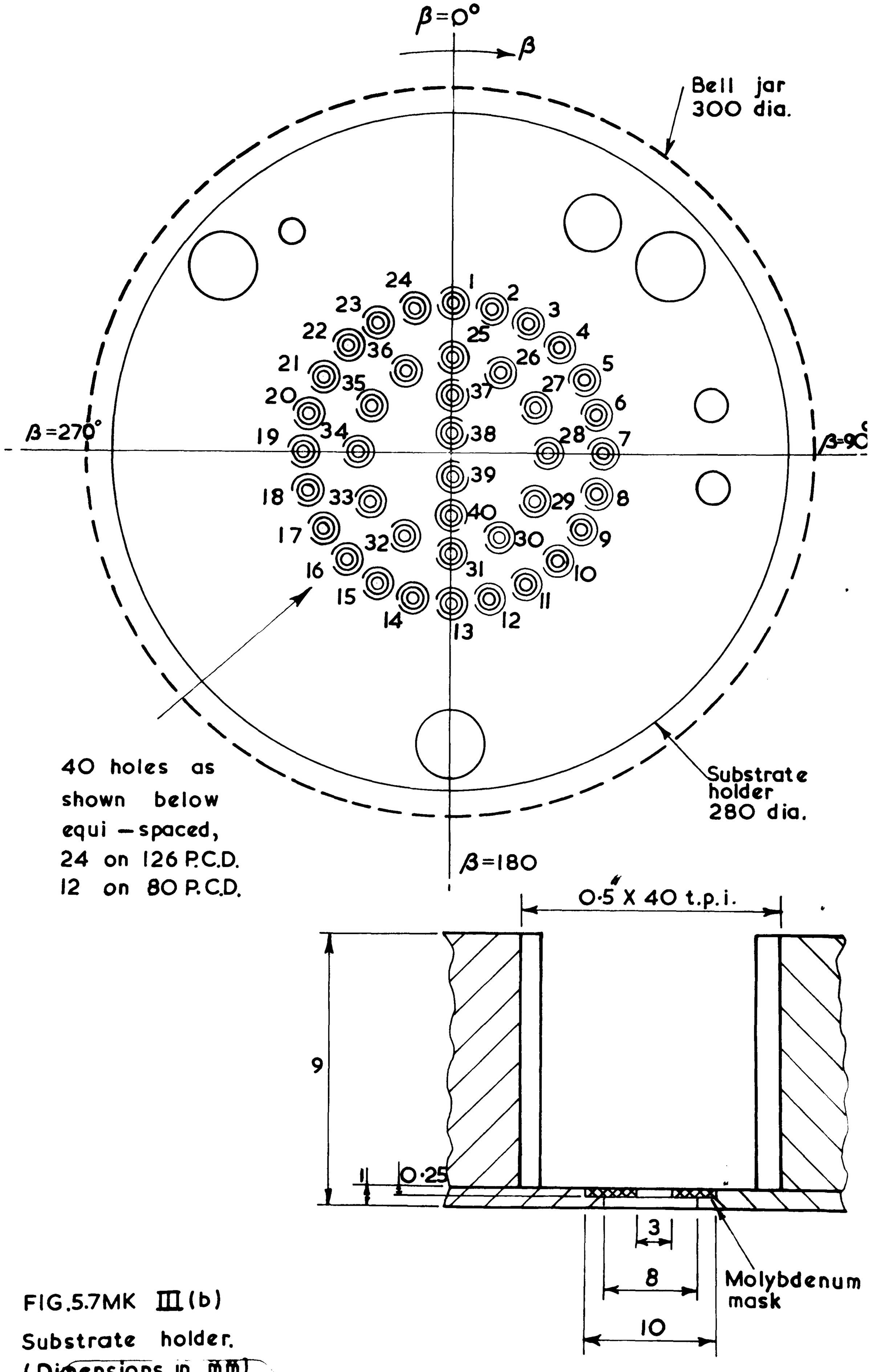

FIG.5.7MK III(b)

Substrate holder.

(Dimensions in mm)

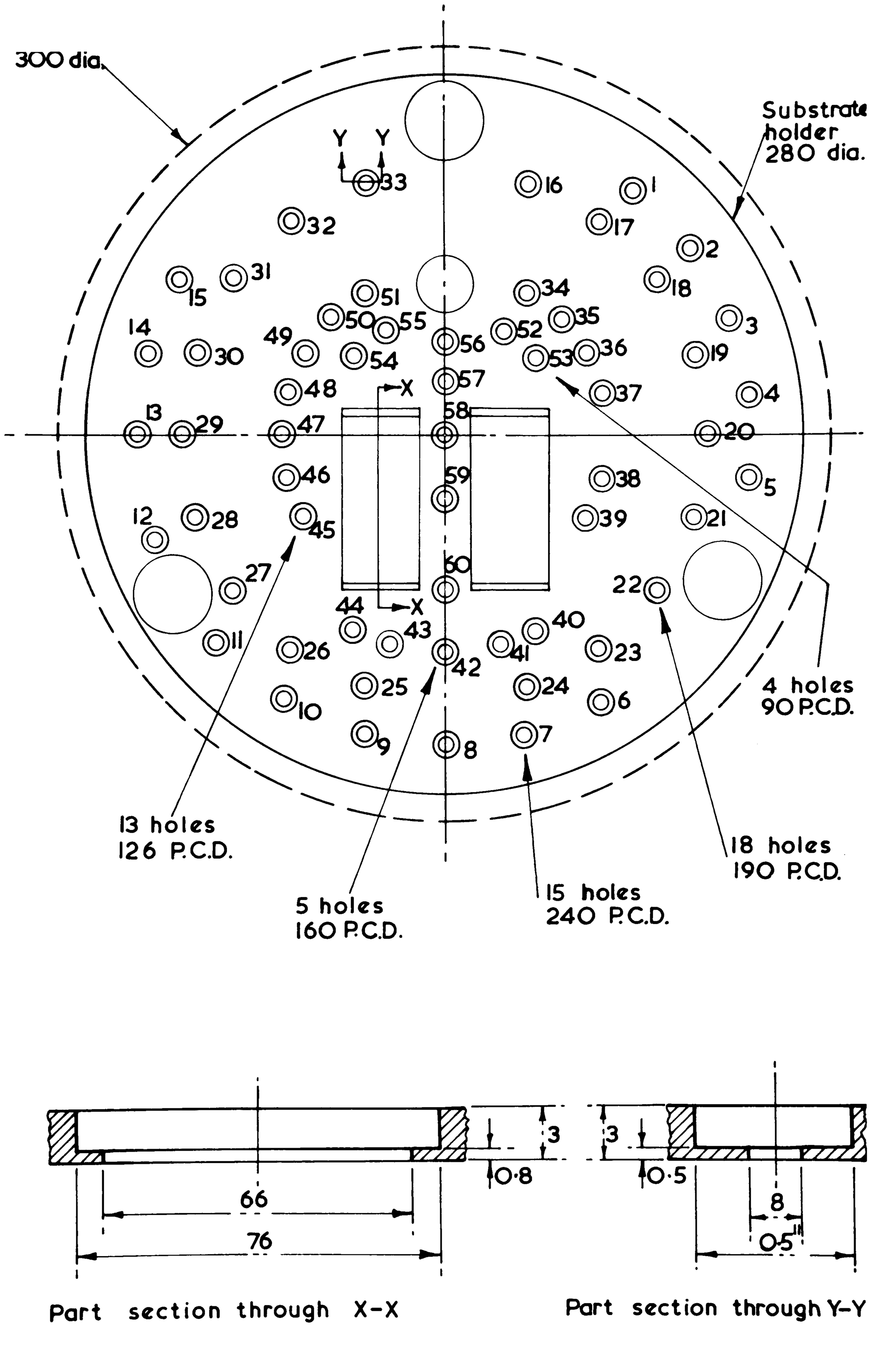

Part section through X-X

Part section through Y-Y

FIG. 5.8 MK II Substrate holder
(Dimensions in m m)

Varying r or h_o alters the film deposition rate and the final film thickness. Film thickness distribution is discussed below (section 5.4) together with the more complicated case when the substrate holder is not horizontal. A big advantage of this type of substrate holding arrangement is the mass production of thin film transducers. As far as is known, most workers who use deposition at an angle, place their substrates vertically above the source with the consequent limitation on the number of substrates used (see section 3.4). The consequent saving in time and evaporant material is even more important when thick films are required. Another advantage of the present arrangement is that it is directly applicable to the deposition of a thin film transducer on a slot milled in a disc wheel-electrode of the type used in seam-welding. This was one of the aims of this project when it started (see Chapter 1 and Chapter 11). The masking arrangements were such that the end products were disc CdS transducers comprising a bottom electrode, an ultrasonically active layer of CdS, and a top (backing) electrode. Molybdenum sheets 250 μm thick were used as masks. For glass slides the masks were rectangular sheets with holes punched in them to give the required size of the backing electrode. These sheets were placed in slots milled in the holder, with the glass slides on top of them (Fig. 5.8). For rod substrates, the masks were in the form of discs which fitted in recesses milled in the substrate holder (Fig. 5.7). The size of a hole punched in the centre of one of these discs determined the area of the substrate exposed to the vapour beam.

5.4. Deposition angle and film thickness distribution

When the substrate holder is horizontal, the deposition angle, ϕ, is given by $\phi = \tan^{-1} \frac{r}{h_o}$, see Fig. 5.2. However, when the plane of the substrate holder is inclined at an angle, γ, to the vertical (Fig. 5.9), the deposition angle is given by :

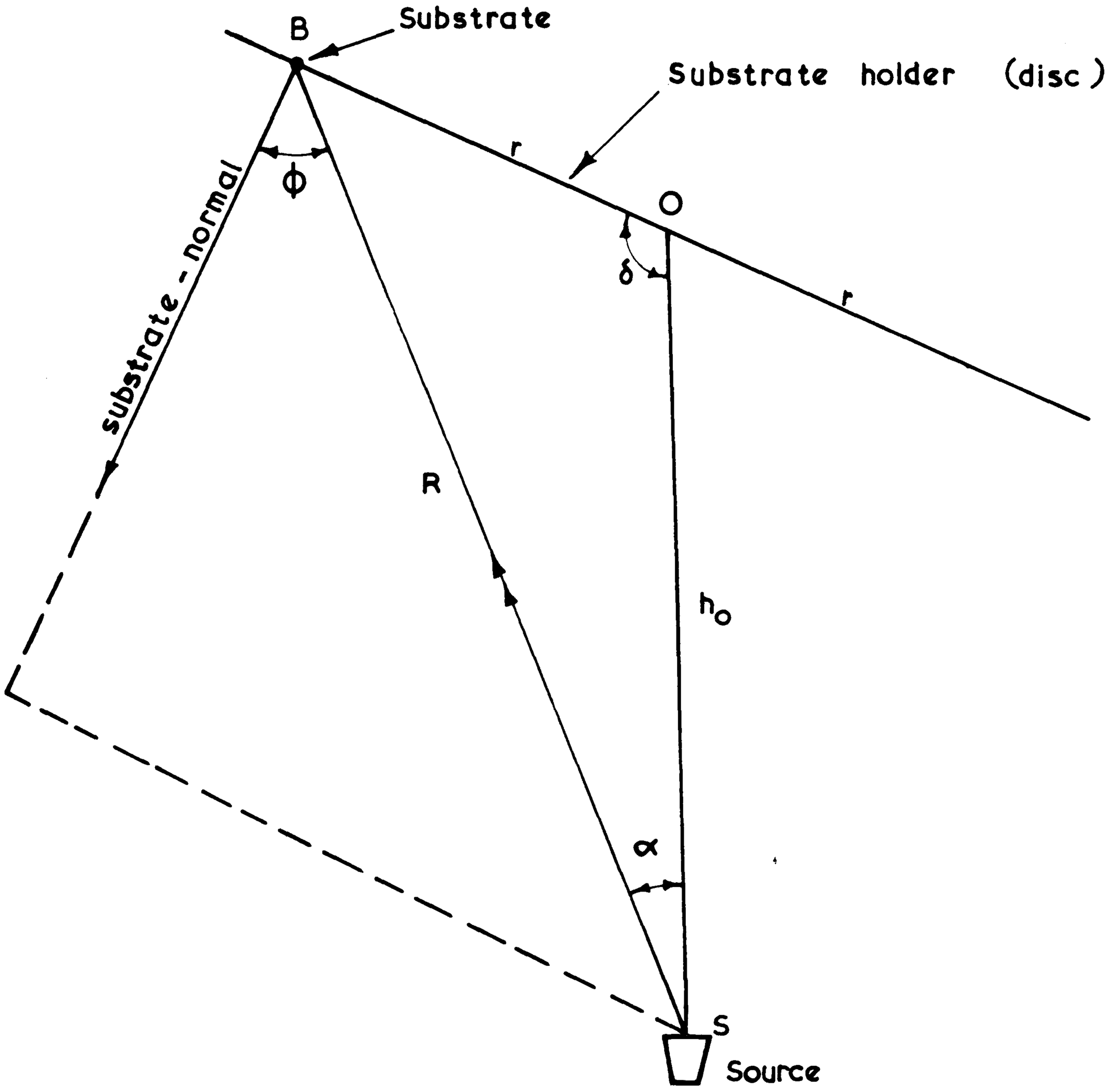

FIG. 5.9 Deposition geometry.

$$\phi = \cos^{-1}\left(\frac{h_o \sin\delta}{R}\right) \qquad \ldots\ldots\ldots (5.1)$$

where δ is the angle between the line joining the substrate to the centre of the disc (holder) and the vertical, and R is the substrate-to-source distance. It is also seen from Fig. 5.9 that $R = h_o^2 + r^2 - 2h_o\, r\, cr\, \delta$. When the substrates (rods) are arranged in concentric circles on the disc, the angle δ is given by :

$$\delta = \cos^{-1}(\cos\beta\, \cos\gamma) \qquad \ldots\ldots\ldots (5.2)$$

where β is the azimuthal angle (see Fig. 5.7). Another useful angle is the angle α between the source-normal, and the line joining the substrate and the source (Fig. 5.9).

$$\text{When } \delta > 90^o \quad \alpha = 90 + \phi - \delta$$

$$\text{and when } \delta < 90^o \quad \alpha = 90 - \phi - \delta \qquad \ldots\ldots\ldots (5.3)$$

When the substrate holder is horizontal, and when e.b.b. evaporation is used, the substrate will no longer be in line-of-sight of the source once α exceeds about 35^o. Therefore, deposition at angles of greater than 35^o is only possible when the substrate holder is tilted.

For a small plane source the film thickness at the substrate, t_r, is given by [7] :

$$t_r = k\,\frac{\cos\alpha\,\cos\phi}{R^2} \qquad \ldots\ldots\ldots (5.4)$$

where k is a constant of proportionality. For a horizontal holder $\alpha = \phi$, and $t_r = k\,\frac{\cos^2\phi}{R^2} = k\,\frac{h^2}{(h_o^2 + r^2)^2}$. Now at the centre of the holder $\phi = 0$, and the film thickness at the centre, t_c, is equal to $k.\,\frac{1}{h^2 + r^2}$. Therefore, $\frac{t_r}{t_c} = \frac{1}{1 + \left(\frac{r}{h_o}\right)^2} = t_{r/c}$ ..... (5.5)

It is seen from this equation that when $r < h_o$ $t_r = t_c$; when $r = h_o$ $t_r = \frac{1}{2}\, t_c$; and when $r > h$ $t_r << t_c$. Equation (5.5) was used to

predict the film thickness deposited on a particular substrate and gave excellent agreement with the actual film thickness. When the substrate holder is inclined at an angle γ to the vertical, the film thickness t_γ may be obtained by substituting equations (5.1), (5.2), and (5.3) in equation (5.4). Thus :

$$t_r = k \frac{h_o}{R} \sin \{\cos^{-1} (\cos\beta \cos\gamma)\} \cdot \cos (90 \pm \emptyset - \delta)$$

..... (5.6)

A desk computer (HP 9100A) was used to give a numerical solution for this equation for various values of γ, β, h_o and r. The computer was programmed in such away that when given values of h_o, γ and r were fed in it would print-out values for α, $\emptyset$, R, t_r, β and δ as-well as the stored values of h_o, γ and r. Normally the computer would only be made to print-out when the condition $30^o < \emptyset < 50^o$ suitable for shear-mode transducer fabrication was met. A flow diagram for this programme is shown in Fig. 5.10, while the actual programme is given in Appendix II. As an example, Table 5.1 shows some of the results.

The computer-predicted film thicknesses where in excellent agreement with the actual thicknesses. With the substrate holder in an inclined position a large range of deposition angles and film thicknesses was obtained in one deposition run. This facilitated the study of the dependence of the crystallographic orientation of a deposited film on its thickness and its deposition angle for a range of thicknesses and angles for films deposited in the same run. This eliminated the influence of other parameters that might affect the growth of films in different deposition runs e.g. the influence of hydrocarbon vapours. As far as is known no such versatile holding arrangement has been reported in the literature. The influence of deposition angle and film thickness on the crystallographic orientation of as-deposited films is discussed below (section 5.6), and in section 8.4.

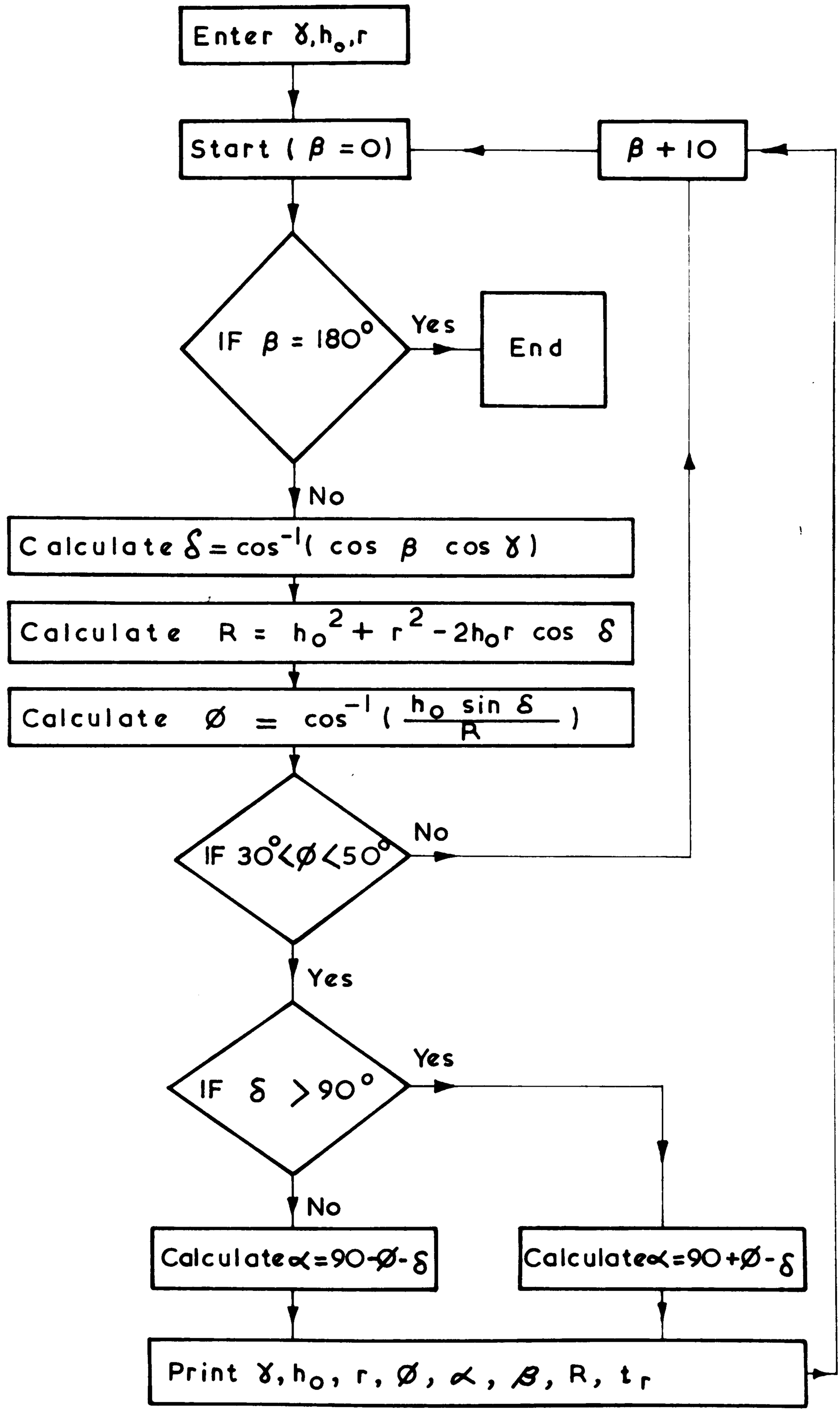

FIG. 5.10 Flow diagram

TABLE 5.1 Deposition data for D15 (Mk IIIb holder)

$\gamma = 60^{o}$, $h_o = 85$ mm

Sample No.	β^{o}	ϕ^{o}	α^{o}	$t_r(\mu m)$	R(mm)	r(mm)	Comments
8	105	41	34	22	112	63	X-rayed
9	120	46	31	19	118	63	Thickness measured with Tayysurf
10	135	49	29	17	122	63	
11	150	52	27	15	126	63	
12	165	54	26	14	128	63	
13	180	-	-	-	-	-	Empty
14	165	54	26	14	128	63	X-rayed
15	150	52	27	15	126	63	
30	150	45	19	25	108	40	

5.5. A typical CdS transducer deposition procedure

One or a combination of the following would be used as substrates : copper, aluminium, duralumin and quartz rods, and glass slides. The copper, aluminium and duralumin (dural) rods would be threaded at 40 threads-per-inch, so that they could be screwed inside the welding electrode of the spot welding machine (Fig. 1.1). The copper and aluminium rods would be machined from standard (drawn) rods 0.5" diameter. The dural rods would be machined from square blocks. The pyrex rods would be cut with a diamond saw to the required length. The faces of these rods (substrates) would be preground using waterproof silicon carbide abrasive paper in four stages (220, 320, 400 and 600 grit sizes). The rods would be carefully washed between stages so that no large abrasive particles could transfer to the smaller sizes. At this stage the centre line average (c.l.a.) of the surface would be about 430 nm, see Fig. 6.3 (in the following Chapter). When a better surface smoothness was required the rods would be transferred to a vibratory polisher (Thorn Electronics "Nashton" Vibratory Polisher, Type M14). The specimens (substrates) would be loaded with brass rod weights and would rest on a tightly stretched nylon cloth impregnated with diamond compounds. The nylon cloth would be stretched and secured by two O-rings in the polishing head casting, and rest on a 30 cm diameter glass disc 6 mm thick on the polishing table. The polishing head could be removed from the polishing table by slackening-off four knobs mounted on the main body of the polisher. The specimens would be placed in holes in the brass loads with their faces protruding a few millimetres. Two polishing heads would be used, one for 3 μm and the other for 0.25 μm diamond compounds. "Dialap" polishing fluid would be used as a lubricant. Vibratory polishing would be achieved by the forward and rotary movement imparted to the specimens. The degree of each movement would be controlled by adjusting the amplitude

of vibration. The specimens would be left to be polished for long periods (10 - 50 hours) depending on the smoothness required. A polythene sheet would cover the polishing head to prevent dust particles from getting to the polishing cloth. At the end of the polishing the c.l.a. would be about 20 nm i.e better than that of a slip-gauge. The glass slide substrates would not be polished, and would have a c.l.a. of about 30 nm "as-supplied". These slides (ordinary soda glass microscope slides) were supplied by Griffin & George Ltd.

All substrates would be washed in a solution of "Teepol", followed by a rinse in a de-ionised water ultrasonic bath. Trichloro-ethylene would then be squirted on the specimen followed by a wash in de-ionised water. Finally, iso-propyl alcohol would be squirted on the substrates and they would be placed in an iso-propyl alcohol bath where they would stay until they were transferred to the deposition chamber. This insured that no specks of dust could settle on the substrates. When it was thought that a substrate had an oxide layer formed on it, it was removed using etching and pickling solutions. For example, if a long time elapsed between polishing and cleaning a substrate and film deposition, oxide layers would form on the surface. For aluminium substrates the pickling and etching would entail immersion in dilute hydrofluoric (HF) acid (10% HF and 90% water). On removal from the pickle the substrates would be swilled in water and immersed in concentrated nitric acid and again rinsed in water. When the substrates had an oxide layer formed on them, or were not ultra-clean the deposited films would not adhere to them.

Once the substrates were secured in their holder, with their masks in position and their heater mounted, the chamber would be evacuated (section 5.2 above). The deposition procedure would start with ionic bombardment cleaning of the substrates for about twenty

minutes at rotary pump pressure (about 0.1 torr). The ionic bombardment results from a glow discharge that is created by applying H.T. voltage between two electrodes inside the deposition chamber. Its cleaning action may be thought of as a physical sputtering process (section 3.4.2), whereby oxide layers are actually removed from the substrate molecule by molecule. It is known [7] that aluminium oxides do not dissociate at high temperatures and low pressures, but they may be removed by ionic bombardment. On the other hand, chemical reactions between adsorbed layers and active gases in the glow discharge may lead to the dissociation of the adsorbed layers e.g. hydrocarbon vapours [7]. The bombardment cleaning process is very complex [7] and no single theory of the cleaning mechanism has been advanced yet.

The temperature controller would be set to hold the substrate temperature at 170^{o}C, and the system would reach thermal equilibrium after about 20 minutes. The chamber would be continuously evacuated until a vacuum of better than 5 x 10^{-5} torr was reached. This would take between 2 and 6 hours depending on the surface area and the number of items to be outgassed. The pump-down would be much quicker when the chamber was not heated, because the number of molecules de-gassed would be so much smaller, see section 4.3. The pressure inside the chamber would rise when the source power supply was turned-on. The system would take about 30 min to go back to its original vacuum when e.b.b. evaporation was used, and about 2 hours when the isothermal furnace was used. The reason behind this is the small mass of evaporant (2g) and crucible (4g) used in the former compared with an evaporant mass of 110g and cells mass of 80g and a furnace mass of 320g in the latter. The source power would be turned off while the source was out-gassing. The evaporant in the cermet crucible would be high purity "Vactron" CdS granules and sulphur granules (sulphur about one-sixth by volume), while that in the cells would be high purity cadmium shots and sulphur powder.

The CdS and sulphur were supplied by BDH Ltd., and the cadmium (grade 6N) was supplied by Metals Research Ltd.

Evaporation would start with the shutter in a position to mask the substrates but not the monitor crystal from the direct vapour beam. The first layer to be deposited would be chromium (few tens of nanometres). This acted as an adhesive between the substrate and consequent deposited layers (section 6.5.1). For metallic substrates the next deposited film would be CdS while for non-metallic substrates the layer would be the bottom electrode (e.g. aluminium or copper films). Chromium would be deposited using e.b.b. evaporation with typical H.T. power of 45 mA at 2 kV and filament current of 26A giving a deposition rate of about 30 nm. min^{-1}. High purity metals supplied by Johnson Matthey were used. CdS would be deposited at a rate of about 150 $nm.min^{-1}$ (approximately 10 μm. $hour^{-1}$) at beam power of 35 mA at 1.2 kV and filament current of 27A. The crucible would contain sulphur and CdS granules with sulphur about $\frac{1}{6}$ th by volume. The presence of excess sulphur, during CdS deposition ensured that the films would turn out more stoichiometric (section 4.5.1). When the cadmium and sulphur isothermal cells were used the chromium would be deposited in a separate (e.b.b.) chamber. The substrates would then be quickly transferred, while still hot, from the e.b.b. chamber to the cells' chamber. Normally the substrates would cool down by about 30^{o} during transfer. This reduced the effect of thermal stresses in the films. CdS would be deposited with cells temperature of $320^{o}C$. The sulphur orifice would have a diameter of 0.5 mm and the cadmium cell would have a gap of 0.7 mm, see Fig. 5.5 This would give a sulphur to cadmium ratio of about 5 (see section 4.5.1). A typical deposition rate would be 160 $nm.min^{-1}$ (approximately 10 $\mu m.hour^{-1}$). The masks would be changed after CdS deposition and the backing electrodes deposited. Only sulphur would be observed to

deposit at the cooler parts of the deposition chamber e.g. the base-plate, which is in good agreement with theoretical predictions (section 4.4). The substrate temperature (170^{o}C) was chosen to give a highly stoichiometric film at the deposition rates used (section 4.4 and Table 4.2). Copper (aluminium) film electrodes would be deposited at rates of about 100 (150) nm.min^{-1} with H.T. power of 50 (40) mA at 3.5 (3.5) kV and filament current of 25 (22) A. When these electrodes form the bottom electrode, the masking arrangements would be changed prior to the deposition of CdS.

The substrate to source distance would be about 80 mm. The residual pressure during deposition would be better than 5 x 10^{-5} torr, giving a mean free path (m.f.p.) for cadmium and sulphur vapour atoms of greater than 830 mm (section 4.3 and Table 4.1). This meant that more than 90% of the vapour molecules hit the substrate at the desired angle (section 4.3 and Table 4.1). It was also shown in section 4.3 that, with e.b.b. evaporation, no interaction between the vapour molecules and the electron beam was likely.

After deposition, the films may be heat treated or etched to investigate various changes in physical properties and crystallographic structure. For example, changes in piezoelectric coupling coefficient due to changes in dislocation density are discussed in section 8.5 changes of crystallographic orientation with thickness in 5.6 below, and changes in resistivity with changes in stoichiometery in sections 4.5.1 and 5.6.

Parenthetically it should be added that the above description of a deposition run is not "typical" in one sense. Often, something would go wrong during a prolonged deposition run. For example, the film thickness monitor would go unstable or its first amplifying stage would burn out, or the e.b.b. gun filament or the substrate heater filament would burn out, or the Penning gauge would give a false indication due to the intrusion of a speck of thin-film between

its anode and ground. The latter tended to happen towards the end of a deposition run. All that could be done when something went wrong was to switch off the source and substrate heater power supply, and wait for the system to cool down before replacing (or repairing) the offending component (or device). This would be done in the shortest possible time to ensure that the substrates were exposed to the atmosphere for a very short time (less than 10 min.). When oxide layers formed on the films or substrates the consequent deposited layers would flake-off.

5.6. A survey of the CdS transducer deposition runs

During the course of this project, nineteen principal deposition runs and hundreds of auxiliary runs were carried out by the author. A principal deposition run involves the deposition of CdS transducers on a mass production basis as described above. For the sake of brevity, every principal deposition run is given a serial number prefixed by the letter "D", e.g. "D9" means principal deposition run number 9. Auxiliary runs are not given serial numbers since they are usually linked with a particular principal deposition run. For example, in an auxiliary run the substrate holder would be baked and outgassed or a thermocouple tested, or a film from a previous deposition run heat-treated. Up to and including principal deposition run number 15, i.e. up to D15, electron beam bombardment (e.b.b.) evaporation was used. Horizontal and inclined substrate holding arrangements gave a wide range of deposition angles (up to 55^{o}) and film thicknesses (up to 100 μm), see section 5.4. In D5 CdS film transducers were successfully deposited at a rate of 300 $nm.min^{-1}$ on highly polished copper rod substrates. They had resistivities of 10^{6} - 10^{7} Ω.m. The resistivity, ρ, of a film transducer may be determined by measuring its resistance, R, and using the equation $\rho = R\frac{A}{y}$, where y is the transducer thickness and A is its electroded area. As discussed in section 9.2.1, when the resistance and the thickness of a CdS disc transducer are known its

resistivity may be read off directly from the graphs of Fig. 9.1. The resistance of deposited film transducers was measured using an Avometer and/or a valve voltmeter. The films deposited in D5 were up to 14 μm thick giving c-mode resonance frequencies down to about 160 MHz. Because the attenuation of acoustic waves in copper is so high at these frequencies, these transducers could not be tested using the pulse-echo technique.

It was decided, before making the films any thicker, to deposit CdS films on glass slides so that they could be tested ultrasonically, and this was done in D6 through D8. In D7 CdS film transducers were also deposited onto quartz rods. The CdS films on glass slides were deposited through molybdenum masks so that there were more than 30 disc electrodes giving rise to the same number of CdS disc transducer on one slide. These transducers could then be tested separately. The CdS transducers on the quartz rods could not be tested because of the presence of pin-holes which short-circuited the backing and the bottom electrodes. Attempts to burn out the pin-holes were unsuccessful. The CdS disc transducers deposited on glass slides in D6 were deposited at a rate of 100 $nm.min^{-1}$ and had resistivities of 10^6 - 10^8 Ω.m. Those deposited in D8 had a deposition rate of 50 $nm.min^{-1}$, and resistivities of 10^8 - 10^{10} Ω.m. The increase in resistivity in the latter run was attributed to the presence of sulphur granules with the CdS granules. Up to D8 only CdS granules were used as the evaporant. As discussed in section 4.5.1, even when CdS is evaporated congruently a deposited film tends to have excess cadmium in it. The presence of excess sulphur during deposition tends to increase the stoichiometry (and resistivity) of the deposited film. From D8 onwards sulphur granules were always included with the CdS granules. After that, deposited CdS films always turned out with their resistivity

higher than 10^8 Ω.m. More than 120 CdS disc transducers were farbicated in D8 above. These transducers were tested individually using the ultrasonic pulse-echo technique. It was found that where the vapour beam hit the substrate at right-angles only c-mode echoes were observed. Where the beam hit the substrate at an angle, however, both s-mode and c-mode excitations resulted. At the maximum deposition angle used (25^o) the c-mode echo amplitude was negligible compared with that of the s-mode echo. This is in excellent agreement with theoretical predictions (section 2.3) and the results of other workers (section 3.4) using different techniques to the present one. The transducers had a typical untuned two-way insertion loss of less than 40 dB in a 50 ohm system (section 9.3.2). These film transducers were heat treated at 350^oC for 3 hours. The heat treatment increased their resistivity by an order of magnitude but did not affect their ultrasonic performance.

Insofar as the resistivity is a measure of the stoichiometry of a deposited film, the higher the resistivity the better the film from a crystal chemistry point of view (section 4.5). In all deposition runs after D7 the CdS film resistivity was greater than 10^8Ω.m. which compares very well with values of resistivity reported by other workers (section 3.4). The value of the resistivity of a piezoelectric film may affect its performance as an ultrasonic transducer by varying its conductivity relaxation frequency, f_c (section 9.2.1). For example CdS films whose resistivities are 10^4, 10^6 and 10^8 Ω.m. have f_c values of 1 MHz, 10 kHz and 100 Hz, respectively. If one takes, as a design rule, the operating frequency to be three orders of magnitude greater than f_c, then CdS films whose resistivities are greater than 10^8 Ω.m. would make useful transducers at frequencies down to 100 kHz.

After the encouraging results of D8 it was decided to go back to the deposition of CdS onto welding electrode inserts. Accordingly in D9, copper rods, aluminium rods, quartz rods and glass slides were

used as substrates. The same deposition procedure as in D8 was executed. The presence of a dark blue powder instead of cadmium sulphide films on the copper substrates was noticed. This blue powder was also noticed on all other copper parts inside the deposition chamber, e.g. the earth shield of the monitor crystal wires. The powder turned out to be cuprous sulphide which resulted from the sulphidation of copper according to the reaction: $S + 2Cu \rightarrow Cu_2S$. The reason why this reaction did not occur in the previous runs is that in the first deposition runs the pumping system was new, and it took some time for sulphur to accumulate at the inlet to the diffusion pump. Also, it was only in the previous run (D8) that excess sulphur started being introduced in the chamber during film deposition. The contamination of copper films during the deposition of CdS films on them has been independently reported by Foster [8]. In D10 copper and aluminium rods, glass slides and gold-plated copper rods were used as substrates. The latter were plated with a film 1 μm thick in a "Zonax" solution (W. Canning & Co.). A plating current density of 30 $\mu A.mm^{-2}$ was used to give a deposition rate of about 200 $nm.min^{-1}$. The copper rods were again contaminated by cuprous sulphide confirming earlier results, while the films on glass slides, and gold-plated copper and aluminium rods were not. CdS film transducers up to 45 μm thick were deposited. Again the transducers were tested with the pulse echo technique. Those on glass slides gave satisfactory results while those on aluminium and gold-plated copper rods did not exhibit any piezoelectric activity. This was attributed to the vibration of these rods during CdS film deposition which took about five hours. Also the CdS film deposition was interrupted to re-charge the crucibles. This entailed the removal of the bell-jar from the base-plate. Because of the tremendous force on the gasket of the bell-

jar when the chamber is under vacuum, the removal of the gasket after admitting air to the chamber normally required a strong push which disturbed the substrate holder when the gasket gave way. Under such circumstances it was possible for a substrate to turn, causing the c-axis of a consequent CdS layer to be oriented in a different direction This would weaken or completely destroy the piezoelectric activity of the film. The rod substrates and glass slides were held more firmly in their holder in D11 by making use of a backing stainless-steel plate. This plate was held firmly on two 2BA steel studdings fixed to the holder. Adjusting screws from the backing plate were then used to load the substrates and keep them firmly in position between the holder and the backing plate. Only aluminium rods and glass slides were used in this run. It was thought that the use of aluminium rods as welding electrode inserts would not introduce any extra problems during the ultrasonic inspection of spot-welds. If anything, aluminium forms a better acoustic match to cadmium sulphide than does copper. Since aluminium rods could be used directly as substrates, whereas copper rods had to be gold-plated, it was decided to use the former. When tested ultrasonically, the films on glass slides gave satisfactory results. Most of the films on the aluminium rods flaked-off or disintegrated. This was thought to be due to the influence of thermal stresses in the films, and, possibly, the formation of oxide layers on the substrates. The oxide layers could be removed using etching and pickling solutions (see section 5.5 above). As discussed in section 6.5.1 the film adherence to the substrate was greatly improved in consequent deposition runs by making the substrate surface "rougher" so that the films could key-in. The surface finish of a "rough" substrate whose centre-line-average (c.l.a.) is 430 nm is shown in Fig. 6.3, where it can be seen that no shadow-masking effects could occur.

In D12 only flat and domed aluminium welding electrode inserts were used as substrates, and the deposition rate was 200 $nm.min^{-1}$. Although a deposition angle of 35^{o} was used the CdS transducers (60 μm thick) gave only c-mode responses when tested by the pulse-echo technique. Practically all of the transducers (about 30) adhered very strongly to the substrate and withstood a rigourous "Scotch-tape" test (see section 6.5.1). The failure of the transducers to respond in the s-mode was attributed to a "stifling process" in which oblique crystallites are smothered by normal crystallites. As discussed in Chapter 8, for a given deposition environment there is a critical thickness above which the film's c-axis starts to tilt towards the substrate normal, depending on the grain size and deposition angle. X-ray crystallographic tests on films deposited in D9 through D15 confirmed the stifling process model. In some runs the substrate holder was tilted so that a wide range of deposition angles and film thicknesses could be achieved for the same deposition environment (see section 5.4 above). After testing the piezoelectric polarity of CdS films deposited on a variety of substrates (section 9.3.3), multi-layer CdS transducers were fabricated in D15. Multi-layering was achieved by depositing a very thin amorphous [9] SiO_2 film on top of the first CdS layer before depositing the second layer, and so on for the third and fourth layers until the desired thickness was reached. The purpose of depositing the very thin amorphous inter-layer was to stop the CdS from being a continuous thick film, but rather a stack of thin films whose c-axes were all inclined at the same angle to the substrate normal. Again X-ray crystallographic test confirmed the stifling process model i.e. multi-layering proved to be a successful way of overcoming the stifling process. However, the multi-layer transducers flaked off on handling, e.g. when loaded by metallic bellows, making them useless from an engineering point

of view. As discussed in section 6.5.1 the multi-layers flaked off due to the enormous thermal stress on the SiO_2 interlayers. A comprehensive search to find a more suitable material for the inter-layer was then undertaken. The desired material had to satisfy the following conditions : (a) It had to be insulating so that it would not short-circuit the CdS layer to the substrate, (b) It had to have a coefficient of linear thermal expansion comparable with that of CdS, (c) It must not be chemically too complex i.e. it must be relatively easy to deposit in thin film form and its melting point had to be above $300^{o}C$, (d) It had to be amorphous when in thin film form so that it would not influence the growth of the CdS film. None of the chemical elements e.g. sulphur, boron, germanium and silicon satisfied the above requirements. The search had to consider simple compounds e.g. Na Cl and alumina which were ruled out as soon as they were proposed because they failed to satisfy one or more of the above requirements. The deposition of a thin amorphous layer of CdS e.g. by increasing the deposition rate abruptly for one minute, was also ruled out because it was thought that the "amorphous" CdS inter-layer would very likely be oriented in the same manner as the CdS layer under it thus preventing the multi-layer from being discontinuous. The search for a material for the inter-layer was finally narrowed down to silicon monoxide (SiO). There was one obstacle, however. A literature search failed to produce a value for the thermal coefficient of expansion, α, for SiO. Nevertheless, it has been suggested [10] that α for SiO should not be very different from that of SiO_2. This meant the ruling-out of SiO as a possible material for the inter-layer. (α for SiO_2, CdS and other relevant materials is given in Table 6.1 at the end of Chapter 6).

At this stage Beecham's paper [5] on the cadmium/sulphur isothermal technique appeared (see section 3.4.1.3), and this

technique was used in D16 onwards. The advantage of using Cd and S instead of CdS and S is that Cd and S have much lower melting points than CdS, and therefore the vapour molecules are less hot. For example, with the e.b.b. CdS/S isothermal technique typical temperatures of molecules were 600-800^{o}C at deposition rates of 0.03 - 0.1 μm.min^{-1} compared with temperatures of 300-400^{o}C with rates of 0.1 - 2 μm.min. in the Cd/S isothermal technique. The present author thought that the latter technique provided another way of overcoming the stifling process, namely by increasing the grain size of the deposited CdS films (see sections 4.5 and 8.4.1). This, indeed, turned-out to be the case, and 50 μm thick CdS s-mode transducers were successfully fabricated at a deposition rate of 160 nm.min^{-1} in D17 using the Cd/S technique. However, there remained one difficulty. The ultrasonic response of these transducers was much weaker than expected. It is possible that this may be due to a high dislocation density in the CdS films (see section 6.5.2). The as-deposited CdS films were then heat treated in a sulphur atmosphere at a temperature of 500^{o}C in an effort to decrease their dislocation density. The CdS films (on aluminium rods) were placed inside a quartz cell with sulphur and were evacuated to a pressure of b.t. 10^{-5} torr, and sealed. The cell was then placed in a programmable furnace (J.L.S. Engineering, Type 9940/0) its temperature raised to 500^{o}C in 24 hours, held there for 50 hours, then cooled-down to room temperature at the same rate as it was heated (20^{o}C.h^{-1}). It was hoped that this slow heating and cooling rate would prevent the films from disintegrating under the enormous thermal stresses generated. Although the films did not disintegrate or flake-off, they presented a short circuit when tested electrically. This is thought to be a result of the appearance of micro-cracks in the films.

In D18, duralumin (dural) rods machined from square blocks were used as substrates, together with the standard (drawn) aluminium (Aℓ) rods. This was done in order to investigate the influence of the size and the orientation of the grains of the substrate on the orientation of CdS films (section 8.4.2). Three kinds of substrate surface finish were used, namely, 20 nm 430 nm, and "as-machined" and pickled (section 5.5). A glass slide was also used as substrate. The deposition conditions were similar to those of D17. At the end of the run, it was found that the CdS films were not continuous but rather small fragments on all of the substrates. The films would have been about 90 μm thick. The disintegration of the films may be attributed to the large compressive forces acting on thick CdS films (section 6.5) or to the formation of oxide layers which weaken the bonding force between film and substrate (section 6.5.1), or to the concerted action of both. It is thought that relatively thick oxide layers were formed in this particular run because the furnace heater burnt-out just after the start of CdS deposition. Although the substrates were kept under vacuum for three hours while the heater was replaced, there was, nevertheless, an appreciable number of air molecules to contaminate the surfaces of the substrates (section 4.2.4).

In D19, the same kinds of substrate and of substrate surface finish as those of D18 were used. Although the resulting CdS films adhered very strongly to the substrates, they had very low resistivity, i.e. they had a lot of excess cadmium in them (section 4.5.1). These films were, therefore, useless as transducers. In view of the fact that the deposition conditions were exactly the same as those of D17, the only variation in the chemical composition (stoichiometry) of the films must have come from a variation in the composition of the vapour beam. This, in its turn, must have come from variations in the orifice areas, since fresh cells were used in each run in order to avoid

contamination. As indicated by equation (4.9), section 4.5.1, for a given source temperature, the ratio of Cd to S atoms, N_{Cd}/N_S in the vapour beam is proportional to the ratio of the Cd to the S cell orifice areas, A_{Cd}/A_S. Now, A_S is proportional to d^2, where d is the diameter of the precision-bore capillary tube from which the orifice is made (Fig. 5.5). Since the tolerance on d is 0.01%, the error in A_S is 0.02%. The error in A_{Cd}, however, is much greater because of the method of manufacture of the Cd cell. The Cd orifice is achieved by blowing the inner pyrex tube until it leaves a gap of the required width, δr, between the blown and the inner wall of the middle tube, see Fig. 5.5. The area of the orifice, A_{Cd}, is given by $A_{Cd} = \pi r\, \delta r$, where r is the diameter of the middle tube (2.5% tolerance). The tolerance on δr is set by the accuracy to which the inner tube can be blown, and is about -0.15 mm for a 0.7 mm gap (Mk II cells), i.e. 21%. Therefore, the error in A_{Cd} is about 24%. Since the error in A_S is much smaller than in A_{Cd}, the error in A_{Cd}/A_S and, therefore, that in N_{Cd}/N_S is equal to the error in A_{Cd}, i.e. 24%. It seems possible, therefore, that in D19 24% more Cd atoms were arriving at the substrate than in D17. A change in the composition of the film of few p.p.m. is sufficient to change the resistivity of the CdS film by orders of magnitude (section 4.5). Beecham reported [5] that a change of 90% in the number of Cd atoms arriving at the substrate, changed the resistivity of the films from very high to very low.

S cell orifice areas of 0.295, 0.196 and 0.049 mm^2 (0.65, 0.50, 0.25 mm diameter, respectively) with Cd cell orifice areas of 74 and 49 mm^2 (1.1 and 0.7 mm gap) were used in various combinations. Source temperatures of 420 and 350°C were used to give S/Cd ratios, at the substrates of greater than five, see section 4.5.1. An S cell orifice of 0.5 mm diameter, a Cd cell orifice gap of 0.7 mm, and a source temperature of 350° gave best results. With the 0.65 mm sulphur orifice, the 1.1 mm cadmium cell gap, and source temperature of 420°C ,

the residual pressure during deposition was too high (> 10^{-4} torr) for oblique deposition. The substrate to source distance in most deposition runs was about 80 mm. For oblique angle deposition this imposed an upper limit on the value of residual pressure during CdS deposition of 5×10^{-5} torr (see sections 4.2.2 and 4.3). When the residual pressure exceeds this value the vapour beam loses its molecular nature and directivity, and complete molecular chaos prevails inside the deposition chamber. Under these circumstances no deposition at an angle is possible. As discussed in section 4.3, one of the parameters controlling the value of the residual pressure is the pumping speed. In the present work the pumping speed had a maximum value of 600 litres.s^{-1}, limiting oblique angle deposition rates to a value of about 10 $\mu m.h^{-1}$.

In order to ensure the repeatability of the deposition environment, the components of the deposition chamber (section 5.3), and the inlet to the diffusion pump (section 5.2) were thoroughly cleaned after every principal deposition run. The cleaning procedure of most components, e.g. substrate holder, was essentially similar to that of substrate cleaning (section 5.5).

Table 5.2 summarizes the various principal deposition runs, while Table 7.2 (at the end of Chapter 7) summarizes the tests carried out on specific samples. The sample numbers are as indicated in Fig. 5.7 or Fig. 5.8 depending on which substrate holder was used. Copper film electrodes were used up to D9, after which aluminium was used.

TABLE 5.2 Deposition runs survey

"D" No.	Substrates	Subst. temp. ^{o}C	Source material	Source temp. ^{o}C	Deposition rate $nm.min^{-1}$	Residual pressure torr	Resistivity Ω.m.	Thickness μm	Comments
4	Cu rods	Room temp.	CdS	700	200	3×10^{-6}	≃0	4 - 6	
5	Cu rods	170 - 200	CdS	800	300	10^{-5}	10^{6} - 10^{7}	8 - 14	Subst. temp. manually contr
6	Glass slides	150 - 200	CdS	800	100	2×10^{-5}	10^{6} - 10^{8}	10 - 15	
7	Cu & quartz rods & glass slides	170	CdS	500	100	2×10^{-5}	10^{6} - 10^{8}	10 - 12	Films on Cu flake off
8	Glass slides	170	CdS/S	650	50	5×10^{-5}	10^{8} - 10^{10}	14 - 16	s- and/or c-mode response depending on deposition angle
9	Cu, Aℓ & quartz rods & glass slides	170	CdS/S	650	160	5×10^{-5}	> 10^{10}	10 - 42	Sulphidation of copper
10	Cu & Aℓ rods	170	CdS/S	800	160	5×10^{-5}	> 10^{10}	15 - 45	
11	Aℓ rods & glass slides	170	CdS/S	800	200	5×10^{-5}	> 10^{10}	80 - 90	Films on Aℓ rods flaked off
12	Aℓ rods	170	CdS/S	750	200	5×10^{-5}	> 10^{10}	60 - 65	Subst. surface made "rougher" c-mode response only
13	Aℓ rods	170	CdS/S	800	200	10^{-5}	> 10^{10}	15 -100	Inclined subst. holder
14	Aℓ rods & glass slides	170	CdS/S	750	120	5×10^{-5}	> 10^{10}	20 - 25	Polarity test
15	Aℓ rods	170	CdS/S	800	150	5×10^{-5}	> 10^{10}	14 - 33	Multi-layers disintegrate on handling
16	Aℓ rods	170	Cd/S	420	200	10^{-4}	-	15 - 20	Excessive residual pressure. Films disintegrate
17	Aℓ rods	170	Cd/S	350	160	5×10^{-5}	> 10^{10}	50 - 55	c- and/or s-mode response
18	Aℓ rods & glass slide	170	Cd/S	350	160	5×10^{-5}	-	80 - 90	Films disintegrate
19	Aℓ rods & glass slide	170	Cd/S	350	160	5×10^{-5}	≃0	50 - 55	Excess cadmium

C H A P T E R 5

REFERENCES

1. D.F. Klemperer et al, *Liquid nitrogen trap copper*, J. Sci. Inst., 1, p. 1232 (1968).

2. N. Irving-Sax, *Dangerous properties of industrial materials*, Reinhold (1963).

3. Dept. of Employment & Productivity, *Dust and fumes in factory atmospheres*, H.M.S.O. (1968).

4. Birvac, *Instruction manual*, 1967.

5. D. Beecham, *Cadmium/sulphur isothermal source for CdS deposition*, Rev. Sci. Inst., 41, p. 1654 (1970).

6. Edwards High Vacuum Ltd., *TFM instruction manual*, Publication No. M1160714 (1966).

7. L. Holland, *Vacuum deposition of thin films*, Chapman & Hall (1966).

8. N.F. Foster, Chapter in *Handbook of thin film technology*, ed. L.I. Maissel et al., McGraw-Hill (1970).

9. K. Mehmet, *Ph.D. Thesis*, University of Warwick (1970).

10. A.E. Hill, *Private Communication*.

11. N. Chubachi et al, *Influence of dislocations in CdS on its coupling factors*, JAP, 42, p. 962 (1971).

C H A P T E R 6

Thermal profiles and stresses in thin films

6.1. Introduction

The rise in temperature of the growing-face of a film during deposition is of interest, because, when appreciable, it may affect the growth environment of the crystal (film) both from the point of view of change in the magnitude of the thermal gradient across the film and change in direction of heat flow across the film, as it grows. It also may increase the stress in a deposited film. In this chapter the general problem of temperature profiles in thin- and thick-films during growth is tackled with particular reference to films deposited in this work. It is concluded that for as-deposited films there is no appreciable rise in growing face temperature. It is also concluded that the direction of heat flow across a CdS film is independent of its crystallographic orientation. Finally intrinsic and extrinsic thermal stresses in thin- and thick-films are discussed in connection with film adherence to the substrate, and their effect on the physical properties of the film. It is thought that these stresses may increase the dislocation density of as-deposited CdS films. A table of thermal and mechanical properties of some relevant materials is given at the end of this Chapter.

6.2. The fundamental laws of heat conduction and radiation

Fourier's law of one-dimensional steady state head conduction states that : $\dot{Q} = -kA \frac{\partial \theta}{\partial x}$, where $\dot{Q}$ is the rate of heat flow across a slab dx, A is the area perpendicular to the direction of flow, $\frac{\partial \theta}{\partial x}$ is the temperature gradient, and k is the thermal conductivity of the material. The minus sign is introduced in order that the positive

direction of heat flow coincides with the positive direction of x. Steady state implies that the temperature at any point does not vary with time and that the temperature gradient is constant provided that k is constant. In such a case heat flow across a slab of thickness x may be written as :

$$\dot{Q} = -kA \frac{\theta_2 - \theta_1}{x} \qquad \ldots\ldots\ldots (6.1)$$

For unsteady one-dimensional flow, the temperature, θ is a function of time t at any point x in the slab. The heat inflow Q, into a layer dx during a time interval dt through an area A is :

$$Q_1 = -kA \frac{\partial\theta}{\partial x} dt$$

The heat out-flow Q_2 is given by :

$$Q_2 = -k \frac{\partial}{\partial x} (\theta + \frac{\partial\theta}{\partial x} dx)\, dt = -kA \left| \frac{\partial\theta}{\partial x} + \left(\frac{\partial^2\theta}{\partial x^2} \right) dx \right| dt$$

The difference between Q_1 and Q_2 must be equal to the heat stored by the layer dx during the time interval dt. The temperature rise of this layer during time dt is $\frac{\partial\theta}{\partial t} . dt$, and, therefore, the heat absorbed by the layer is $(\rho A\, dx)c \frac{\partial\theta}{\partial t} dt$, where ρ is the density of the material and c its specific heat,

$$\therefore \quad Q_1 - Q_2 = \rho c\, A dx \frac{\partial\theta}{\partial t} dt$$

$$\text{i.e.} \quad kA \frac{\partial^2\theta}{\partial x^2} dx\, dt = \rho c\, A dx \frac{\partial\theta}{\partial t} dt$$

$$\therefore \quad \frac{\partial\theta}{\partial t} = \alpha \frac{\partial^2\theta}{\partial x^2} \qquad \ldots\ldots\ldots (6.2)$$

where $\alpha \left(= \frac{k}{\rho c} \right)$ is the thermal diffusivity of the material.

When radiation impinges on matter it may be totally or

partially reflected, transmitted through it, or absorbed. The ratio of the reflected to the total incident energy is called the reflectivity, ρ, of the material; the ratio of the transmitted to the total incident energy is called the transmittivity, τ, and the ratio of the absorbed to the total incident energy is called the absorptivity α. Practically all solid materials used in engineering are opaque to thermal radiation (even glass is only transparent to a fairly narrow range of wavelengths) and the radiation is either reflected or absorbed within a very shallow depth of matter [1]. When radiation is absorbed by a material, it normally increases the random molecular energy and therefore the temperature of the absorbing material. A material whose absorbitivity is unity is called a "black body". The Stefan-Boltzmann law gives [1] the heat radiated by a black body, $\dot{Q}_b$, at temperature θ by : $Q_b = \sigma A \theta^4$, where A is the surface area of the black body, and σ is the Stefan-Boltzmann constant which is equal to 5.7×10^{-8} $W.m^{-2}.K^{-4}$.

When two black-body surfaces, A_1 and A_2, are at different temperatures, θ_1 and θ_2, the heat energy flow, dQ_{b1-2}, from the hotter to the colder body is given [1] by :

$$dQ_{b1-2} = dQ_{b1} - dQ_{b2} = \sigma (\theta_1^4 - Q_2^4) \int\int \frac{\cos\phi_1 \cos\phi_2 \, dA_1 dA_2}{\pi R^2}$$

where ϕ_1 and ϕ_2 are the angles the normals to A_1 and A_2 make with the line joining them, and R is the distance between the two bodies.

or $$dQ_{b1-2} = \sigma (\theta_1^4 - \theta_2^4) F_{1-2} \, dA_2 \qquad \ldots\ldots\ldots (6.3)$$

where F_{1-2} is known as the geometric factor and is defined as the fraction of the radiation of the surface A_1 in all directions which is intercepted by surface A_2. No real material emits and absorbs radiation according to the laws of the black body, but the behaviour of many materials may be studied through their emissivity. The emissivity, ε,

is defined [1] as the ratio of the total energy, Q, emitted by a surface to the total energy, Q_b, emitted by a black surface at the same temperatures : $\varepsilon = \left(\frac{Q}{Q_b}\right)_\theta$. The emissivity of a surface 1 at θ_1 is equal to its absorbtivity for radiation received from a surface 2 at the same temperature, $\theta_2 = \theta_1$, i.e. $\varepsilon = \alpha$. For example polished aluminium, polished steel, asbestos paper, and quartz glass have emissivities of 0.04, 0.1, 0.94, 0.89, at 260°C, respectively [1]. If the emissivity of a surface is independent of the wavelength of the heat radiated, the material is called a "grey-body". The laws of black-body radiation may then be applied to a grey-body using ε as a multiplication factor in the expression for heat radiated or emitted by it, i.e.

$$Q_g = \varepsilon \sigma A\theta^4 \qquad \ldots\ldots\ldots (6.4)$$

When the heat transfer between two small areas whose distance is greater than their major dimensions is considered, then to a good approximation [1] equation (6.3) may be written as :

$$dQ_{b1-2} = \sigma (\theta_1^4 - \theta_2^4) \frac{\cos\phi_1 \cos\phi_2 A_1 A_2}{\pi R^2} \qquad \ldots\ldots\ldots (6.5)$$

6.3. Heat flow inside a vacuum evaporation chamber

Inside a vacuum chamber heat flow by convection may be ignored i.e. the residual vapours and gases are assumed to be perfect transmitters of heat energy. There are various sources of heat inside a vacuum chamber e.g. substrate heater, the vapour source itself and its heater. Heat is also released when vapours condense to form a film, e.g. on a substrate. The fundamental laws of heat flow will be used to investigate the change in temperature of the substrate both due to condensation heat and radiation heat. As stated in section 4.4, condensation heat, Q_{con} is given by :

$$Q_{con\ f} = (m\ \Delta H_c)_f \quad J$$

$$Q_{con\ f} = (A\rho y \Delta H_c)_f \quad J$$

$$\text{or} \quad \dot{Q}_{con\ f} = (\dot{m}\ \Delta H_c)_f \quad W \qquad \ldots\ldots\ldots\ (6.6)$$

where m_f is the mass of film deposited, $\dot{m}_f$ rate of deposition of mass, y is the film thickness and ΔH_{cf} is the heat of condensation of the film material per unit mass. The film then cools down from its initial (crucible) temperature, θ_c, to that of the substrate, θ_s, releasing an amount of heat, Q_f, given by : $Q_f = m_f\ c_f\ (\theta_c - \theta_s)$, where c_f is the specific heat of the film material. Even when $\theta_c - \theta_s = 1000$, $Q_f << Q_{con\ f}$, and, therefore, Q_f may be neglected. As an example, take the deposition of a 100 μm thick cadmium sulphide film at a very fast rate of 10 μm.min, i.e. total deposition time = 100 min = 6000 second. Now for CdS $\Delta H_c = 2.1 \times 10^6\ J.kg^{-1}$, $\rho = 4.8 \times 10^3\ kg.m^{-3}$, $k = 20\ W.m^{-1}.K^{-1}$.

$$\therefore \quad \dot{Q}_{con\ f} = A\rho \frac{y}{t} \Delta H = 8.2\ mW \qquad \ldots\ldots\ldots\ (6.7a)$$

If the deposition rate is decreased ten times, condensation heat is also decreased 10 times i.e.

$$\dot{Q}'_{con\ f} = .82\ mW \qquad \ldots\ldots\ldots\ (6.7b)$$

Radiation heat energy flows toward the substrate from the vapour source. In e.b.b. heating two sources of radiation may be considered. The first is the electron gun itself and the second is the crucible. The temperature of the crucible is plotted against electron beam power in Fig. 5.4 (Chapter 5). The rise in temperature of the face of the electron gun that may radiate heat to the substrate was also determined experimentally, and it was found that it reached thermal equilibrium at about 120^oC. Since the

substrate temperature is normally held at 170^{o}C, no heat will flow from the ring gun to the substrate. The surface areas of the crucible and the substrate are small compared with the source to substrate distance, R, and equation (6.5) applies for the heat flow from the crucible to the film, $Q_{rad\ c\text{-}f}$. The surface area of the crucible that is seen by the substrate is that of the top face of the crucible (= 1.1 x 10^{-4} m^2). The surface area of the CdS film is 5 x 10^{-5} m^2. For a deposition angle of 35^{o} with a horizontal substrate holder, the radiation heat flow from crucible to film is given by

$$\dot{Q}_{rad\ c\text{-}f} = 1.6 \times 10^{17} \frac{(\theta_c^4 - \theta_s^4)}{R^2}$$

where R is the substrate-to-crucible distance, assuming that the film and crucible behave as black-bodies. Now in most deposition experiments

$\theta_c > 2\ \theta_s$

$$\therefore \quad \theta_c^4 - \theta_s^4 = \theta_c^4$$

$$\therefore \quad \dot{Q}_{rad\ c\text{-}f} = 1.6 \times 10^{-17} \frac{\theta_c^4}{R^2} \qquad \ldots\ldots\ldots (6.8)$$

For θ_c = 1000 K, and R = 1.1 x 10^{-1} m

$$\dot{Q}_{rad\ c\text{-}f} = 1.3\ mW \qquad \ldots\ldots\ldots (6.9)$$

A comparison between equation (6.9) and (6.7) reveals that for deposition rates greater than 10 $\mu m.min^{-1}$, condensation heat is greater than radiation heat from the crucible. However, for deposition rates of less than 1 $\mu m.min^{-1}$ condensation heat may be ignored.

It is seen from equation (6.8) that when the crucible

temperature is reduced to 900, 800 and 1000 kelvin (K), the heat radiated is reduced by 1.5, 2.4 and 4 times, respectively. On the other hand when the temperature is increased to 1100 and 1200 K the heat is increased 1.5 and 2.1 times, respectively. The isothermal furnace area is about 64 times that of the crucible used in e.b.b. evaporation. Therefore, the radiation heat received by the film, $\dot{Q}'_{rad\ c\text{-}f}$, is given by

$$\dot{Q}'_{rad\ c\text{-}f} = 64\ \dot{Q}_{rad\ c\text{-}f}$$

However the furnace temperature is about 700 K instead of 1000 K.

$$\dot{Q}'_{rad\ c\text{-}f} = 16\ \dot{Q}_{rad\ c\text{-}f} \qquad \ldots\ldots\ldots\ (6.10)$$

For example, for a source to substrate distance of 1.1×10^{-1} m

$$\dot{Q}'_{rad\ c\text{-}f} = 21\ mW \qquad \ldots\ldots\ldots\ (6.10a)$$

It can be seen from equation (6.5) that, other things being equal, for deposition at right angles six times more radiation heat is received by the substrate than that with deposition at an angle of 35^{o}. Also when R is reduced from 110 mm to 90 and 60 mm the heat is increased 1.5 and 5 times respectively. Therefore, for a horizontal substrate which is 90 mm above the crucible, the heat received is 9 times that given in equations (6.9) and (6.10).

As a first approximation the radiation heat received by the substrate holder, $\dot{Q}_{rad\ c\text{-}sh}$, may be similarly worked out using equation (6.5) for the case of e.b.b. evaporation. For the isothermal furnace, however, both emitter (furnace) and receiver (substrate-holder) have major dimensions greater than the distance between them, and the geometric factor $F_{c\text{-}sh}$ may be taken as unity. In this case radiation heat is given by

$$\dot{Q}'_{\text{rad c-sh}} = \sigma \theta_c^4 A_{\text{furnace}} \quad \ldots\ldots\ldots (6.11)$$

The heat actually absorbed by the holder will be less than that given above by a factor ε, the absorbtivity of the substrate holder. It is known [1] that the absorbtivity of polished steel at 260°C is 0.1. However, when an oxide layer is formed on its surface, its absorbtivity increases to 0.8 at the same temperature. During cadmium sulphide deposition the stainless steel holder is continuously coated with a dark film. It is reasonable to assume that the film has the same effect on the absorbtivity of the holder as that of an oxide layer, i.e. the absorbtivity of the holder is 0.8. Now the area of the holder is about one thousand times that of the substrate,

$$\dot{Q}_{\text{rad c-sh}} = 0.8 \times 1.3 \times 10^{-3} \times 10^{3} = 1 \quad W \quad \ldots\ldots (6.12)$$

Also from equation (6.11)

$$\dot{Q}'_{\text{rad c-sh}} = 0.8 \times 5.7 \times 10^{-8} \times (700)^4 \times 70 \times 10^{-4} = 75 \text{ W}$$

$$\ldots\ldots\ldots (6.13)$$

Hence, radiation heat from the isothermal source is 75 times that from the e.b.b. crucible.

6.4. Temperature profile in a growing film

6.4.1. Rise in temperature of the growing face of the film

In order to investigate the temperature profile in a film during growth (Fig. 6.1) the following assumptions are made :

(i) The growing face temperature, θ_g, is higher than that of the bottom face (substrate), θ_s.

(ii) The substrate temperature stays constant during deposition, i.e. θ_s = constant.

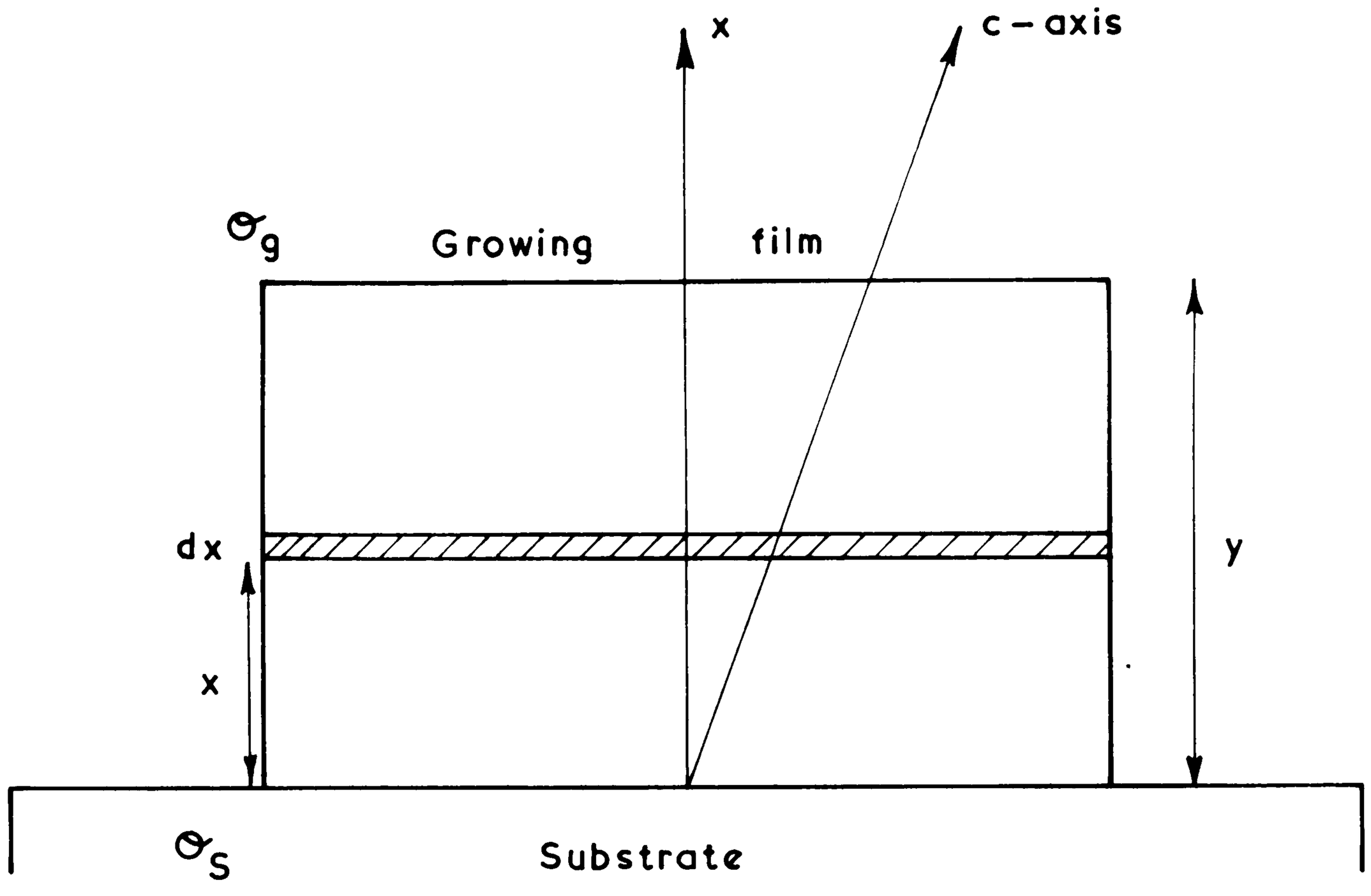

FIG. 6.1 Temperature profile in a growing film

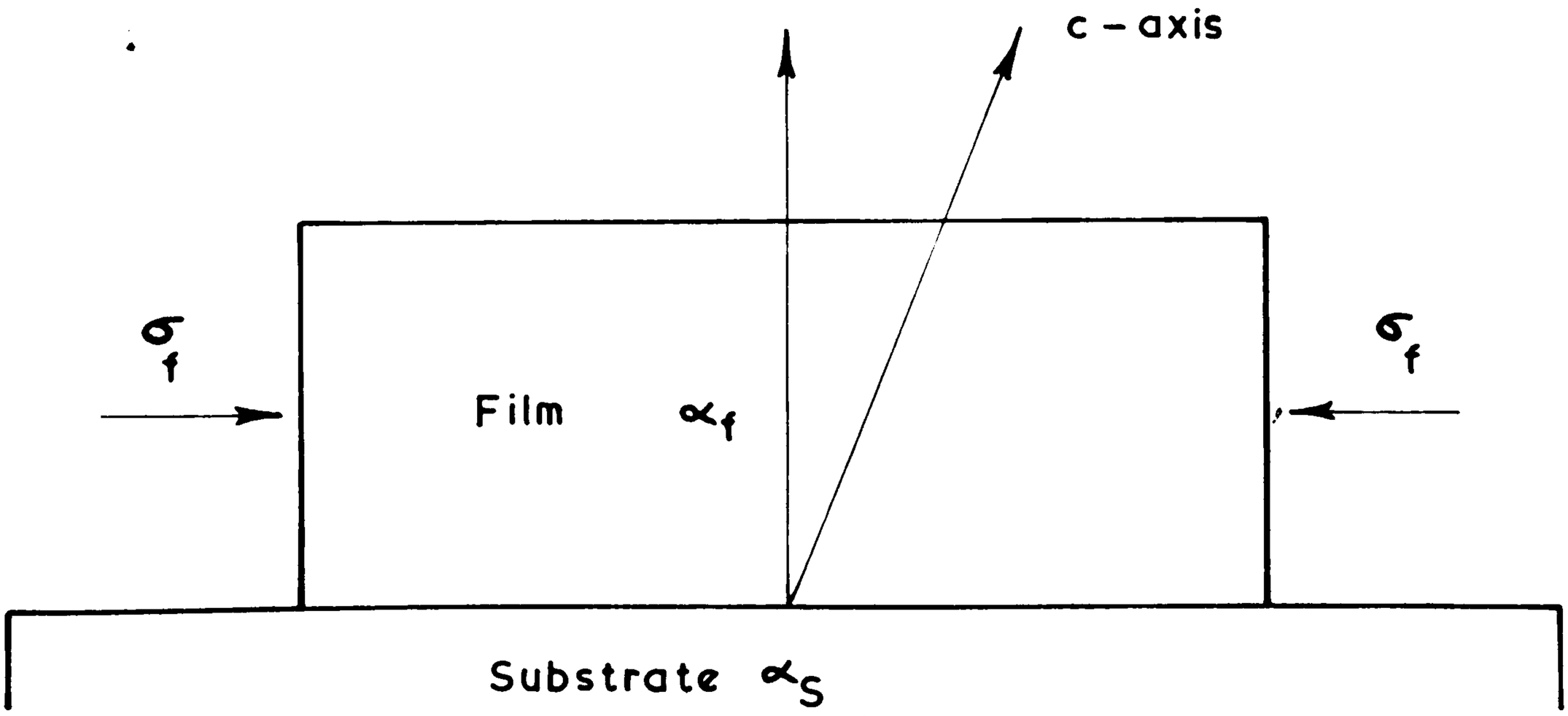

FIG. 6.2 Differential expansion stress.

(iii) Steady state heat flow conditions hold.

Using equation (6.1) the rise in growing face temperature, θ_g, may then be calculated. Assumption (ii) is not valid because it is known empirically that θ_s does rise during film deposition. Nevertheless, it is convenient to assume θ_s constant to see how far θ_g might rise above it. The rise in θ_s could be worked out later, and the two rises may, then, be superimposed since the system may be assumed linear. Assumption (iii) is justified in view of the fact that the time constant of the transient heat flow, t_c, is small (few seconds) compared with the deposition time (typically thousands of seconds). For example, for cadmium sulphide the thermal diffusivity α in equation (6.2) is $1.03 \times 10^{-4}\ m^2.s^{-1}$, and even for an extremely thick film of 1000 μm $t_c = \frac{y^2}{\alpha} = 10$ ms. The transient is over in less than one second, and steady state conduction takes place, i.e. the temperature gradient across the film is linear. Therefore, equation (6.1) may be used to calculate the rise in growing face temperature:

$$\Delta\theta_{gs} = \theta_g - \theta_s = \frac{\dot{Q}}{kA} \cdot y \qquad \ldots\ldots\ldots (6.14)$$

The temperature rise, $\Delta\theta_{con\ gs}$, due to condensation heat, $\dot{Q}_{con}$, may be superimposed on that, $\Delta\theta_{rad\ gs}$, due to radiation heat, $\dot{Q}_{rad}$, to yield the total temperature rise.

An order-of-magnitude estimate may be worked out for the thickness of a film, x_c, below which no appreciable changes in growing face temperature occur relative to that of the substrate.

$$x_c \simeq \sqrt{\alpha t}$$

for times greater than 100 seconds

$$x_c \simeq \sqrt{103 \times 10^{-6} \times 10^2}$$

$$\simeq 100 \text{ mm}$$

i.e. so long as the film is thinner than 100 mm, there is no appreciable rise in surface temperature. In thin film technology the films are often less than 10 μm thisk, and films are considered to be very thick indeed if they are more than 100 μm. It could be stated, therefore, that from a thermal point of view a film is homogeneous i.e. its temperature does not vary with thickness. Nevertheless, it is useful to get an exact value for the temperature gradient across a thin film because this small temperature gradient may be responsible for the existence of stresses in the films.

From equation (6.6), $\dot{Q}_{con\ f} = \dot{m}_f \Delta H_{cf} = A\rho \frac{y}{t} \Delta H_{cf}$ and from equation (6.14)

$$\Delta\theta_{con\ gs} = \frac{Q_{f\ con}}{k_f A_f} \cdot y$$

$$\therefore \quad \Delta\theta_{con\ gs} = \frac{\rho_f \Delta H_{cf}}{k_f t} y^2 \qquad \ldots\ldots\ldots (6.15)$$

where t is deposition time. It is to be noted from equation (6.15) that the rise in temperature due to condensation is proportional to the square of the film thickness, and inversely proportional to its thermal conductivity and its time of deposition i.e. the lower the deposition rate the lower the temperature rise. Again taking as an example the deposition of a 100 μm thick CdS film in 10 min, equation (6.15) gives, after substituting $Q_{con\ f}$ from equation (6.7a), $\Delta\theta_{con\ gs} = 4\ m^oC$ i.e. the temperature gradient is 40 degrees per metre. Similarly the rise in growing face temperature, $\Delta\theta_{rad\ gs}$, due to radiation heat may be worked out by substituting $\dot{Q}_{rad}$ instead of $\dot{Q}_{con\ f}$ in equation (6.15). From equations (6.7), (6.9) and (6.10), it is seen that $\dot{Q}_{con\ f}$ is six times greater than the e.b.b. radiation heat $\dot{Q}_{rad\ c-f}$, and 12 times smaller than the isothermal

furnace radiation heat $\dot{Q}'_{rad\ c\text{-}f}$. Therefore, the temperature rise of the growing face of a 100 μm thick CdS film is still very small and is of the order of 10's of millidegrees per 100 μm. It is to be noted however that this temperature gradient (approximately 100 $K.m^{-1}$) may be responsible for the so-called intrinsic stresses in thin films, i.e. stresses which exist in thin films during deposition and come into play before the film cools down to room temperature when thermal stresses start acting on the film. Experimental values of intrinsic stresses have been reported for silicon monoxide [2], and silver and gold [3] films. It is reported [4] that for most materials intrinsic stresses have the same magnitude as the thermal stresses. Stresses in thin films are discussed later.

6.4.2. Rise in temperature of substrate

In this case the temperature of the film, the substrate and the substrate holder are assumed to be equal. This is justified by the fact that (a) the substrates are screwed into the holder to make very good thermal contact, and (b) the mass of the film and substrate (6g) is much smaller than that of the holder (3.5 kg). The holder acts as a heat sink whose temperature determines that of the substrate which in its turn determines the film temperature. The rise in temperature of the substrate holder, $\Delta\theta_{sh}$, may be calculated in a similar manner as was done in section 6.4.1. The total amount of condensation heat released by a film, $Q_{tf\ con}$, deposited on the face of the substrate holder and on the substrates is given by :

$$Q_{con\ tf} = A_{sh}\ (\rho y\ \Delta H_c)_f$$

$$= \Delta\theta_{con\ sh}\ [\ (mc)_{sh} + (mc)_s + (mc)_f\ ]$$

where the subscripts f, s and sh denote film, substrate, and substrate

holder respectively. Now $(mc)_f << (mc)_s << (mc)_{sh}$

$$\therefore \quad \Delta\theta_{con\ sh} = \frac{A_{sh}\ (\rho y\ \Delta H_c)_f}{(mc)_{sh}}$$

This assumes that the CdS film is unifcrm over the whole area. However, as discussed in Chapter 5 (section 5.4), film thickness varies with the cosine of the deposition angle, having a maximum value at the centre, and practically zero at the edges. To a good approximation the film may be assumed uniform with a thickness equal to $\frac{y}{2}$.

$$\therefore \quad \Delta\theta_{con\ sh} = \frac{1}{2}\ \frac{A_{sh}\ (\rho y\ \Delta H_c)_f}{(mc)_{sh}} \qquad \ldots\ldots\ldots\ (6.16)$$

Now for stainless steel $c_{sh} = 510\ J.kg^{-1}.K^{-1}$, $m_{sh} = 3.5\ kg$, $A_{sh} = 6.25 \times 10^{-2}\ m^2$.

For a 100 μm film

$$\Delta\theta_{con\ sh} = \frac{1}{2} \cdot \frac{6.25 \times 10^{-2} \times 4.8 \times 10^{3} \times 10^{-4} \times 2.1 \times 10^{6}}{3.5 \times 510}$$

$$= 35^{o}C$$

Similarly the substrate-holder temperature rise due to radiation heat may be worked out from the equation :

$$\Delta\theta_{rad\ c\text{-}sh} = \frac{\dot{Q}_{rad}\ t}{(mc)_{sh}} \qquad \ldots\ldots\ldots\ (6.17a)$$

where t is deposition time

$$\therefore \text{ Temperature rise per second } = \dot{\Delta\theta}_{rad\ c\text{-}sh} = \frac{\dot{Q}_{rad}}{mc_{(sh)}} \qquad \ldots\ldots\ldots\ (6.17b)$$

From equation (6.12) for e.b.b. evaporation $\dot{Q}_{rad\ c\text{-}sh}$ = W, for a deposition time of 6000 s (100 min)

$$\Delta\theta_{rad\ c\text{-}sh} = 3^{o}C \qquad \ldots\ldots\ldots\ldots (6.18a)$$

For a deposition time of 36000 s.(10 hours)

$$\Delta\theta_{rad\ c\text{-}sh} = 24^{o}C \qquad \ldots\ldots\ldots\ldots (6.18b)$$

From equations (6.12) and (6.13) it is seen that the radiation received by the substrate holder from the furnace at 700 kelvin is 75 times that received by it from e.b.b. crucible at 1000 kelvin. Therefore, the rise in temperature in 6000 seconds is given by :

$$\Delta\theta'_{rad\ c\text{-}sh} = 225^{o}C \qquad \ldots\ldots\ldots\ldots (6.19a)$$

This is an over estimate for two reasons. First because the geometric factor was assumed unity as an approximation to give the most extreme care. Second it was assumed that the substrate holder does not lose any heat to its environment. This is true for convection and conduction heat because the substrate holder is in vacuum and is thermally insulated from its supporting pillars. However as soon as the substrate-holder temperature, θ_{sh}, increases appreciably above that of the bell jar ($\simeq 60^{o}C$), its top surface (i.e. the one that is not facing the furnace) starts losing heat by radiation. The amount of heat lost is proportional to the fourth power of its temperature (equation 6.4), and becomes appreciable when the substrate temperature is greater than twice that of the bell jar. Thus the equilibrium temperature will be about half of that predicted by equation (6.19a), i.e. :

$$\Delta\theta'_{rad\ c\text{-}sh} = 112^{o}C \qquad \ldots\ldots\ldots\ldots (6.19b)$$

It is to be noted, however, that when a film is deposited on a very thin substrate whose thermal inertia is very small and whose thermal conductivity is much lower than that of aluminium, e.g. quartz or mica, its temperature rise would be much more than in the present case. A deposited thin-film temperature sensor has been used to measure the rise in temperature at the interface between a film and its 1 mm thick glass substrate, due to condensation heat from aluminium, copper and tungsten evaporated from an e.b.b. source. A typical temperature rise is $10^{o}C$ for an aluminium film 1.2 μm thick deposited in one minute. The temperature rise due to radiation heat was also determined experimentally and it was found to be negligible when e.b.b. evaporation was used which is in agreement with the results presented above in connection with the present deposition experiments. Experimentally determined [3] time constants for deposition of silver and gold films of 16 and 11 s, on thin substrates have been reported. Again this is in agreement with theoretical predictions discussed in section 6.4.1.

6.4.3. Thermal state of a substrate during film deposition when its temperature is automatically controlled

In this case the substrate temperature is raised above that of its environment and held there by an automatically controlled heater. Thus, another source of heat is introduced into the evaporation chamber, i.e. the substrate heater, in addition to the other sources of heat discussed above. In all deposition experiments the substrate temperature reaches equilibrium before deposition starts. The substrate temperature rise time is normally of the order of few minutes depending on the power rating of the heater and on heat losses from the substrate and its holder. When steady state is reached, the heater only supplies as much heat as is needed to keep the substrate temperature at its set value.

Let the total heat losses from the substrate and its holder at temperature, θ_{set}, be $\dot{Q}_{\ell}$, and let $\dot{Q}_h$ be the heat supplied by the heater at equilibrium. Then before deposition starts $\dot{Q}_{\ell} = \dot{Q}_n$. When deposition starts, however, condensation heat, $\dot{Q}_{con}$, and radiation heat, $\dot{Q}_{rad}$, start acting on the system, and, in order that the substrate temperature stays at its set value the following condition must hold :

$$\dot{Q}_{\ell} = \dot{Q}'_h + \dot{Q}_{rad} + \dot{Q}_{con} \qquad \ldots\ldots\ldots (6.20a)$$

where $\dot{Q}'_h$ is the power supplied by the heater during deposition. Therefore the temperature of the substrate will not rise above its set value provided that :

$$\dot{Q}_{\ell} > \dot{Q}_{rad} + \dot{Q}_{con} \qquad \ldots\ldots\ldots (6.20b)$$

In deposition experiment in the present work Q_{ℓ} is of the order of few hundred watt depending on substrate temperature, and it is always greater than the sum of $\dot{Q}_{rad}$ and $\dot{Q}_{con}$. The substrate temperature, therefore, never rises above its set value. This is confirmed by the fact that during film deposition, the indicated substrate temperature stays constant throughout the process. If the substrate temperature rises above its optimum (set) value, the resulting film may have a different chemical composition from that intended (see Chapter 4, section 4.5.1). Also an appreciable rise in substrate temperature may affect the growth environment of a film whose crystal orientation may depend, among other things, on the substrate temperature, and heat flow across the film. Another factor that may affect crystal growth is the possibility that film (crystal) anisotropy may change the direction of heat flow during growth even when the substrate temperature stays constant, thus altering the temperature gradient across the film. The effect of cadmium sulphide crystal anisotropy on heat flow across a thin film

is discussed below.

6.4.4. Effect of film (crystal) anisotropy on heat flow

In all the above, it was assumed that the growing film was completely isotropic, and that heat flow always directed at right angles to the plane of the film i.e. the film's surface was isothermal. However when the film is not isotropic i.e. when it has a crystallographic orientation, the crystal anisotropy may affect the direction of thermal flow. In particular, when a CdS film grows with its c-axis either normal to the substrate or inclined at angle to the substrate-normal the direction of heat flow may not be the same in these two cases. Further, if the film is composed of oblique and normal crystallites, then its surface may not be isothermal i.e. heat may flow from one grain on the surface where the thermal conductivity is low to another grain where the conductivity is higher. This would affect the growth environment of the film (crystal), and was advanced [6] as a hypothesis to explain why changes in film orientation occurred as the deposited film grew thicker. This hypothesis assumes that in hexagonal cadmium sulphide crystal anisotropy affects thermal flow i.e. that the thermal conductivity of cadmium sulphide is anisotropic. This, indeed, appears to be the case from theoretical crystal symmetry considerations [7]. However, Moore [8] has measured the thermal conductivity in cadmium sulphide single crystals along the c-axis and in the basal plane at various temperatures. His experimental results show that the thermal conductivity of cadmium sulphide is isotropic i.e. there is no variation of heat flow with crystallographic orientation. It would seem unlikely therefore that temperature-gradient changes would occur in a cadmium sulphide film during growth, and an alternative explanation is offered in Chapter 8 (section 8.4.1) as to why orientation changes occur in

thick films.

6.5. Stresses in thin films

During film deposition the substrate temperature is above ambient temperature either because of condensation heat and radiation heat from the source, or because the substrate is deliberately heated to a certain temperature to give a film of given chemical composition and crystallographic structure. As the substrate and film cool down to ambient temperature, the film undergoes a state of stress. The stress arises from the constraint imposed by the substrate when the film attempts to change its volume. Assuming that the film and the substrate are elastically isotropic and that the substrate is much thicker than the film so that it does not bend, the substrate constraint causes a strain in the plane of the film and a Poisson's contraction normal to the film surface. This strain results in a bi-axial stress distribution in the plane of the film with a zero stress component normal to the surface. The stress may be compressive i.e. the film would like to expand parallel to the surface so that in extreme cases it may buckle up on the substrate or disintegrate completely. Alternatively, the film may be in a state of tensile stress, i.e. the film would like to contract and in certain cases the forces may be high enough to exceed the elastic limit of the film so that it breaks up into fragments. Movement of the film relative to the substrate will take place only if the adhesive bond between film and substrate is broken, otherwise the stress will deform the film either elastically or plastically. When thermal stresses are considered, compressive stresses result when the thermal coefficient of linear expansion of the film, α_f, is smaller than that of the substrate, α_s, and vice versa. Let the film and substrate (Fig. 6.2) cool from temperature θ_s to θ_a, then the strains in the substrate, ε_s, and film, ε_f, are

given by :

$$\varepsilon_s = \alpha_s (\theta_s - \theta_a), \text{ and } \varepsilon_f = \alpha_f (\theta_s - \theta_a).$$

Therefore, the net strain in the film, $\varepsilon_{net} = \varepsilon_s - \varepsilon_f = (\alpha_s - \alpha_f)(\theta_s - \theta_a)$.

Therefore, the stress in the film is given by :

$$\sigma_f = E_f (\alpha_s - \alpha_f) (\theta_s - \theta_a) \quad \ldots\ldots\ldots (6.21)$$

where E_f is the Young's modulus of the film. With this equation the convention is that compressive stresses are positive and vice versa. This equation also indicates that stress is independent of film thickness; a fact confirmed by experiment [2, 3]. When the substrate is not thick compared with the film, the film and substrate bend and the stress in the film is related to the radius of curvature. This enables stresses to be determined experimentally [4]. When a thin film is sandwiched between two thick films, then by a proper choice of top and bottom films the net stress in the middle film may be zero. For instance, if the top film gives a compressive stress, then the bottom film may be chosen to give a tensile stress of the same magnitude. This has been done for optical coating films [4]. Another interesting case is that of a very thin inter-layer between to thick films of the same material but different from that of the inter-layer. In such a case the net stress on the inter-layer is twice that of a single thin film of the inter-layer material. In the present investigation cadmium sulphide multi-layers have been fabricated with silicon dioxide (SiO_2) as a very thin inter-layer, as part of the investigation into orientation dependence on film-thickness.

For crystalline (anisotropic) fiims the relation between stress and strain is more complex than that given in equation (6.21). The stress tensor can have any orientation within a crystal, and it does not represent a crystal property but is akin to a "force"

impressed on the crystal which can have an arbitrary direction in the crystal i.e. the stress tensor is a "field tensor". This is in contrast to tensors which measure crystal properties i.e. "matter tensors", such as the piezoelectric tensor, of Chapter 2, which has a definite orientation within a crystal and must conform to the crystal symmetry. Although hexagonal crystals are elastically anisotropic, it has been pointed out that the ratios c_{11}/c_{33}, c_{12}/c_{13} and $\frac{2\,c_{14}}{c_{11} - c_{12}}$, of the elastic constants, of wurtzite CdS are close to unity, indicating that it is very nearly elastically isotropic [8]. This is not surprising in view of the closely related atomic arrangements in hexagonal and cubic CdS, as discussed in Chapter 2 (section 2.4). To a very good approximation, therefore, a deposited hexagonal CdS film may be taken as elastically isotropic, and equation (6.21) may be used to work out the stress in the CdS films and in the amorphous SiO_2 inter-layers.

As indicated in Table 6.1 (at the end of the Chapter), for CdS the value of the thermal coefficient of linear expansion, α, in a direction parallel to the basal plane, α_{basal}, is about twice that parallel to the c-axis, $\alpha_{//c}$. However, both α_{basal} and $\alpha_{\perp c}$ are small compared with α of the aluminium substrate, α_s. Therefore, $\alpha_s - \alpha_{basal} = \alpha_s - \alpha_{//c}$; and the strain in the CdS film is nearly independent of its crystallographic orientation. Substituting the appropriate values of α_s and α_f from Table 6.1 into equation (6.21) the thermal stress is in the plane a CdS film deposited at $170^{o}C$ on an aluminium substrate may be written as :

$$\sigma_{CdS/Al} = 1.5 \times 10^{3} \text{ pascal } (1 \text{ pascal} = 1 \text{ N.m}^{-2}) \quad \ldots\ldots\ldots (6.22)$$

This is a very large stress (approximately equivalent to 1.5 atmosphere or 20 p.s.i.) and may affect the film in a number of ways (see later).

This stress may, of course, give rise to peizoelectric charges on the surface of the film depending on the crystallographic orientation of the film. However, because the stress is static the resulting static charge will leak away through the film to ground. The changes [9] in elastic stiffnesses due to piezoelectric stiffening during straining CdS crystals perpendicular to the c-axis are less than 2%. There may be a small component of stress perpendicular to the plane of the film, due to the small anisotropy of CdS hexagonal crystals. The value of this component will depend on the crystallographic orientation of the film. When duralumin is used as a substrate instead of aluminium the stress in the deposited CdS film will be about 1.2 times greater. If, instead, the CdS film is deposited on soda lime glass (microscope slide) or sapphire at the same temperature its stress will be 3.5 times less, but still compressive. However, if the film is deposited on fused quartz, at the same temperature, its stress will be tensile and will have a value 15 times smaller than that given in equation (6.22). Similarly, the stress on the very thin amorphous inter-layer sandwiched between two CdS films (see Fig. 2.4d) may be written as :

$$\sigma_{SiO_2/CdS} = 3.4 \times 10^7 \text{ Pa (pascal)} \qquad \ldots\ldots\ldots (6.23)$$

As discussed in section 6.4.1, two kinds of stress in thin films may be distinguished: (a) intrinsic stress due to the top layer of the film being hotter than its interface with the substrate during deposition, (b) extrinsic stress due to differential thermal expansion between film and substrate as they cool down to ambient temperature. It is known [10] that the intrinsic stress in CdS films is compressive. It would seem possible, then, to obtain a stress-free CdS film by depositing it on a rigid fused quartz substrate e.g. a quartz rod. In section 6.4.1, the temperature difference across a 100 μm thick film was stated to be of the order of 10 millidegrees. Therefore

the intrinsic stress, σ_{in}, in the film is of the order of 10^3 Pa. This stress is much smaller than the extrinsic stress, σ_{ex}, of equation (6.22). Thus, intrinsic thermal stresses may be neglected in films deposited in the present investigation. However, in deposition experiments where the substrate thermal inertia is a few orders of magnitude smaller than that in the present work, and the thermal conductivity is also much smaller, the intrinsic stress could be comparable with, or much larger than the extrinsic stress [4, 10]. Intrinsic stresses have been measured in silicon monoxide [2] (SiO) and gold and silver films [3], using a cantilever deflection technique. The intrinsic stress in SiO was found [2] to be dependent on deposition angle. This may be due to the elastic anisotropy of the film. Non-destructive methods of evaluating residual stress in thin films have been studied [11]. Stresses may affect a deposited film in a number of ways : (a) They may be strong enough to overcome the forces that bind the film to the substrate causing it to flake off, (b) If the binding forces are very strong and the film stays on the substrate, these stresses may deform it elastically or plastically causing the film to reticulate or disintegrate, and (c) If the film does not disintegrate, these stresses may affect its physical properties by influencing its crystallographic structure e.g. by increasing the dislocation density.

6.5.1. Effect of stress on film adhesion

In most deposition experiments a film is required to adhere very strongly to the substrate. The most obvious exception is the use of films in replica techniques for electron microscopy where poor adhesion is expressly required. Three degrees of adhesion may be distinguished: (a) Very poor adhesion: where the film flakes off from the substrate on its own accord, e.g. due to the substrate being not very highly clean (b) Poor adhesion: where the film stays

on the substrate, but flakes off or disintegrates on handling, e.g. when a metallic bellows is impressed on it to make electrical contact (c) Good adhesion: where the film stays on the substrate even when handled. A simple criterion for testing film adhesion is the widely used simple "Scotch-tape" method. In this method adhesive tape is applied to the film surface and subsequently stripped off, whereby the film stays on the substrate if its degree of adherence is very good. This is a "go-no-go" technique and obviously gives no measure of the degree of good adhesion. The film either stays on or comes off with the tape. More sophisticated techniques are used to determine the exact value of the binding force between film and substrate. All the deposited films that withstood the Scotch tape test in the present investigation never flaked off or disintegrated throughout their life as test pieces undergoing various mechanical operations, e.g. being lapped with silicon carbide wheels (Chapter 8) and being "hammered" with a probe (Chapter 9). Adhesion energy values [4] may vary from tenths of electron volts (10^{-20} J) to 10 eV (10^{-18} J) or more, and because this is a wide range it is necessary to invoke two different mechanisms [4] to explain the nature of the binding forces. For low values of adhesion, the adsorbed atoms keep their electron shells intact and the forces holding them to the surface are of the van der Waals type (physi-sorption), i.e. the force is physical in nature and is primarily electrostatic due to the difference in work function between film and substrate. For higher adhesion energies, chemical bonds must exist between substrate and film, i.e. sharing of electrons takes place between substrate and film atoms (chemi-sorption). Thus, oxygen-active metals form chemical bonds to the substrates and are strongly adhesive, whereas those which form only physical bonds are easily removed [4]. Chromium has a higher work function [12] than that of gold, silver, aluminium and copper, and is widely used as an "adhesive"

between substrate and film in the form of a very thin inter-layer. The cleaner the substrate surface, the higher the degree of adhesion between it and the deposited film. When the substrate is not very highly clean the films always flake off even before being handled in any way (see Chapter 5). A deposited film has been observed to leave the substrate in one of two manners. In the first, the whole film comes off, i.e. it does not reticulate or disintegrate. This was observed in the earlier deposition experiments and is attributed to the "dirtiness" of the substrate i.e. the binding forces between film and substrate are not very strong because the substrate surface is not very clean. The second process by which a film left the substrate occured in stages. The top layer of the film crinckled and flew away in the air in small flakes followed by the fragmentation of other layers, and finally the film would fracture. The mechanism of final fracture is one of localised plastic deformation with a resultant thinning of the film. This gives a rise in the stress level and small cracks appear and when they join up the film fails. This may indicate that stress in the film is inhomogeneous. It was always found that once a film had passed the Scotch tape test it always stayed on the substrate. When CdS films were observed to peel-off as a whole, it was always found that they curled-up, indicating that the stress in them was inhomogeneous.

So far adhesion has been thought of as a mechanical property of the whole film. However, on an atomic scale the removal of a film consists of the breaking of bonds between the individual atoms of the film and of the substrate so that macroscopic adhesion can be considered as the summation of individual atomic forces. It is, then, possible to relate the adsorption energy, E_a, of a single atom on the substrate to the total adhesion energy of the film [4]. E_a is

defined as the energy required to remove an atom from a substrate, and is related to the probability of evaporation, β, of a single atom on the substrate surface by : $\beta = \nu \exp \frac{-E_a}{k\theta_s}$, where k is Boltzmann's constant, ν is a vibrational frequency and θ_s is the substrate temperature. Electron microscope nucleation techniques may be used to measure the adsorption energy E_a, and comparison between adsorption-energy values from this technique and adhesion as obtained from a mechanical point of view has only been done in one or two cases because of the difficulties in measuring E_a, and making meaningful quantitative measurements by mechanical techniques [4].

It was stated above that the stress on a deposited film is independent of its thickness. However the total force acting on the film (per unit width) is directly proportional to its thickness. It is to be expected, therefore, that if the film thickness is increased n times, the force acting on it, F_1, increases likewise. When considering film adhesion to a substrate this force may be thought of as trying to overcome the binding forces, F_2, between film and substrate. The film remains bonded to the substrate provided that $F_1 < F_2$. Now F_2 is independent of the film thickness since its field does not penetrate beyond the interface between substrate and film. As the film thickness increases, however, F_1 increases and when a certain thickness is reached this inequality may be reversed, and the film flakes off. In the present investigation, cadmium sulphide films deposited on very highly polished aluminium rod substrates were observed to have a critical thickness of about 30 μm, above which deposited films flaked off. This is in agreement with the results of Llwellyn et al [13] where it was found that CdS films thicker than 10 μm deposited on cadmium single crystal rod substrates flaked off, whereas thinner films adhered very well to the substrate. This flaking off of thick vacuum deposited films has an analogy with earlier observations [4] of stress in optical coatings, where it was

found that too thick a coating tended to crack or peel off from the substrate. Another factor that may help the film to flake off is a stress perpendicular to the plane of the film due to its elastic anisotropy, giving rise to a large component of force perpendicular to the plane of the film as discussed in section 6.5 above. In later deposition experiments CdS films up to 100 μm thick were made to adhere very strongly to the aluminium rod substrates by making the substrate surface "rougher". In the early experiments the substrates were polished in six stages giving a final centre-line-average (c.l.a.) of 20 nm. For the deposition of thick films the substrates were only polished in four stages giving a c.l.a. of 430 nm, see Fig. 6.3. As can be seen from this figure, the surface profile is still smooth on a microscopic scale, and should not give any shadow-masking effects when deposition at an angle is used. When shadow-masking occurs the crests on the film surface mask the vapour beam from the troughs, making the growth of oblique nuclei much more difficult compared with that of normal nuclei (see Chapter 8). With this surface finish all the CdS films stayed on the substrate. This is because of the key-in action between film and substrate which makes it much more difficult for the thermal forces, which are in the plane of the film, to move the film relative to the substrate. Putting it another way, the films are so well "dug-in" that their resistance to peeling-off the substrate is much increased.

6.5.2. Effect of stress on physical properties of films

Very little [14] data is found in the literature for the effect of stress on the physical properties of thin films. This is because the major effort in thin-film technology has been concentrated on controlling the deposition parameters so that a successful device could be made. In this respect, the stress is only of importance so far as the mechanical integrity of the film in a device is concerned. However, as discussed above, the stress in thin films

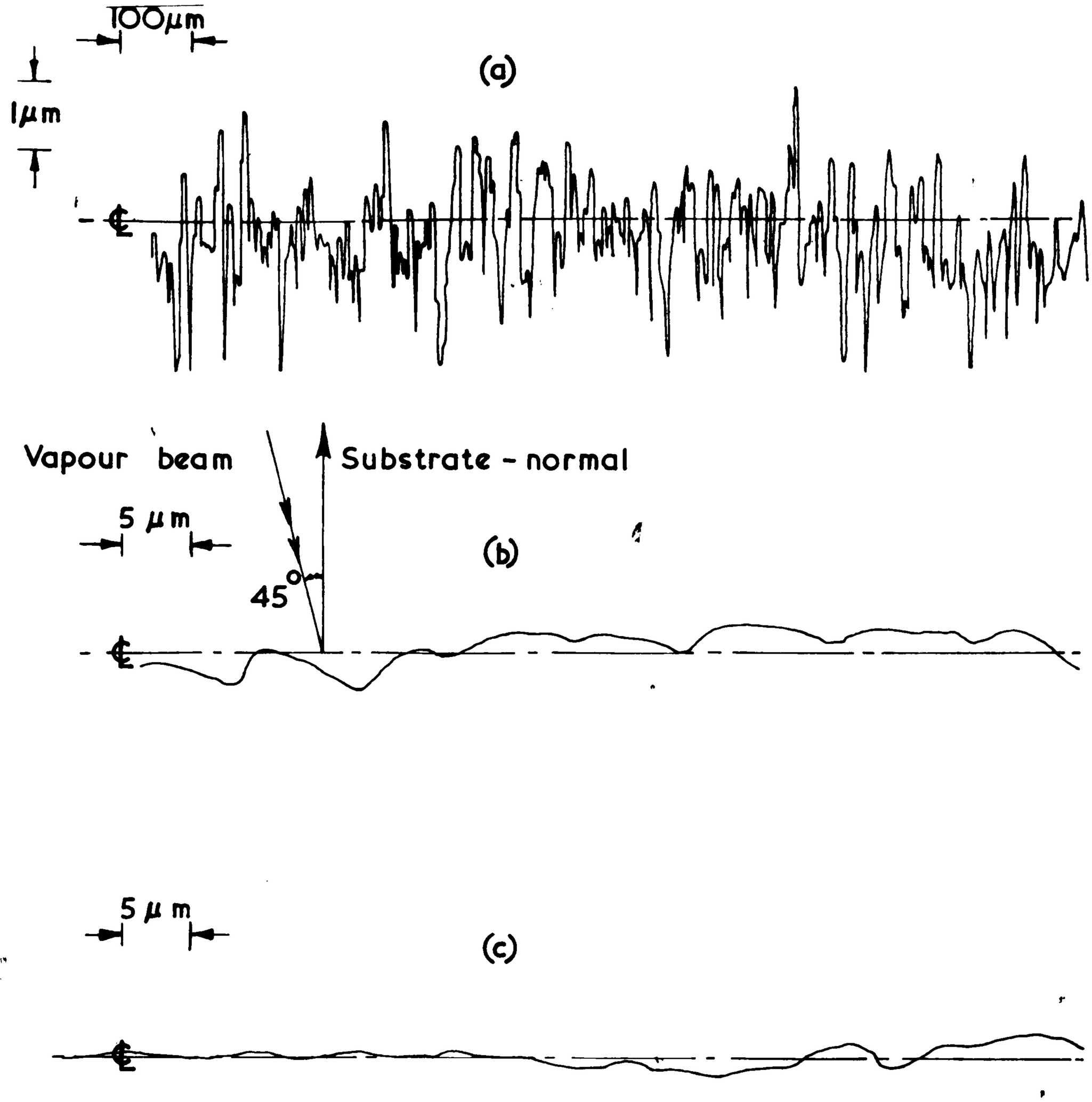

FIG. 6.3 Surface finish of aluminium substrate after lapping with silicon carbide (600 grit) (a) Along a diameter perpendicular to polishing "lines" (b) Same as (a) with horizontal magnification increased twenty times (c) Along a diameter parallel to polishing lines ("Talysurf" traces)

Centre line average = 0·43 μm

is often large and comparable to the stress used in high pressure investigations [14]. Since the elastic properties of thin films are in general similar to those of bulk materials, data obtained with bulk single crystals may be used to explain phenomena that may occur in thin films. Some of the phenomena observed in the present work, that may be linked with stresses in the films are discussed below.

(a) It is known [15] that when a single crystal bar of CdS is bent, the dislocation density increases a hundred times at the centre of the bar. Thus the stress in CdS films on Aℓ rods may be expected to increase the dislocation density in the films. However, because the stress in CdS films on glass is much less, this phenomenon may not be significant in such a case. It has also been found [16] experimentally that the thickness-mode piezoelectric coupling coefficient, k_t, is a function of dislocation density in bulk CdS single crystals. The value of k_t stays constant over a wide range of values of dislocation density but starts rolling down to zero very abruptly once a critical value of dislocation density has been reached [16], see Fig. 6.4. The weak ultrasonic performance of as-deposited CdS films on Aℓ (section 9.3.1) may be due to a high dislocation density in the films.

(b) Although the ultrasonic response of as-deposited films on aluminium was weak, it was, nevertheless, possible to distinguish between shear-mode and compressional-mode echoes (see Chapter 9). However, the shear-mode echo from one transducer deposited on aluminium that had been observed, disappeared when the same transducer was tested two days later, leaving only the c-mode echo. This may be due to plastic flow taking place in the film. As discussed in Chapter 2 (section 2.3), for a CdS film to give s-mode and c-mode echoes simultaneously its c-axis must be inclined at an angle to the substrate-normal. Alternatively, the film may be composed of microcrystals

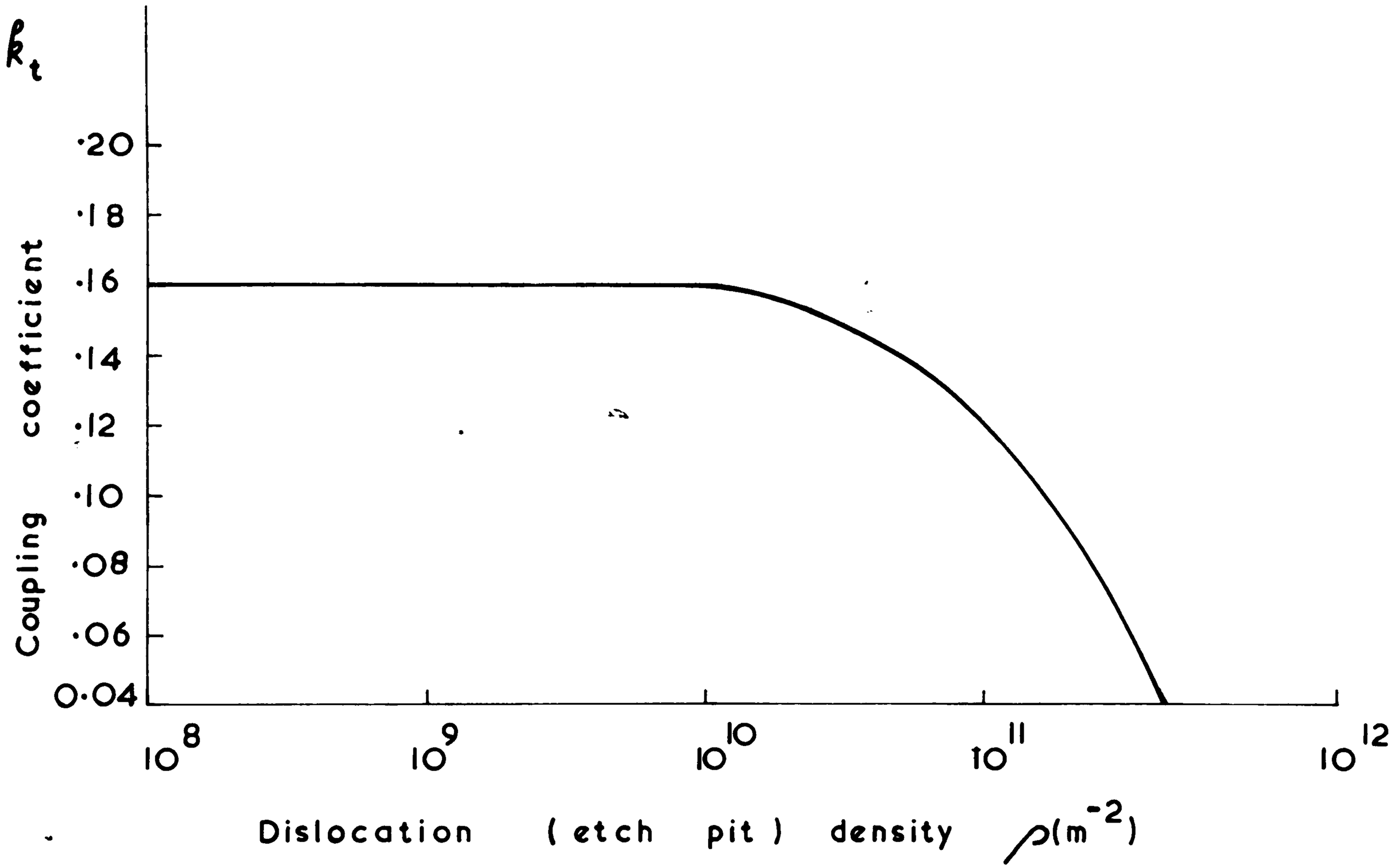

FIG. 6.4 Experimentally determined values of thickness-mode piezoelectric coupling coefficient versus dislocation density for single crystal CdS (after Chubachi.[16])

(crystallites) the c-axis of some of which is normal to the substrate while that of the others inclined at an angle. It is known that the critical shear-stress for plastic flow in bulk CdS is 3×10^6 Pa at a temperature of 420^o, and that plastic flow also occurs at room temperature [15]. It is also known that hexagonal crystals are plastically anisotropic and that the basal plane has the lowest shear stress. Some confirmation for this for bulk CdS has been given by Shiozawa [15] who found that the microhardness is greatest for indentation normal to (001), i.e. when the shear stress on (001) is minimum. If plastic flow were to take place then the oblique crystallites would be the ones which were deformed with a consequent increase in their dislocation density. This increase in dislocation density may weaken the piezo-electric performance of these crystallites (see above), leaving the normal crystallites to give the c-mode echo.

Very little is known on the effect of stresses and of dislocation density on piezoelectricity in thin films of CdS, or indeed in any other piezoelectric material. However, the effect of stress on the Curie temperature of some magnetic thin films, the transition temperature of superconducting thin films, and the resistivity of epitaxial silicon films, has been recently reported [14]. The Youngs modulus of copper thin films was reported to be independent of film thickness, while its breaking strength like that of silver, gold and nickel films, was found to *decrease* with thickness [17]. This may be due to the thicker films being under the influence of a larger force than the thinner ones, as discussed above.

Plastic deformation has been observed in gold films under stress of the order of 2×10^7 Pa, when the film is stretched beyond its elastic limit [4]. Even below the elastic limit there is evidence for creep, and creep elongations of 0.06% in 80 minutes have been reported [4] for evaporated silver films stressed below the elastic limit. Creep in magnetic films has also been observed [18].

Property	Material	Value	Comments	Ref
Thermal coefficient of linear expansion α (K^{-1})	CdS	2.1×10^{-6}	//c	19
		4×10^{-6}	basal	
	Al_2O_3	7.8×10^{-6}	//c	12
		7.1×10^{-6}	basal	
	SiO_2	0.4×10^{-6}	Fused	20
	Soda glass	8×10^{-6}		20
	Al	23.2×10^{-6}	Polycrystalline	20
	Dural	27		20
Thermal conductivity k ($W.m^{-1}.K^{-1}$)	CdS	20	At $30^{o}C$	19
	Al	230	At $20^{o}C$	12
	Stainless steel	25	At $200^{o}C$	20
Specific heat c ($J.kg^{-1}.K^{-1}$)	CdS	390	At $50^{o}C$	21
	Al	900	At $20^{o}C$	22
	SiO_2	790	At $20^{o}C$	21
	Stainless steel	510	At $100^{o}C$	20
Heat of condensation ΔH_c ($J.kg^{-1}$)	CdS	2.1×10^{6}		23
Young's modulus E Pa	CdS	4.6×10^{10}	Isotropic	24
	SiO_2	7×10	Isotropic	20

TABLE 6.1. Thermal and mechanical constant of some relevant materials

C H A P T E R 6

REFERENCES

1. G.F.G. Rogers et al, *Engineering thermodynamics*, Longmans (1964).

2. A.E. Hill et al, *Stress in films of SiO*, Brit. J. Appl. Phys. 18, p. 13 (1967).

3. J.D. Wilcok et al, *The internal stress in evaporated silver and gold films*, Thin Solid Films, 3, p. 13 (1969).

4. D.S. Campbell chapter in, *Handbook of thin film technology*, ed. L.I. Maissel et al, McGraw-Hill (1970).

5. G. Breitweiser et al, *Influence of film condensation and source radiation on substrate temperature*, J. Vac. Sci. Tech. 7, p. 274 (1970).

6. R.G. Rhodes, *Private Communication.*

7. J.F. Nye, *Physical properties of crystals*, Oxford Univ. Press (1964).

8. G.E. Moore et al, *Thermal conductivity of doped and pure CdS*, Phys. Rev. 179, p. 722 (1969).

9. B.N. Das et al, *Stacking fault energy and polygonization in vapour grown CdS*, Mat. Res. Bull. 5, p. 751 (1970).

10. R.R. Addis, *Recrystallization of CdS films*, Trans. 10th Nat. Vacm. Symp. Am. Vacm. Soc. p. 354, Macmillan N.Y. (1963).

11. G.A. Walker, *Structural investigation of thin films*, J. Vac. Sci. Tech. 7, p. 465.

12. *American Institute of Physics Handbook*, McGraw-Hill (1963).

13. J.D. Llewellyn et al, *Apparatus for the deposition of low frequency CdS transducers*, J. Sci. Inst. (Journal of Phys. E) 2, p. 535 (1969).

14. E. Klokhom, *Effect of stress on the physical properties of thin films*, J. Vac. Sci. Tech. 8, p. 148 (1971).

15. L.R. Shiozawa, *II-VI compound semiconductors*, AD Report No. 620297 (1968).

16. N. Chubachi et al, *Influence of dislocations in CdS crystal on its electro-mechanical coupling factors*, JAP 42, p. 962 (1971).

17. H. Leidheiser et al, *Mechanical properties of copper films*, JAP 41, p. 402 (1970).

18. L.I. Maissel et al ed., *Handbook of thin film technology*, McGraw-Hill (1970).

19. EPIC, *II-VI semiconducting compounds data tables*, by M. Neuberger (1969).

20. G.W.C. Kaye et al, *Tables of physical and chemical constants*, Longmans (1966).

21. N.A. Lange, *Handbook of chemistry*, McGraw-Hill (1956).

22. *Chemical Rubber Company Handbook*, (1970).

23. G.A. Somarjai, *The evaporation rate and mechanism of CdS and CdSe*, Proc. Intl. Symp. Evapn. Condn. Dayton, Ohio (1962).

24. O.L. Anderson chapter in *Physical Acoustics*, Vol. 3B, Academic Press (1965).

C H A P T E R 7

Determination of crystallographic structure of deposited films (theory and techniques)

7.1. Introduction

In this chapter the theory and techniques of crystallography are introduced on the lines presented in standard texts [1,2,3]. The significance of the Bragg law and the Bragg angle, and of the Laue equations is discussed in relation to their use in determining the crystal structure of various materials. The experimental procedure used by the author to determine the preferred orientation of cadmium sulphide films is presented together with values for the Bragg angle, for various crystallographic planes, for hexagonal (wurtzite), and cubic (sphalerite) cadmium sulphide (Table 7.1). A theoretical value for the X-ray mass absorption coefficient in cadmium sulphide is worked-out.

7.2. Crystals, crystal systems and classes

A single crystal is homogeneous, in the sense that it has identical properties at all points within it. However, it is not, in general, isotropic, that is to say, directed properties such as thermal or electrical conductivity or the coefficient of thermal expansion or the velocity of propagation of acoustic waves within the crystal depend upon the direction in the crystal which is being considered. Parallel to any given direction, thus, the properties at all points in the crystal are the same, but at any point the same property differs in different directions. Crystal homogeneity is a consequence of the regular geometrical form of a crystal which, in its turn, is a consequence of the regular arrangement of the atoms of which the crystal is built. The regularity is that of a 3-dimensional

pattern (the space lattice) in which a certain unit of structure (the unit cell) is repeated over and over again in space. The dimensions a, b, and c of the unit all (Fig. 7.1a) may or may not be equal, and the inter-axial angles α, β, and γ may or may not be equal, and may or may not be right angles depending on the crystal considered. If all combinations of equality and inequality in inter-axial angles and in lengths are considered, it is found [1] that a total of 14 kinds of lattice are possible. The term "lattice" is used to refer to the scheme of repetition of the unit cell in the crystal, and not to the actual arrangement of atoms in a crystal. The atomic arrangement is called the "structure" of a crystal, and an unlimited number of structures (e.g. various materials) can be conceived while only 14 lattices are possible.

In order to specify a given point in a lattice (or atom in a structure), its co-ordinates are referred to the crystal axes $\vec{a}$, $\vec{b}$ and $\vec{c}$ (Fig. 7.1a). Each space lattice has some convenient set of crystallographic axes that is conventionally used with it. For example, for cubic and hexagonal crystals the axes are referred to the three contiguous edges of a cube, and the three edges of a single hexagonal cell, respectively, Fig. 7.1b and c. A total of seven different systems of axes each with specified equality or inequality of lengths and angles are chosen, giving the seven "crystal systems". For example in the cubic and hexagonal systems $a = b = c$, $\alpha = \beta = \gamma = 90^{o}$, and $a = b \neq c$, $\alpha = \beta = 90^{o}$ and $\gamma = 120^{o}$ respectively. The seven crystal systems are : cubic, hexagonal, trigonal (rhombohedral), tetragonal, orthorhombic, monoclinic and triclinic. Each system is subdivided into a definite number of classes according to the degree of symmetry within the system e.g. among cubic and hexagonal crystals five and seven classes exist, respectively, possessing progressively more and more elements of symmetry until the full symmetry of the perfect cube or hexagon is attained. The symmetry elements of all crystals consist

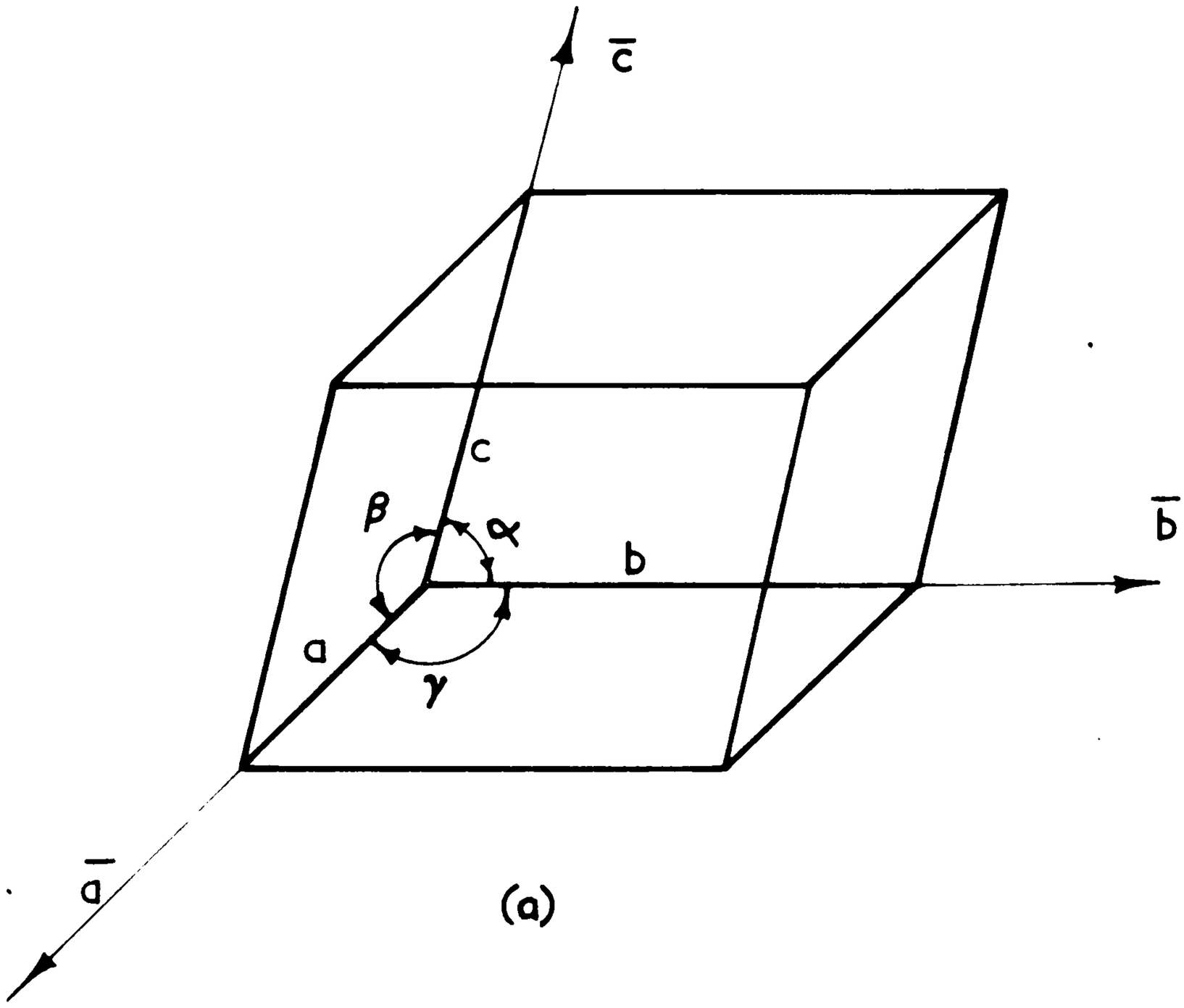

FIG. 7.1 Unit-Cell (a) general,

(b) cubic , (c) hexagonal.

of a combination of one or more rotation axes, planes of symmetry and centres of symmetry. In a combination of these elements all the members may be regarded as passing through a single point giving rise to the symmetry elements of various point-groups (classes). It can be shown [4] that there are only 32 different point groups, and accordingly crystals are divided into 32 "crystal classes" with respect to the point-group symmetry they posses. Every crystal class is given a symbol which summarises its essential symmetry elements, e.g. 6 mm is the symbol used to represent a class of crystals that have a 6-fold rotation axis (i.e. hexagonal) and two mirror planes.

If the vector from the origin to the point x, y, z in a crystal lattice is $\vec{r}_{x,\,y,\,z} = x\vec{a} + y\vec{b} + z\vec{c}$ where $\vec{a}$, $\vec{b}$, $\vec{c}$ are the vectors representing the unit cell (Fig. 7.1a) then the co-ordinates of the point are x, y, and z i.e. they are expressed in terms of the unit cell dimensions and not in absolute units of length. This is a consequence of the Law of Rational Indices governing the existance of crystal planes. For example, with an origin chosen at a lattice point, the point at position 3, 2, 1 lies at the end of the vector $\vec{r}_{321}$ and is reached by moving along the $\vec{a}$ axis a distance of three times a, then parallel to $\vec{b}$, a distance twice b, and finally parallel to $\vec{c}$ a distance equal to c. Similarly the position of an atom in a unit cell is specified in terms of a, b and c, e.g. in the hexagonal close packed (h.c.p.) crystal structure (class 6/mmm), e.g. cadmium and zinc crystals, the atoms are centred at the positions which have co-ordinates o, o, o and $\frac{2}{3}$, $\frac{1}{3}$, $\frac{1}{2}$ in each unit cell.

7.2.1. Indices of lattice directions

The notation [uvw] is used to indicate the direction of a line from the origin to a point whose co-ordinates are uvw. It is customary to use square brackets, to avoid fractional indices, and to use the smallest integers that will locate a point on the line. Negative

indices and written with a bar above them. Because of symmetry, various directions in a crystal are equivalent e.g. the cube edges of a unit cell of a cubic crystal are equivalent. Such (equivalent) directions are indicated by carets : <uvw> e.g. <100> for the example above. Some crystal directions are shown in Figs. 2.1d and 2.2e (Chapter 2).

7.2.2. Indices of lattice planes

Miller indices are universally used as a system of notation for faces of a crystal or planes within a crystal or a space lattice. These indices are based on the intercepts of a plane with the three crystal axes, each intercept with an axis being measured in terms of the unit cell dimensions (a, b, and c) along that axis (not in absolute units of length). To determine the Miller indices of a plane the following procedure is used : (1) the intercepts on the three crystallographic axes are found, (2) the reciprocals of these intercepts are taken, (3) these are then reduced to the three smallest intergers having the same ratio, (4) enclose in parenthesis : (hkℓ). The indices of some crystal planes are illustrated in Fig. 7.2. For example, the Miller indices of the basal plane of a hexagonal crystal are (001) because such a plane is parallel to the a- and b- axes (intersection at infinity, and, therefore, the reciprocal of the intersection is zero, i.e. h = k = o), and it intersects the c-axis and a distance equal to one "c", and, therefore, ℓ = 1. Certain sets of planes of a crystal meet along a line or along parallel lines, e.g. the vertical sides of a hexagonal prism intersect along lines that are parallel to the c-axis. Such planes are known as planes of a zone, and the direction of their intersection is the zone axis. The important zones are the ones to whom many planes belong. Equivalent planes are indicated by curly brackets : { }.

7.3. Diffraction of X-rays by crystals

It has long been recognised [3] that a theory of the type presented above would account for the observed facts of crystalline form and

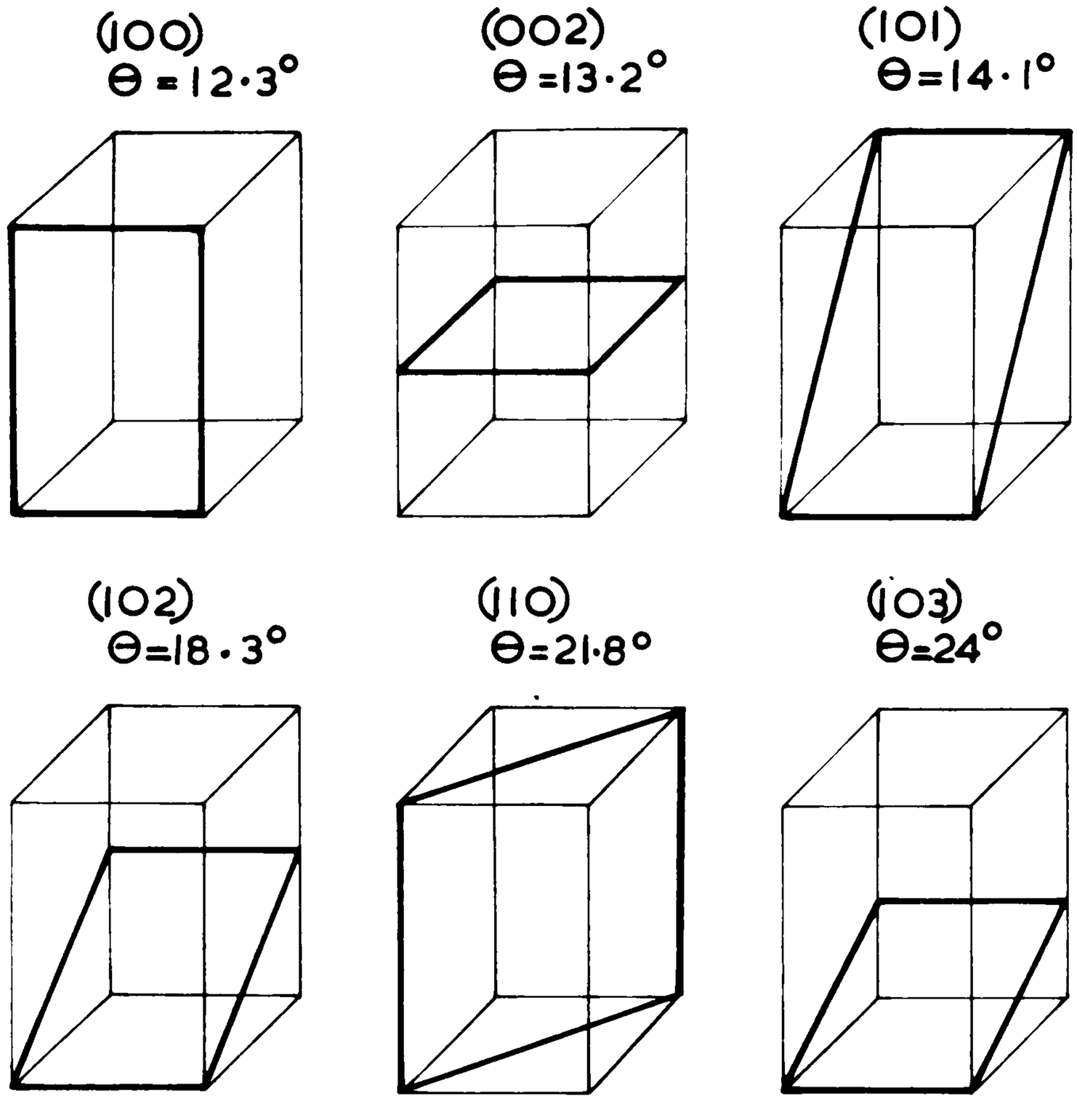

FIG.7.2 Various lattice planes for hexagonal cadmium sulphide, Θ is Bragg angle.

symmetry, and the geometry of such space patterns (the 14 lattice kinds) had been fully worked out, but it was not until the development of X-ray crystallography that it became possible to determine the actual nature of the unit cell and of the pattern in any crystal. The diffraction of X-rays by a crystal lattice will now be discussed.

7.3.1. Bragg's law and the Bragg angle

Consider a set of parallel planes of atoms in a crystal (atomic planes) AA and BB (Fig. 7.3a). Suppose that a beam of monochromatic X-ray is directed at the planes in the direction LM which makes an angle θ with the planes. The line LL, represents one of the crests in the approaching waves and is perpendicular to the direction of wave propagation. As this crest reaches each of the atoms in the plane it generates a scattered wave crest. Bragg's law states that reinforcement of scattered waves takes place when the incident beam and the scattered beam make equal angles with the atomic plane. It is then possible to regard the plane of atoms as a mirror reflecting a portion of the X-rays at an angle of reflection equal to the angle of incidence. It can be shown [1] that, the requirement tc be met, so that rays reflected from successive planes may reinforce each other, is :

$$n\lambda = 2\, d \sin\theta \qquad \ldots\ldots\ldots (7.1)$$

where n is an integer, λ is the wavelength of the X-ray, d is the spacing between the planes and θ is the Bragg angle.

7.3.2. The Laue equations

Diffraction from a crystal plane has been considered above as analogous to reflection from a series of semi-transparent mirrors, but it is also to be considered as a diffraction from a 3-dimensional grating analogous to the diffraction of light from a one-dimensional optical grating. If an X-ray beam is directed at a row of equally spaced atoms (Fig. 7.3b), each atom will be a source of scattered waves spreading

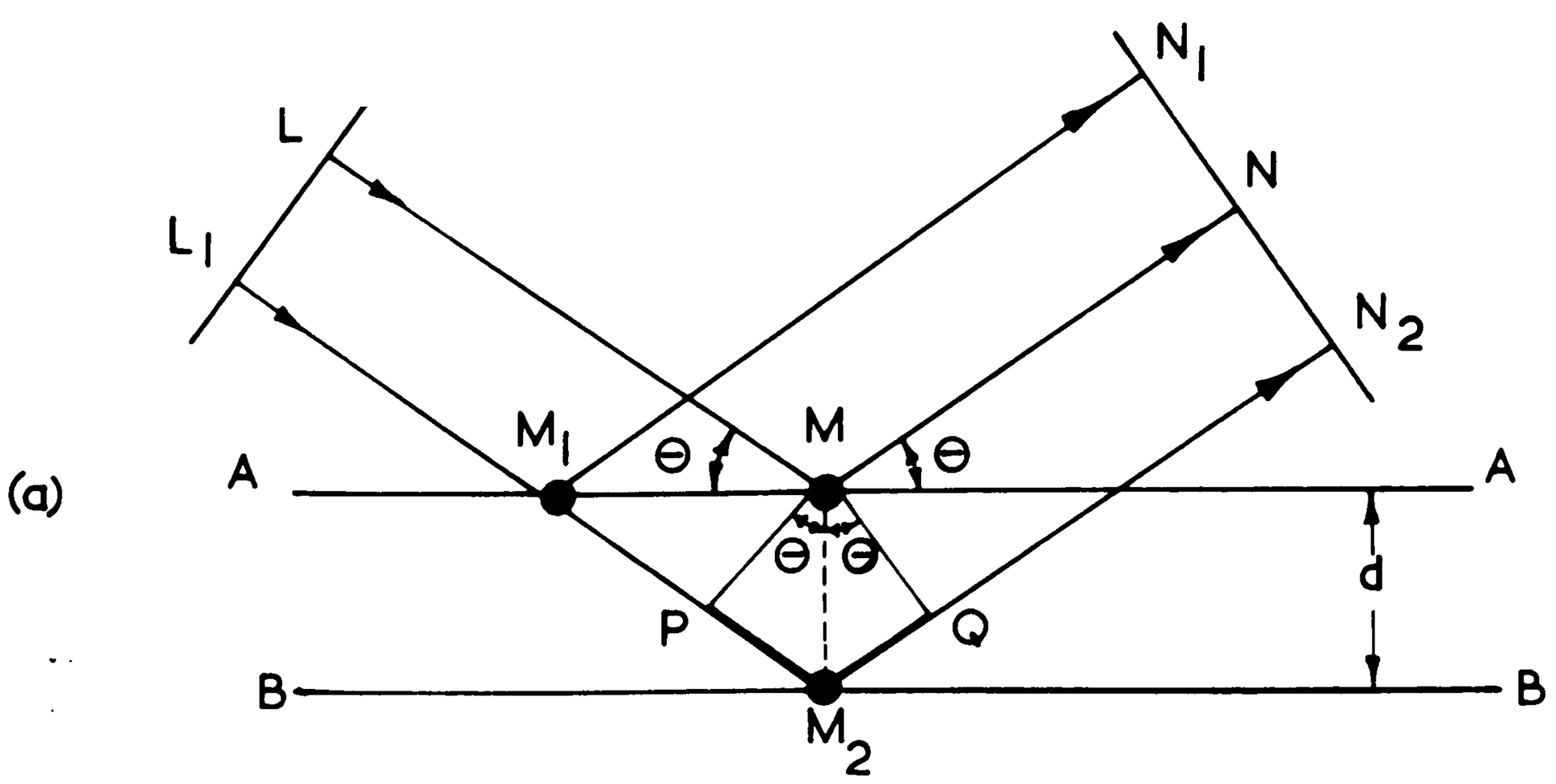

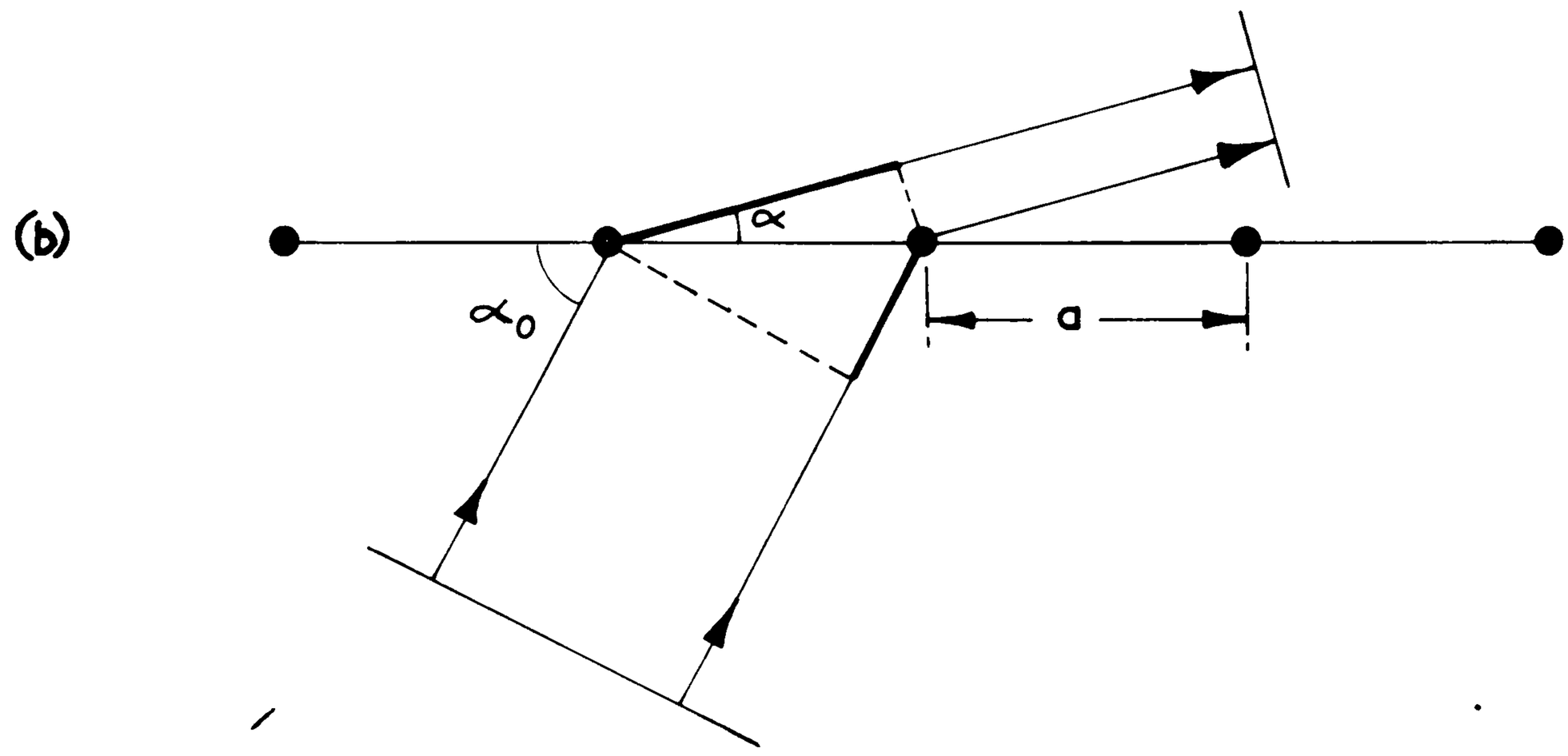

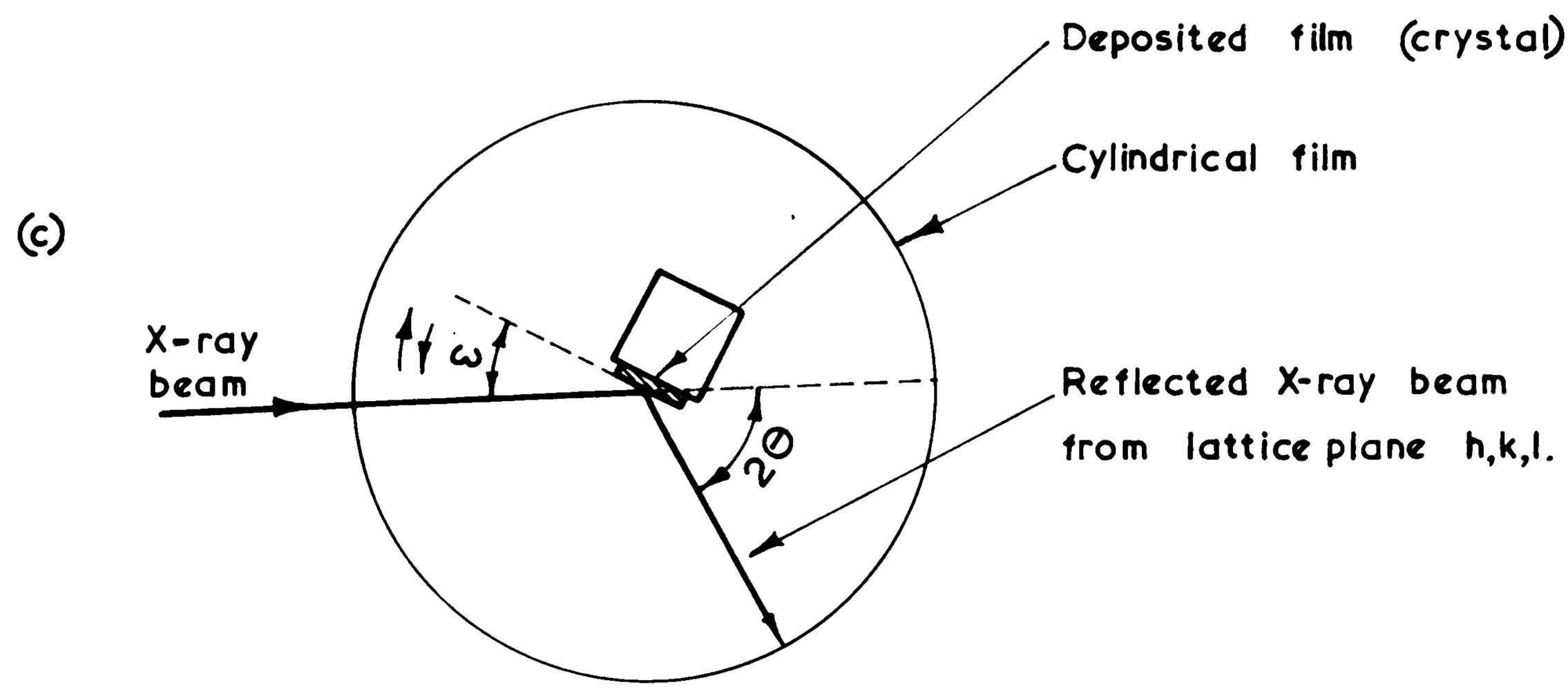

FIG. 7.3 (a) Bragg's law (b) Laue equations

(c) Schematic of oscillation camera X-ray diffraction set up,

Θ is the Bragg angle and ω is the rocking angle.

spherically which re-inforce in certain directions (Bragg angle) to produce a diffracted beam. Successive waves can be indicated by concentric arcs. The condition for re-inforcement can be derived [1] in terms of the wavelength of the X-rays, λ, the atomic spacing, a, and the angles of the incident, α_o, and diffracted, α, beams :

$$h\lambda = a\,(\cos\alpha - \cos\alpha_o)$$

where h is an integer representing the order of the diffraction. This equation will be satisfied by all the generators of a cone whose axis is concentric with the line of atoms and that has the semi-apex angle α. Thus for any given angle of incidence, α_o, there will be a series of concentric cones surrounding the rows of atoms each cone being made-up of one order of diffracted rays. If there is a two-dimensional network of atoms with spacing a in one direction and b in another, there will be two simultaneous equations to be fulfilled for intense diffracted beams :

$$a\,(\cos\alpha - \cos\alpha_o) = h\lambda$$
$$b\,(\cos\beta - \cos\beta_o) = k\lambda$$

where α_o, α, and β_o, β are the angles which the incidental diffracted beams make with the a- and b- rows of atoms respectively, and h and k are integers giving the order of reflection w.r.t. a- and b- rows respectively. A crystal is a 3-dimensional network of atoms and, therefore, for diffraction by crystals three simultaneous equations must be satisfied :

$$a\,(\cos\alpha - \cos\alpha_o) = h\lambda$$
$$b\,(\cos\beta - \cos\beta_o) = k\lambda$$
$$c\,(\cos\gamma - \cos\gamma_o) = \ell\lambda \qquad \ldots\ldots\ldots\ (7.2)$$

These equations are the Laue equations, in which the first two have the same significance as before, and the third relates to the periodicity

of the atoms in the third direction, the c-axis of the crystal, with which the incident beam makes an angle γ_o and the diffracted beam an angle γ. The interger ℓ is the order of diffraction w.r.t. the c-axis, and hkℓ can be called the indices of the diffracted beam. These indices are not enclosed in parentheses as the Miller indices are, for these may differ from the Miller indices of the reflecting plane by a common factor.

Bragg showed that [1] fulfilling the Laue equations is equivalent to a reflection from a lattice plane. The first order reflection is given the same indices as the plane e.g. the first order reflection from the (110) plane is written 110, while the second order is 220. With this scheme of notation the nth order reflection from (hkℓ) plane is equivalent to the 1st-order reflection from an imaginary plane spaced $\frac{1}{n}$th the spacing of (hkℓ). All higher-order reflections can be regarded as first-order reflections from such imaginary planes, and if the spacing of these planes is $d' = \frac{d}{n}$, where d is the true spacing of the lattice planes, then the Bragg equation (equation 7.1) may be written as

$$\lambda = 2d' \sin a \qquad \ldots\ldots\ldots (7.3)$$

where d' is the inter-planar spacing.

The Bragg angles for various lattice planes may then be computed from the various values of d' allowed in a given structure, and assuming that the wavelength of the X-rays is known. The inter-planar spacing, d', between various atomic planes (hkℓ) for various materials are published by the American Society for Testing of Materials (A.S.T.M.) from which the values for hexagonal and cubic cadmium sulphide were taken [5]. The Bragg angles were then computed using the HP 9100A desk computer, and the results are shown in Table 2.1 (see section 7.6).

7.4. X-ray diffraction techniques

It has been shown in the previous sections that the directions

of the reflected X-ray beams are governed entirely by the geometry of the lattice i.e. by the orientation and spacing of the atomic planes (Bragg's law, equation (7.1)) and by the periodicity of the lattice in three dimensions (Laue's equations, equation (7.2)). The intensities of diffracted beams, however, are determined by the arrangement of atoms within the unit cell. For example certain diffracted beams are extinguished because waves scattered by body-centred atoms are exactly out of phase with those scattered by atoms at the corners of the unit cell. Such is the case with the 001 reflection from the (001) plane of a cadmium sulphide crystal, and, therefore, no 001 reflection will appear on a diffraction pattern. However the 002 reflection is possible (i.e. reflection from planes whose spacing along the c-axis is half that of the unit cell, see Fig. 7.2).

Various techniques are used to obtain diffraction patterns from single crystals and from polycrystalline materials with preferred orientation. Some of the more important techniques are summarised below.

7.4.1. The Laue Method

In this method an achromatic ("white") X-ray beam is limited to a fine pencil about 500 micrometre in diameter by means of a collimator, and falls upon a thin slice of a stationary crystal. The unabsorbed transmitted beam impinges normally upon a light-proof photographic film yielding an intense centre-spot which is surrounded by a pattern of spots produced by the various diffracted beams. A fundamental property of the Laue pattern is the symmetry of the pattern which reveals the (unknown) symmetry of the crystal. If the X-ray beam were mono-chromatic, reflections would be purely a matter of chance, and their occurance would be very rare since in this method, the direction of the X-ray beam is fixed and the crystal is stationary,

the angles made by the incident beam with every possible set of planes is fixed in advance, the only variable being n (equation 7.1) which must be an integer.

7.4.2. The powder method (Debye and Sherrer method)

A powder photograph is obtained by allowing a narrow beam of mono-chromatic X-rays to fall upon a small specimen of the powder under investigation. Since the orientations of the crystal fragments (crystallites) are perfectly random, a certain number of them will be in such a direction that the Bragg condition for reflection is satisfied. The crystallites giving rise to these reflections must each be set at a grazing angle θ to the incident beam, about which they may have any orientation. The result is that the diffracted beams with the same hkℓ indices all lie upon the surface of a cone which has a semi-apex angle 2θ. When a flat photographic film is used the diffraction patterns are concentric rings, the centre being the spot at which the direct X-ray beam hits the film. The powder method presents a means whereby a compound may be identified, since no two powder-patterns are the same in all detail. The powder method may also be used for phase identification e.g. to find out whether the wurtzite (hexagonal) phase or cubic (sphalerite) phase of cadmium sulphide is present in a certain specimen.

The powder method was initially used in the present investigation to establish that the deposited cadmium sulphide were films of the hexagonal (alpha) phase, and that no cubic (beta) phase was present. In later experiments the oscillating crystal method was used to obtain more precise orientation measurements on deposited films, with the aid of a goniometer.

7.4.3. Oscillating (or rotating) crystal method

When an X-ray beam enters a crystal in an arbitrary direction there may be no simultaneous solution for the three Laue equations which

is necessary for reflections to occur. However, if a crystal is made to oscillate (or rotate) about the direction of the X-ray beam, with the axis of oscillation (or rotation) perpendicular to the X-ray beam, then the X-ray beam angle will have a wide range of values, making it more likely for reflections to occur. When a flat photographic film is used in such a set-up, then it is possible that some of the reflections may miss the photographic paper. In order to ensure that all possible reflections will fall on the photographic film a cylindrical film is used (Fig. 73c). This method has been used in the present work and the experimental procedure is described later.

The biggest advantage of the oscillating-crystal method is its separation of the reflections into layer-lines (Fig. 7.4). Not only does this prevent some overlapping of reflections that would superimpose in powder photographs but it makes assigning indices (i.e. indexing of various reflections) much easier. All planes that are parallel to the oscillation axis reflect to the zero layer line. On a photograph with the a-axis as the axis of oscillation in the crystal, these will be planes of the type (okℓ). Similarly planes of the type (1kℓ) will reflect to the first layer line above the central one, (2kℓ) to the second, etc. The general rule [1] is that reflections on the nth layer line will have indices hkℓ that satisfy the equation

$$hu + kv + \ell w = n$$

where [uvw] are the indices of the axis about which the crystal is rotated.

When a crystal is mounted for oscillation around the a-axis, say, the spacings of the layer lines give immediately the spacing between lattice points in the direction of the oscillation axis. This follows from the Laue equations (equations (7.2)). For each layer line is produced by diffracted rays forming the generators

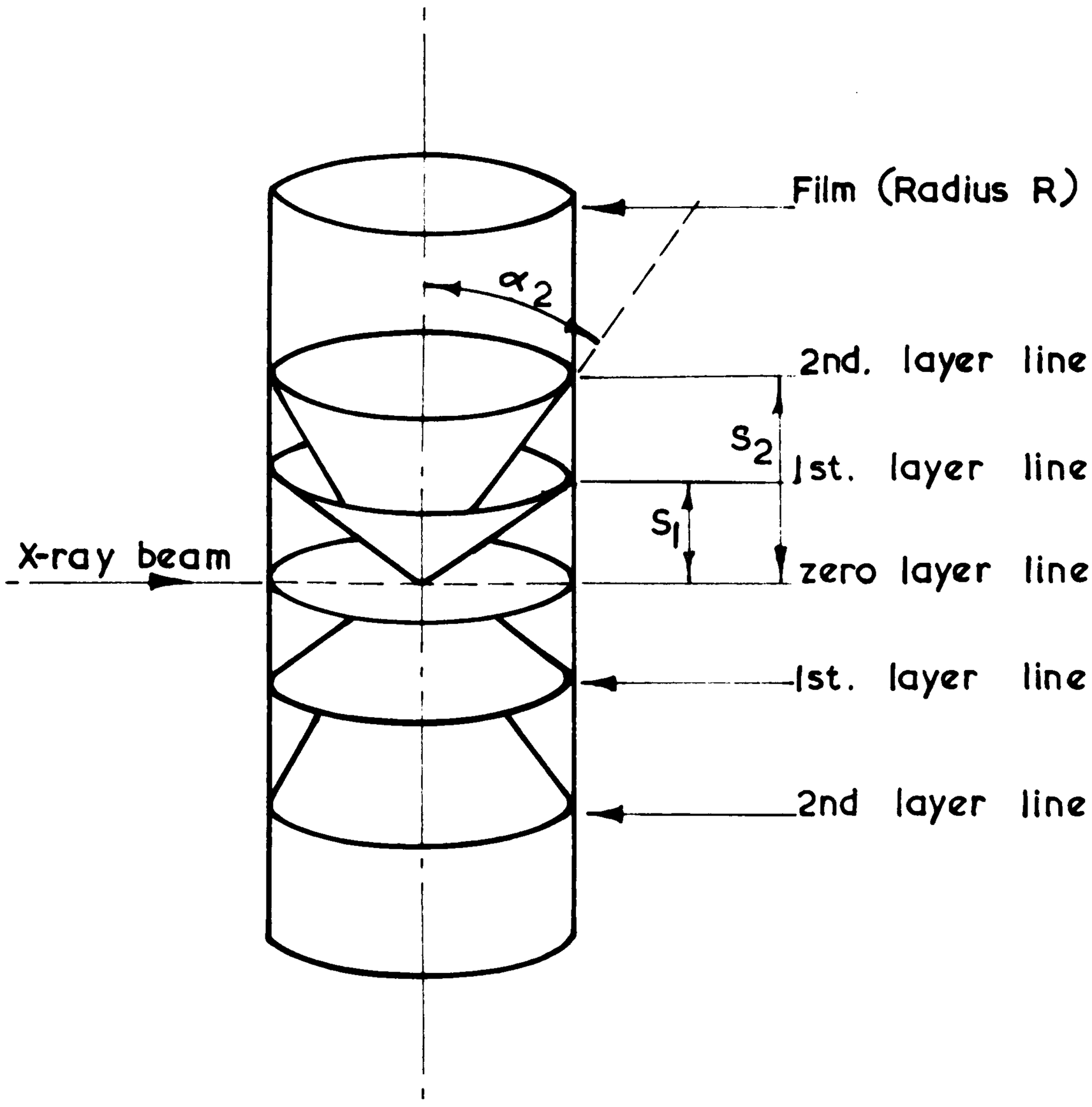

FIG. 7.4 Formation of layer lines from cones of diffracted beams.

of a cone co-axial with the rotation axis (Fig. 7.4). The Laue equation that applies here is

$$a\ (\cos\ \alpha\ -\ \cos\ \alpha_o)\ =\ h\lambda$$

and if the incident beam is perpendicular to the axis of rotation (as is the case in most experiments), then $\alpha_o = 90^o$ and the Laue equation reduces the

$$a\ \cos\ \alpha\ =\ h\lambda$$

$$\therefore\quad a\ =\ \frac{h\lambda}{\cos\ \alpha}$$

where α is semi-apex angle of the diffracted cone, λ is the wavelength of the X-rays, a is the inter-planar spacing, and h is an integer (the order of reflection for the cone) which is 0 for the horizontal layer line through the central spot, 1 for the first layer above this, etc. Similar equations hold for rotation about any other direction in the crystal. The above equation may be generalised to apply to oscillations about any direction in the crystal, and if the measured distance S_n on the film (Fig. 7.4) from the zero line to the nth layer is inserted then :

$$I\ =\ \frac{n\lambda}{\cos\ \alpha_n}$$ where I is the identity distance, and

$\alpha_n = \frac{S_n}{R}$, R being the radius of the cylindrical film.

7.5. Absorption of X-rays

An X-ray beam loses intensity in traversing matter both by true absorption which is a transformation from X-rays into kinetic energy of ejected electrons and atoms, and by scattering which is a transfer of radiant energy from the primary beam to scattered beams originating in the atoms of the absorbing matter. It is found [1] that the intensity of a mono-chromatic beam of X-rays decreases with

distance traversed according to the law given below :

$$I = I_0 e^{-\mu x} \qquad \ldots\ldots\ldots (7.4)$$

where I_0 is the initial value of the intensity I is the value of the intensity after traversing a thickness x, and μ is the linear absorption coefficient. When the mass rather than the thickness traversed is of interest, then, the above equation may be written as :

$$I = I_0 e^{-\frac{\mu}{\rho} \cdot \rho x}$$

where $\frac{\mu}{\rho}$ is the mass absorption coefficient.
Most tables [1] list $\frac{\mu}{\rho}$ rather than μ because $\frac{\mu}{\rho}$ is independent of the physical state (solid, liquid or gas) whereas μ is not. The mass absorption coefficient of a binary compound may be calculated from the weight percentages w_1, w_2 and the values $(\frac{\mu}{\rho})_1$, $(\frac{\mu}{\rho})_2$ for its constituents as follows [1] :

$$(\frac{\mu}{\rho})_{compound} = \frac{w_1}{100} (\frac{\mu}{\rho})_1 + \frac{w_2}{100} (\frac{\mu}{\rho})_2$$

For cadmium sulphide it can be shown (see section 4.2.1) that cadmium forms 77.5% by weight of the compound. Using the equation above, and published values [1] of $\frac{\mu}{\rho}$ for cadmium and sulphur, the mass absorption coefficient for cadmium sulphide has been calculated as 199 ($cm.gm^{-1}$), and μ as 955 cm^{-1}. This compares well with the experimental values of μ quoted by Brummer [6] as 976 cm^{-1}, and by Schnurer [7] as about 1000 cm^{-1}, for copper K_α radiation.

From equation (7.4), the thickness traversed, $x_{\frac{1}{2}}$, by an X-ray beam before it loses half of its intensity may be worked-out, and for cadmium sulphide : $x_{\frac{1}{2}} = 7.2$ μm. This distance represents the depth of penetration of an X-ray beam which is normal to the specimen. However, when the X-ray beam is inclined at an angle

(Fig. 7.5), the actual depth of penetration, x_ρ, is less than $x_{\frac{1}{2}}$. It is, in fact, given by $x_\rho = x_{\frac{1}{2}} \sin\theta$, where θ is the grazing angle of the X-ray beam. For grazing angles of 5^o, 10^o, 15^o, and 20^o x_ρ has values of 0.06, 0.12, 1.9 and 2.5 μm respectively. In most of the experiments performed in the present investigation, the grazing angle had a maximum value of 20^o, and, therefore, all the diffraction patterns obtained are pertinent only to the top few micrometres (< 2.5 μm) of the deposited films investigated.

7.6. Experimental procedure

A Hilger micro-focus X-ray generator was used to produce copper K_α radiation using a nickel filter. The beam was collimated to a pencil 0.5 mm in diameter. The specimen was mounted on a goniometer inside a cylindrical "Unicam" oscillation camera. The dimensions of the cylindrical photographic film (Fig. 7.6) are such that when it is loaded inside the camera, using the locating pin, every 1 mm along the width of the film subtends an angle of 2^o at the axis of the cylinder which is also the axis of oscillations. This simplifies the angular measurements to be made on the diffraction patterns on the film. The X-ray beam was always perpendicular to the axis of oscillations (Fig. 7.3c). With the aid of the goniometer, the plane of the deposited film (crystal slab), was made to contain the axis of oscillations. The X-ray beam was made to hit the deposited film (crystal slab) at grazing angles from 5^o to 20^o, using the oscillation attachment provided with the goniometer. Typically the photographic film would be exposed to the X-rays for about 10 hours, with H.T. power of 0.7 mA at 40 kV, and filament current of 5 A.

Various diffraction patterns were obtained using exactly the same procedure as above, except that the deposited film would be rotated, in its own plane, through an angle β (Fig. 7.7a), from its initial position. When the (001) plane of a deposited film is

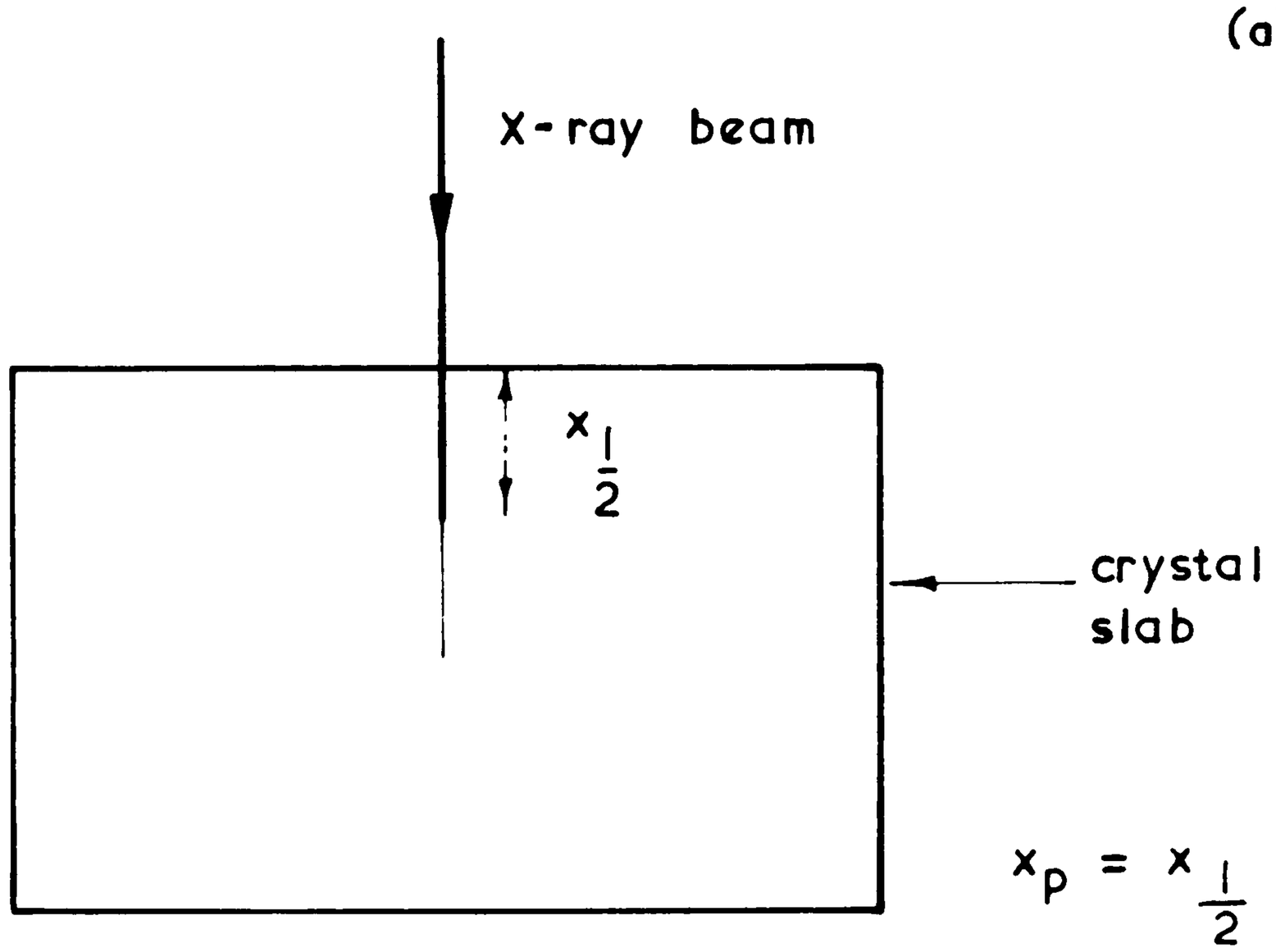

FIG 7.5 Absorption of X-rays, (a) beam normal to face of slab, (b) beam inclined at angle (90-θ) to normal.

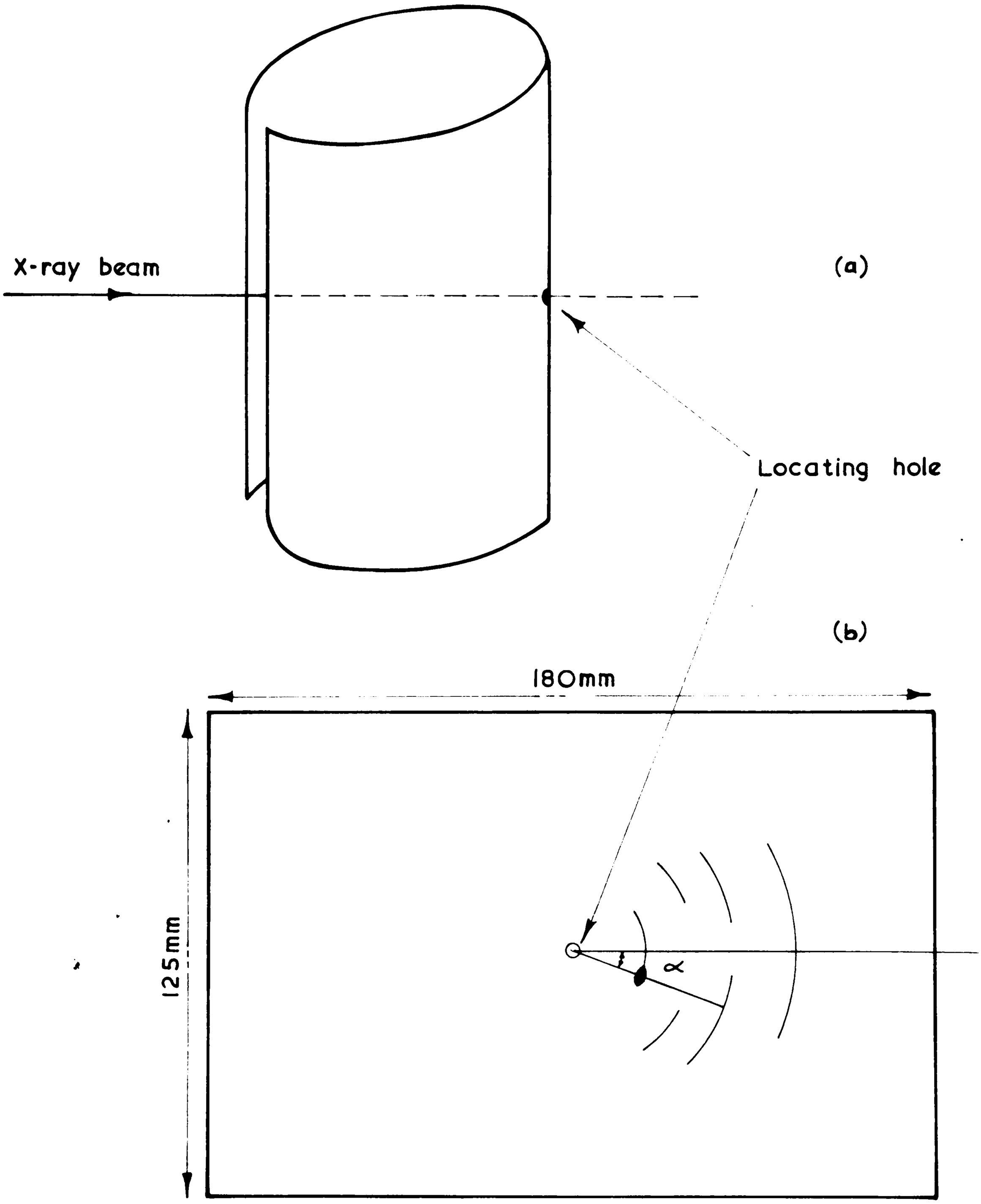

FIG. 7.6 Cylindrical Film (a) inside camera, (b) opened - up, arcs are diffracted beams.

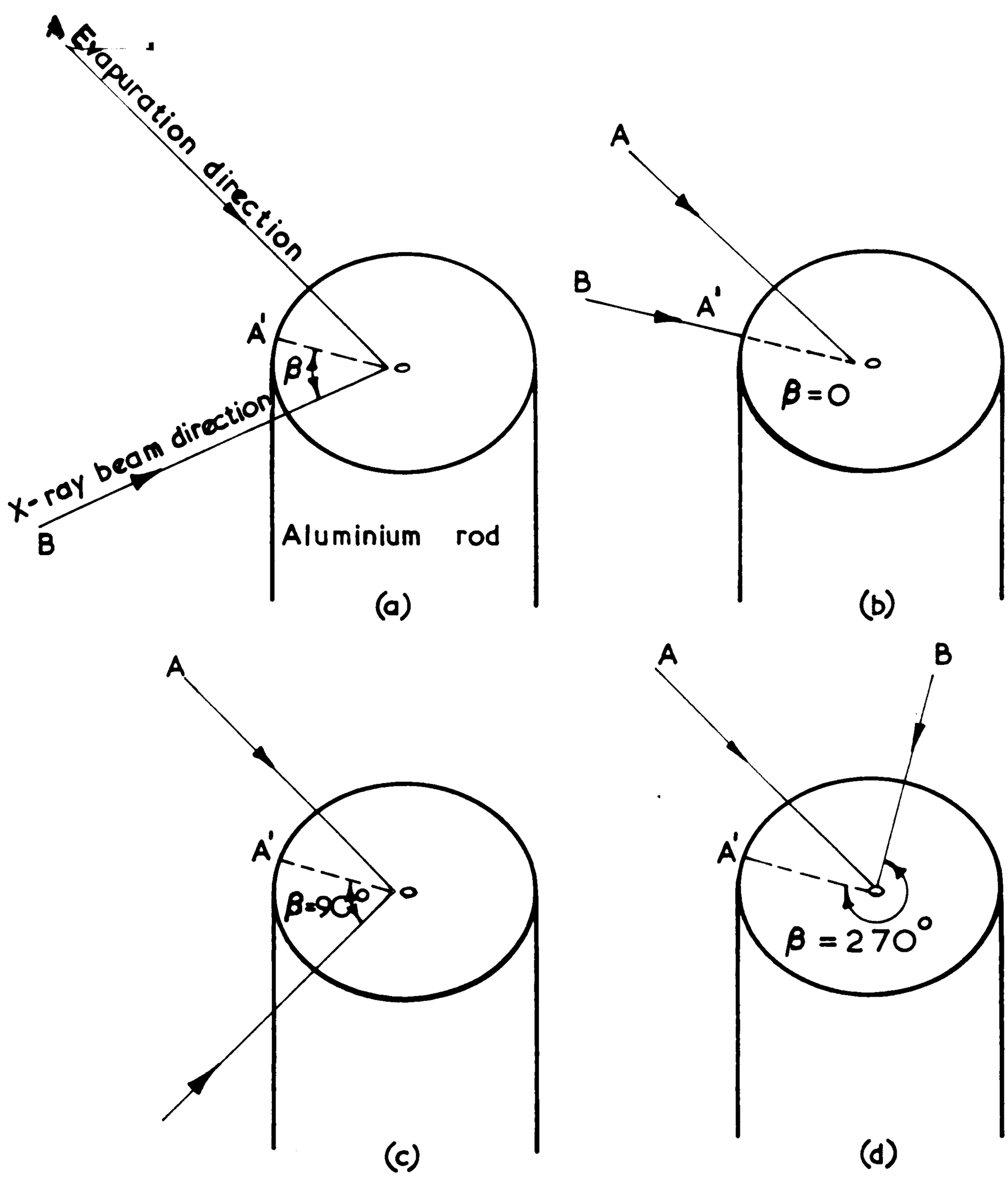

FIG. 7.7 Relation between X-ray beam direction (BO) and evaporation direction AO, OA' is the projection of the evaporation direction (OA) on the plane of the deposited film.

(a) X-ray beam inclined at angle β to OA'

(b) X-ray beam parallel to OA'

(c) X-ray beam at right angles to OA'

(d) X ray beam at 270° to OA'

parallel to the substrate, the rotation of the crystal (deposited film) in the azimuthal plane does not alter the orientation of the crystal relative to the X-ray beam, since crystals of class 6 mm are completely isotropic in the (001) plane (see Chapter 2). When the c-axis of the deposited film is inclined at an angle to the substrate-normal, however, the X-ray beam would hit different planes at different angles as the azimuthal angle is changed.

In order to investigate the influence of the direction of the vapour beam on the preferred orientation, the X-ray beam was made to hit the deposited film in two extreme directions.

(1) The X-ray beam parallel to the projection, on the plane of the film of the direction of evaporation i.e. $\beta = 0^{o}$ or 180^{o}, Fig. 7.7b.

(2) The X-ray beam perpendicular to the projection of the direction of evaporation i.e. $\beta = 90^{o}$ or 270^{o}, Fig. 7.7c and d.

In some (earlier) experiments values of β of 30^{o}, 45^{o}, 60^{o} were used as well as the above values, but it was decided on inspection of the various diffraction patterns obtained, that (1) and (2) above were sufficient [7] to determine, the inclination of the c-axis to the substrate normal.

A diffraction pattern from a cadmium sulphide film is shown in Fig. 7.8, where the various layer lines are indexed. The layer lines were indexed according to the values of the Bragg angles of various crystallographic planes of hexagonal cadmium sulphide. The Bragg angles (Table 7.1) were calculated using equation (7.3) and published values [5] for the inter-planar spacing of various planes and the wavelength of copper K_{α} radiation. The interpretation of the X-ray diffraction patterns (Fig. 7.8 and 7.9) will now be discussed. Let the diffracted beam fall at point P_1 on the cylindrical film (Fig. 7.10a). When the film is opened-up P_1 moves to a point P_2 in

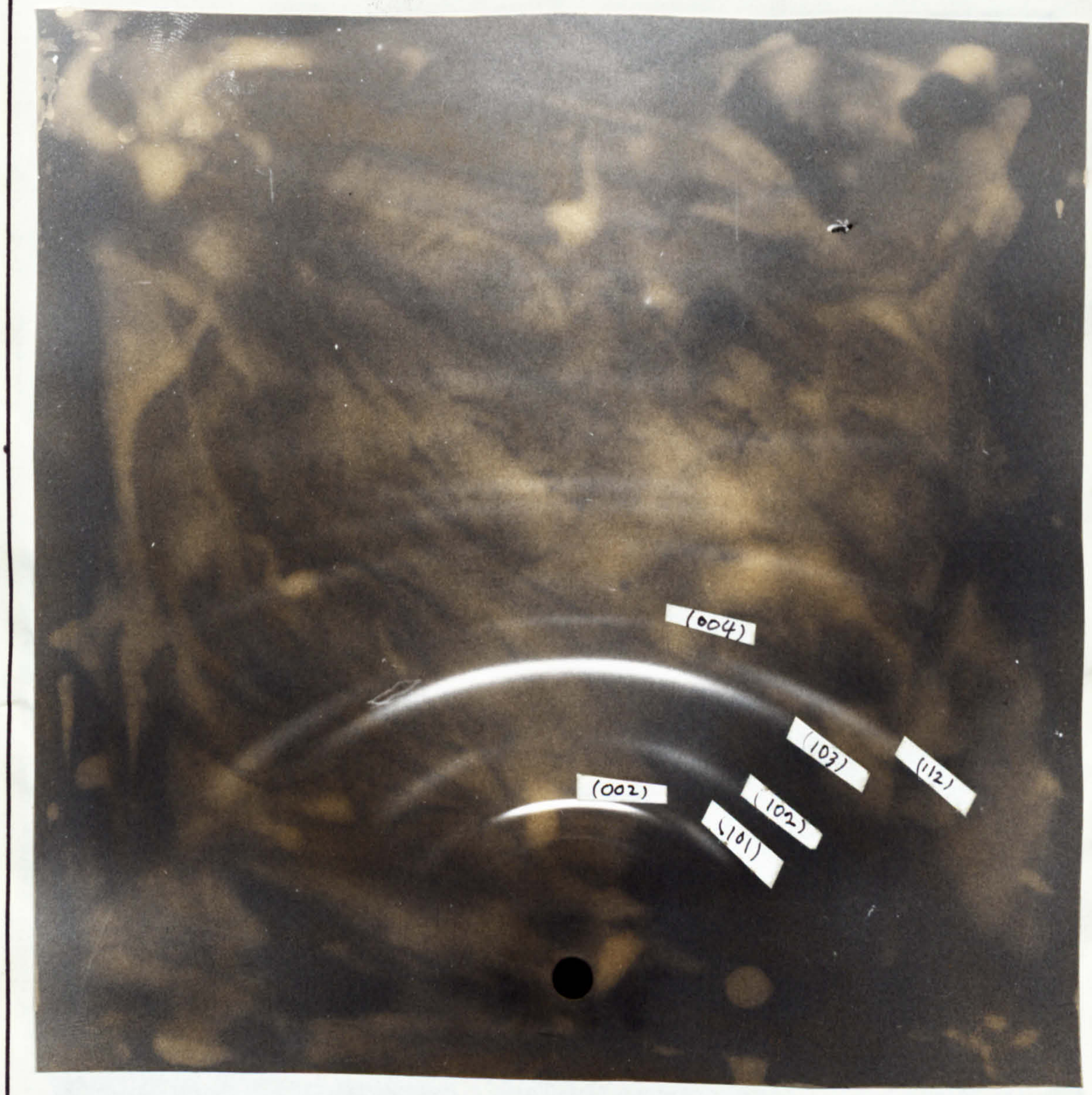

FIG. 7.8

Diffraction pattern from a CdS film whose c-axis is normal to the substrate. X-ray beam perpendicular to the projection of the evaporation direction, $5° \leftrightarrow 20°$ rocking angle. (D9/58)

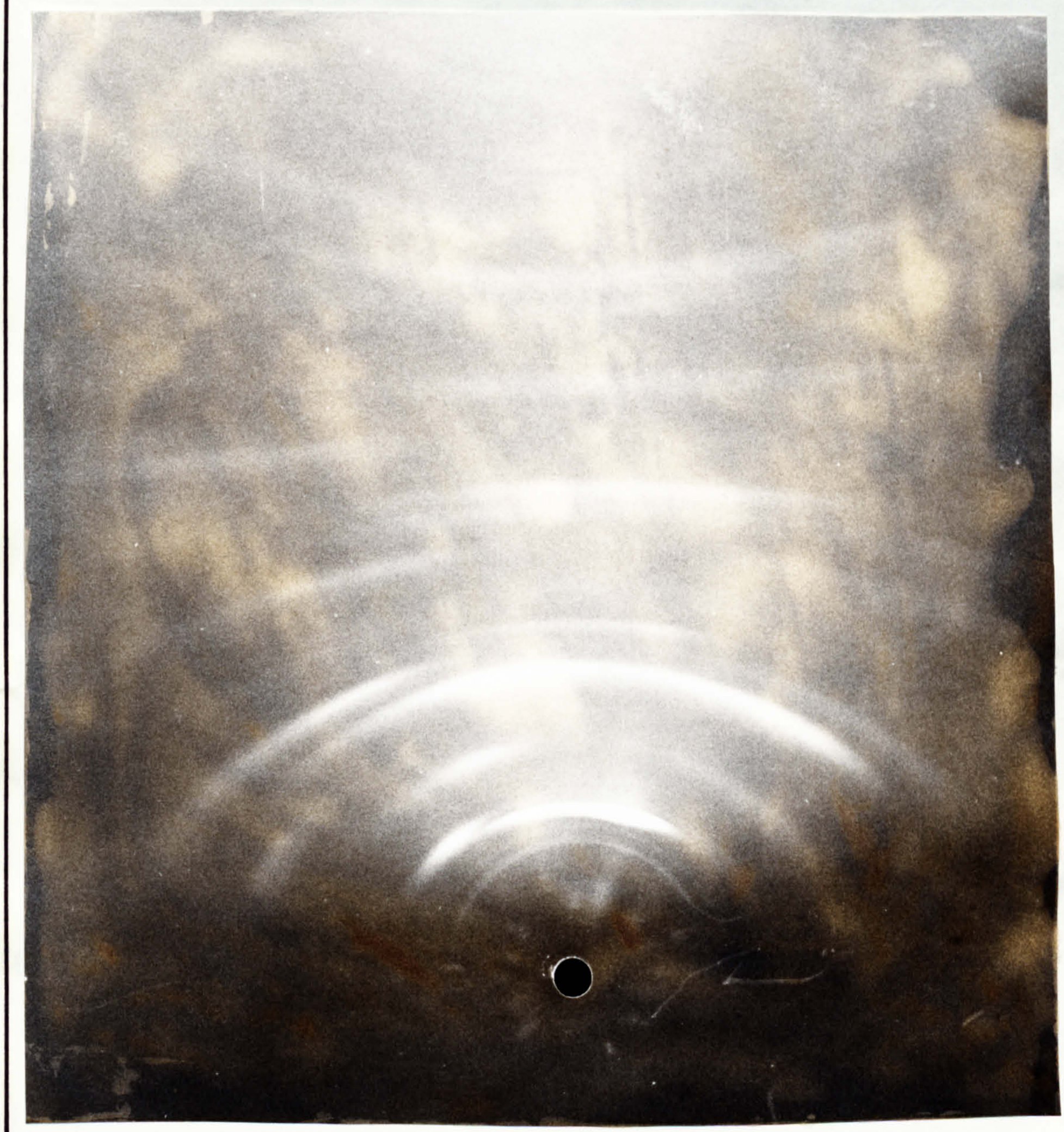

FIG. 7.9

Diffraction pattern from a CdS film whose c-axis is inclined at an angle of about 20° to the substrate-normal. X-ray beam perpendicular to the projection of the evaporation direction, $5° \leftrightarrow 20°$ rocking angle. (D13/39)

WURTZITE CdS

Plane (hkℓ)	Random Intensity (Reference 5)	Bragg angle (θ^o)	Inclination to basal plane
(100)	75	12.4	90^o
(002)	59	13.3	0^o
(101)	100%	14.1	62^o
(102)	25	18.3	43^o
(110)	57	21.9	90^o
(103)	42	23.9	32^o
(200)	17	25.5	90^o
(112)	45	25.9	49^o
(201)	18	26.4	56^o
(004)	4	27.3	0^o
(202)	7	29.1	62^o
(104)	2	30.4	25^o
(203)	15	33.4	49^o

SPHALERITE CdS

(hkℓ)	Random Intensity (Reference 5)	Bragg angle (θ^o)
(111)	100%	13.3
(200)	40	15.4
(220)	80	22.0
(311)	60	26.1
(222)	10	27.3
(400)	20	32.0
(331)	30	35.2
(420)	10	36.4
(422)	30	40.5
(333), (511)	30	43.5
(440)	5	48.5
(531)	20	51.4

TABLE 7.1

Crystallographic data for CdS

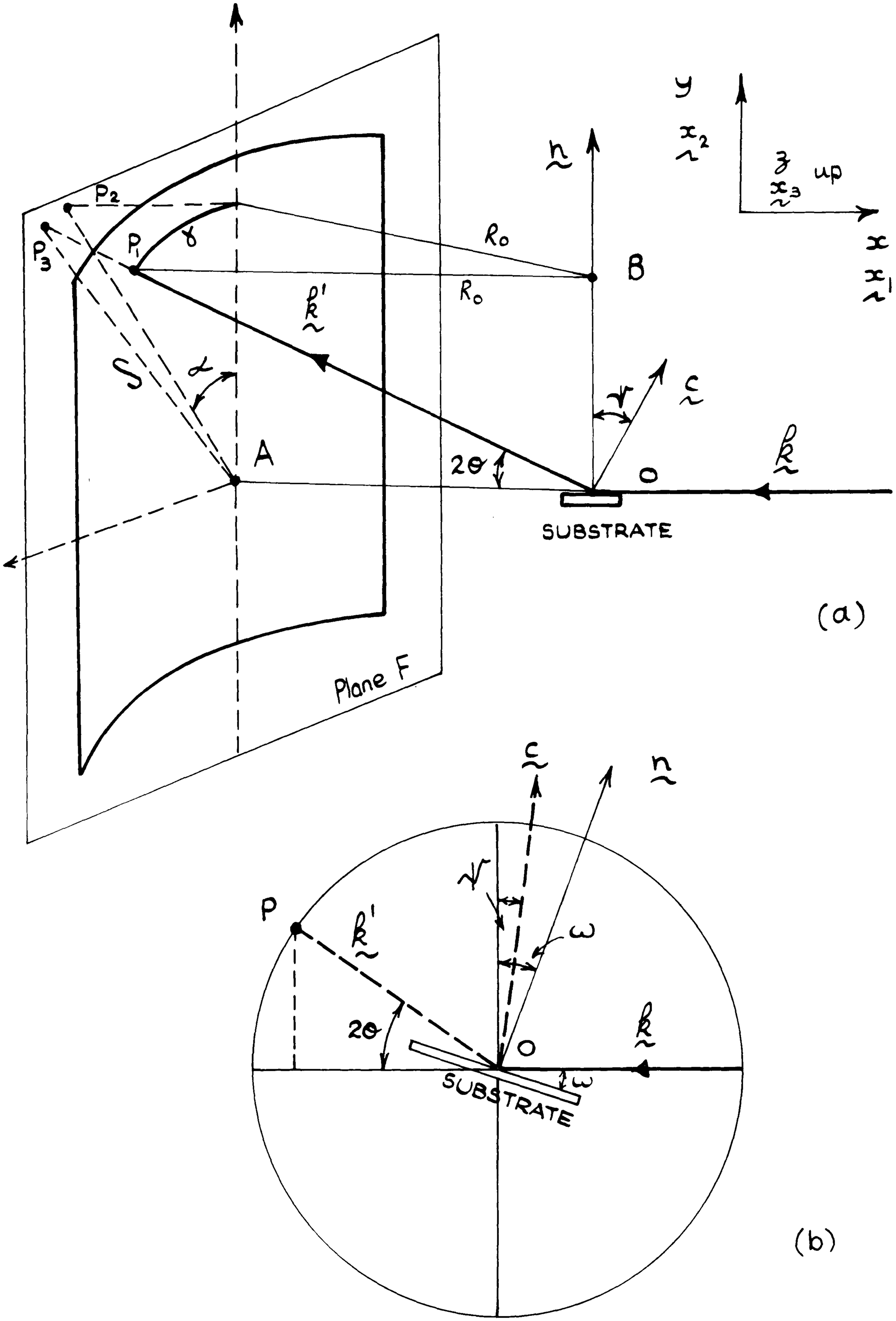

Fig 7.10 Diffraction geometry

the plane F. Let P_3 be the spot formed by the diffracted beam when a flat film perpendicular to the X-ray beam is used (plane F). With choice of axes as shown in Fig. 7.10 and with O as origin, let the coordinates of P_1, P_2 and P_3 be, respectively, (x_1, y_1, z_1), (x_2, y_2, z_2) and (x_3, y_3, z_3). Since P_2 and P_3 lie in the plane F, $x_2 = x_3 = -R_o$, where R_o is the radius of the cylindrical camera.

It can be seen from Fig. 7.10a that $x_1 = -R_o \cos \frac{\gamma}{R_o}$ and $z_1 = R_o \sin \frac{\gamma}{R_o}$ where γ is the cylindrical arc subtended by P_1 at the axis of the cylinder. For diffraction from the (002) planes in the present set up $\frac{\gamma}{R_o} < 0.3$ radians. With an error of 4%, $\cos \frac{\gamma}{R_o} = 1$, and an error of 0.4%, $\sin \frac{\gamma}{R_o} = \frac{\gamma}{R_o}$. To a good approximation, then, $x_1 = -R_o$ and $z_1 = \gamma$. But $x_2 = -R_o$, $z_2 = \gamma$, and $y_2 = y_1$. Therefore, P_1 and P_2 are very nearly the same point. Since P_1 and P_3 lie on the same line, their coordinates, must be in the same ratio, i.e. $\frac{x_3}{x_1} = \frac{y_3}{y_1} = \frac{z_3}{z_1}$. But $x_3 = -R_o$, and, within 4%, $x_1 = -R_o$, therefore, to the same approximation $y_3 = y_1$ and $z_3 = z_1$. The points P_1, P_2 and P_3 are very nearly the same point, P, in space, when 002 reflections are considered. Since the diffraction geometry is much simpler when the photographic film is flat, the point P will be assumed to lie on the plane F. When the specimen has no preferred orientation, the diffraction spot traces out a Debye circle whose radius S is given by : $S = R_o \tan 2\theta$, where θ is the Bragg angle. However when the specimen has a fibre texture, the diffraction spot becomes an intense arc which forms part of the Debye circle. When the X-ray sample is oscillated only about fibre axis, the width of the arc is a measure of the spread from the ideal single crystal.

Consider now a deposited CdS film whose c-axis is inclined at an angle ψ to the substrate normal (Fig. 7.10). The texture of the film is sufficiently described by specifying the direction of the c-axis, i.e. the angle ψ. Let the vectors $\underset{\sim}{c}$, $\underset{\sim}{n}$, $\underset{\sim}{k}$ and $\underset{\sim}{k}'$ represent

the c-axis, the substrate-normal, the incident and the diffracted beams, respectively. In Fig. 7.10(b), $\underset{\sim}{n}$ and $\underset{\sim}{k}$ are in the plane of the paper while $\underset{\sim}{k'}$ and $\underset{\sim}{c}$ are not. Let the plane of the deposited film make an angle ω with the incident X-ray beam. Let $\underset{\sim}{k}_1$ and $\underset{\sim}{k}_1'$ be unit vectors along $\underset{\sim}{k}$ and $\underset{\sim}{k'}$, respectively.

Bragg's law gives :

$$\underset{\sim}{c} = \underset{\sim}{k}_1' - \underset{\sim}{k}_1 \qquad \ldots\ldots\ldots \qquad (7.3)$$

With choice of axes as shown in Fig. 7.10, one may write :

$$\underset{\sim}{k}_1 = [-1, 0, 0] \qquad \ldots\ldots\ldots \qquad (7.4)$$

and $\underset{\sim}{k}_1' = \left[-\cos 2\theta\ ,\ \frac{-X_2 \cos 2\theta}{R_o}\ ,\ \frac{X_3 \cos 2\theta}{R_o}\right]$, where X_2 and X_3 are the coordinates of P along $\underset{\sim}{x}_2$ and $\underset{\sim}{x}_3$, respectively. But $X_2 = S \cos\alpha = R_o \tan 2\theta \cos\alpha$, and $X_3 = R_o \tan 2\theta \sin\alpha$.

$$\therefore\ \underset{\sim}{k}_1' = [-\cos 2\theta, -\sin 2\theta \cos\alpha, \sin 2\theta \sin\alpha] \qquad \ldots\ldots\ldots \qquad (7.5)$$

From equations (7.3) to (7.5) one gets

$$\underset{\sim}{c} = [2\sin^2\theta, -\sin 2\theta \cos\alpha, \sin 2\theta \sin\alpha] \qquad \ldots\ldots \qquad (7.6)$$

Hence $$|\underset{\sim}{c}| = 2\sin\theta \qquad \ldots\ldots\ldots \qquad (7.7)$$

Now $$\underset{\sim}{n}_1 = [\sin\omega, -\cos\omega, 0] \qquad \ldots\ldots\ldots \qquad (7.8)$$

But $$\underset{\sim}{n}_1 \cdot \underset{\sim}{c} = |\underset{\sim}{c}| \cos\psi$$

Therefore, $2\sin\omega \sin^2\theta + \cos\omega \sin 2\theta \cos\alpha = 2\sin\theta \cos\psi$

and, $$\cos\psi = \sin\omega \sin\theta + \cos\omega \cos\theta \cos\alpha \qquad \ldots\ldots\ldots \qquad (7.9)$$

The HP 9200 desk computer was used to work out values of ψ versus α for the 002 reflection ($\theta = 13.3^o$), for values of ω from 5^o to 20^o. The results are shown in Fig. 7.11 where it can be seen that to a good approximation $\psi = \alpha$. This is checked by inspection of equation (7.9) for $\omega < 20^o$ and $\theta = 13.3^o$: $\sin\omega \sin\theta \simeq 0$, and $\cos\omega \cos\theta \simeq 1$,

$$\gamma = \cos^{-1}\left[\sin\omega \sin\theta + \cos\omega \cos\theta \cos\alpha\right]$$

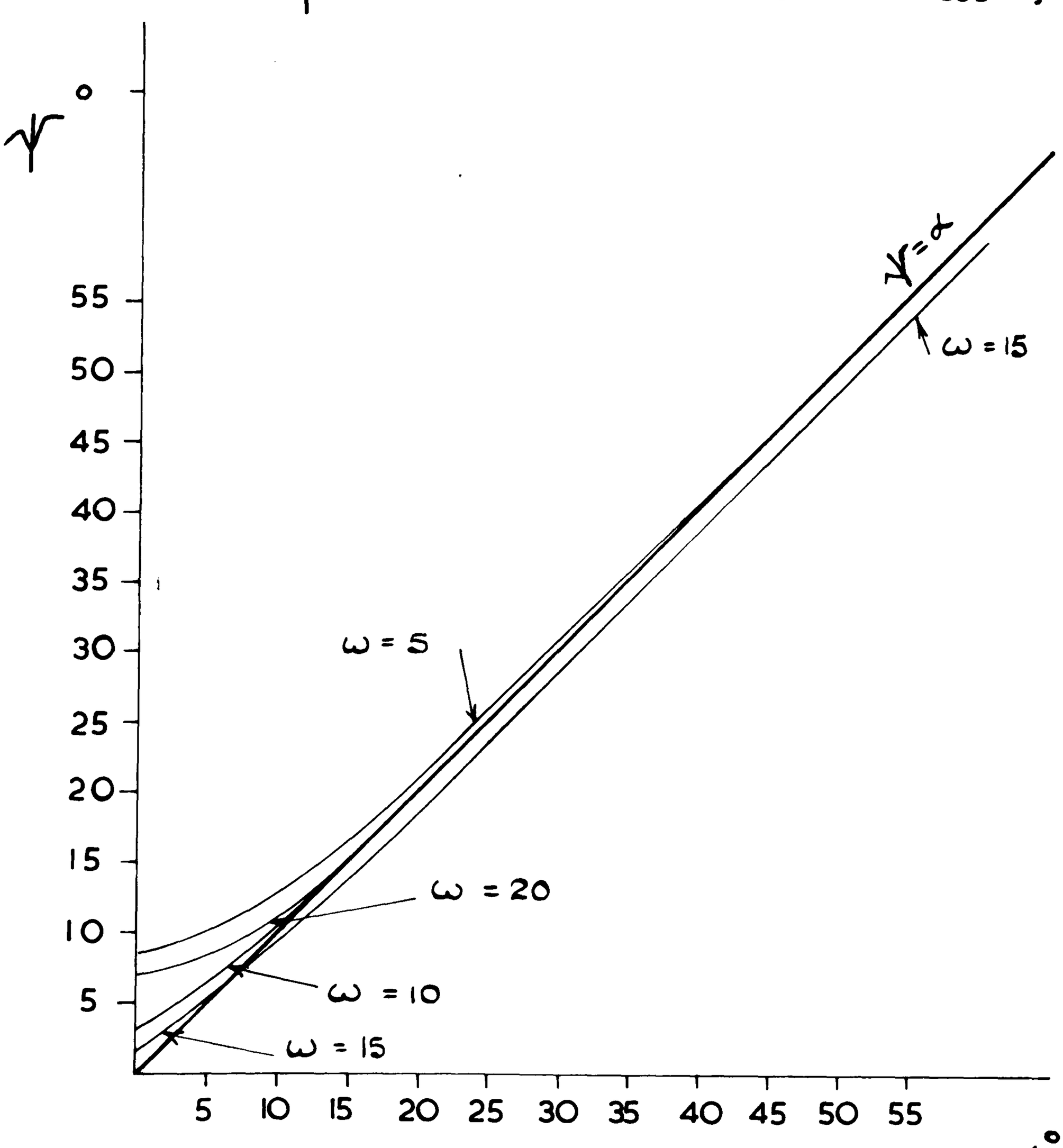

Fig 7.11 γ versus α for $\theta = 13 \cdot 3^{\circ}$

and therefore $\psi \simeq \alpha$. From Fig. 7.11 it is seen that for $\alpha > 10^{o}$, the error in assuming $\psi = \alpha$ is less than 3^{o} and that the maximum uncertainty in ψ (2^{o} - 8^{o}) occurs when $\alpha = 0$. However, this uncertainty is offset by the fact that two diffraction patterns are obtained one with the X-ray beam parallel and one with it normal to the projection of the evaporation direction (see above). When both patterns give $\alpha = 0$, then ψ must also be nearly zero. Since the photographic method for determining α, used in the present work, is accurate within one or two degrees, and since the error involved in assuming the photographic film flat, is about 5%, it could be stated that, to a good approximation, the value of the azimuthal angle, α, measured on the film is equal to the inclination, ψ, of the c-axis to the substrate-normal.

Using the experimental procedure described here, the orientation of CdS films deposited under various conditions (e.g. deposition rate, source temperature and film thickness) were studied and the results are given in Table 7.2. The crystallographic orientation of a deposited CdS film may be inferred from its ultrasonic response (section 9.3.1) e.g. whether s-mode and/or c-mode response is observed when an electric field is applied across the film thickness. The X-ray results may then be correlated with the ultrasonic response of the as-deposited films. The ultrasonic tests carried out on the films are described in Chapter 9 where it is stated that ultrasonic and X-ray results are in good agreement. The X-ray results are discussed in the following Chapter, where the dependence of c-axis orientation on film thickness is discussed in terms of the "stifling process".

Various techniques have been used by a number of workers [9-18] to determine the texture of deposited CdS films.

TABLE 7.2. X-ray results and ultrasonic pulse-echo response for CdS films deposited on Aℓ rods

"D" No.	Sample No.	Deposition angle (ϕ^o)	Inclination of c-axis to subst.-normal ψ^o (X-ray results)	Film thickness (μm)	Ultrasonic response	Comments
9	19	38	30	15	-	Attenuation too high for ultrasonic pulse-echo tests to be carried out
	58	0	0	20	-	
12	2	35	15	60	c- & s-mode	Weak diffraction spot
	3	35	15	60	c-mode	
	4	35	15	60	c-mode	
	20	35	15	60	c-mode	
13	39	30	0	100	c-mode	Before etching
			20	40	-	After etching
14	55	26	18	20		
15	8	41	0	22		
	9	46	25	19		Domed substrate. Weak diffraction spot
	12	54	20	14		Single-layer
	13	54	20	28		Multi-layer
	14	37	10	32		Multi-layer
17	35	35	30	50	s- & c-mode	Very strong diffraction spots
	38	5	5	55	c-mode	
	2	35	30	50	s- & c-mode	
	5	35	30	50	s- & c-mode	

CHAPTER 7

REFERENCES

1. C.S. Barret et al, *Structure of metals : crystallographic methods, principles and data*, McGraw-Hill (1964).

2. R.W. James, *X-ray crystallography*, Methuen (1965).

3. A. Taylor, *X-ray metallography*, Chapman and Hall (1952).

4. J.F. Nye, *Physical properties of crystals*, Oxford Univ. Press (1964).

5. A.S.T.M. Index Card Nos. 6-0314 and 10-454 (1964).

6. O. Brummer et al, *Anomalous X-ray absorption and photo-current in CdS single crystals*, Phys. Stat. Sol., 36, p. 617 (1969).

7. E. Schnurer, *Absorption von Rontgens-strahlen in CdS*, Arbeitstagung Festkoerperphysik, 2. Dresden, ed. K.W: Boer (1955).

8. N.F. Foster, *Crystallographic orientation of ZnO films deposited by triode sputtering*, J. Vac. Sci. Tech., 6, p. 111 (1969).

9. M. Weinstein et al, *The growth of wurtzite CdTe and sphalerite type CdS single crystal films*, App. Phys. Lett., 6, p. 73 (1965).

10. G.A. Rozgonyi et al, *Epitoxial thin films of ZnO on CdS and sapphire*, J. Vac. Sci. Tech., 6, p. 115 (1969).

11. J. DeKlerk, *C-axis flipping for multilayer piezoelectric film transducers*, App. Phys. Lett., 13, p. 102 (1968).

12. N.F. Foster et al, *CdS and ZnO thin film transducers*, IEEE Trans., SU-15, p. 28 (1968).

13. B.J. Curtis, *CdS ultrasonic transducers*, Mullards Res. Labs. Rep. No. 2608 (1966).

14. A.F. Andrushko, *Orientation of the micro crystals of t.f. of CdS*, Sov. Phys. Cryst., 7, p. 172 (1962).

15. J. Dresner et al, *Crystallinity and electronic properties of evaporated CdS films*, JAP, 34, p. 2390 (1963).

16. I. Lagando et al, *R.F. sputtered CdS thin crystals*, J. Vac. Sci. Tech., 7, p. 318 (1970).

17. J.D. Llewellyn et al, *Apparatus for the deposition of low frequency CdS transducers*, J. Sci. Inst. (J. Phys. E), 2, p. 535 (1969).

18. P.J. King, *The optimum conditions for the evaporation of CdS films*, Brit. J. App. Phys. 2, p. 1349 (1969).

C H A P T E R 8

Orientation effects in as-deposited CdS thin- and thick-film crystals

8.1. Introduction

In this chapter the theories of film crystal nucleation and growth [1-3], and of film crystal form and growth habit [4,5] are outlined before discussing the orientation effects in as-deposited CdS thin- and thick-film crystals. The orientation dependence on thickness in as-deposited CdS is explained in terms of the "stifling process". The influence of the preferred orientation of the substrate and of its surface finish, and of deposition rate on the orientation of CdS films is also discussed. It is pointed out that there is no reference in the literature to CdS film orientation dependence on thickness. The reader is referred to Chapter 7 for an introduction to crystals and crystallography.

8.2. Nucleation and growth of film crystals

Many phase transformations take place via the processes of nucleation and growth, i.e. the new phase is created first in the form of microscopic aggregates which then accrete further material and attain macroscopic size. Condensed atoms agglomorate into relatively stable units (nuclei) whose probability of future growth is greater than that of re-evaporation. In all theories [3,2] of t.f. nucleation, the initial step is the impingement of vapour molecules on the substrate. After impingement the vapour molecules can either be adsorbed permanently ($\alpha = 1$), or be adsorbed for a short time after which they re-evaporate ($\alpha < 1$), or immediately bounce off the substrate in a specular reflection manner ($\alpha = 0$), where α is the accommodation coefficient. The defining

equation for α is [3]

$$\alpha = \frac{E_m - E_r}{E_m - E} = \frac{T_m - T_r}{T_m - T}$$

where E_m is the kinetic energy of the incident vapour molecule, E_r its energy before reaching equilibrium, and E is that after reaching equilibrium on the substrate. The T's are corresponding temperatures. This predicts that the likelihood of complete thermal accommodation ($\alpha = 1$) increases if the ratio of the mass of the impinging atoms to that of the mass of the substrate lattice atoms increases. The atomic weights of copper (Cu) and chromium (Cr) are [6] 63 and 52. Thus, for the deposition of a given film, e.g. CdS, there should be no appreciable difference in the value of α on Cr and Cu substrates. Most theories postulate [2,3] that once a cluster has reached a certain critical size it will no longer dissociate into monomers, but will grow to form a stable condensate. In essence, nucleation theory predicts that there is a critical nucleus size below which no condensation is possible. It is widely accepted that α of a vapour molecule, on a clean surface of a crystal of the same material as the vapour, is independent of deposition angle, $\emptyset$, and is equal to unity (section 4.4). However, it has been suggested [4] that α is in fact a function of $\emptyset$ and of film orientation, according to the equation :

$$\alpha = \alpha_0 + \alpha_1 \sin^2\emptyset + \alpha_2 \cos^2\emptyset \sin\lambda$$

where λ is the angle between the projection of the vapour beam direction onto the crystal surface and the direction of the greatest packing density in the surface, and α_0, α_1 and α_2 are constants of the material. The

above equation is based on the assumption that adsorbed vapour molecules behave in the same manner as inelastically scattered thermal neutrons in a crystal. It is also claimed [5] that vapour molecules have an analogy in ion impact phenomena rather than neutron impact, and α is assumed to depend only on cosØ or on sinØ. At present no quantitative theory of the accommodation coefficient exists [4]. In section 4.4, where film condensation was discussed, it was assumed that the condensation process was equivalent to a raining down on the substrate of sticky atoms which were adsorbed where they impinged. However, there is generally sufficient surface diffusion (mobility of atoms) on the substrate to lead to the formation of well defined islands of film material on the substrate. Larger critical nuclei result [3] if the surface energy of the condensate material is large and if the surface energy of the substrate material is low. The binding energy, E_a, of adsorbed single atoms to the substrate (section 6.5.1) is important in determining the critical size of the nuclei. The stronger the binding between adsorbed atoms and substrate, the smaller the critical nucleus and the higher the nucleation frequency. If the substrate is not homogeneous, smaller critical nuclei are formed at sites where the binding energy is greater. A step on a substrate is an often [3] observed strong binding site. Increasing the substrate temperature for a given deposition rate increases [3] the size of the critical nucleus (increased probability of re-evaporation). Increasing the deposition rate, R_{ar}, at a given substrate temperature results in smaller islands and a higher frequency of formation of islands (section 4.5). However, a change in R_{ar} of few orders of magnitude is necessary [3] before any effect can be observed on the size of the critical nucleus. Immediately after formation a nucleus will grow by acquiring more atoms which migrate on the substrate surface in search of a tight binding site, depending on the amount of surface diffusion. As soon as the islands grow large enough to touch each other, grain boundaries or lattice defects

become incorporated in the film unless the islands coalesce to form a single grain. These processes have been observed using in situ electron microscopy techniques [1,7,8]. These techniques have also been used to observe the four stages of film growths:formation of islands, coalescence of islands, formation of channels, and bridging of channels to form a continuous film. Only single systems e.g. some of the element, have been studied to date, and very little is known on the growth of inorganic compounds [1]. It is found, with these simple systems, that the nuclei and, very often, the islands are perfect single crystals. Usually an island is formed by the coalescence of tens of nuclei. It is known [1] that dislocations and tarnish (e.g. oxide) layers on metals affect the nucleation of deposited films. The dislocation density in epitaxially grown [1] films is of the order of 10^4 m^{-2}. The morphology of the nuclei and their number per unit area depend upon the orientation of the substrate [1].

8.3 The form and growth habit of film crystals

Most chemical compounds and elements exist in crystalline forms characterised by their external geometrical shape (morphology). They crystallize out of a solution or solidify from the melt or from the vapour. In the process of crystallization the atoms (or molecules) arrange themselves in a regular fashion, and thereby settle down into positions of minimum energy. It is usual [9] that the slower the rate of crystallization the more perfect are the resulting crystals. As long as crystals grow without mutual interference their habit, i.e. their external form, is decided [10] by temperature and supersaturation, owing to the different surface free energies of different crystal planes. The development of the growing faces of crystals is often favoured [10] by vapour concentration gradients which enhance the importance of surface migration of condensed atoms. The equilibrium form of a crystal is determined [4] by Wulff's law :

$\frac{\sigma_1}{h_1} = \frac{\sigma_2}{h_2} = \ldots\ldots \frac{\sigma_i}{h_i}$, where σ_i is the specific free energy of the crystal plane F_i, and h_i is the distance of this plane from the centre of the crystal. The validity of this law is limited to cases where : (a) σ_i is independent of the size and shape of the surface, and (b) the geometrical ideal shape of the crystal coincides with its ideal shape from the point of view of its crystal chemistry (e.g. the stoichiometry of a binary compound, section 4.5.1). The equilibrium form depends upon the growth environment of the crystal e.g. it may be influenced by residual gases. Experimentally the equilibrium form is obtained only [4] if the whole crystal surface is supplied with a sufficient amount of molecules so that the growth rate in any direction is not limited by the rate of supply of molecules. If the supply of molecules is anisotropic, the growth form can deviate considerably from the equilibrium form. However, these deviations will consist [4] in general in the abnormal development of certain planes of the equilibrium form e.g. in the formation of a platelet or a columnar habit instead of the isometric (equilibrium) form. In free growing (e.g. natural) crystals the directions of fastest growth are those from the centre towards the remotest point of the crystal, and they are [4,5] the <001> and the <110> directions for hexagonal crystals. The significance of the directions of fastest growth is that during crystal growth in a confined space many orientations develop, but only those orientations whose direction of fastest growth is along the direction of crystal growth survive [4,5,11]. For example [12], when bulk crystals are grown from the melt in a tube, it is purely a matter of geometry for the crystallite whose greatest speed of growth is along the axis of the confining tube to overtake and restrict the space left for the other crystallites until finally there is no room left for them to grow in. The behaviour of film crystals is analogous to that of bulk crystals : the crystallites

whose chances of survival are greatest [5] are those whose direction of fastest growth is along that of film growth (normal to the substrate).

Vacuum deposited film crystals grow in the same [4,5] manner as free growing crystals provided there is an isotropic supply of vapour molecules (i.e. the vapour molecules are random, see section 4.3). Thus, hexagonal film crystals deposited onto amorphous substrates grow with their c-axes either parallel or perpendicular to the plane of the substrate when random evaporation is used. Although the latter orientation has been frequently obtained with CdS and ZnO films on a variety of substrates, the former orientation has only been reported once for ZnO (section 3.3). Even if the initial nuclei are randomly oriented, certain orientations predominate as the film grows thicker. As discussed in section 2.4, the wurtzite (hexagonal) structure has complete dielectric, piezoelectric and elastic isotropy in the basal plane. Therefore, the orientation of a wurtzite film crystal can be sufficiently described by specifying the [001] direction (the c-axis). Hereafter, a film crystal whose c-axis is normal to the substrate will be referred to as a crystal with "normal" orientation, that whose c-axis is inclined at an angle to the substrate as an "oblique" orientation, and that whose c-axis is parallel to the substrate as a "parallel" orientation. When the vapour beam is directional (i.e. when the molecules hit the substrate at a certain angle, section 4.3), the molecular supply is necessarily anisotropic. The effect of this anisotropy on the orientation of a deposited film depends on the amount of surface diffusion (mobility of arriving molecules on substrate or crystal surfaces). When there is no surface diffusion at all, the molecules freeze at the positions where they hit the substrate surface or the growing crystal surface. In this case, the anisotropy of the vapour supply favours the growth of thos crystallites whose direction of fastest growth is aligned with that of the supply of

molecules. For hexagonal films, this means that the c-axis of a film crystal aligns itself with the direction of the vapour beam. This was confirmed by experiment more than forty years ago for cadmium films [4], and more recently for CdS films (section 3.3). On the other hand when there is infinite surface diffusion, crystal growth proceeds in the same manner as when the vapour supply is isotropic i.e. a hexagonal film grows with its c-axis either parallel or perpendicular to the substrate. Other orientations result [5] if different surface diffusion conditions are assumed, e.g. infinite surface diffusion only along the crystal faces, or only along the crystal. These orientations also depend [5] on the accommodation coefficient, α, e.g. whether α is assumed to be independent of deposition angle, $\emptyset$, or to be dependent on $\sin\emptyset$ or $\cos\emptyset$. Again, even if all the nuclei are initially randomly oriented, certain orientations predominate as the film grows thicker. Deviation from stoichiometry may also affect [4] the orientation of the film crystal of a compound.

8.4 Orientation effects in as-deposited CdS film crystals

8.4.1 Orientation dependence on film thickness : the "stifling process"

As discussed above, when a film is polycrystalline, i.e. when it consists of crystallites of various orientations, then as the film grows a conflict for survival develops between the various orientations. In particular, in oblique deposition a conflict develops between normal crystallites (which are favoured because their direction of fastest growth is along the direction of film growth), and oblique crystallites (which are favoured because their direction of fastest growth is along the direction of supply of vapour molecules). This assumes that all random orientations have disappeared at this stage of growth. From a purely geometric consideration it is much easier for normal crystallites to survive rather than oblique ones. This is because, as the film grows thicker, the oblique crystallites eventually reach the wall of the

confining masking hole, while the growth of normal crystallites proceeds unimpeded (Fig. 8.1a). This is analogous to the growth of bulk crystals in a tube (see above). When an oblique CdS crystallite meets a normal one the latter overtakes the former because its speed (rate of growth) along the film thickness is greater. Thus the growth of the oblique crystallite is stifled by the normal one, and this process will be referred to as the "stifling process". After the two crystallites meet, they both grow as a single normal crystallite, see Fig. 8.1a. In this figure, which was inspired by diagrams in Ref. 5 and 11, the lines depict the c-axes of the CdS crystallites, i.e. their directions of fastest growth. Fig. 8.2b shows the orientation of a polycrystalline film eight times thinner than that in (a). It is clear from these two figures that it is much easier for oblique crystallites to survive in thin rather than thick films. In Fig. 8.1b the mean value of the inclination of the c-axes of most crystallites to the substrate-normal is 30^{o}. Molecules deposited between the favoured crystallites may form random or oriented nuclei. These nuclei can grow in the same manner with the disadvantage of growth in depth. This may make the preferred orientation weaker. The stifling process model discussed so far is two dimensional. Although the three dimensional case is more complicated, the same process may be imagined to take place. Fig. 8.2 is a three-dimensional perspective model of the stifling process. This process may be helped by the fact that the (001) face is slightly "hotter" than other crystal faces thus increasing surface diffusion along this crystal face. It is known [13] that, in crystals grown from the melt, the fastest growing faces are hotter than other faces.

So far, the existance of the stifling process has been postulated on purely geometrical, and theoretical crystal growth considerations. However, the strongest support for the existance of this process comes from the experimental results obtained in the present work concerning the orientation of CdS thin- and thick-films. These results clearly

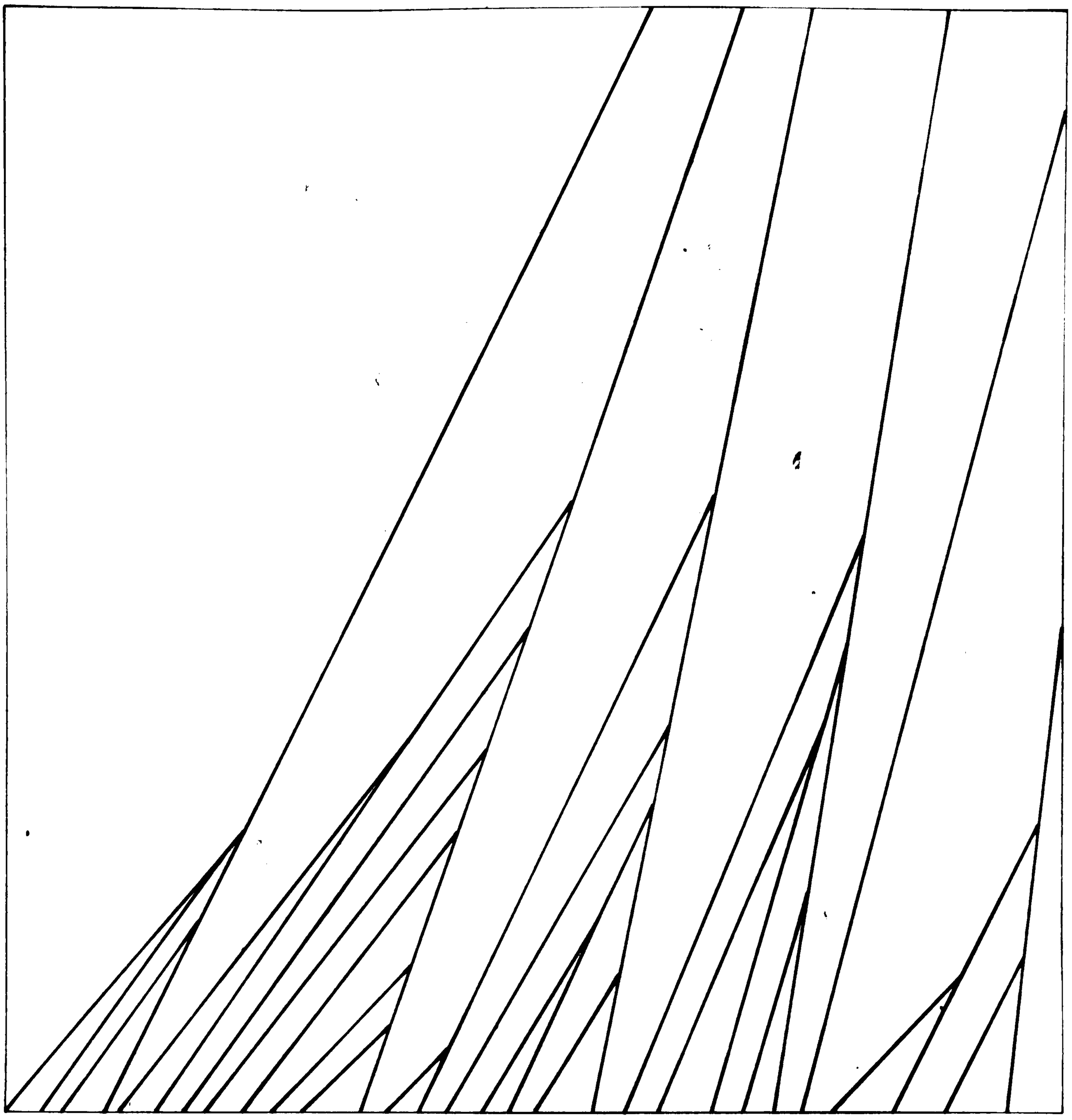

FIG. 8.1
Direction of c-axis preferred orientation. (a) thick film, (b) same film as (a) but about eight times thinner.

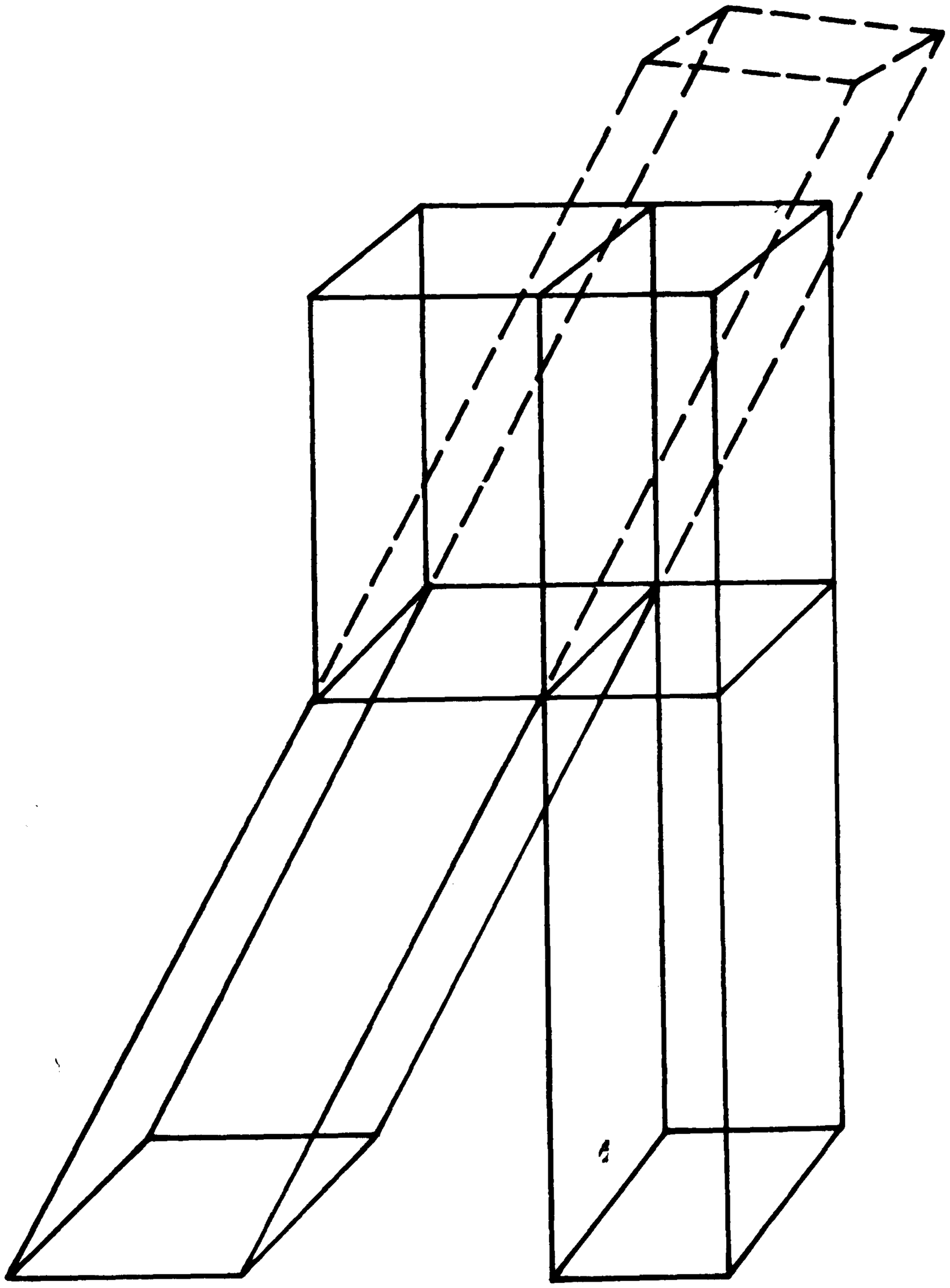

FIG. 8.2

Shows how growth of an obligue crystallite may be inhibited by presence of a normal crystallite (Stifling Process), dotted lines show growth of obligue crystallite if it had not encountered normal crystallite.

showed orientation dependance on thickness (see below). It is clear from the model of Fig. 8.1 that one of the parameters affecting the stifling process is the grain size, Δx, relative to the rationalised film thickness $\frac{t}{\Delta x}$. The bigger Δx, the thicker the film can grow without the oblique crystallites being smothered. Another factor, is the angle, ψ, at which the oblique crystallite is inclined to the substrate normal. For a given Δx, the bigger ψ, the smaller is the critical thickness, t_c, of the film (i.e. the thickness at which the crystallite inclined at angle ψ is smothered). Two crystallites inclined at ψ_1 and ψ_2 are smothered at thicknesses t_{c_1} and t_{c_2} related geometrically by the equation :

$$\frac{t_{c_1}}{t_{c_2}} = \frac{\cot\psi_1}{\cot\psi_2}$$

Thus when the critical thickness, t_{c_1}, is known at which crystallites inclined at 20^o, say, are smothered, one can predict thicknesses at which crystallites inclined at, say, 10^o, 30^o and 40^o will be smothered. By depositing CdS film crystals, with varying thicknesses, at various values of the deposition angle, $\emptyset$, in the same deposition run (section 5.4), it was possible to confirm the stifling process model using X-ray diffraction techniques. The inclination, ψ, of the c-axis to the substrate-normal of the top 2 μm of as-deposited CdS films with various values of t and $\emptyset$ were determined from their respective diffraction patterns. These patterns were obtained using the oscillation crystal technique (section 7.4.3), and following the experimental procedure described in detail in section 7.6. The (002) diffraction arcs from some as-deposited CdS films are given in Fig. 8.3. In this figure the "D" numbers refer to the various deposition runs and the numbers in parenthesis refer to sample numbers

(a) D9, on Cu film, Ø = 38° (19)

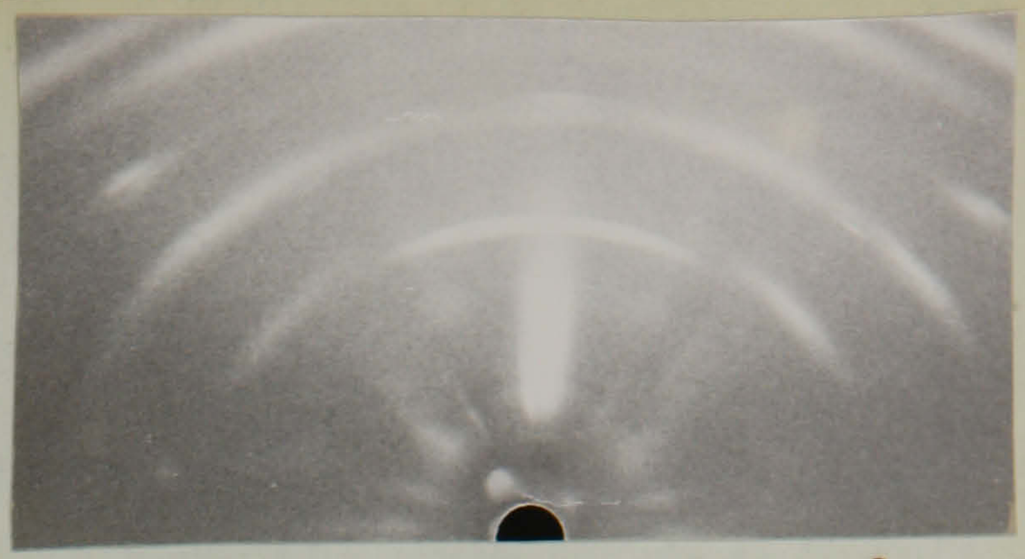

(b) D12, on Cr film, Ø = 35° (2)

(c) D13, on Cr film, Ø = 30°
Befor etching (39)

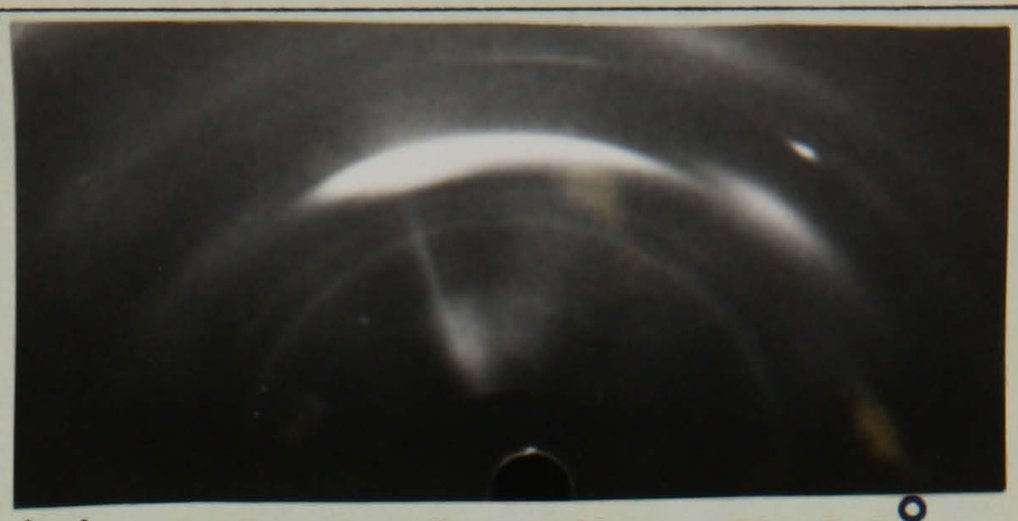

(d) D13, on Cr film, Ø = 30°
After etching (39)

(e) D14, on SiO_2 film, Ø = 26° (55)

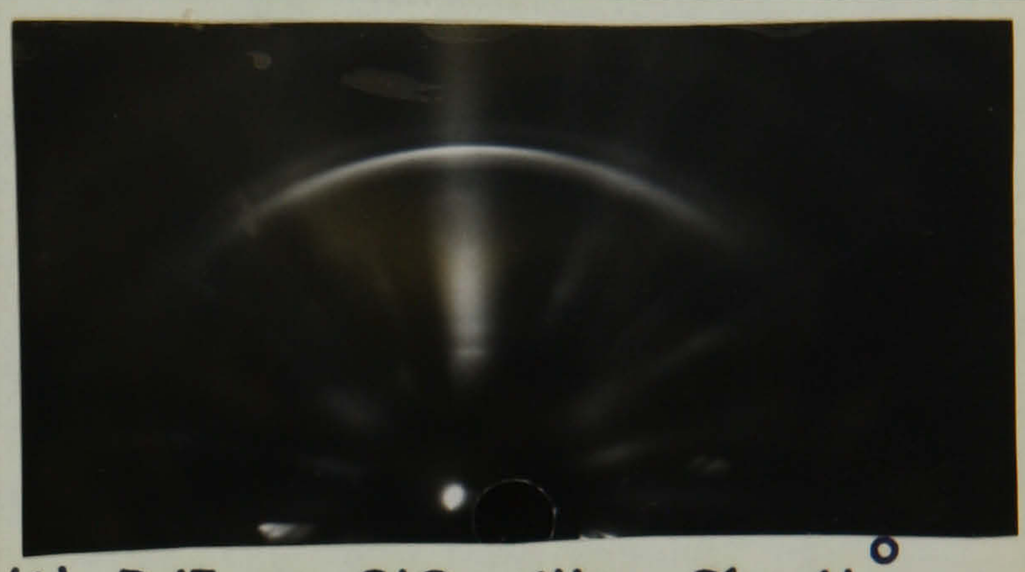

(f) D15, on SiO_2 film, Ø = 41° (8)

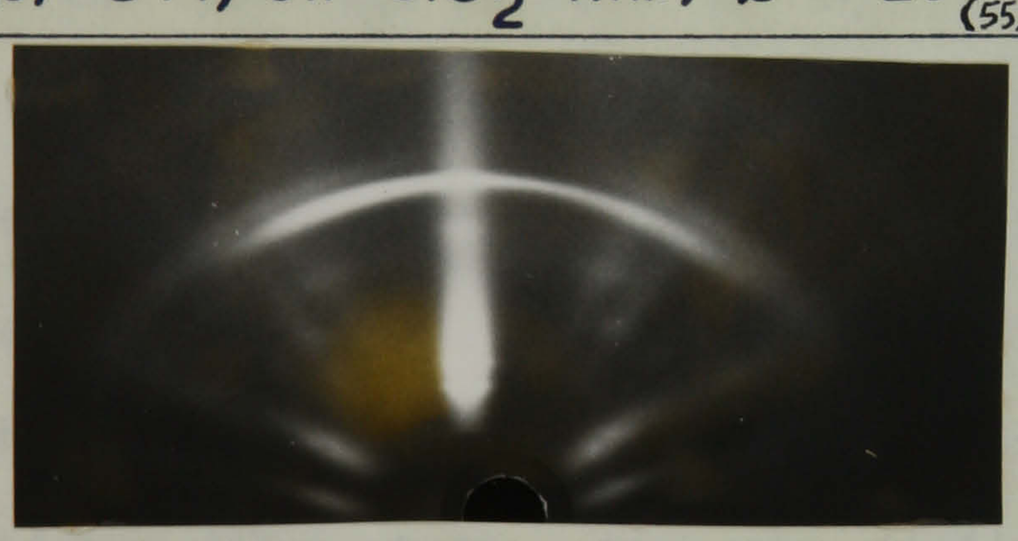

(g) D15, on Cr film, Ø = 46°
Domed substrate (9)

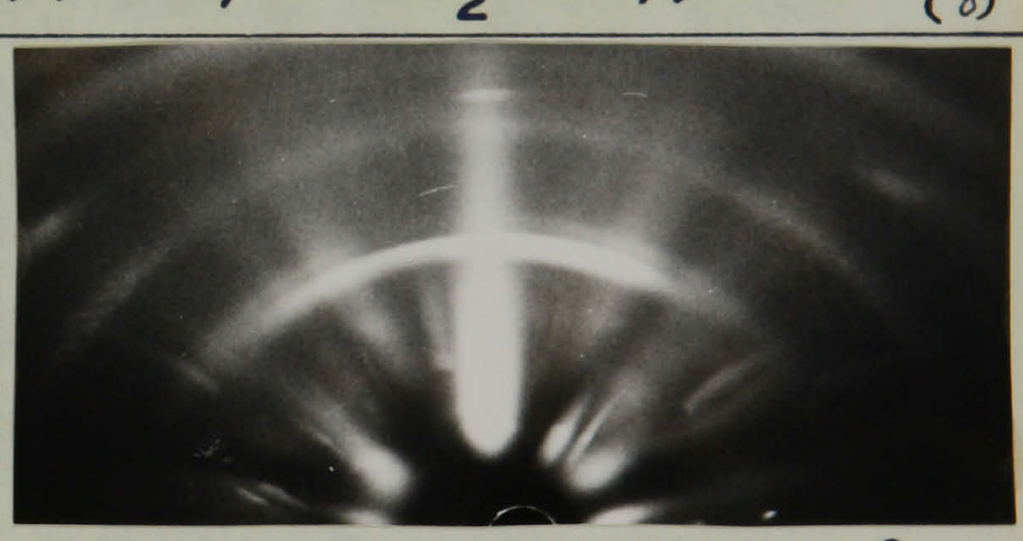

(h) D15, on Cr film, Ø = 54°
Flat substrate (12)

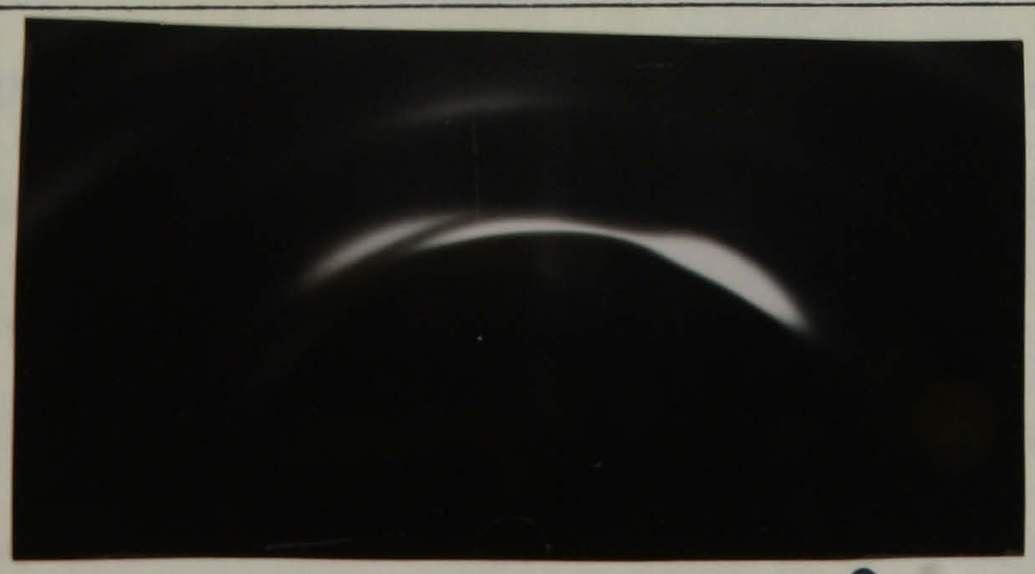

(i) D17, on Cr film, Ø = 35° (2)

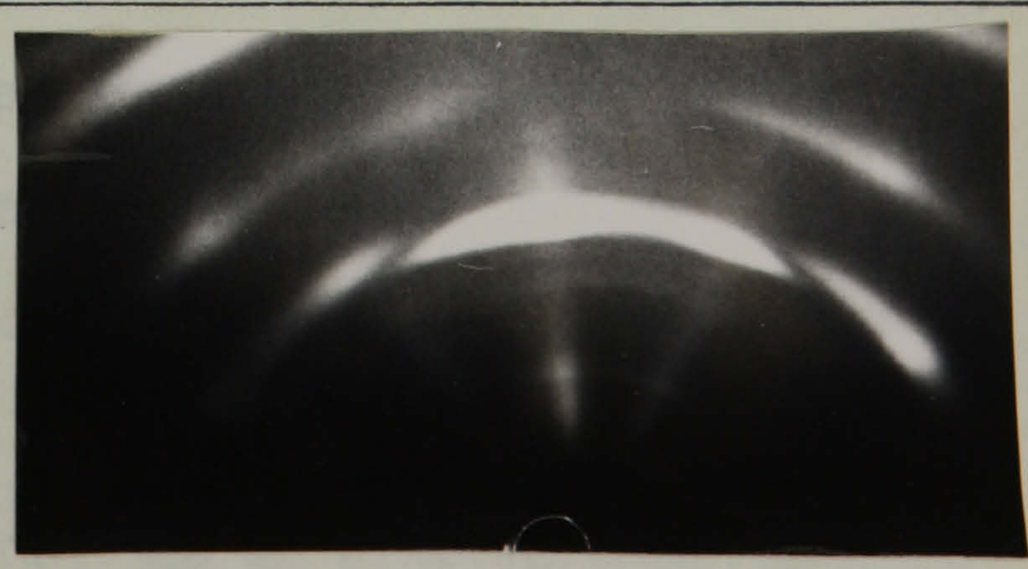

(j) D17, on Cr film Ø = 5° (38)

FIG. 8.3 (002) difraction arcs for as-deposited cadmium sulphide on aluminium rods. X-ray beam perpendicular to evaporation direction, 5° ↔ 20° rocking angle (Ø is deposition angle)

(see Table 7.2). From the diffraction patterns, the inclination of the c-axes of the various CdS films was determined. Fig. 8.4 shows c-axis variation with thickness for as-deposited CdS films up to 100 μm thick. In this figure the angle $\eta(= \emptyset - \psi)$ was chosen as the variable instead of ψ in order to facilitate comparisons between films deposited with various t's and $\emptyset$'s ($\emptyset$ has a maximum of 35^{o} in this figure). The stifling process model was further confirmed by three independent experiments which were primarily intended for the fabrication of thick CdS s-mode transducers. In the first a 100 μm thick CdS film which was deposited at an angle of 30^{o} was etched down to about 40 μm using dilute hydrochloric acid. X-ray diffraction patterns were obtained before and after etching (Fig. 8.3c and d). These patterns showed very clearly that whereas the bottom layers of the film aligned themselves with the vapour beam, the top layers moved nearer and nearer to the substrate normal. In the second experiment, the CdS film was prevented from being continuous by using a multilayering arrangement. Very thin amorphous silicon monoxide inter-layers were deposited between the CdS layers to form SiO/CdS/SiO/CdS stacks (section 5.6). This was a successful way of overcoming the stifling process, i.e. thicker films whose c-axes were inclined at an angle to the substrate-normal were fabricated. In the third experiment, the grain size of the deposited CdS film crystal was made to increase. This was done using cooler vapour molecules (i.e. the Cd/S isothermal source, section 5.6). This decreased surface diffusion, thus making it more favourable for oblique crystallites to grow (see above). The amount of surface diffusion on the film's surface may be inferred from its smoothness. The relative smoothness (see Fig. 9.12) of the CdS films deposited using the CdS/S e.b.b. isothermal technique would indicate

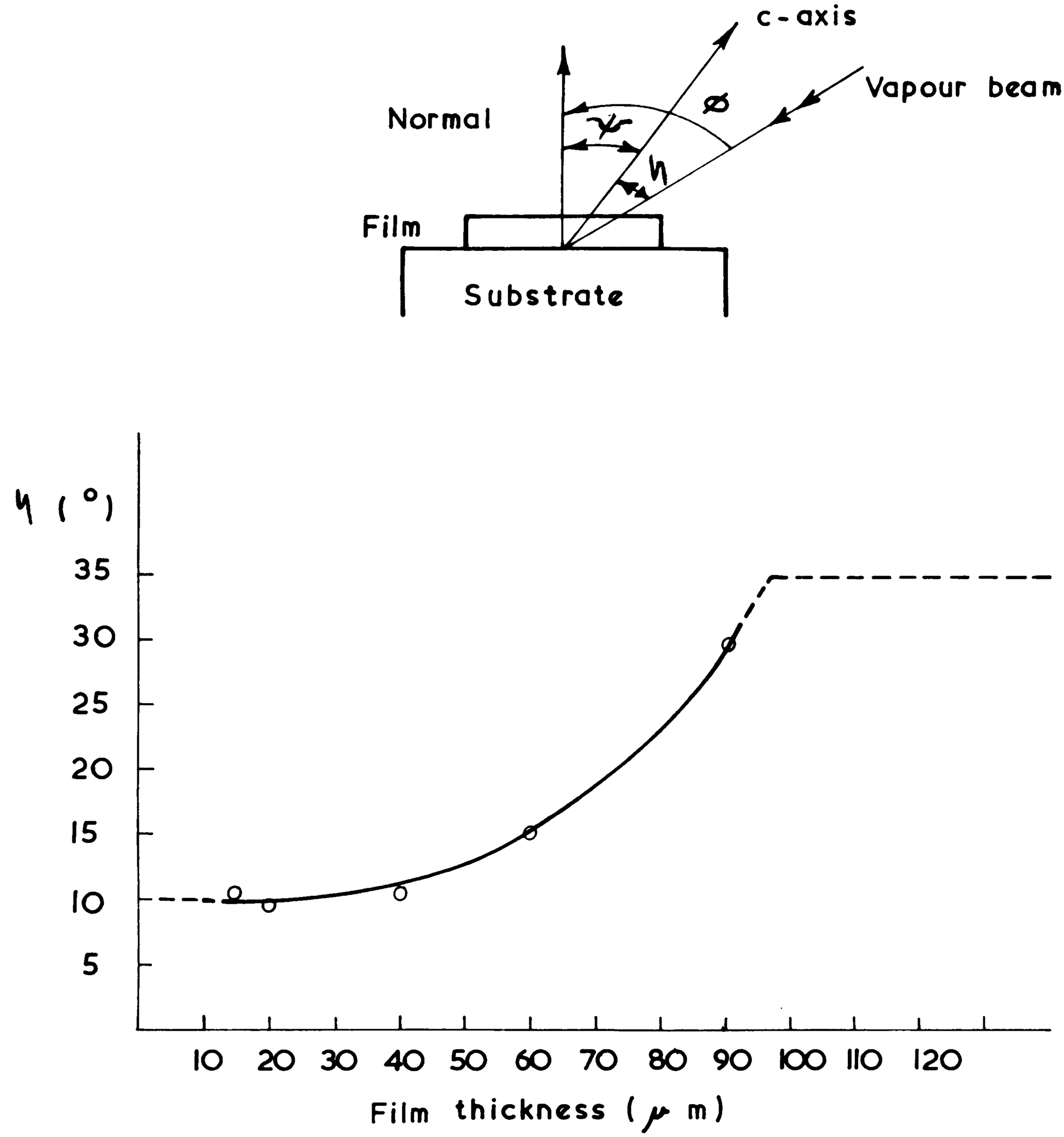

FIG. 8.4 Variation of c-axis inclination with film thickness,

—o— experminental point.

that there is some surface diffusion on the growing face of these films. Migration of impinging molecules leads to a filling of the valleys and a levelling of the peaks on the surface of the film. When there is no surface diffusion, the surface roughness of the film is equal to ^{3} the square root of its thickness, i.e. the troughs and peaks in the as-deposited CdS film of Fig. 9.13 would be about 4 μm.

To the author's knowledge, no other worker has reported on the growth of thick (> 20 μm) oblique CdS film crystals. There is no specific reference in the literature to orientation changes in CdS with film thickness, although recently Mitchell [14] reported that the deposition of oblique CdS film crystals "was always unreliable". Foster has also recently reported some "not well understood" differences between the orientations of very thin and thin films of CdS [15] and of ZnO [16].

8.4.2 Influence of substrate preferred orientation and its surface finish on the orientation of CdS film crystals

So far, the substrate has been assumed to play a passive role in the deposition of oriented film crystals. Its role has been regarded merely as that of a surface where the depositing atoms lose their condensation heat. However. the atomic arrangement on the surface of the substrate (i.e. its crystal structure), may influence the arrangement of the arriving atoms or molecules. For example, in homo-epitaxy the arriving atoms are induced to arrange themselves in the same manner as those of the substrate, i.e. the deposited film crystal is induced to have the same orientation as that of the substrate. Under certain conditions [1], epitaxy may also be used to deposit films of a certain orientation on a substrate of a different material. To the author's knowledge, to date epitaxial CdS films have neither been grown with their c-axis inclined at an angle to the substrate-normal, nor with their c-axis parallel to the substrate. Practically all of the work on thin film crystals is concerned either with deposition onto single

crystal substrates or onto amorphous substrates. Although epitaxial studies provide a valuable insight into the growth and orientation effects of film crystals, the substrate materials used in most of these studies are of little value from an engineering strength of materials view point. In applications where the substrate required has to be metallic, strong and easily machined, polycrystalline metals or alloys are used e.g. drawn or extruded rods or rolled sheets. The strength characteristics of such materials are determined primarily by their grain size and grain orientation. The deposition of film crystals on polycrystalline substrates has scarcely been investigated. In the present work, copper (Cu) and aluminium (Aℓ) polycrystalline (drawn) rods, and polycrystalline duralumin (dural) rods machined from square blocks have been used as substrates. The latter provided rods whose preferred orientation was different from that of drawn rods. However, as discussed in section 5.6, the CdS films deposited on dural rods disintegrated in one deposition run, and in a consequent run they had very low resistivity rendering them useless as transducers. Also, the use of Cu rods as substrates was abandoned because of the reaction between Cu and sulphur. The preferred orientation of the grains of an Aℓ rod substrate is shown in Fig. 8.5. Most of the grains are oriented either with their [111] or [200] direction, normal to the rod face (substrate). This double preferred orientation is frequently [17] observed in drawn wires and rods of Aℓ. Complete epitaxy of as-deposited CdS films on the Aℓ rods may be ruled out for three reasons. Firstly, the orientation of some as-deposited CdS crystallites is that with their c-axes inclined at an angle to the substrate-normal. If there was any epitaxy the c-axis of the CdS film would be parallel to the [111] or the [200] directions of the Aℓ substrate, i.e. its c-axis would be normal to the substrate. Secondly, a very thin chromium (Cr) layer is always deposited on the substrate before CdS deposition. It is not likely that such a thin layer (tens of nm) will have any preferred

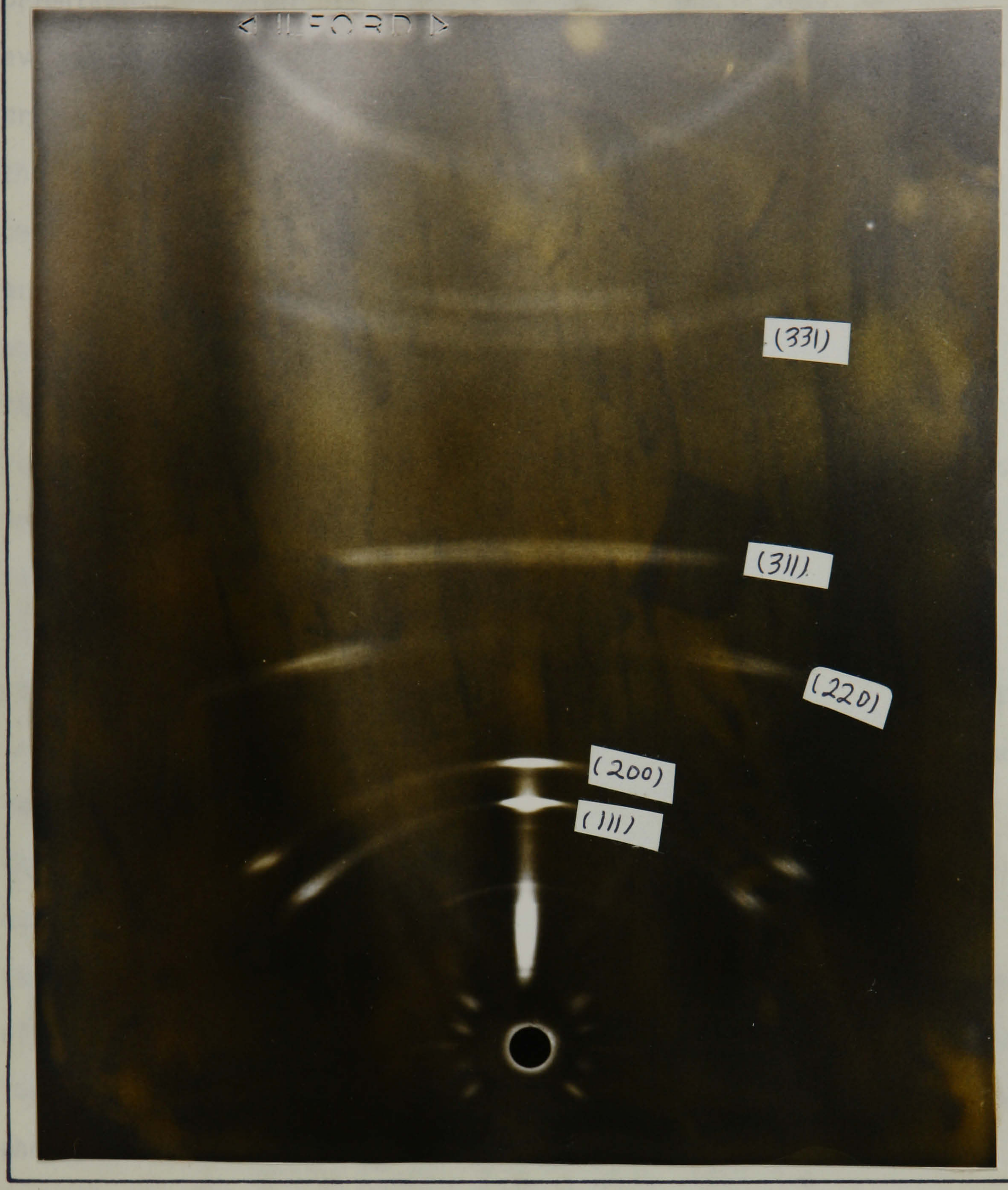

FIG. 8.5

Diffraction pattern from aluminum rod face (substrate).
X-ray beam at grazing incidence, 5° ↔ 20° rocking angle.

orientation. However, it has been reported [18] that epitaxy *does* occur even when a very thin amorphous inter-layer exists between a single crystal substrate and a film crystal. In view of this it would seem that although total epitaxy of CdS films as-deposited onto Aℓ rods may be ruled out, the Aℓ substrate may still have an influence on the orientation of the films. For example, the Aℓ substrate may induce some of the initial nuclei to be oriented with their c-axis normal to the substrate. This is consistent with the stifling process model (above) where it is stated that normal and oblique orientations co-exist in the earlier stages of film growth. The third reason why epitaxy is ruled out, is that the Aℓ rod is not single crystal but rather poly-crystalline with double strong orientation. It was found that there was no marked difference between the orientations of CdS films deposited on flat and domed Aℓ rods (Fig. 8.3g and h). To the author's knowledge, the present investigation is the first in which piezoelectric film deposition on curved substrates has been studied. Because the as-deposited Cr film is about 10 nm, the X-ray beam penetrates it very easily and little diffraction occurs. In fact, the diffraction pattern of Fig. 8.5 was taken with the Cr film deposited onto the Aℓ rod surface. The faint (not indexed) arc nearest to the dark spot in the bottom of the photograph is certainly not that of Cr, but may be of a chromium oxide. To study the orientation of very thin films electron instead of X-ray diffraction is used [19]. Because the vacuum system used in the present investigation is high vacuum (HV), and not ultra high vacuum (UHV), it is possible that during the Cr deposition, oxides became incorporated in the film. It is known [20] that at HV Cr, reacts strongly with oxygen. Studies of the structure of Cr thin films revealed that they consisted of relatively pure islands of metal in a matrix of insulating chromium oxide[21].

Nagao [22] has deposited oblique CdS film crystals onto fused

quartz and onto single crystal sapphire substrates. He found that the orientation of CdS depended both on the angle of CdS deposition and the angle of deposition of the bottom Aℓ electrode. It is generally accepted [23] that f.c.c. metals (e.g. Cu, Aℓ and Ag) grow with their (111) plane parallel to an amorphous substrate. However, Nagao does not mention the preferred orientation of the Aℓ films.

The surface finish of the substrate may also affect the orientation of a deposited film. A smooth (rough) surface may be defined as that whose smoothness (roughness) is small (large) compared with the nucleus of a deposited film. Practically all the work on thin films is concentrated on deposition onto very smooth surfaces. Film deposition on rough surfaces has received very little [4] attention. One of the findings of the present investigation is that, whereas thin films adhered very strongly to the Aℓ rod substrates, thick films did not. As discussed in section 6.5.1, in order to make the films "key-in", the substrate surface was made rougher. This enabled the fabrication of thick films which adhered very well to the substrate. The surface profile of a rough Aℓ substrate is shown in Fig. 6.3 where it can be seen that no shadow masking effects take place. Therefore, the oblique nuclei (and oblique crystallites) are not screened, by the peaks on the surface, from the supply of vapour molecules. There should be less surface diffusion on rough surfaces since the mobility of the initial deposited atoms is reduced by the barriers (peaks) on the substrate surface. Thus, provided that no shadow masking effects occur, the initial growth of as-deposited CdS oblique crystallites should be favoured to that of normal ones (section 8.3). Therefore, it would appear that the stifling process, and the orientation of the substrate rather than its surface finish are the factors controlling the orientation of as-deposited CdS films. This is further supported by the fact that the orientation of CdS films,

deposited under similar conditions, was the same on a variety of surface finishes (20 nm and 430 nm c.l.a., and "as-machined" and etched, (section 5.5).

8.4.3. Other factors influencing the orientation of CdS films, particularly the deposition rate

Numerous other factors may affect the orientation of thin films, in addition to those discussed above. For example the following may be mentioned, namely, deposition rate, temperature of substrate and of vapour molecules, atomic nature of substrate e.g. its atomic weight and atomic radius, stresses in the film, and the nature of the residual gases. In the deposition of stoichiometric film crystals of CdS, the substrate temperature is held constant at a certain value (section 4.4). However, it is known [24] that the orientation of film crystals of some of the Elements varies with substrate temperature. Residual gases e.g. hydrocarbon vapours are known to induce a change in the habit of growth of hexagonal ZnO films [16]. For the deposition of a given film, the heavier the substrate atom, the smaller is the accommodation coefficient, α (section 8.2 above). The value of α has an influence on the growth habit of film crystals (section 8.3). The effect of stresses in as-deposited CdS films on their physical properties is discussed in section (5.5.2).

As discussed in section 3.4.1.5, in most CdS deposition methods, increasing the deposition rate necessarily increases the temperature of the vapour molecules. Also, for a given pumping speed, increasing the deposition rate increases the residual pressure, P_o, during deposition, and thus decreases the directionality of the vapour beam (section 4.4). Further an increase in P_o increases the number of nucleation sites and

therefore decreases the grain size, Δx, of the deposited film crystal (see above). Thus, depending on the particular deposition method used, slow or fast deposition rates may be desirable. For example, for a given vacuum pumping speed, the slower the deposition rate the more directive is the vapour beam, and therefore, the better the preferred orientation of the film crystal, provided that the temperature of the vapour molecules stays the same. If one assumes that the vacuum pumping speed can be increased at will so that the directivity of the vapour beam does not change, then an increase in the deposition rate merely increases the rate of arrival, R_{ar}, of (identical) molecules. From statistical [25] crystal faulting considerations, the slower the rate of arrival of molecules, the more perfect the crystal. This is in agreement with experimental growth results where it is found [9] that the slower the crystallization rate the better the crystal. However, qualitatively one could argue that when the identical vapour molecules are arriving at a very fast rate, they do not have time to move about because of the "quickness" with which they are attracted to the (fast growing) film crystal lattice (little surface diffusion). On the other hand, when R_{ar} is a few orders of magnitude slower, then the atoms can move about before they are finally adsorbed into the lattice (appreciable surface diffusion). From surface diffusion considerations, it would therefore appear that the faster the rate of arrival of molecules the more favourable is the growth of oblique crystallites (section 8.3). Nevertheless, when R_{ar} is increased by increasing the temperature of the vapour source (molecules), the mobility of the molecules (surface diffusion) is also increased. It may be because of these (hidden) changes in other deposition parameters, which accompany changes in R_{ar}, that there is disagreement on the "optimum" deposition rate for good oblique CdS film crystals. For example, Foster [15] found that deposition rates of 0.33 $\mu m.min^{-1}$ rather than 0.02 $\mu m.min^{-1}$ gave better results. Later he reported [26] a deposition rate of

0.2 μm.min^{-1} for the first 0.5 μm of the CdS film, and 0.03 μm.min^{-1} for the remaining CdS film thickness (4 μm). Foster claims [15,26] that the first 0.5 μm of the CdS film has its c-axis normal to the substrate. On the other hand Beecham[27] reported a rate of about 2 μm.min^{-1}, and that the faster the rate, the better the CdS film crystal. Most workers (see section 3.3) who reported an evaporation of CdS (rather than Cd/S) used slow deposition rates in order to ensure the stoichiometry of the deposited film. It is reported [3] that a change in deposition rate of few orders of magnitude is necessary, before any orientation changes occur in deposited films. In the present investigation CdS films were deposited using the CdS/S e.b.b. isothermal technique at rates of 0.03 - 0.1 μm.min^{-1}, with corresponding vapour molecule temperatures of 600 - 800^{o}C. The slower rates gave sharper oblique c-axis preferred orientation, and larger grain size on glass slides substrates. CdS films were also deposited onto Aℓ rods using the Cd/S and CdS/S isothermal techniques at rates of 0.1 and 0.16 μm.min^{-1} with vapour molecule temperatures of 800 and 350^{o}C. The films deposited using the former technique had sharper oblique c-axis orientation than the latter, and also slightly bigger grain size. It is thought that this improvement is due to a decrease in surface diffusion (cooler vapour molecules).

As CdS film crystal orientation depends on the many parameters necessary to characterise a deposition (more than ten named above), the difficulty in formulating a comprehensive model is apparent. However, it seems likely that in oblique CdS film crystal growth, the surface diffusion, and, therefore, the temperature of the vapour molecules is more important a parameter than the rate of arrival of molecules.

Another factor which may affect the orientation of film crystals is a change in thermal gradients either across the film thickness or along its growing face. These gradients may change either

due to the anisotropy of the crystal to heat conduction, or due to rise in temperature of the growing face of the film as it grows thicker, see section 6.4. However, it is shown in that section that as-deposited CdS films are isothermal both along their thickness, and along their surface, i.e. no temperature gradient changes occur during film growth.

C H A P T E R 8

REFERENCES

1. D.W. Pashley, *The nucleation, growth, structure and epitaxy of thin surface films*, Advan. Phys. 14, p. 327 (1967).

2. D.R. Frankl et al, *Nucleation on subs-rates from the vapour phase*, Advan. Phys. 19, p. 409 (1970).

3. C.A. Neugebauer, Chapter in Ref. 20.

4. E. Bauer, Chapter in, *Single crystal films*, ed. M.H. Francombe et al, Pergamon (1964).

5. A. Von der Drift, *Evolutionary selection*, Philips Res. Repts. 22, p. 267 (1967).

6. *American Institute of Physics Handbook*, McGraw-Hill (1963).

7. G.A. Basset, *Continuous electron microscope study of vacuum evaporated metal films*, Proc. Intl. Symp. Condn. Evapn., Dayton, Ohio (1962).

8. I.H. Khan, Chapter in Ref. 20.

9. A. Taylor, *X-ray crystallography*, p.33, Chapman & Hall (1952).

10. D.C. Shotton et al, *The growth of CdS crystals*, G.P.O. Res. Dept. Rept. No. 6 (1968).

11. H.E. Buckly, *Crystal growth*, J. Wiley & Sons (1961).

12. " " " " p. 263

13. " " " " p. 262

14. R.F. Mitchel, *Mullard Research Labs. Rept. No. 2732* (1970).

15. N.F. Foster, *Structure of CdS evaporated films in relation to their use as ultrasonic transducers*, JAP 38, p. 149 (1967).

16. Chapter in Ref. 20.

17. C.S. Bassett et al, *Structure of metals*, p. 546, McGraw-Hill (1966).

18. C.A.O. Henning, *Orientation of vacuum condensed overgrowths through amorphous layers*, Nature, 227, p. 1129 (197).

19. S. Mader, Chapter in Ref. 20.

20. L.I. Maissel et al ed., *Handbook of thin film technology*, p.2-107, McGraw-Hill (1970).

21. " " p.18-17

22. M. Nagao, *High efficiency CdS film transducers for the shear-mode*, JAP 37, 4591 (1966).

23. P.J. Dobson et al, *Preferred orientation in metal films deposited on glass*, Thin Solid Films 5, p. 97 (1970).

24. T.N. Rhodin, Chapter in *Single crystal films*, ed. M.H. Francombe, Pergamon (1964).

25. B.G. Bagley, *On the origin of pseudosymmetry*, J. Cryst. Growth, 6, p. 323 (1970).

26. N.F. Foster et al, *CdS and ZnO thin film transducers*, IEEE trans. SU-15, p. 28 (1968).

27. D. Beecham, *Cd/S isothermal source for CdS deposition*, Rev. Sci. Inst. 41, p. 1654 (1970).

CHAPTER 9

Electrical, ultrasonic and piezoelectric, and mechanical measurements on as-deposited films

9.1. Introduction

In this chapter the following measurements on as-deposited films are described and results presented : CdS film resistivity and CdS/copper junction characteristics, film and junction capacitance, pulse-echo and insertion loss, piezoelectric polarity determination, film adhesion and film thickness. Theoretical values for donor density and conductivity relaxation frequency for as-deposited films are also given. It is stated that the as-deposited films are insulating rather than semiconducting and of negative piezoelectric polarity. It is also stated that the Cu/CdS/Cu junction is equivalent to a single CdS/Cu junction.

9.2. Electrical measurements

9.2.1. CdS film resistivity and CdS/copper junction I-V characteristics

The resistivity, ρ, of as-deposited films was determined from resistance measurements using the defining equation : $\rho = R \frac{A}{y}$, where R is the resistance of the film, A its electrode area and y its thickness. For convenience the ratio ρ/R was plotted against film thickness for three different electrode areas (Fig. 9.1). Once the resistance of a CdS film was measured, its resistivity could be read off directly provided that its thickness and electrode area were known. The resistance was measured using an Avometer and/or a valve voltmeter, and the measurements jig shown in Fig. 9.2. As discussed in section 4.5.1 the resistivity of CdS may vary by more than 15 orders of magnitude (10^{1} - 10^{16} Ω.m.) depending on its stoichiometry, and the higher the stoichiometry the higher the resistivity. Up to D7 (deposition run number 7,

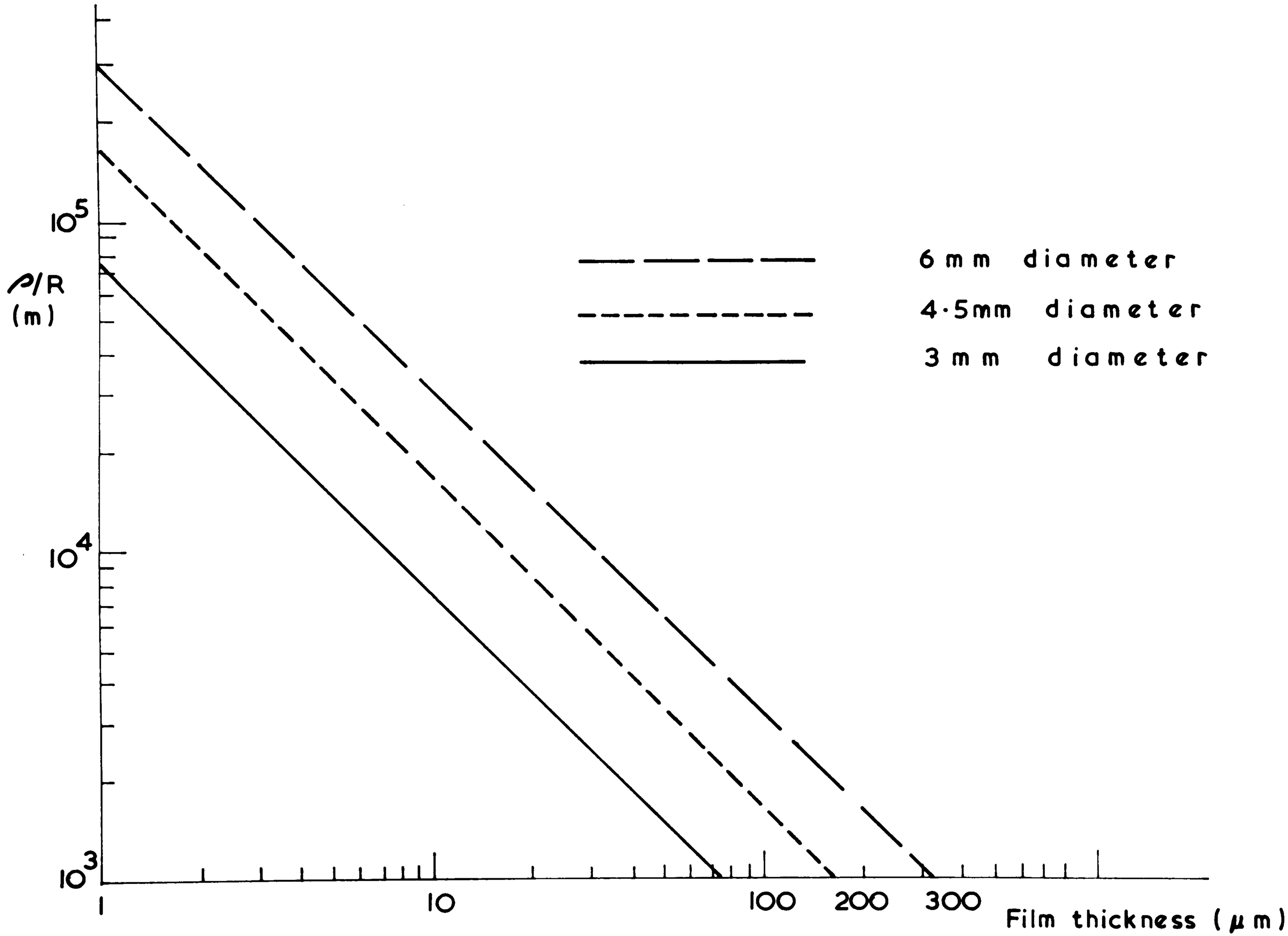

FIG. 9.1 Ratio ρ/R versus film thickness for a CdS disc transducer.

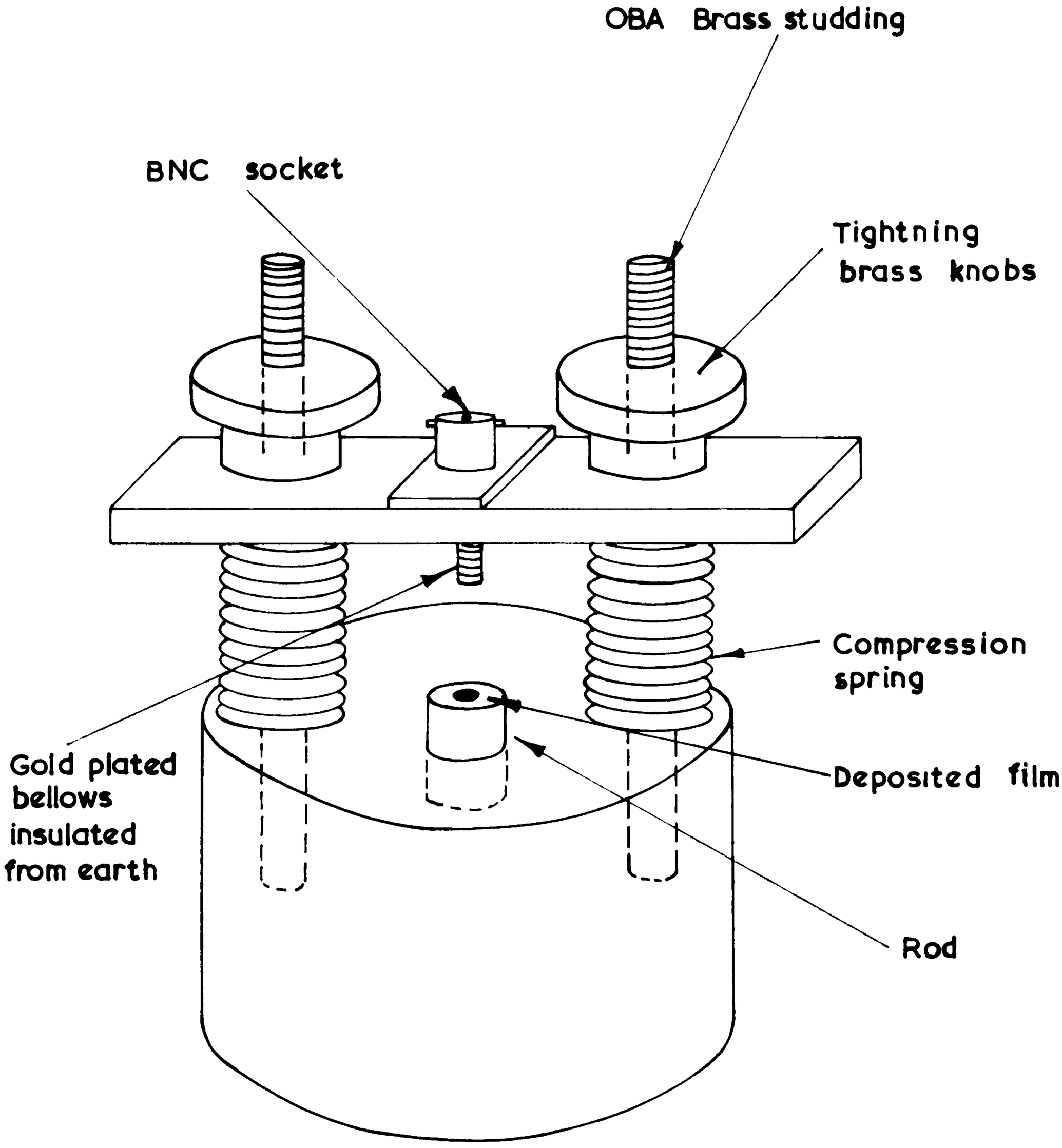

FIG. 9.2 Jig used in electrical and ultrasonic measurements on thin films

see section 5.6) the as-deposited films had resistivities of the order of 10^8 Ω.m. The resistivity of films deposited in D8 was 10^{10} Ω.m. and was observed to increase after heat treatment to 11^{11} Ω.m. This is in agreement with the results of Foster [1], and may be attributed to the creation of acceptor centres in the CdS lattice (see below). The ultrasonic performance of heat-treated films was not any different from that before treatment. Because in consequent deposition runs the as-deposited CdS films had high resistivities (> 10^{10} Ω.m.), they were not heat treated. Films thicker than 50 μm presented an open circuit to the Avometer even when it was on the Ω x 100 range. No photo-conduction in any of the CdS films was observed.

When the lattice site of a sulphur atom is vacant, two electrons must be supplied for every missing sulphide ion (S^{--}) in order to maintain charge neutrality in the crystal ($Cd^{++}S^{--}$). In the vicinity of the vacancy there is a net positive charge, and there is a strong tendency for the extra electrons to be held near the vacancy site. The electrons trapped in the anion vacancy may be regarded as a donor centre which is analogous to the substitutional centre created by doping an elemental semiconductor (e.g. doping germanium with arsenic). If by some means these trapped electrons are released (e.g. by exposing the crystal to light radiation) they enter the conduction band of the crystal and increase its conductivity (e.g. photo-conduction). Another way in which the stoichiometry of a compound may affect its conductivity is the presence of atoms of its constituent elements on inter-stitial sites. The electrical consequences of an inter-stitial donor are entirely similar to those of substitutional donors. No case of interstitial acceptor centres has been established in semiconductors [2]. This may be attributed [2] to the difficulty of fitting large negative ions into inter-stitial sites. CdS is always n-type i.e. the carriers are always electrons.

This is because the donor levels are near the conduction band and so remain ionised but the acceptor levels are about 0.5 eV above the valence band [2]. The behaviour of CdS is typical of the Group II-VI compounds where it is found that either hole conduction (p-type) or electro-conduction (n-type) takes place but not both [3]. In order to determine the density of donors in as-deposited CdS films the following equation [2,4] may be used : $\sigma_n = ne\ \mu_n$, where σ_n is the conductivity of the crystal, n is the donor density, μ_n is the Hall electron mobility and e is the electronic charge. Taking μ_n for CdS as [2] 0.2 $m^2.V^{-1}.s^{-1}$, and a typical conductivity of as-deposited films of 10^{-10} $S.m^{-1}$, n has a value of about 10^{16} m^{-3}. Thus, assuming an atomic density of the order of 10^{29} m^{-3}, the donor density in as-deposited films is of the order of one part in 10^{13}. This donor density is very low indeed and the as-deposited films may be regarded as insulators rather than semiconductors. The forms of controlling conductivity discussed so far are intrinsic. The conductivity may also be controlled extrinsically, e.g. by the diffusion of a suitable impurity. As discussed in section 3.4 impurity doping has been used to decrease the conductivity of CdS films. For example, because copper (Cu) and silver (Ag) belong to Group I of the Periodic Table, the substitution of Ag or Cu atoms in a lattice site of Cd atoms (Group II) results in acceptor centres which decrease the conductivity. However doping of thick CdS films may induce orientation changes and is therefore unreliable. The orientation changes may arise from the necessary alteration in the crystal lattice in order to accommodate the dopant atom which has a different number of electronic charges (Atomic Number Z) associated with it. For example Z_{Cd} and Z_{Al} are, respectively, 48 and 13. Of course, factors other than the stoichiometry of the compound may affect its conductivity. For example it is known that the conductivity is influenced by the crystallographic structure (section 4.5).

It is known [5] that metals may form ohmic or non-ohmic (rectifying) junctions when deposited onto semiconductors (or insulators) depending on the height of the potential barrier between the metal and the semiconductor (or insulator). The barrier may be thought of either as an abrupt or as a graded p-n junction, or a Schottky barrier junction. It is claimed [6] that the height of the potential barrier, ϕ_b, is given by :

$\phi_b = \psi_n - \chi$, where ψ_n is the electronegativity of the metal and χ is the electron affinity of the semiconductor (or insulator). It has been reported [6-9] that metals with low electronegativity e.g. Aℓ, Cr and In form ohmic contacts while the high electronegativity metals e.g. Pt, Au, Ni and Cu form rectifying contacts on CdS. It is claimed [10] that ohmic contacts can be obtained with almost any metal on CdS by tunnelling through the junction barrier with an intense current pulse. The I-V characteristic of an as-deposited Cu/16μmCdS/Cu junction is shown in Fig. 9.3, with the convention that when the top (backing) electrode is positively biased the junction is forward biased and vice-versa. Because of the very low currents involved no measurements on thicker films was possible, and because of breakdown no higher voltages could be applied. The breakdown of one as-deposited film was observed to occur when the electric field was of the order of 2 $kV.mm^{-1}$ although other films had a higher value. This compares with a breakdown value for bulk [11] CdS of 33 $kV.mm^{-1}$. As seen from Fig. 9.3 the Cu/CdS/Cu junction gives a rectification ratio of about 10, and is therefore not a good rectifier. CdS junctions with rectification ratios of up to 10^6 at 5 V have been reported [8]. If an ohmic junction is defined as offering nearly the same resistance for forward and negative bias, then this Cu/CdS/Cu junction is nearly ohmic. However, it is not, strictly speaking, ohmic because the current through it is proportional to the nth power of the voltage across it. For the junctions tested,

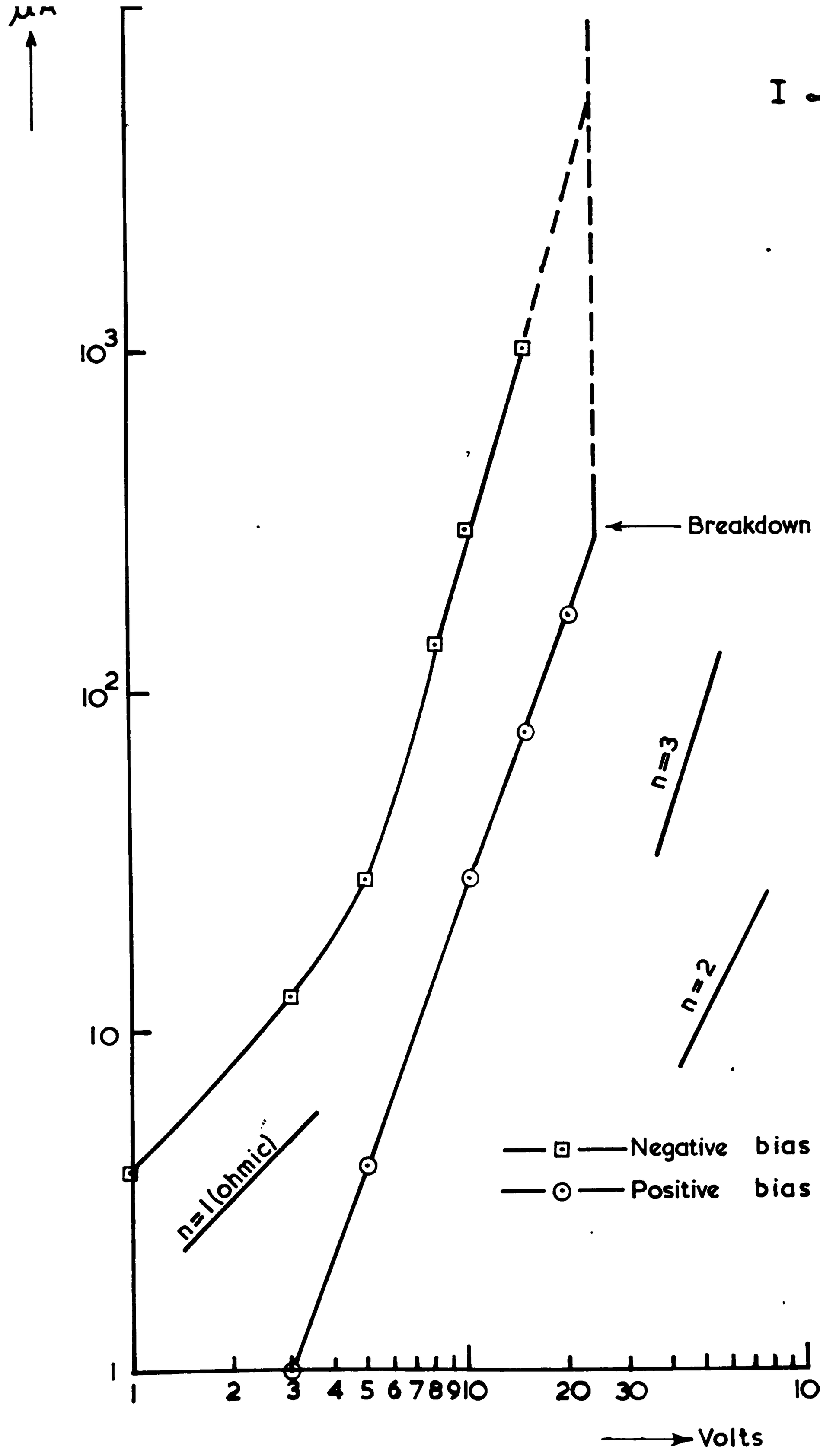

FIG. 9.3 Current versus voltage for a 16μm thick CdS film on glass slide (copper electrodes)

n was about 2.4 for forward and reverse currents of greater than 10 μA. One would have expected the forward and reverse characteristics of a Cu/CdS/Cu junction to be identical since the junction should be equivalent to two identical diodes back to back (or front to front). However, the graphs of Fig. 9.3 show that the two diodes are not identical, that is to say a CdS/Cu junction does not behave in the same way as its geometric inverse i.e. the Cu/CdS junction. This anomalous behaviour of Cu/CdS junctions has also been reported by other workers [7] where it was found that when CdS was deposited onto copper the junction was ohmic, whereas when copper was deposited onto CdS a rectifying junction resulted. This anomalous behaviour may be explained in terms of the reaction between sulphur and copper to form cuprous sulphide (Cu_2S) reported in the present work (section 5.6). It is possible that when CdS is deposited onto Cu a very thin layer of Cu_2S forms onto which the CdS consequently grows forming a CdS/Cu_2S junction instead of the CdS/Cu junction. When Cu is deposited onto CdS it is much more difficult for a Cu_2S layer to form. The I-V characteristics of Fig. 9.3 are in good agreement with those reported [12] for Indium (In) ohmic contacts on CdS. On some junctions tested the current measured was observed to drift with time. This may be attributed to the release of electrons from their traps as discussed above.

The value of the resistivity of a piezoelectric film may affect its performance as an ultrasonic transducer by varying its conductivity relaxation frequency. The conductivity relaxtion frequency, f_c, of a crystal is defined as [13] $f_c = \frac{\sigma}{2\pi\kappa}$, where σ is the conductivity and κ is the permittivity of the crystal. For piezoelectric crystals two types of behaviour are to be expected as the frequency spectrum is scanned. The first occurs when the ultrasonic frequency, f, is much lower than f_c. In this case the carriers, e.g. electrons, will be able to redistribute themselves quickly

enough so that their field will essentially cancel the piezoelectric field. When f is much larger than f_c, however, the carrier distribution will not be able to respond quickly enough to "short-circuit" the piezoelectric field. In this case the piezoelectric field will be nearly as strong as when the crystal is a perfect insulator. It is because ultrasonics has traditionally concerned itself with low frequencies that it has been using insulating piezoelectric materials as transducers. However, with the advent of microwave ultrasonics, semiconducting piezoelectric materials are being used. For example, CdS films whose resistivities are 10^4, 10^6 and 10^8 Ω.m., have conductivity relaxation frequencies of 1 MHz, 10 kHz and 100 Hz, respectively. If one takes, as a design rule, f to be three orders of magnitude greater than f_c, then CdS films whose resistivities are greater than 10^8 Ω.m. would make useful transducers at frequencies down to 100 kHz.

9.2.2. Film and junction capacitance

The capacitance measurement set-up consisted of a Marconi Type TF 1246 oscillator connected across a standard resistance (1 kΩ or 10 kΩ) in series with the CdS transducer. In order to investigate the dependence of capacitance on bias voltage a variable "Microreg" d.c. supply was connected in series with the oscillator. The voltage V_R across R was measured, on a Tektronix Type 545B oscilloscope, and taken as reference. The voltage V_C across C and its phase angle, Ø, w.r.t. the reference voltage was also measured. The capacitance of the film was calculated from the equation $\tan \emptyset = \omega RC$. The capacitance of the 50 Ω coaxial lead which connected the film in the measurements jig (Fig. 9.2) to the scope, and the input capacitance of the scope were substrated from the calculated value to yield the capacitance of the film, C_o. The capacitance was measured at 100 kHz, 1 MHz and 10 MHz, and no dependence of capacitance on frequency was observed.

The value of C_o measured agreed very well with the geometric capacitance which was calculated assuming bulk conditions (Fig. 9.4). However, the film capacitance, C_o, varied with d.c. bias as shown in Fig. 9.5. With positive bias (i.e. the top electrode positive w.r.t. the bottom one) the capacitance was found to be independent of bias voltage. With negative bias, however, the capacitance varied approximately linearly with $V^{-\frac{1}{3}}$. This would indicate that the CdS/Cu/CdS junction is equivalent to a single CdS/Cu junction in agreement with the junction I-V characteristics discussed above. Further, the dependence of C_o on $V^{-\frac{1}{3}}$ would indicate [4] that this CdS/Cu junction is equivalent to a linearly graded diffusion-layer junction rather than an abrupt p-n junction. Other workers [9] have reported the linear dependence of C_o on $V^{-\frac{1}{3}}$ for a CdS/In junction. The use of the diffusion layer as the active part of a low-resistivity CdS slab enabled the fabrication of UHF CdS transducers before the advent of vacuum-deposited thin film transducers. The thickness of the diffusion layer determined the resonance frequency since the conductivity of the rest of the slab was negligibly small compared with that of the layer. The resonance frequency could, therefore, be tuned electronically. Frequency tuning of CdS s-mode platelets has been performed [14] by voltage, temperature and loading. It was found that, depending on the conductiviy of the CdS crystal the frequency either decreased or increased with bias voltage. The as-deposited film capacitance, C_o, was also found to vary with the amplitude of the a.c. voltage across the film. Other workers [12] have studied the variation of the capacitance of CdS/In junctions for various a.c. and d.c. bias conditions.

9.3. Ultrasonic and piezoelectric measurements

9.3.1. The pulse-echo technique

The pulse-echo technique is widely used in ultrasonics in its single-ended mode, i.e. the same transducer is used for both

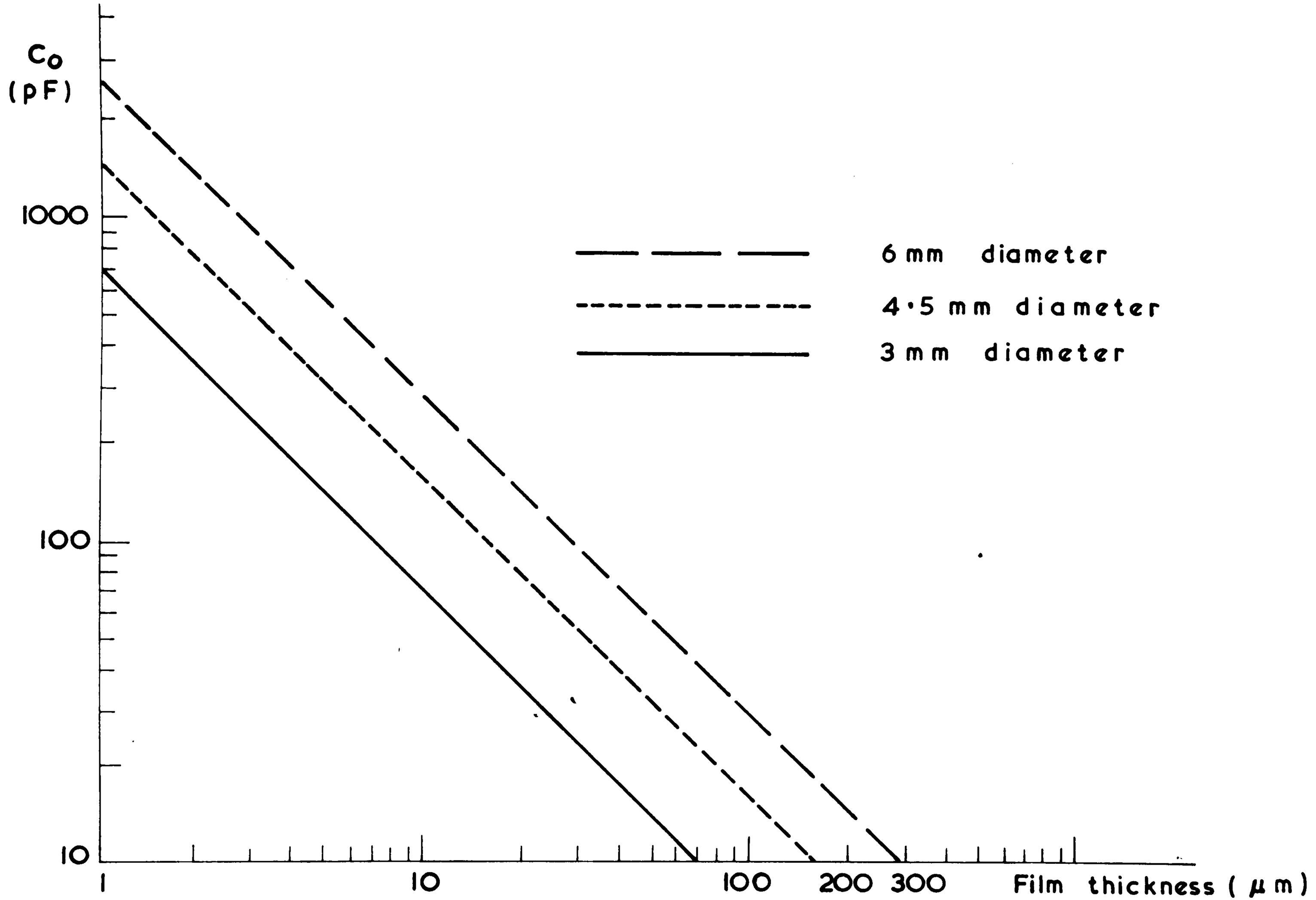

FIG. 9.4 Static capacitance, C_o, versus film thickness for a CdS disc transducer.

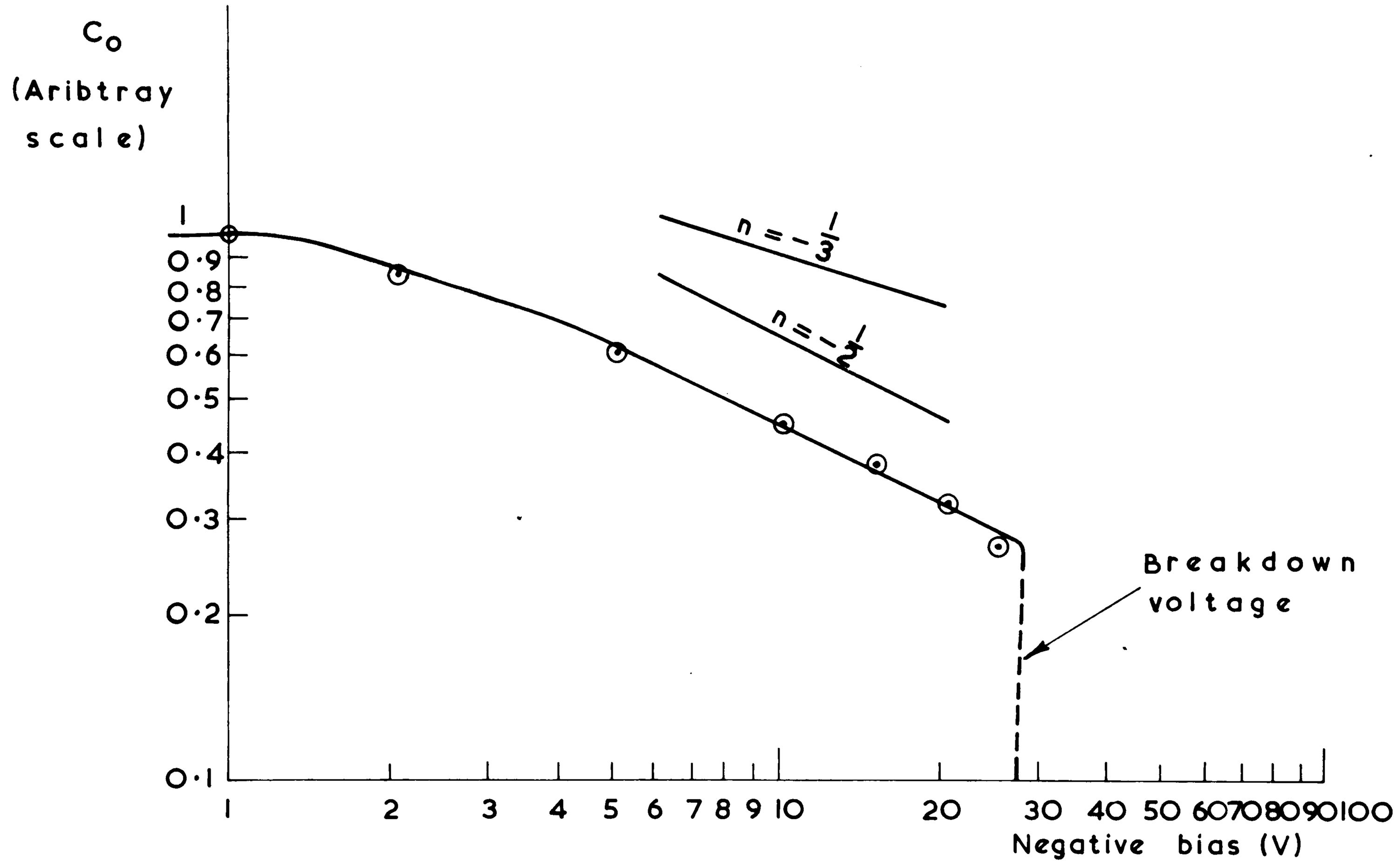

FIG.9.5 Variation of capacitance, C_o, with bias voltage for a 16 μm thick CdS film on glass slide (copper electrodes).

transmitting and receiving. The transducer sends a pulse of ultrasonic waves into the medium onto which it is bonded (or deposited). The ultrasonic pulse wave undergoes reflection at a discontinuity, e.g. a solid/fluid interface or a crack in the propagation medium. The reflected wave is received by the transducer. Many measuring and non-destructive testing techniques make use of short ultrasonic wave pulses. In the generation of ultrasonic wave pulses a transient electrical signal is applied to the transducer which, in its turn, produces a transient mechanical vibration. Likewise, in detection the transient mechanical signal (ultrasonic wave reflection) is converted to an electrical impulse by the transducer. A number of practical problems involve the application of a transient electrical signal to a piezoelectric transducer. For example, the static capacitance of the transducer, C_o, lengthens the rise time of the driving electrical pulse. This is why transducer materials with low permittivity, e.g. CdS, are preferred, since their low capacitances make them much easier to drive. Another problem with single-ended pulse-echo set-ups is the difficulty to provide isolation between the high-power r.f. transmitter which drives the transducer and the sensitive receiver which amplifies the ultrasonic echos converted by the transducer. Often, this isolation problem sets the limit on how hard a transducer is driven, rather than the breakdown voltage of the transducer. In general it is best to drive the transducer as hard as possible so as to make the echo amplitude large compared with the noise level in the first stage of the receiver.

CdS transducers as-deposited onto glass slide and aluminium flat and domed rod substrates were tested by the pulse-echo technique (Fig. 9.6). A nonosecond pulse generator (E-H Model 120B) and an oscilloscope (H-P Type 1410A) and the measurements jig of Fig. 9.2 were used. The echoes from the back wall of the substrate were as shown in Fig. 9.7. For CdS films up to 45 μm thick onto glass slides

it was observed that where the CdS vapour beam hit the substrate at right-angles, the resulting transducer generated only c-mode waves (Fig. 9.8). Where the vapour beam hit the substrate at an angle, however, both s-mode and c-mode excitations resulted (Fig. 9.7). When the vapour angle was at about 30^{o} to the substrate normal the c-mode echo amplitude was very much smaller than the s-mode echo, i.e. the transducer acted as an s-mode transducer with little coupling to the c-mode. This is in excellent agreement with the predicted response of CdS films whose c-axes are inclined at angle to the substrate-normal (section 2.4). Some of the as-deposited films on aluminium substrates gave both s-mode and c-mode responses simultaneously while the majority gave only c-mode echoes although their deposition angle was 35^{o}. This anomalous behaviour is explained in Chapter 8 in terms of orientation changes with CdS film thickness. The first echo amplitude from CdS transducers on 1.5 mm thick glass slides was typically 45 dB down on the transmitter pulse (12V). The best response from CdS transducers on aluminium rod substrates was that obtained from a 90 μm thick film. The echo amplitude (c-mode) was 26 dB down on the transmitter pulse (4V). This was obtained when the rod substrate was machined down until it was about 2 mm long. the transducer driving pulse is shown in Fig. 9.9 together with the c-mode and s-mode echoes from the back of the glass slide onto which the transducer was deposited. These echoes have approximately the ideal "chad" shape predicted from theoretical considerations (see section 2.4.2). The transmitter and echo pulses shown here were recorded on an X-Y plotter.

9.3.2. Insertion loss

Although the amplitude of the first echo in the pulse-echo technique gives a good idea of the insertion loss of the transducer, it is, nevertheless, not an exact measure of it. In

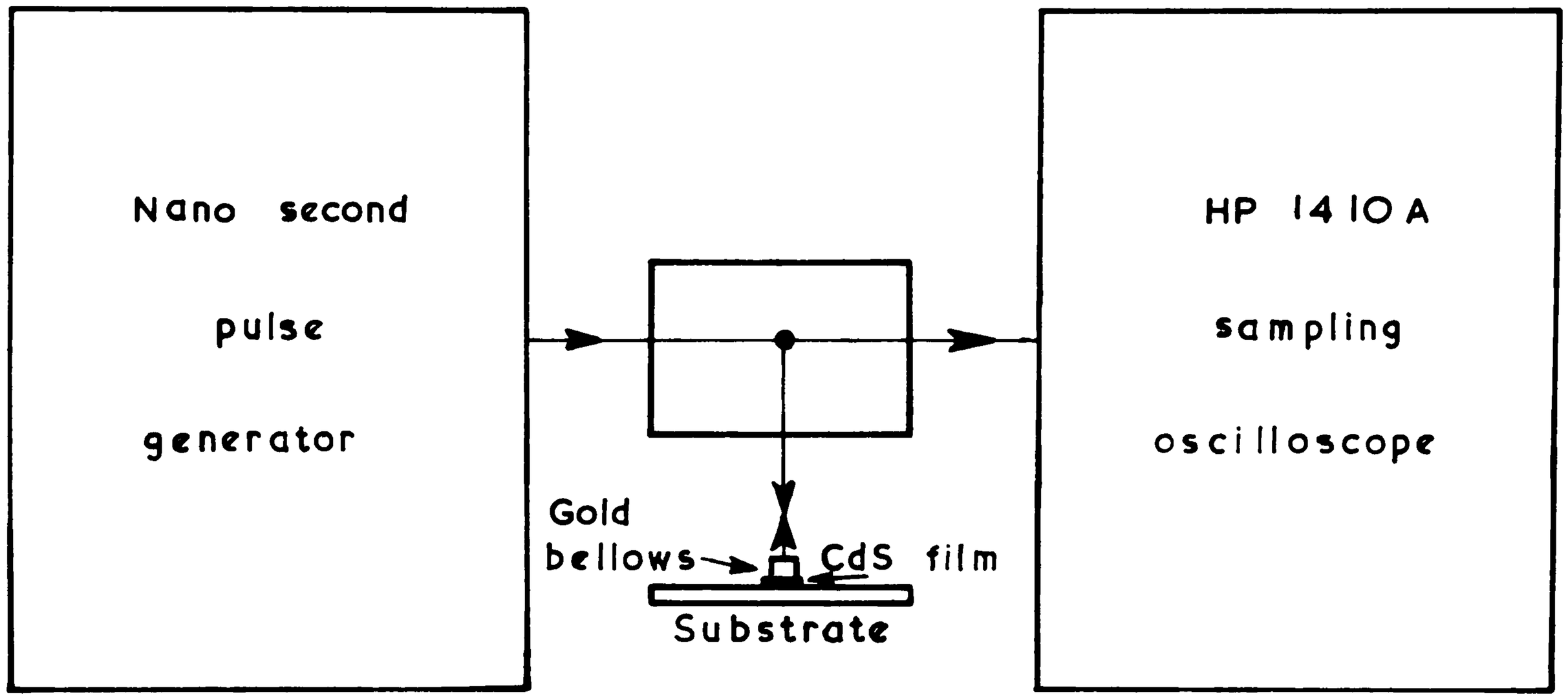

FIG. 9.6 Schematic diagram of pulse echo set up

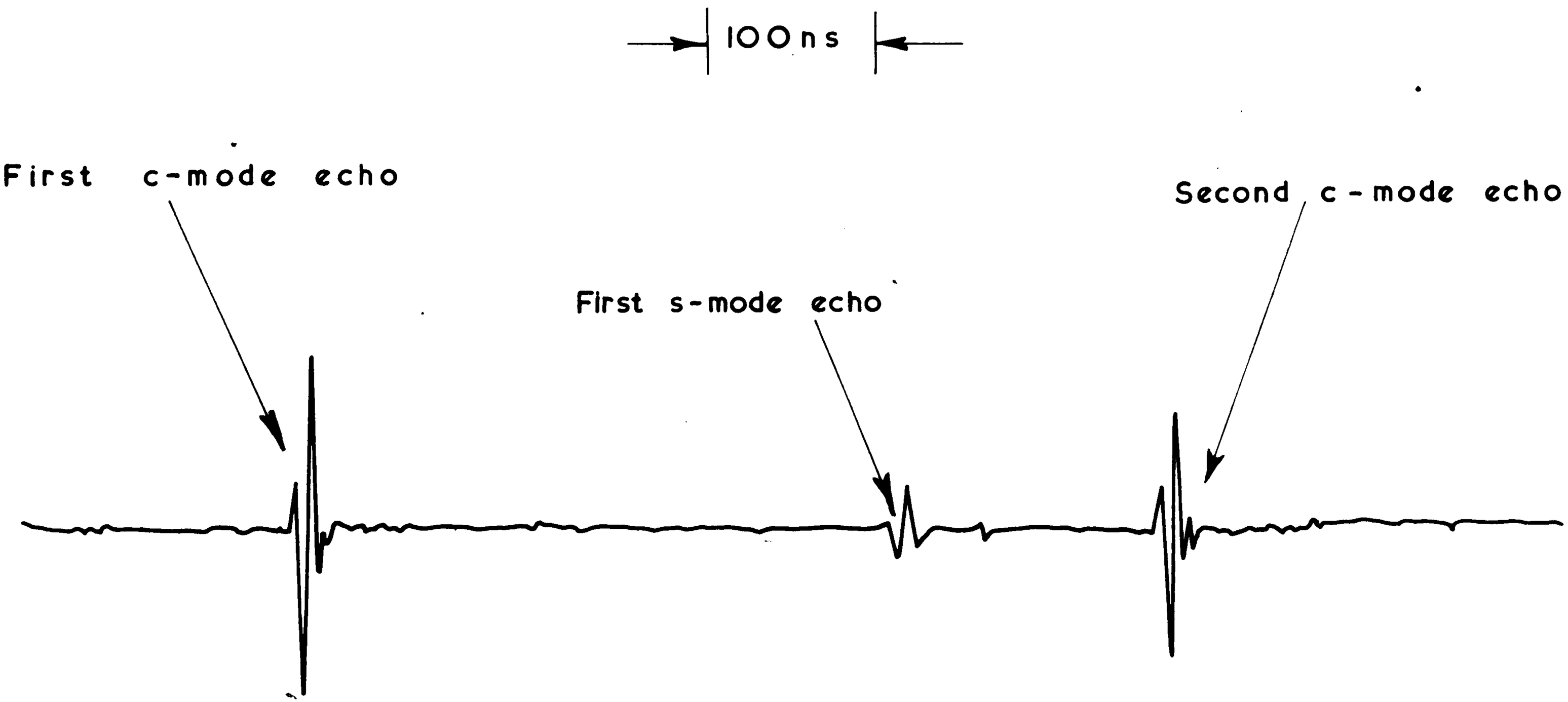

FIG. 9.7 Compressional-mode and shear-mode echoes on glass slide 1.5mm thick (CdS film 16 μm thick.

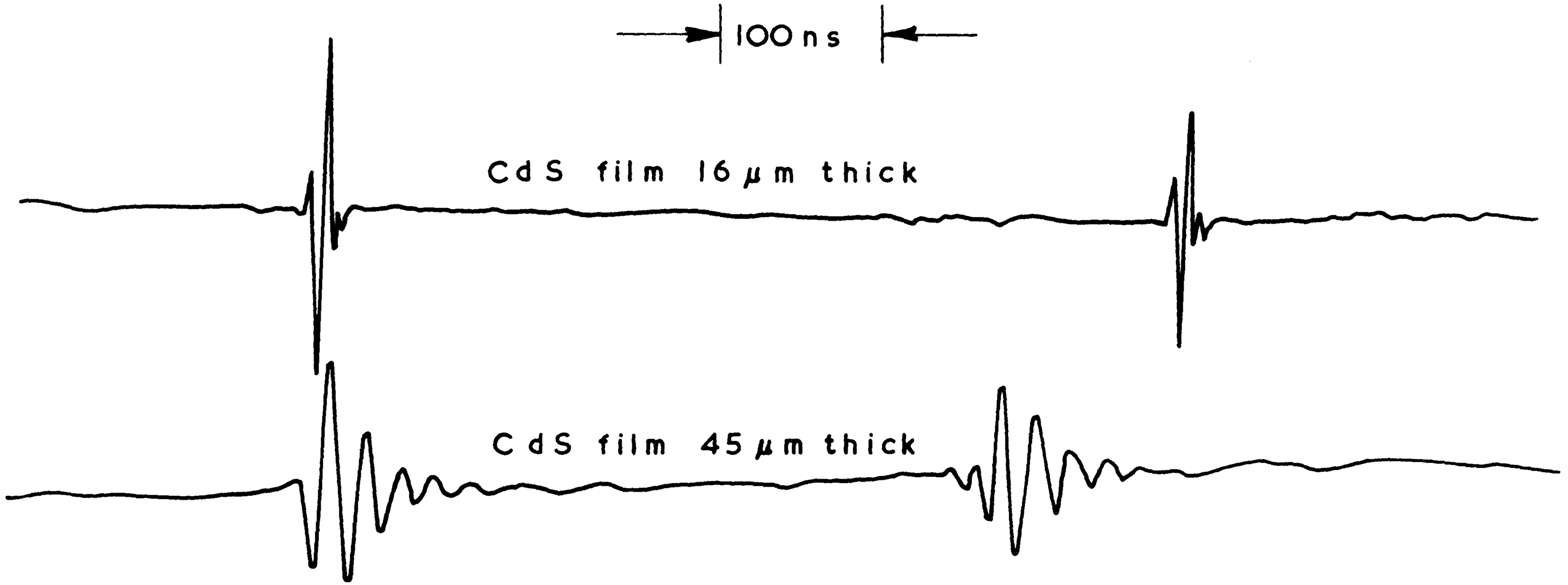

FIG. 9.8 Compressional-mode echoes on glass slides for different values of transducer thickness.

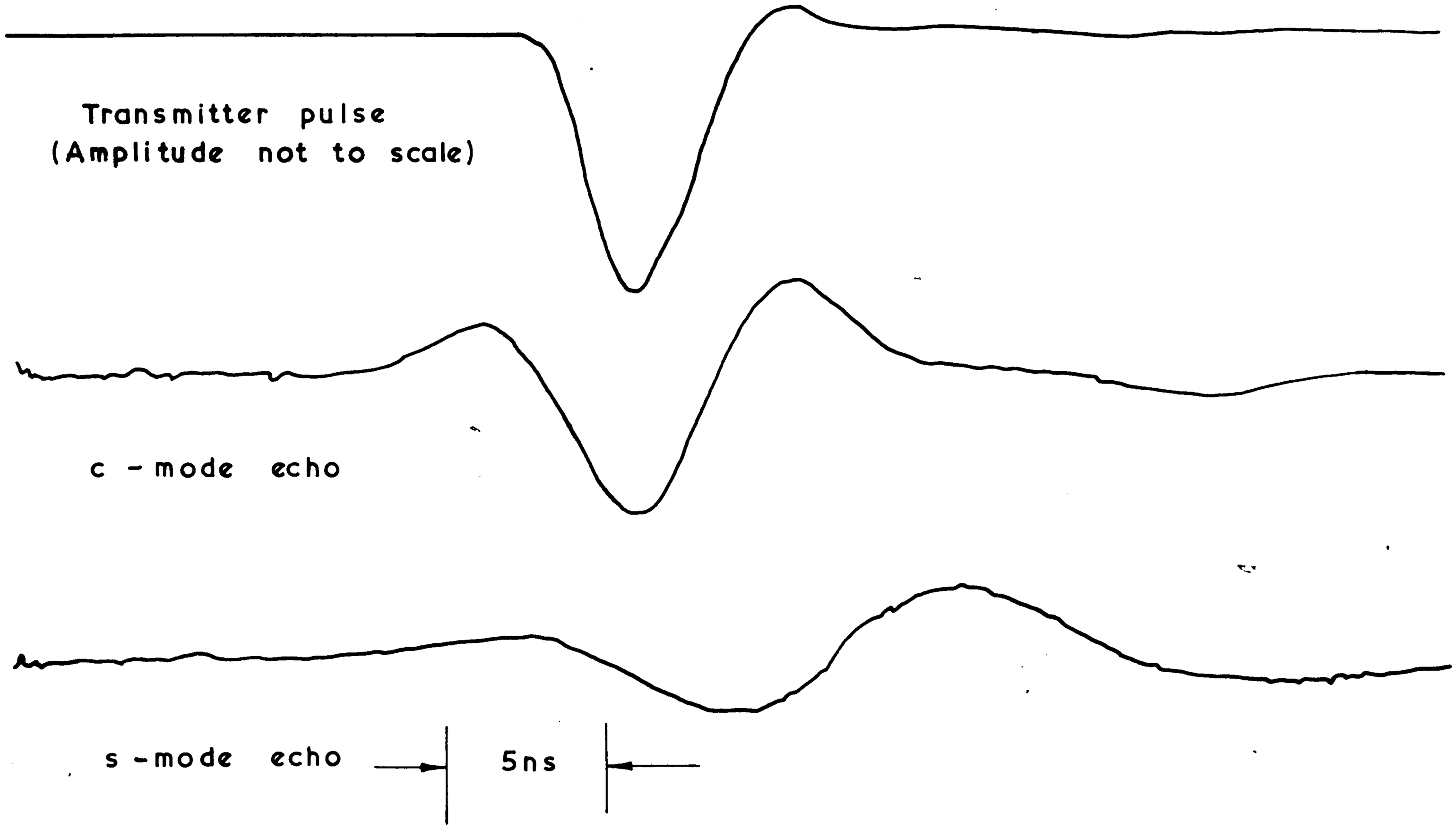

FIG. 9.9 Transmitter pulse and echoes on glass slide 1.5 mm thick (CdS film 16 μm thick.)

order to measure the insertion loss properly, sine waves must be used to drive the transducer instead of a single pulse. To this end the author designed and built a pulsed Hartley oscillator, the circuit diagram of which is given in Fig. 9.10. This oscillator was used to drive the transducer instead of the nanosecond pulse generator. The oscillator had an output resistance of about 50 Ω, and the transducer insertion loss was measured in a 50 Ω system in the frequency range 60-90 MHz. This was done in the early part of this project where thin CdS films were deposited onto glass slides. A pulse repetition frequency of 100 Hz, and an r.f. pulse width of 100 ns were obtained. A typical un-tuned two-way insertion loss was 35 dB. Because of the difficulties encountered with the fabrication of low-frequency CdS transducers on aluminium rod substrates (section 5.6), no insertion loss measurements were carried out on these transducers.

9.3.3. Piezoelectric polarity determination

As discussed in section 2.4.2, it is sometimes necessary to determine the absolute configuration of a piezoelectric film (crystal). For CdS films this means the determination of the absolute arrangement of Cd and S atoms in the CdS crystal (Fig. 2.1), i.e. whether the top layer of a deposited film is composed of Cd or S atoms. Because of the anisotropy (which is responsible for piezoelectricity) along the c-axis of a hexagonal CdS crystal, it is possible to establish the absolute configuration by applying a force impulse to the CdS films. The resulting charge (and current) generated through the piezoelectric effect would be either positive or negative depending on whether the top atomic layer is composed of S or Cd atoms (see later). As-deposited films were tested using the rig shown in Fig. 9.11. A high input impedance FET probe was used as a "hammer" applying a force impulse to the film and detecting the resulting current impulse. A miniature gold bellows (Servometer Type 2012)

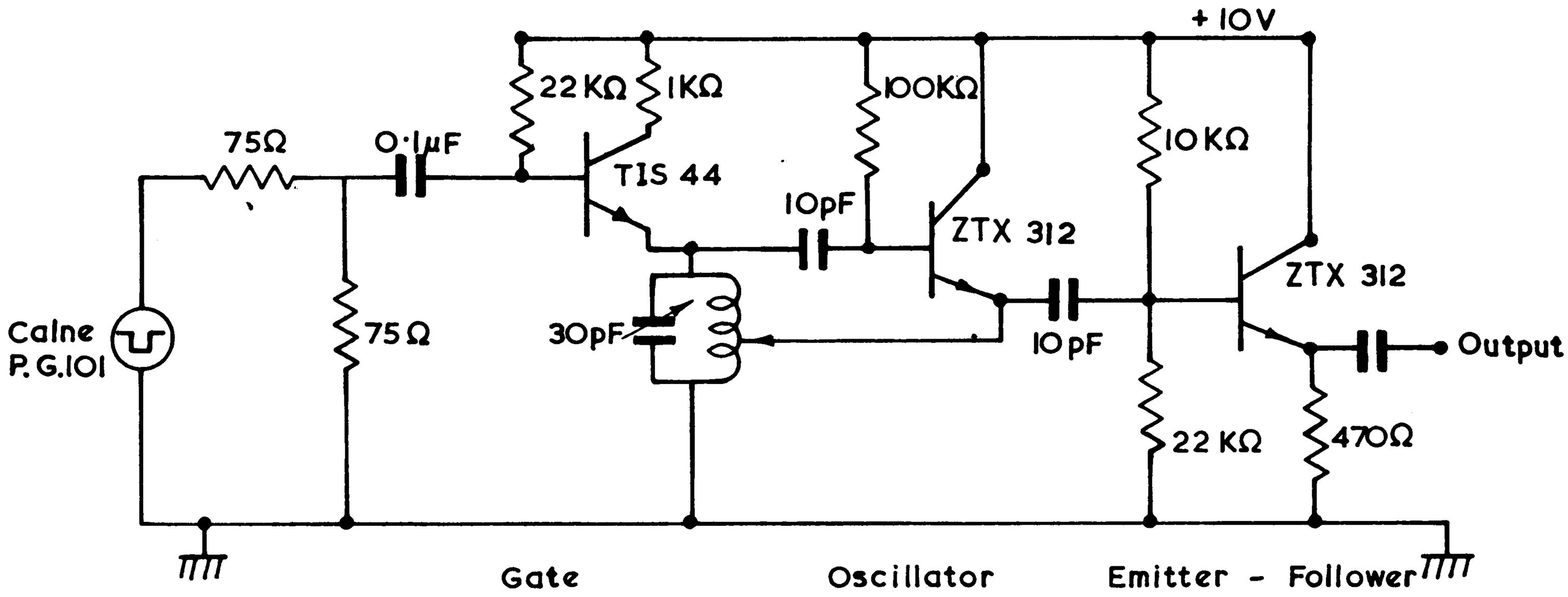

FIG. 9.10 50 ohm output pulsed Hartley oscillator.

(a)

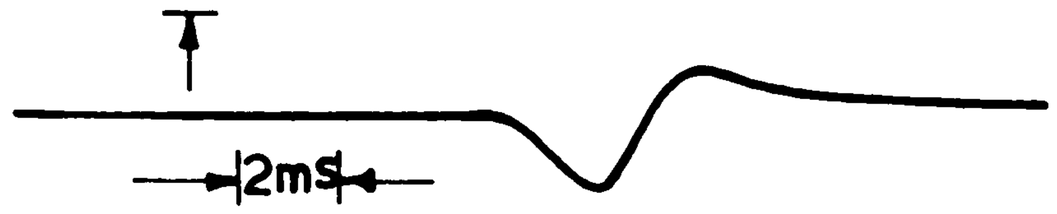

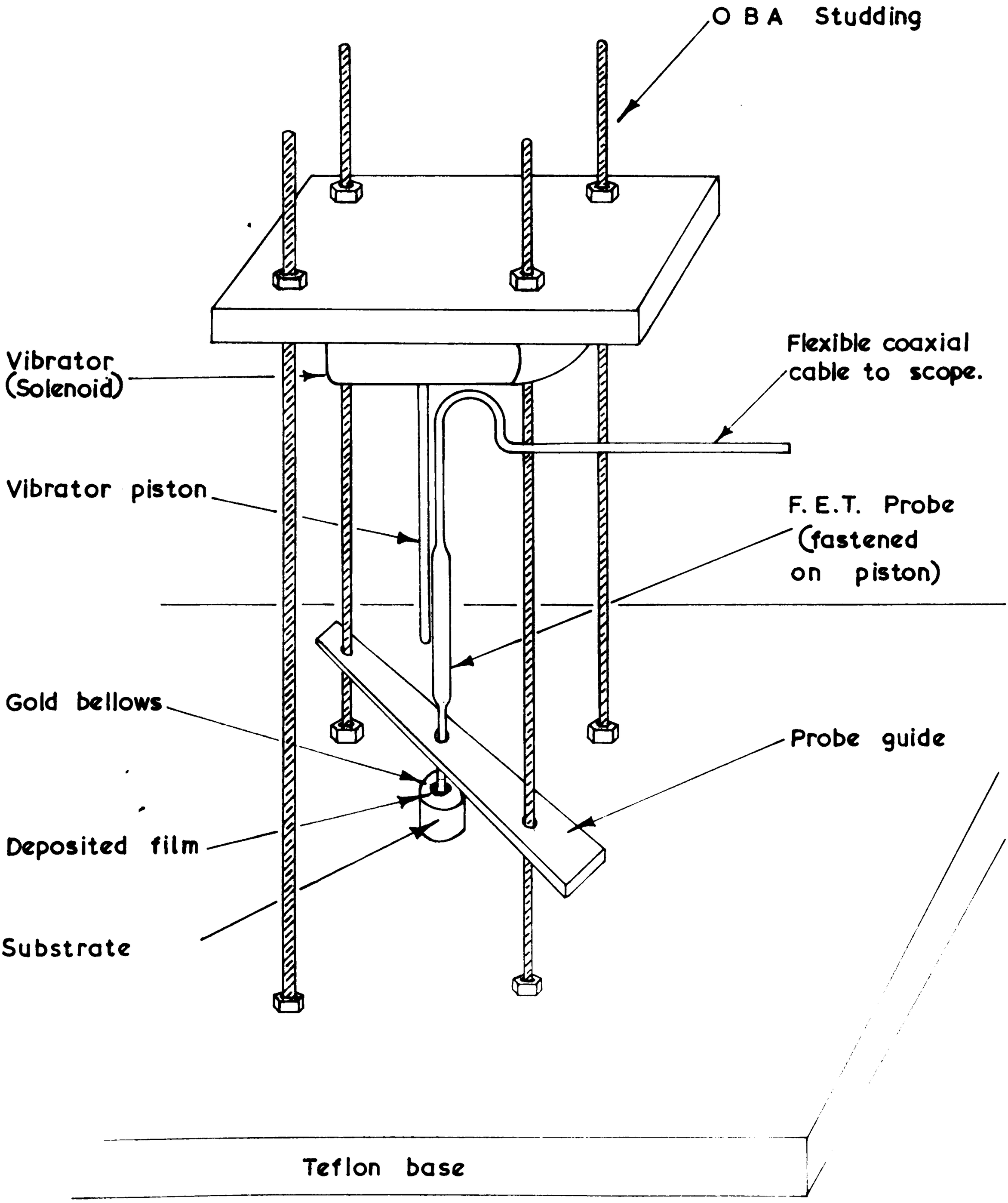

(b)

FIG. 9.11: (a) Piezoelectric voltage impulse.
(b) Polarity test rig.

acted as a cushion between the film and the sharp-pointed probe (H-P Type 1123A). The probe was fastened onto the piston of a vibrator which was driven by a power amplifier fed from a pulse generator (Advance Type PG 5002D). The pulse generator also provided the trigger signal for the oscilloscope display. The force impulse and the scope display were thus synchronised. Typical pulse repetition frequencies of 5 Hz were used. A typical film response to the force impulse is shown in Fig. 9.11a. This is a tracing of a Polaroid photograph taken from the screen of the oscilloscope. CdS films deposited onto copper film, silicon dioxide film, and chromium film substrates were tested, and they all had the same (negative) polarity. (The polarity is assigned according to whether the leading edge of the piezoelectric impulse goes positive or negative). Because this technique essentially involves a compression of the crystal, it is only suitable for testing the polarity of c-mode films, i.e. films whose c-axes are normal to the substrate. Thus, films whose c-axes were inclined at an angle to the substrate normal did not respond electrically to the force impulse applied to them.

Using an elementary electrostatic model it has been shown [15] that compression along the c-axis gives rise to a negative charge on the (001) cadmium face of the crystal. This has been confirmed by experiments on single crystal slabs [15]. It would appear, then, that the as-deposited CdS films had a top layer composed of cadmium atoms. This means that the bottom layer (i.e. the layer in contact with substrate) is composed of sulphur atoms. Theoretical treatment [16] based on the assumption that the predominant interaction across the film-substrate interface is of an ionic nature predicts that it is more favourable for a sulphur layer rather than a cadmium layer to be immediately adjacent to the substrate. The theory is based on

a minimum energy criterion. Rozgonyi and co-workers [15] have also reported on polarity testing of deposited CdS films. They distinguished between two types of film. The first type were highly oriented, from a crystallographic point of view, and were of negative polarity. The second type were of positive polarity and were not highly oriented. Since the films tested in the present work had a negative polarity and were highly oriented (section 7.6) Rozgonyi's assertion that highly oriented films are of negative piezoelectric polarity should be supported. Again, the shape of the piezoelectric voltage impulse is in good agreement with that predicted [17] when a force step-impulse is applied to a transducer.

9.4. Mechanical and other measurements

As a check on the Edwards Film Thickness Monitor (section 5.3), the thickness of as-deposited films was measured using a "Talysurf" and a "Talystep" (Taylor-Hobson Model 4 and 1 respectively). The "Talysurf" instrument makes use of a sharply pointed (2.5 μm tip) diamond stylus to trace the profile of the surface irregularities. A rounded skid is used to provide a datum. The pick-up carrying the stylus and skid is traversed across the surface by means of a motorised drive unit. The up and down movements of the stylus relative to the skid are converted into corresponding changes in an electric current using an inductive transducer. These changes are amplified and then used to control either a Rectilinear Recorder which plots the surface profile, or an Average Meter which shows the centre line average (c.l.a.). The "Talystep" has two kinds of stylus. The first is conical with 12.5 μm radius while the second is a truncated pyramid 0.1 x 2.5 μm. A typical Rectilinear Recorder plot is given in Fig. 9.12. The "Talysurf" was also used to determine the surface finish of substrates. The substrates had c.l.a. values between 20 and 430 nm. These results are discussed

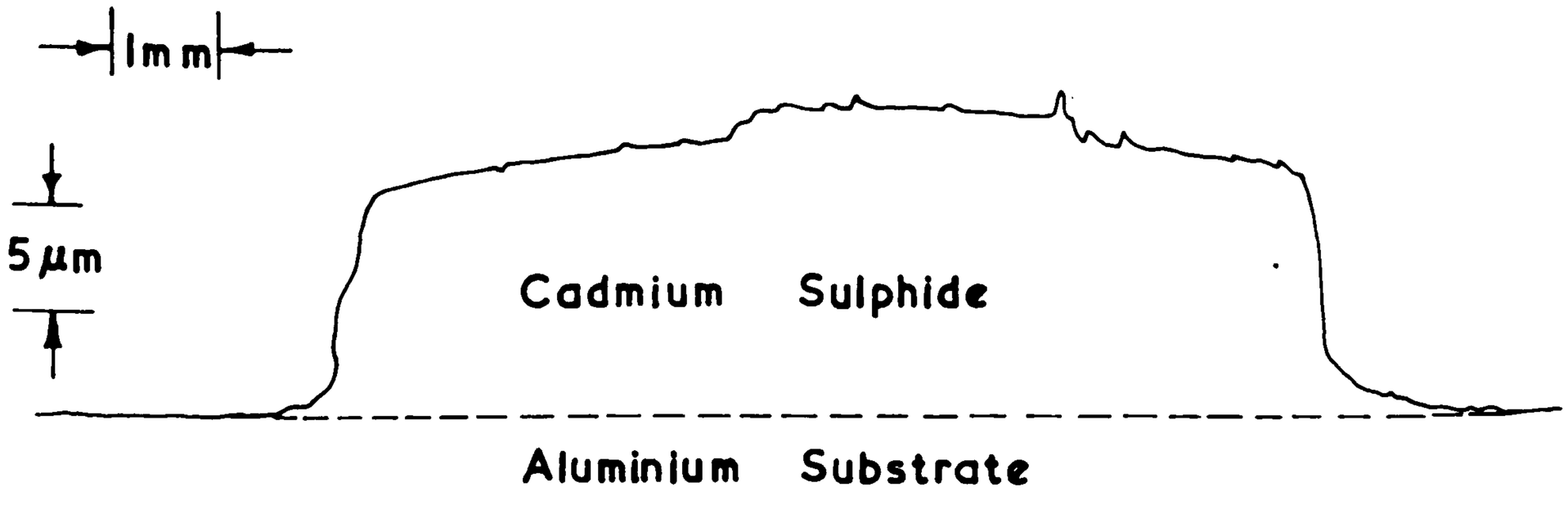

(a)

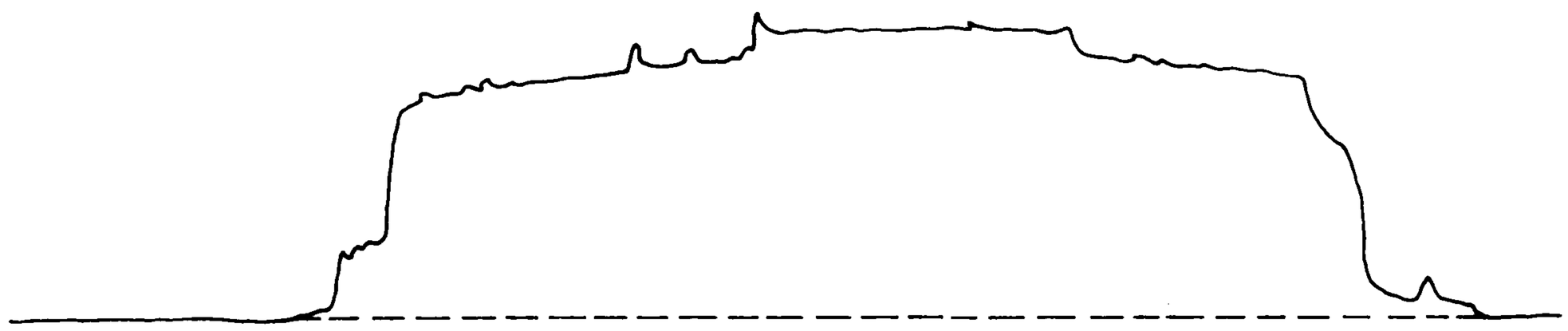

(b)

FIG. 9.12 Typical "Talysurf" traces for a cadmium sulphide film deposited on aluminium rod (a) along a diameter (b) along a diameter perpendicular to (a).

in detail in sections 5.6 and 6.5.1.

From a technological point of view one of the most important properties of a deposited film is its mechanical integrity. For a film that disintegrates or even flakes off its substrate is of no use as far as device fabrication is concerned. The "Scotch-tape" test to measure film adhesion to the substrate is discussed in detail in section 6.5.1, where the effect of deposited film thickness and substrate surface finish on film adhesion are also discussed. In that section the manner in which a film disintegrates or flakes-off due to thermal stresses or "dirtiness" is described.

X-ray crystallographic studies on as-deposited films are described in Chapter 7. Optical microscopy was also used to determine the thickness of very thin CdS films. A travelling microscope was used and the results agreed with those obtained from the "Talysurf".

CHAPTER 9

REFERENCES

1. N.F. Foster, *CdS evaporated-layer transducers*, Proc. IEEE 53, p. 1400 (1965).

2. N.B. Hannay ed., *Semiconductors*, Chapman & Hall (1960).

3. M. Aven et al ed., *Physical & chemical properties of II-VI compounds*, North Holland (1967).

4. D. Le Croissette, *Transistors*, p. 79, Prentice-Hall (1963).

5. J.G. Simmons chapter in *Handbook of thin film technology*, ed. L.I. Maissel et al, McGraw-Hill (1970).

6. M. Aven et al, *Electrical transport and contact properties of low resistivity n-type ZnS crystals*, App. Phys. Lett. 7, p. 8 (1965).

7. A.J. Learn et al, *Barriers at evaporated metal-polycrystalline CdS interfaces*, App. Phys. Lett. 8, p. 144 (1966).

8. J.A. Scott-Monk et al, *Rectifying contacts under evaporated CdS*, Proc. IEEE, 56, p. 68 (1968).

9. R. Zuleeg et al, *Space charge limited currents and Schottky emission currents in thin film CdS diodes*, Sol. Stat. Electronics, 1, p. 575 (1964).

10. G. Thomas ed., *II-VI semiconducting compounds*, p. 1267 Benjamin (1967).

11. W.A. Crofut, *High power operation of CdS t.f. transducers*, Proc. IEEE, 55, p. 715 (1967).

12. B. Binggeli et al, *Capacitance changes in thin CdS crystals under d.c. bias*, JAP, 38, p. 4984 (1967).

13. J.H. McFee chapter in *Physical Acoustics*, Vol. 4A, ed. W.P. Mason, Academic Press (1964).

14. A. Gopinath et al, *Frequency tuning of CdS platelets*, Elect. Lett., 5, p. 622 (1969).

15. G.A. Rozgonyi et al, *Orientation inversions in polycrystalline CdS bulk crystals and thin films*, JAP, 38, p. 5172 (1967).

16. W.H. Strehlow et al, *Epitaxy of CdS on SrF*, Physl. Rev. 188, p. 188 (1969).

17. M. Redwood, *A study of waveforms in the generation and detection of short ultrasonic pulses*, App. Mat. Res., p. 76, April 1963.

C H A P T E R 10

Conclusions

Attempts to deposite efficient thick-film (low-frequency) s mode CdS transducers directly onto inserts which formed part of a spot-welding-electrode, to enable the quality of the welds to be evaluated "on-machine", have not been successful. However, a number of contributions to the state-of-the-art have been made.

It has been found that the temperature of the vapour molecules is an important parameter in influencing the orientation of CdS films and that the cooler the molecules the sharper the oblique c-axis preferred orientation. Provided that the temperature of the vapour molecules is less than 400^{o}C, and that the pumping speed can be increased at will, then, the faster the deposition rate the sharper the oblique c-axis preferred orientation, and the better the piezoelectric performance of the films. Fast deposition rates (few $\mu m.min^{-1}$) at oblique vapour incidence are difficult to achieve because of the limit imposed on the rate by the speed of the vacuum pumping system. If the pumping speed is not high enough, the pressure builds up and the vapour molecules lose their directionality. The high vacuum (HV) system used in the present investigation had a maximum pumping speed of 600 litre $.s^{-1}$ which limited deposition rates to 10 $\mu m.h^{-1}$.

It has been established that no appreciable temperature gradients exist in CdS films during growth, either across their thickness or along their surface. No changes in temperature gradients occur in deposited CdS films due to changes in film orientation, and vice versa.

Appreciable stresses exist in deposited CdS films, and appreciable forces, proportional to film thickness, induce the thick films to flake off or disintegrate. Nevertheless, thick CdS films were made to adhere to the substrate by making the substrate surface "rougher" so that the

films keyed-in.

It has been established that up to a certain (critical) thickness, the c-axes of most CdS film crystallites aligned themselves with the direction of the vapour beam. Once the thickness of the film exceeded this critical thickness, the growth of oblique crystallites was stifled, and the film's c-axis tilted towards the substrate-normal and eventually became parallel to it. Nevertheless, thick oblique c-axis films have been fabricated, either by making the grain size of the film bigger, or by multi-layering CdS films so that the thickness of each layer was less than the critical thickness. Very thin amorphous Si O_2 layers were deposited between the CdS layers to prevent the multi-layered CdS from being crystallographically continuous. CdS films have also been deposited on curved substrates, and no marked difference was found between their orientation and that of those on flat substrates.

Highly stoichiometric (deviations from stoichiometry of the order of 1 part in 10^{13}) and highly resistive (> 10^{10} Ω.m.), and highly oriented CdS films up to 100 μm thick have been successfully deposited on Aℓ rod substrates. However, these films made very poor transducers : it is possible that their dislocation density was too high. Good s-mode transducers, with untuned two-way insertion loss of 35 dB in a 50 Ω system were successfully fabricated on glass slides for operation at frequencies down to 20 MHz. The stress in CdS films on glass slides was much less than that on Aℓ rods. It is possible that the higher stress in CdS films on Aℓ rods weakened their piezo-electric performance.

Copper substrates, and indeed copper parts inside the deposition chamber, cannot be used because of the corrosive action of sulphur on them. It has been found that Cu/CdS junctions are nearly ohmic, and the anomalous behaviour of these junctions has been explained in terms of the reaction between Cu and S to form Cu_2 S.

C H A P T E R 11

Future work

An obstacle to the fabrication of good CdS s-mode transducers on polycrystalline metal may be due to a high dislocation density in the films. A high dislocation density may be caused by the roughness of the substrate, the stress in the films, and the high dislocation density in the substrate. So long as the substrate is metallic, the stresses are always appreciable and nothing can be done to reduce them. Something can be done, however, to decrease the dislocation density of the substrate surface, namely, to use substrates with very large grains. For example duralumin or aluminium rods may be machined from square blocks with large grain size. The rod surface finish has to be relatively rough so that a thick-film keys-in and thus adheres very strongly to the substrate. If it is found that, even with large grain rods the dislocation density in the films is still high, the rough surface finish will have to be made smoother but not so smooth that the films flake off. Spark-machined surface finishes may prove useful here.

The Cd/S isothermal technique should be used instead of the CdS/S electron beam bombardment, to achieve faster deposition rates at lower temperatures of vapour molecules. To ensure repeatability, the same cadmium cell should be used in successive deposition runs. The area of the cadmium orifice could be measured accurately using a polar planimeter. Different sulphur to cadmium ratios could then be achieved using different diameter sizes of precision bore (0.01% tolerance) capilary tubes for the sulphur orifice. The remanent cadmium (from a previous deposition run) could be dissolved in a solution of ammonium nitrate, and the cell cleaned.

A vapour diffusion pump with a pumping speed of at least one order of magnitude higher than that in the present work should also

be used. For example the Edwards Model 24M4 or Model F3606 (price at time of writing £2000) could be used, together with a faster backing rotary pump. Much faster CdS deposition rates (few $\mu m.min^{-1}$) could then be achieved making the oblique c-axis preferred orientation of the films sharper, and their dislocation density lower. As a bonus a run for the deposition of a 100 μm film will take hours instead of days, with actual deposition times of minutes instead of hours. The high pumping speed will also be useful in shortening interruption times, when air has to be admitted to the chamber to repair or replace some components. This makes the formation of oxide layers on the surfaces of the substrates less likely.

In view of the fact that no marked difference was found between the orientations of CdS films deposited onto flat and domed aluminium rods, it seems likely that once useful transducers can be made on domed rods, they should also work on other curved substrates. The only limitation being the radius of curvature, where shadow-masking effects may come into play and alter the growth environment of the film crystal. The radius of curvature of the side of the slot in the seam-welding-electrode, onto which the CdS film is to be deposited, is about 10 times greater than that of the domed aluminium rod. It seems likely, therefore, that s-mode CdS films could be deposited directly onto the slot. Since welding electrodes are made of copper, a CdS film cannot be deposited directly onto the slot. This is because of the corrosive action of sulphur on copper. However, a gold-plated seam-welding-electrode with a slot suitable for oblique angle deposition already milled in it is available.

No problems are anticipated with the fabrication of s-mode CdS transducers for microwave applications, for frequencies up to at least 1 GHz. For this application, the CdS/S e.b.b. isothermal technique should be used since it is much easier to carry out than the Cd/S technique.

A P P E N D I X I

- R.F. sputtering apparatus

In this appendix the r.f. sputtering electrodes and vacuum chamber top seal designed by the author are described together with the power supply for the r.f. oscillator which was designed and built by the author (see section 3.4.2).

The sputtering electrodes consisted of two segments of a copper disc 6 mm thick. The r.f. field is developed across the 4 mm gap between these segments (Figs. A1.1 and A1.2). Copper pipes served as both electric connectors and carriers of circulating cooling water. the chamber top seal consisted of a stainless steel disc-plate 300 mm diameter and 12 mm thick. The copper electrodes were housed in this plate using P.T.F.E. bushes (Fig. A1.4) and a P.T.F.E. disc (Fig. A1.5). The electrodes-plate assembly was made vacuum-tight by the use of O-rings. The whole assembly is shown in Fig. A1.6 where it is seen that the target to be sputtered is held in position below the electrodes by a stainless steel retaining push. The top seal rests on the gasket of the bell jar of the deposition chamber. The Admiralty Materials Laboratory has kindly presented us with a P.Z.T. sputtering target to suit this apparatus.

The circuit diagram for the 1.5 kW variable power supply for the r.f. oscillator is shown in Fig. A1.7. A microswitch attached to the Variac which supplied the H.T. transformer ensured, with the help of a relay, that H.T. power would only be supplied starting from zero. Another relay ensured that no H.T. power was available unless the deposition chamber was evacuated. This worked in conjunction with a vacuum switch. The valves of the oscillator were also protected against heater failure.

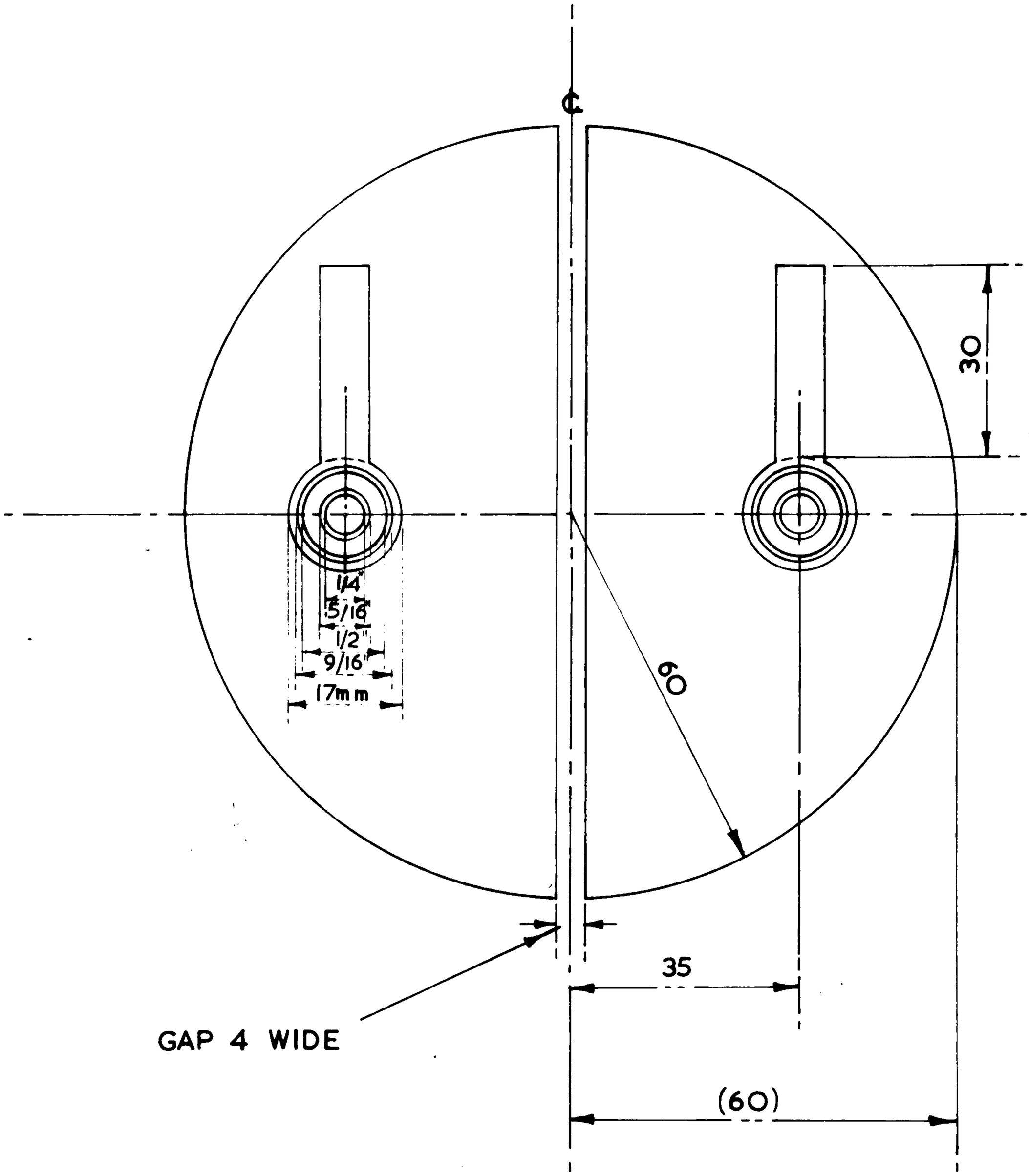

FIG. A1·1 Copper electrodes and cooling copper pipes (PLAN), for elevation see FIG. A1·2. Dimensions in mm, unless shown otherwise

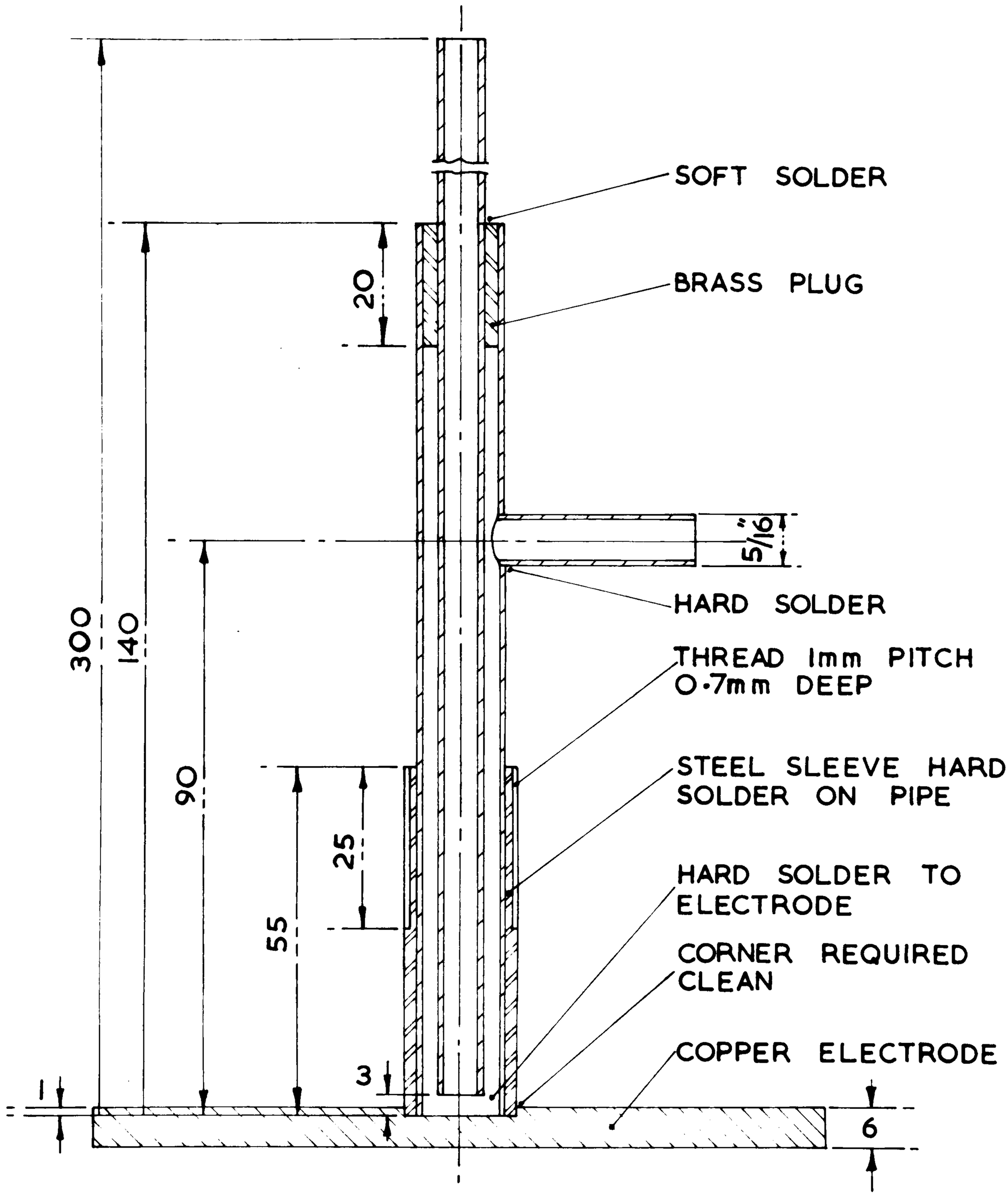

FIG. A1·2 Copper electrode and cooling copper pipes (ELEVATION). Dimensions in mm, unless shown otherwise.

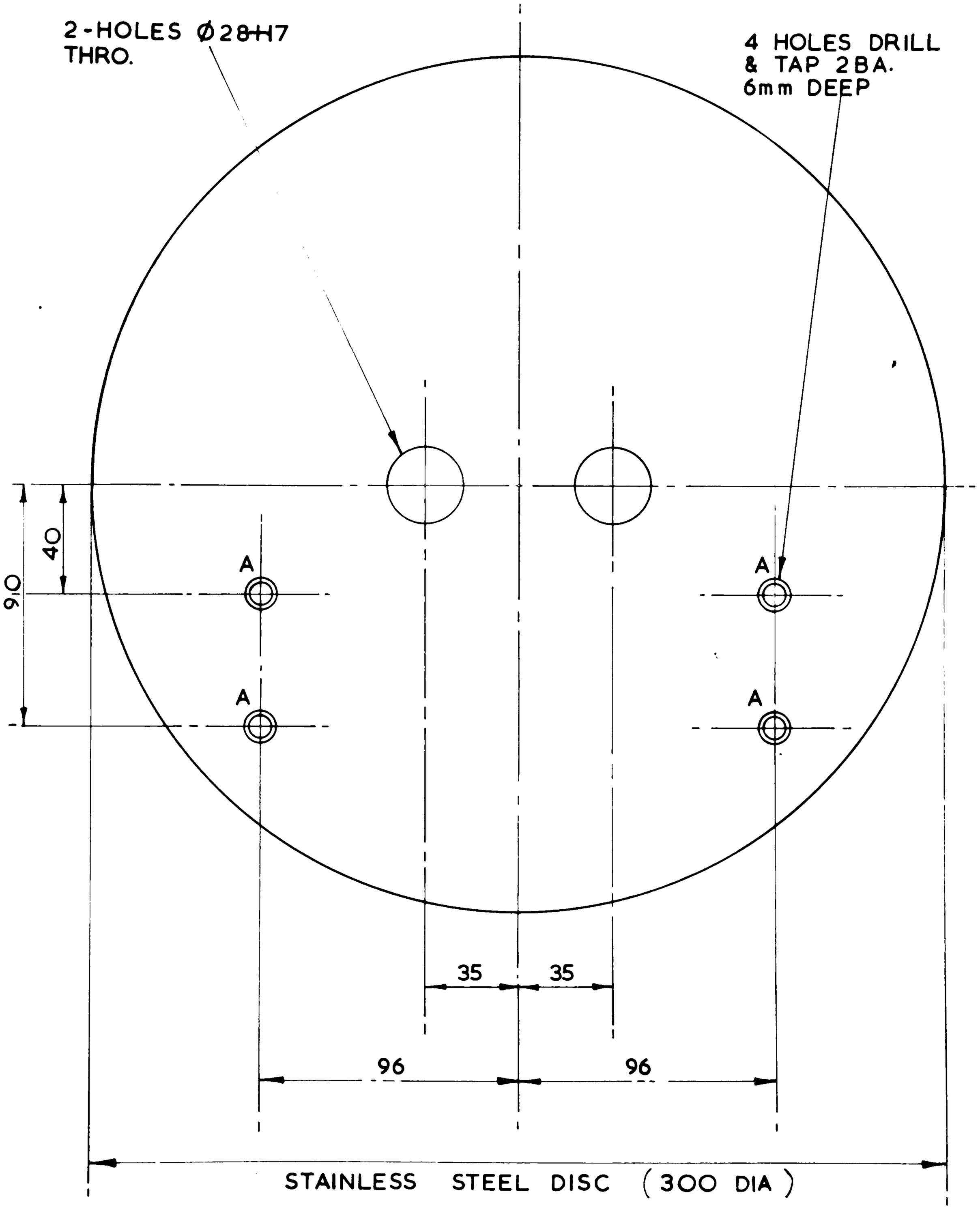

FIG. A1·3 R.F. sputtering chamber top disc-plate (houses copper electrodes) see FIG. A1·6 for assembly. Dimensions in mm

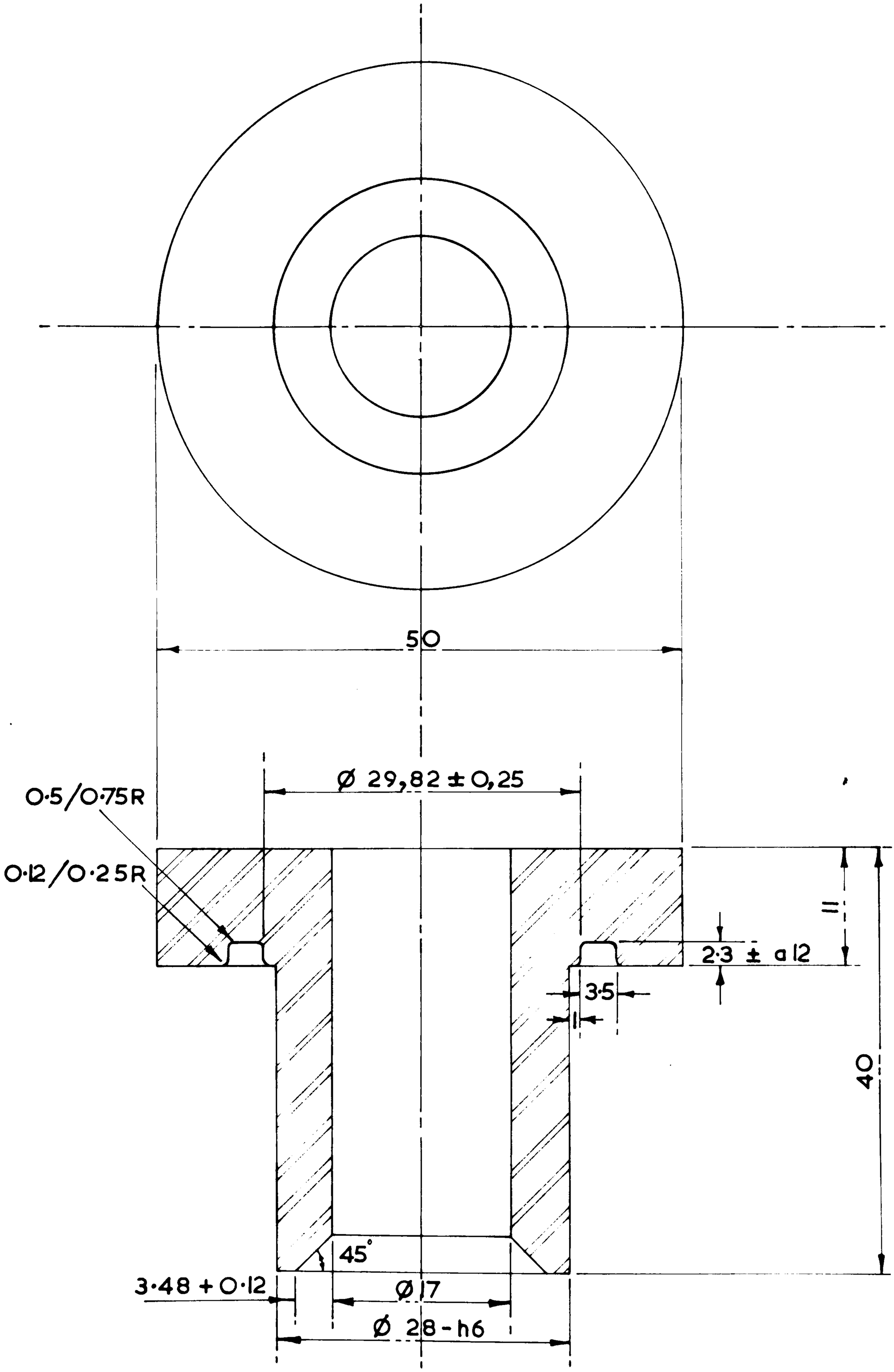

FIG. A1·4 P.T.F.E. bush, see FIG. A1·6 for assembly. Dimensions in mm.

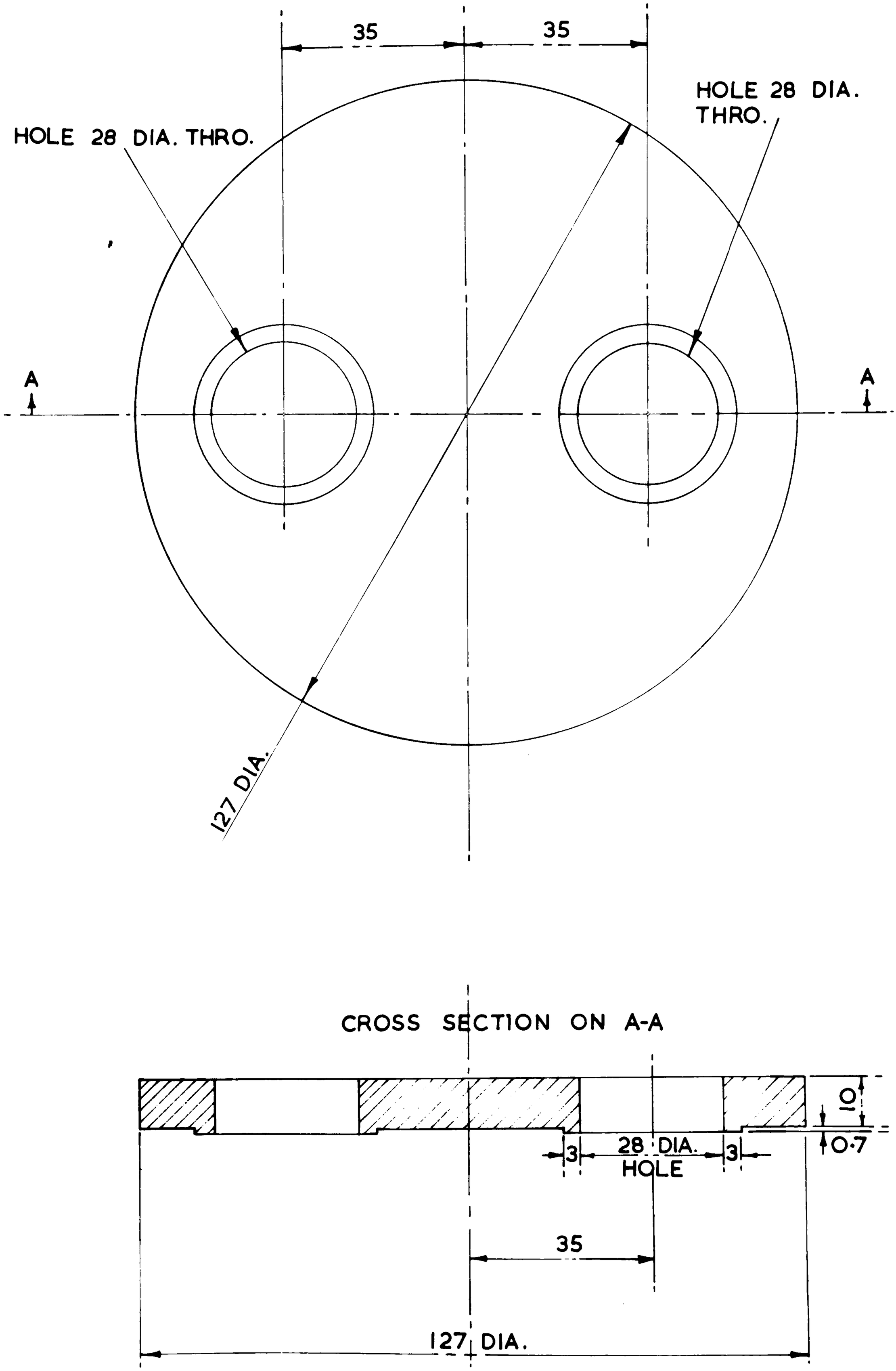

FIG. A1·5 P.T.F.E. disc, see FIG. A1·6 for assembly. Dimensions in m m

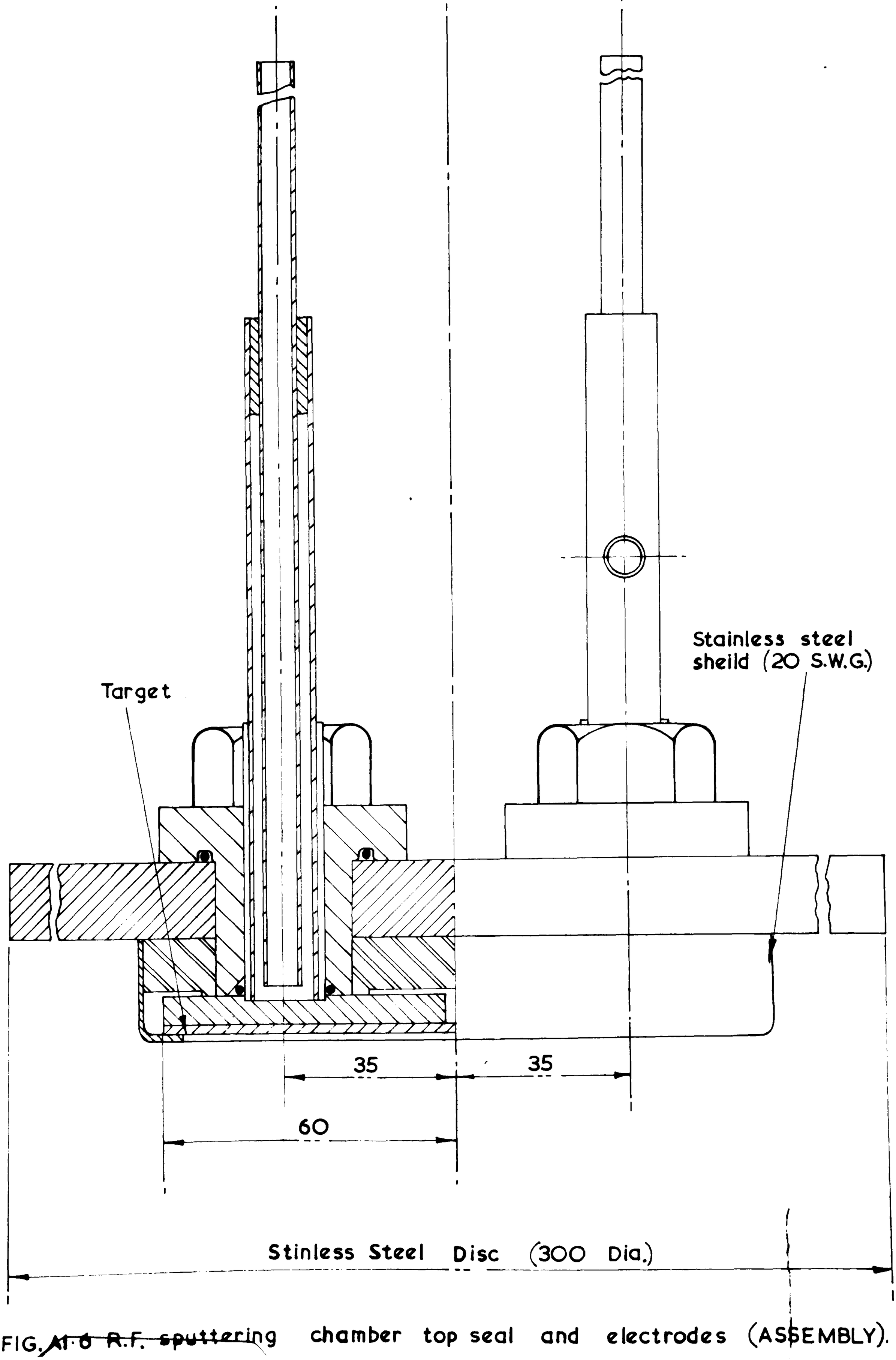

FIG. A1·0 R.F. sputtering chamber top seal and electrodes (ASSEMBLY).

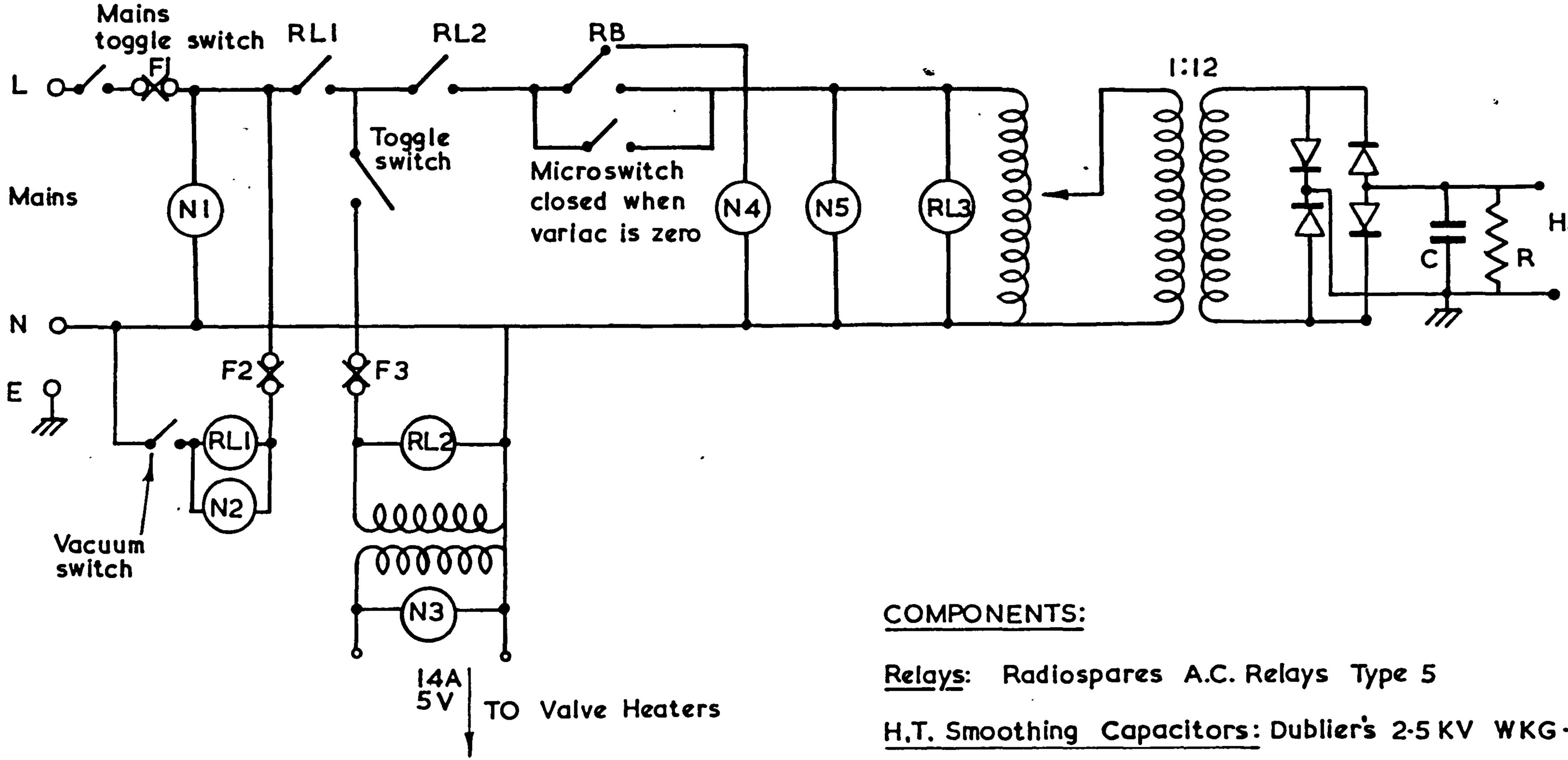

FIG A1.7 Power-Pack for r.f. oscillator

COMPONENTS:

Relays: Radiospares A.C. Relays Type 5

H.T. Smoothing Capacitors: Dublier's 2·5 KV WKG – (8μF)

Rectifiers: Mullard's Silicon Rectifiers Type OSS670

A P P E N D I X II

Desk Computer Programme

Given here is the programme for the Hewlett-Packard 9100A desk computer which was used to predict deposition angles and deposited film thicknesses when the substrate holder was tilted (see section 5.4). The programme prints-out values for film thickness, t_r, substrate to source distance, R, and the angles $\emptyset$, α, δ and β defined in section 5.4 and in Figs. 5.7 and 5.9. It also prints out the data fed-in, namely h_0, r and γ. The programme is self-cycling, i.e. when values of h_0, r and γ are fed-in, it automatically starts with $\beta = 0^o$ and works out values for the other parameters, then it works out these values when $\beta = 15^o$, 30^o, ... etc., until $\beta = 180^o$ when it will stop. It only prints-out when $30^o < \emptyset < 50^o$.

Step	Key	x	y	z	a	b	c	d
00	Clear				h_o	r	γ	
1	f	β						
2	cos	cosβ						
3	↑		cosβ					
4	c	γ						
5	cos	cosγ						
6	X		cosδ					
7	↻	cosδ						
8	arc							
9	cos	δ						
a	x( )							
b	e							
c	a	h_o						
d	↑		h_o					
10	X		h_o^2					
1	b	r						
2	↑		r	h_o^2				
3	X		r^2					
4	↓	r^2	h_o^2					
5	+		$h_o^2 + r^2$					
6	↑			$h_o^2 + r^2$				
7	$\sqrt{x}$	r						
8	↻		r					
9	a	h_o						
a	X		$h_o r$					
b	2	2						
c	X		$2h_o r$					
d	e	δ						

Step	Key	x	y	z	a	b	c	d
20	cos	cosδ	$2h_o r$	$h_o^2 + r^2$				
1	X		$2h_o r \cos\delta$					
2	↓	$2h_o r \cos\delta$	$h_o^2 + r^2$					
3	-		R^2					
4	↻	R^2						
5	$\sqrt{x}$	R						
6	↑		R					
7	x( )							
8	d							R
9	e	δ						
a	sin	sinδ						
b	↑		sinδ	R				
c	a	h_o						
d	X		$h_o \sin\delta$					
30	↓	$h_o \sin\delta$	R					
1	↻	R	$h_o \sin\delta$					
2	÷		cosØ					
3	↷	cosØ						
4	arc							
5	cos	Ø						
6	↑		Ø					
7	3							
8	0	30						
9	IF x < y							
a	5							
b	1							
c	f	β						
d	↑		β					

Step	Key	x	y	z	a	b	c	d
40	1		β					
1	8							
2	0	180						
3	IF x = y							
4	9							
5	1							
6	1							
7	5	15						
8	↻		15					
9	Clear x	0						
a	↻	15	0					
b	Acc +							
c	Go to							
d	0							
50	1							
1	5		Ø					
2	0							
3	IF x > y							
4	5							
5	9							
6	Go to							
7	3							
8	c							
9	↻	Ø						
a	↑		Ø					
b	↑			Ø				
c	9							
d	0	90						

Step	Key	x	y	z	a	b	c	d
60	+	90	90 + Ø	Ø				
1	e	δ						
2	-		α					
3	f	β						
4	Print							
5	Print							
6	↓	α	Ø					
7	cos	cosα						
8	↻	Ø	cosα					
9	cos	cosØ						
a	X		cosØcosα					
b	d	F						
c	÷							
d	÷		t_r					
70	↺	t_r						
1	↑		t_r					
2	↑			t_r				
3	a	h_o						
4	X		h_o t_r					
5	X		h_o t_r^2					
6	e	δ						
7	sin	sinδ						
8	÷		$t_{r/c}$					
9	d	R						
a	Roll	$t_{r/c}$	t_r	R				
b	Print							
c	Print							
d	Print							

Step	Key	x	y	z	a	b	c	d
80	a	h_0						
1	↑		h_0					
2	b	r						
3	↑		r	h_0				
4	c	γ						
5	Print							
6	Print							
7	Print							
8	Print							
9	Go to	50	ø					
a	3							
b	c							
c	End							
d	6							
90	Go to							
1	3							
2	c							
3	↑			ø				
4	c	γ						
5	↻		γ					
6	f	β						
7	Print							
8	Print							
9								
a								
b								
c								
d								

A P P E N D I X III

PUBLICATIONS